LATE QUATERNARY PALAEOENVIRONMENTAL RECONSTRUCTION FROM LAKE OHRID

Jack H. Lacey

Thesis submitted to the University of Nottingham

for the degree of Doctor of Philosophy

July 2016

School of Geography &

British Geological Survey

ABSTRACT

Lake Ohrid is a large, deep, ancient lake located on the Balkan Peninsula and has an extraordinary degree of endemic biodiversity. A deep drilling campaign was carried out in 2013 as part of the Scientific Collaboration on Past Speciation Conditions in Lake Ohrid (SCOPSCO) project to better understand the influence of climate and environmental change on evolutionary patterns and endemism. Initial results from a 569 m sediment succession drilled in the centre of the basin indicate continuous lacustrine conditions over the past ca. 1.2 Ma. This thesis presents new stable isotope data from carbonate within the upper 248 m of the composite profile, covering the last ca. 640 ka at a millennial-scale resolution (≈ 0.5 ka). Isotope data are used to provide a long-term palaeoenvironmental reconstruction, which is supported by a quantitative model of modern lake water isotope composition and a detailed multi-proxy investigation of climate evolution since the last glacial period.

Water balance calculations confirm Ohrid to be an evaporative system with a complex hydrology. Variations in the isotope composition of modern lake water are suggested to represent long-term fluctuations in water balance. A trend from wetter to drier conditions through the Holocene is consistent with regional and hemispheric processes related to changes in insolation. Over the last ca. 640 ka, endogenic calcite is precipitated in abundance during warm stages, however carbonate is negligible during glacial periods with the exception of discrete horizons comprising early diagenetic authigenic siderite. The oxygen isotope composition of lake water, calculated using calcite and siderite, indicates more evaporated conditions during warm stages and fresher lake water in glacial phases. Low frequency variability shown by calcite isotope data suggests relatively stable conditions before ca. 450 ka, a transition to a wetter climate between ca. 400-250 ka, and a trend to drier climate conditions after ca. 250 ka. Higher frequency millennial-scale oscillations and abrupt climate events observed during warm stages are likely associated with regional climate change as a function of orbital forcing.

This study emphasises the potential of Lake Ohrid as a valuable archive of climate change in the central Mediterranean region and demonstrates the efficacy of isotope data for palaeoenvironmental reconstruction at Lake Ohrid.

AUTHOR'S PUBLICATIONS

Published

Lacey, J. H., Leng, M. J., Höbig, N., Reed, J. M., Valero-Garcés, B., Reicherter, K. 2015. Western Mediterranean climate and environment since Marine Isotope Stage 3: a 50,000-year record from Lake Banyoles, Spain. Journal of Palaeolimnology, 55 (2), 113-128.

Lacey, J. H., Francke, A., Leng, M. J., Vane, C. H. and Wagner, B. 2015. A high-resolution Late Glacial to Holocene record of environmental change in the Mediterranean from Lake Ohrid (Macedonia/Albania). International Journal of Earth Sciences, 104 (6), 1623-1638.

Cvetkoska, A., Levkov, Z., Reed, J. M., Wagner, B., Panagiotopoulos, K., Leng, M. J., **Lacey, J. H.** 2015. Quaternary climate change and Heinrich Events in the southern Balkans: Lake Prespa diatom palaeolimnology from the last interglacial to present. Journal of Palaeolimnology, 53 (2), 215-231.

Wagner, B., Wilke, T., Krastel, S., Zanchetta, G., Sulpizio, R., Reicherter, K., Leng, M. J., Grazhdani, A., Trajanovski, S., Francke, A., Lindhorst, K., Levkov, Z., Cvetkoska, A., Reed, J. M., Zhang, X., **Lacey, J. H.**, Wonik, T., Baumgarten, H., and Vogel, H. 2014. The SCOPSCO drilling project recovers more than 1.2 million years of history from Lake Ohrid. Scientific Drilling, 17, 19-29.

Wagner, B., Leng, M. J., Wilke, T., Böhm, A., Panagiotopoulos, K., Vogel, H., **Lacey, J. H.**, Zanchetta, G., and Sulpizio, R. 2014. Distinct lake level lowstand in Lake Prespa (SE Europe) at the time of the 74 (75) ka Toba eruption. Climate of the Past, 10, 261-267.

Submitted

Lacey J. H., Leng, M. J., Francke A., Sloane, H. J., Milodowski, A., Vogel, H., Baumgarten, H., Wagner B. 2015. Mediterranean climate since the Middle Pleistocene: a 640 ka stable isotope record from Lake Ohrid (Albania/Macedonia). Biogeosciences Discussions, 12, 13427-13481.

Zanchetta, G., Regattieri, E., Giacco, B., Wagner, B., Sulpizio, R., Francke, A., Vogel, H., Sadori, L., Masi, A., Sinopoli, G., **Lacey, J. H.**, Leng, M. J., Leicher, N. 2015. Aligning MIS5 proxy records from Lake Ohrid (FYROM) with independently dated Mediterranean archives: implications for core chronology. Biogeosciences Discussions, 12, 16979-17007.

Francke, A., Wagner, B., Just, J., Leicher, N., Gromig, R., Baumgarten, H., Vogel, H., **Lacey, J. H.**, Sadori, L., Wonik, T., Leng, M. J., Zanchetta, G., Sulpizio, R., and Giacco, B. 2015. Sedimentological processes and environmental variability at Lake Ohrid (Macedonia, Albania) between 640 ka and present day. Biogeosciences Discussions, 12, 15111-15156.

Zhang X. S., Reed J. M., **Lacey J. H.**, Francke, A., Leng M. J., Levkov, Z., Wagner B. 2015. Complexity of diatom response to Lateglacial and Holocene climate and environmental change in ancient, deep, and oligotrophic Lake Ohrid (Macedonia/Albania). Biogeosciences Discussions, 12, 14343-14375.

ACKNOWLEDGEMENTS

Over the course of this project, I have had the especial privilege of meeting and working with a wide range of people, all of whom have positively benefitted the PhD. In particular, the project would not have been possible (or as enjoyable) without assistance from the following people.

First and foremost, I would like to thank my supervisor, Melanie Leng, who has provided advice and encouragement throughout the PhD. I am sincerely grateful for the breadth of scholarly undertaking, invaluable opportunities, and profound support Melanie has afforded me over the past years.

I am very grateful to Matthew Jones for taking on the role of secondary supervisor and providing additional guidance. In particular, our discussions on isotope mass balance models have greatly improved the thesis.

I am thankful to Bernd Wagner for welcoming me into the SCOPSCO science team and providing sample material. I would also like to thank Alexander Francke for many constructive discussions and scientific support.

Staff at BGS have provided excellent training and assistance with preparative and analytical work, particularly Hilary Sloane, Christopher Kendrick and Jonathan Dean. Andrea Snelling is thanked for initial training on the carbonate line, Christopher Vane for conducting the Rock-Eval analysis and Antoni Milodowski for help with SEM work.

The PhD was funded by the BGS University Funding Initiative (GA/12S/016/C2), and Jonathan Naden and Michael Patterson are acknowledged for their understanding and support.

Being part of such a large interdisciplinary collaboration, as well as working on other research projects, means there are a number of other people to thank (in no particular order): Jane Reed and Xiaosen Zhang for providing diatom data and manuscript collaboration; Hendrik Vogel for FTIR data and along with Gianni Zanchetta providing a great insight into Mediterranean palaeoclimate; Laura Sadori and Alessia

Masi (and the pollen group) for palynological data; Katja Lindhorst for seismic data plots; Henrike Baumgarten for advice on writing up the 5045-1 age model and manuscript comments; Janna Just, Konstantinos Panagiotopoulos, Andreas Koutsodendris for fruitful discussion; Ascelina Hasberg, Raphael Gromig (and Alexander Francke) for 12-hour night shifts on the barge; the DOSECC team for drilling the SCOPSCO cores; Nicole Höbig, Klaus Reicherter and Blas Valero-Garcés for collaboration on Lake Banyoles; David Ryves for collaboration on Rostherne Mere; Doris Wagner for providing XRD data; John Fletcher for producing excellent thin sections; University of Nottingham School of Geography staff and postgraduates for providing such a welcoming environment and copious palaeo-based discussions; and the University of Leicester Department of Geology, in particular Nick Marsh and Cheryl Haidon for their technical assistance during the early stages of the PhD.

CONTENTS

Chapter 7 | SCOPSCO 5045 162

LIST OF FIGURES

LIST OF TABLES

CHAPTER 1 | INTRODUCTION

1.1 Ancient lakes

Although there are estimated to be in excess of 100 million lakes worldwide covering almost 4% of the Earth's non-glaciated land surface (Downing et al., 2006; Verpoorter et al., 2014), the majority are short-lived (<18,000 years) and only very few have continuously existed since before the last glacial maximum (Albrecht et al., 2006). This select group of long-lived extant lakes are referred to as 'ancient lakes' (Figure 1.1; Brooks, 1950), and are classically defined as having a limnological age of at least 100,000 years (Gorthner, 1994).

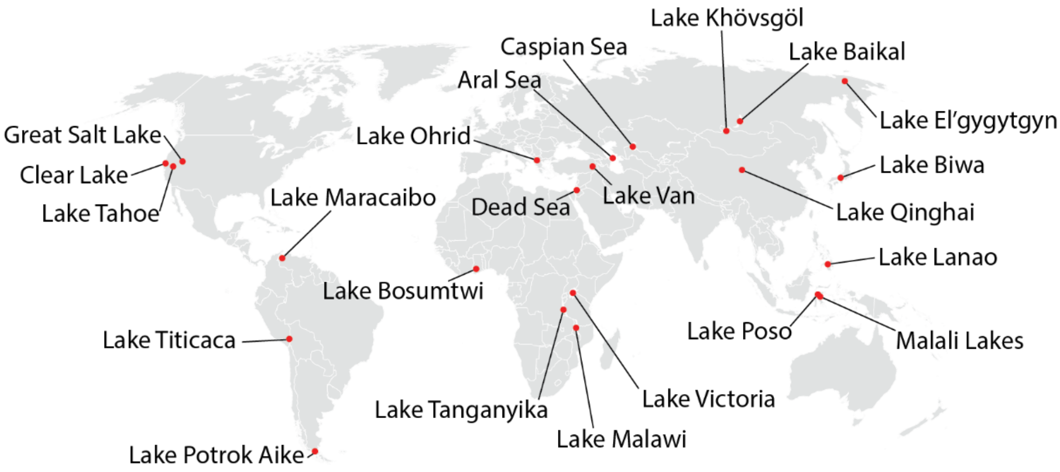

Figure 1.1 *Map showing the location of major ancient lakes of the world.*

The oldest lakes in the world have survived far beyond this, for example Lake Baikal (Russia) is thought to originate within a Paleogene rift zone (ca. 30 Ma; Williams et al., 2001) and Lake Tanganyika (East Africa) has age estimates between 9 and 12 Ma (Table 1.1; Cohen, 2003). However, most ancient lakes are younger, such as Lake Biwa (Japan) and Lake Titicaca (South America) at between 2 and 4 Ma (Dejoux, 1994; Kawanabe et al., 2012) or the relatively youthful Lake Victoria (East Africa) at <1 Ma (Johnson et al., 1996).

In addition to longevity, ancient lakes are recognised as hotspots of biodiversity and endemism that provide excellent research systems for better understanding speciation mechanisms and the processes that govern the generation of endemic populations

(Brooks, 1950; Cristescu et al., 2010). Moreover, a high faunal species diversity is often used as a proxy indicator for ancient lake status (Martens, 1997), correlating with lake longevity in both a modern and geological context (Gierlowski-Kordesch and Park, 2004).

Table 1.1 *Physical and biological features of ancient lakes with high rates of endemism (modified from Martens, 1997; Matzinger et al., 2007; Cohen, 2011).*

Lake	Maximum Age (My)	Surface Area (km^2)	Endemic Species	Index of Endemic Biodiversity*
Ohrid	2	348	212	0.92
Baikal	30	31500	982	0.67
Tanganyika	20	32600	632	0.62
Biwa	4	674	54	0.61
Victoria	0.75	70000	240	0.49
Malawi	8.6	30800	200	0.51
Titicaca	4	8448	61	0.45

(*index of endemic biodiversity = log $N_{\text{endemic species}}$ * log $A_{\text{surface area}}^{-1}$, see Figure 1.3)

Ancient lakes are commonly associated with active tectonic rift zones where basin subsidence compensates sedimentation (Schon and Martens, 2004; Albrecht and Wilke, 2008), important examples of which include lakes Baikal, Tanganyika, Biwa, Titicaca, Victoria, Khövsgöl (Mongolia), and Malawi (East Africa) (Mackay et al., 2010). Alternatively, ancient lakes can form as a direct result of volcanism (e.g. Lake Challa, East Africa), meteorite impacts (e.g. Lake El'gygytgyn, Russia), or in karst basins (e.g. Ioannina, Greece).

This unique group of extant lakes often contain an extensive sedimentary archive as, in contrast to other depositional environments, sedimentation is relatively rapid and continuous (Cohen, 2011). Therefore, ancient lakes can hold highly resolved records that span (at least) the full Quaternary period (2.6 Ma) providing an unparalleled opportunity to study the relationship between past processes (climate, geology, tectonics, volcanism) and diversity patterns through multi-proxy analysis of lake sediments (Schon and Martens, 2004).

1.2 Lake Ohrid

In Europe, the majority of lakes considered to be of ancient status are located in the Balkan region (Figure 1.2; Albrecht and Wilke, 2008). The largest and perhaps most exceptional of these is Lake Ohrid, a transboundary lake shared between the Former Yugoslav Republic of Macedonia (henceforth Macedonia) and the Republic of Albania (henceforth Albania). Lake Ohrid is located in a steep-sided graben that formed through rift tectonics, similar to lakes Baikal and Tanganyika for example, during the late Miocene-Pliocene (Dumurdzanov et al., 2004) and is thought to have a limnological age of at least 1.2 Ma (Wagner et al., 2014).

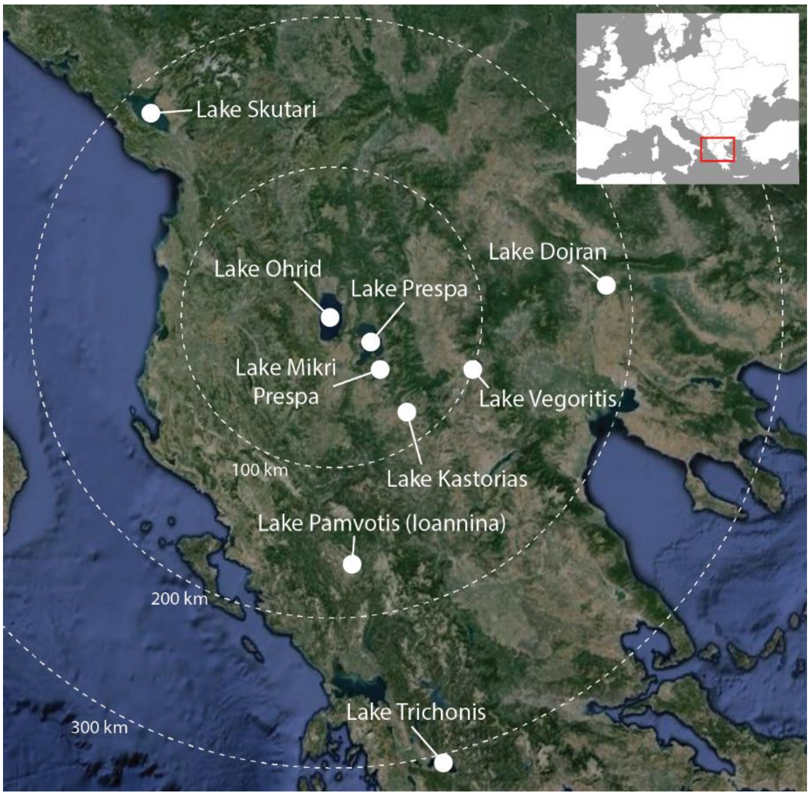

Figure 1.2 *Map showing the location of Lake Ohrid and other European ancient lakes (after Albrecht and Wilke, 2008, their figure 1; Landsat image: Google Earth).*

The lake harbours a remarkable degree of natural biological diversity (Stankovic, 1960), and has 212 described endemic species, which, when lake surface area is taken into account, makes Ohrid the most diverse in the world (Table 1.1, Figure 1.3; Albrecht and Wilke, 2008). Unlike ancient lakes in Africa and Southeast Asia where vertebrate species comprise the majority of endemic fauna, European ancient lakes are typically characterised by their invertebrate endemism, in particular among benthic and semi-benthic taxa (Albrecht and Wilke, 2008). The benthic communities of Lake Ohrid are no exception, Watzin et al. (2002) estimated the degree of benthic endemism to be up to 86%, with the highest diversity present in gastropods (Table 1.2). Endemism is also recognised in several other groups, such as diatoms, sponges and bivalves. This impressive biodiversity was an important contributing factor for establishing Lake Ohrid as a UNESCO World Heritage Site in 1979 and the Ohrid-Prespa Transboundary Biosphere Reserve in 2014.

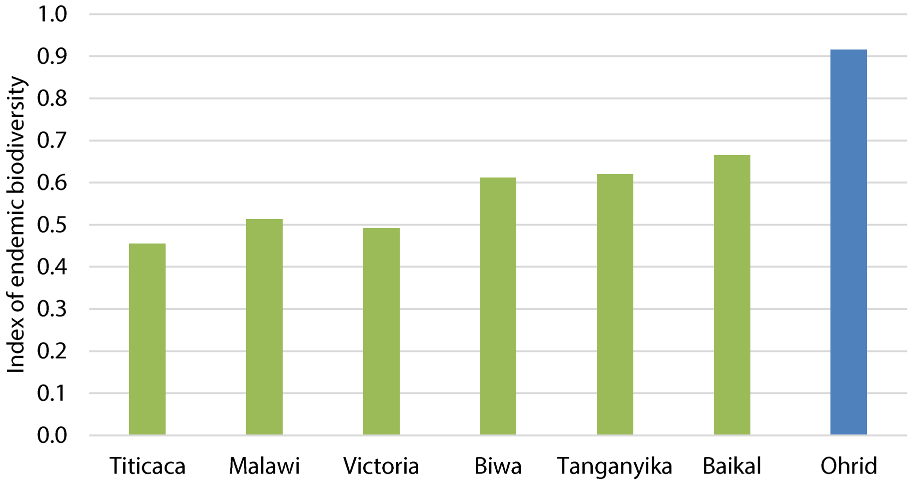

Figure 1.3 *Index of endemic biodiversity for selected ancient lakes, taking surface area into account (Table 1.1; after Albrecht and Wilke, 2008, and references therein).*

Table 1.2 *The degree of endemism for various benthic animal taxa in Lake Ohrid (data from Watzin et al., 2002).*

Class	Endemic taxa (%)
Gastropoda (snails)	86
Tricladida (flatworms)	81
Oligochaeta (worms)	47
Hirudinea (leeches)	52
Ostracoda (seed shrimp)	71
Amphipoda (lawn shrimp)	60
Isopoda (woodlice)	75

1.3 Scientific drilling of ancient lakes

High temporal resolution records from ancient lakes can provide data on the timing and extent of environmental change over long time scales, and represent valuable archives for coordinating palaeolimnological reconstructions and phylogenetic work (Cohen, 2011). The outstanding characteristics of ancient lakes as sites of global significance have allowed several to be targeted within the scope of the International Continental scientific Drilling Program (ICDP) over the last two decades (Figure 1.4; Harms et al., 2007). In the Mediterranean, this encompasses the Dead Sea in Israel/Jordan (Stein et al., 2011), Lake Van in Turkey (Litt and Anselmetti, 2014), and Lake Ohrid in Macedonia/Albania (Wagner et al., 2014).

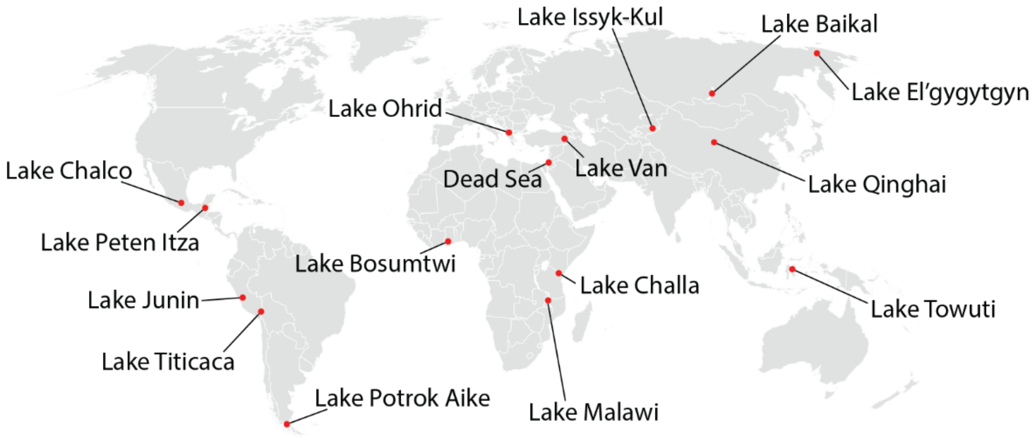

Figure 1.4 *Map showing the location of recent and proposed ICDP ancient lake drill sites.*

The Mediterranean is a climatically sensitive region at the confluence between subtropical and mid-latitude regimes (Lionello et al., 2012), which has made it a key location for palaeoenvironmental research. However, a significant proportion of current studies are restricted to the Holocene (Wick et al., 2003; Baroni et al., 2006; Eastwood et al., 2007) or the Last Interglacial (Drysdale et al., 2005; Regattieri et al., 2015), and only a very limited number of records cover several glacial-interglacial cycles (Martrat et al., 2004; Tzedakis et al., 2006; Gasse et al., 2015). Therefore, Lake Ohrid provides a rare example of a large extant Mediterranean ancient lake from which climate and environmental variability can be reconstructed over multiple glacial-interglacial cycles, and where such changes can potentially be linked with rates of evolutionary change and faunal diversity.

1.4 SCOPSCO project

Previous sedimentary records from Ohrid show that the lake was sensitive to changes in climate over the last glacial-interglacial cycle (Wagner et al., 2009a; Vogel et al., 2010a), and reveal that it is a valuable archive of volcanic ash dispersal (Caron et al., 2010; Sulpizio et al., 2010b) and tectonic events (Wagner et al., 2008a; Reicherter et al., 2011) (see later disscussion on previous work in Chapter 2). These sequences demonstrate the great potential for environmental reconstruction from the Ohrid sediments, but only span the last 140 ka. Previous research does not have the temporal range necessary to address key research questions in regard to the age and origin of the lake, and importantly the mechanisms (e.g. environmental change) controlling endemism and evolution (Wagner et al., 2009b). Moreover, the Mediterranean has been identified as a prominent ‘hot-spot’ in future climate change scenarios (Giorgi, 2006) and an understanding of past environmental change is crucial to enable the accurate prediction of future variations, especially during past interglacials when orbital geometries were similar to the present configuration (Vogel et al., 2013).

Given that Lake Ohrid is a site of global importance for better understanding Quaternary climate change and the generation of endemic fauna, it became the target site for an ICDP deep drilling campaign in 2013. The Scientific Collaboration On Past Speciation Conditions in Lake Ohrid (SCOPSCO) project is an international multi-disciplinary research initiative which aims to investigate the impact of major environmental and geological events on the unique biodiversity of the lake, with the aim of obtaining more precise information on (i) the age and origin of the lake, (ii) past seismotectonic activity in the region, (iii) central Mediterranean climate and environmental change through the Quaternary, and (iv) how evolution is influenced by major geological events and the triggers for speciation.

1.5 Research aims and objectives

This thesis presents isotope and geochemical stratigraphy data from SCOPSCO cores and provides an environmental reconstruction covering the last 640 ka, which will support other evidence on long-term climate change and short-term climate events.

This work will address SCOPSCO aims (iii) and (iv), in part, as the cores cover the past 1.2 Ma. The reconstruction will ultimately be used as a reference record for climate change across the Mediterranean and Northern Hemisphere, to infer teleconnections between other long and continuous records, and to aid assessment of whether speciation in Lake Ohrid is reliant on stable or catastrophic conditions.

In addition to the central aims of the SCOPSCO project, and to provide information on palaeoenvironmental and palaeoclimate conditions at Lake Ohrid, this thesis aims to address three primary synoptic research questions primarily using isotope and geochemical data.

- What is the response of Lake Ohrid to recent (Holocene) shifts in climate and environmental change?
- How has Lake Ohrid responded to long-term variations in climate over the last 640 ka?
- Is this response constant and is there evidence for hydroclimate variations both between and within interglacials?

The main objectives of this thesis are:

i. Further assess the modern isotope hydrology of Lake Ohrid and investigate climate and environmental change over the Late Glacial to Holocene using a high-resolution (ca. 30-year) record (core Co1262) and multi-proxy approach to provide a calibration for longer-term reconstructions that can be correlated with previous Lake Ohrid multi-proxy records and compared to those from the wider Mediterranean region.

ii. Produce an environmental reconstruction over the past 640 ka (at ca. 425-year resolution) using the SCOPSCO composite profile (core 5045-1) and determine interglacial (and if possible glacial) variability to evaluate long-term hydroclimate change in the central Mediterranean region, which forms the basis to better understand the consistency of environmental conditions and their influence on the endemic biodiversity of the lake.

1.6 Thesis outline

The thesis has been divided into the following chapters:

Chapter 2: Background presents an overview of Lake Ohrid and its catchment, providing information on physiography and hydrology, geological setting, controls on climate and summarises previous coring work.

Chapter 3: Theoretical framework reviews the controls on lacustrine stable isotope and organic geochemistry datasets.

Chapter 4: Analytical methodology explains the laboratory work conducted during this study.

Chapter 5: Modern isotope hydrology reviews the modern isotope data available for Lake Ohrid and presents new calculations to refine the understanding of isotope systematics at Lake Ohrid.

Chapter 6: Lini Co1262 presents the results from a high-resolution Late Glacial to Holocene core from Lake Ohrid, discusses climate and lake hydrology, as well as the terrestrial and aquatic response to climate.

Chapter 7: SCOPSCO 5045-1 presents the results from the SCOPSCO composite profile over the past 640 ka, discusses interglacial (and glacial) variability through the Middle and Late Pleistocene, and compares the Ohrid reconstruction to other long and continuous records from both marine and terrestrial realms.

Chapter 8: Summary of research reviews the overall conclusions from the thesis and assesses the potential for future work.

CHAPTER 2 | BACKGROUND

2.1 Physiography and hydrology

Lake Ohrid (40°54’-41°10’N, 20°38’-20°48’E) is located in the north-eastern Mediterranean on the Balkan Peninsula and spans the border between Macedonia and Albania (Figure 2.1). It forms part of the Dessaretes lake group, which also consists of Lake Prespa, Lake Mikri Prespa and Lake Maliq (Figure 2.2; Albrecht and Wilke, 2008). The lake is situated at an altitude of 693.5 m above sea level (asl), has a maximum N-S length of 30.8 km, a maximum E-W width of 14.8 km wide and covers an area of around 358 km^2 (Stankovic, 1960); of the total surface area 251 km^2 belong to Macedonia and 107 km^2 to Albania (Popovska and Bonacci, 2007). Lake Ohrid is surrounded by high mountain chains, bounded to the west by the Mokra Mountains (1500 m asl) and to the east by the Galičica Mountains (2262 m asl) and the Mali i Thatë Mountains (2287 m asl). The lake basin has a bathtub-shaped morphology with an estimated volume of 50.7 km^3, a maximum water depth of 293 m and an average water depth of 150 m (Popovska and Bonacci, 2007; Lindhorst et al., 2015).

***Figure 2.1** Map of the north-eastern Mediterranean showing the location of Lake Ohrid (red dot).*

Lake Ohrid has a relatively small direct topographic watershed of around 1002 km^2 (Popovska and Bonacci, 2007), which increases to 2600 km^2 when tributaries and aquifer input from neighbouring Lake Prespa are also taken into account (Figure 2.2; Matzinger et al., 2006b). Lake Prespa, located 9 km to the east and 155 m above Lake Ohrid at 848.5 m asl (Leng et al., 2013), delivers water to Lake Ohrid through a network of karst aquifers which account for approximately half of total water input to the lake (Figure 2.3; Matzinger et al., 2006a). The karst spring water is depleted in nutrients and has a low mineral content (Wagner et al., 2008a; Vogel et al., 2010a). The underground connection between lakes Ohrid and Prespa, first hypothesised by Cvijić (1906), has been confirmed using environmental tracer methods (Anovski et al., 1991; Amataj et al., 2007). The remaining water input comprises direct precipitation on the lake's surface and river inflow. The water input balance from karst aquifers can be further divided between sublacustrine springs and surface springs (water balance is discussed in detail in Chapter 5; Matzinger et al., 2006b).

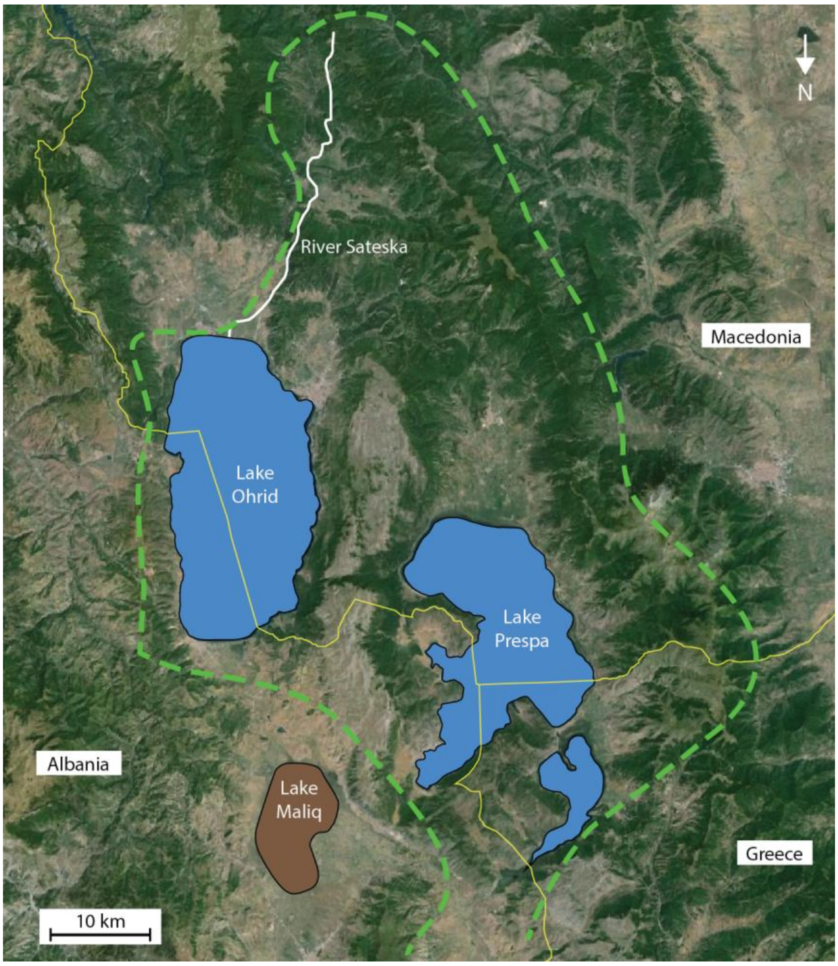

Figure 2.2 *Map showing the geographical setting of Lake Ohrid, Lake Prespa, Lake Maliq and the River Sateska (map: Google Earth, 2013). International boundaries (yellow solid line) and the watershed boundary (green dashed line) are shown (Popovska and Bonacci, 2007, their figure 2). Lake Maliq was drained after World War II for agricultural purposes (Bordon et al., 2009).*

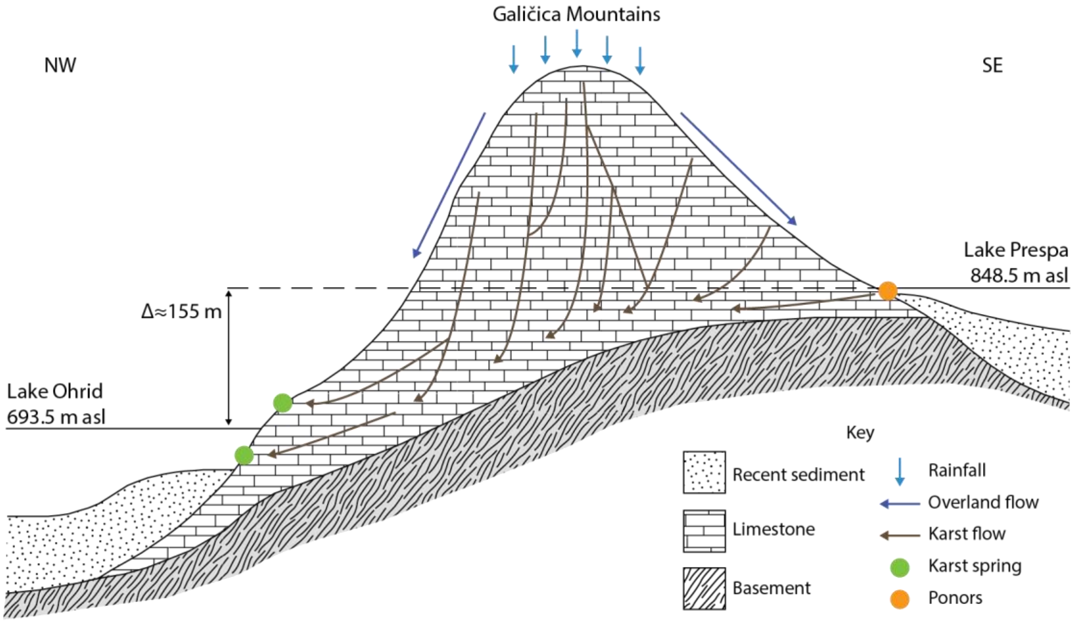

Figure 2.3 *Schematic section through the Galičica Mountain range, showing the hydrological connection between Lake Ohrid and Lake Prespa and the karst spring system (after Popovska and Bonacci, 2007, their figure 3). The Galičica range contains aquifers within karstified carbonates that have a large hydraulic conductivity due to a high secondary porosity (Eftimi et al., 2001).*

The largest surface spring area is located at the southern edge of Lake Ohrid near the Monastery of Saint Naum in Macedonia, with a second important spring complex nearby at Tushemisht in Albania (Figure 2.4), both of which have been shown to receive water from Lake Prespa (Eftimi and Zoto, 1997; Matzinger et al., 2006a). There are several smaller spring complexes on the north-western and north-eastern shores of Lake Ohrid (Albrecht and Wilke, 2008).

The main riverine inflow to Lake Ohrid is the Sateska on the northern shore (Figure 2.4), which comprises the majority of river input (Matzinger et al., 2006b). The River Sateska was artificially diverted into the lake in 1962, extending the Lake Ohrid watershed northwards (Figure 2.2) and leading to an increase in average annual inflow by around 200 x 10^6 m^3 (Popovska and Bonacci, 2007). Previous to being diverted the Sateska was a tributary of the River Crn Drim (Figure 2.4), the primary surface outflow from Lake Ohrid (Matzinger et al., 2006b). The remainder of water output from Lake Ohrid is through evaporation, which is greater than direct precipitation on the lake's surface (Matzinger et al., 2006b). Although groundwater outflow is also a possibility, it has not yet been demonstrated (see Chapter 5).

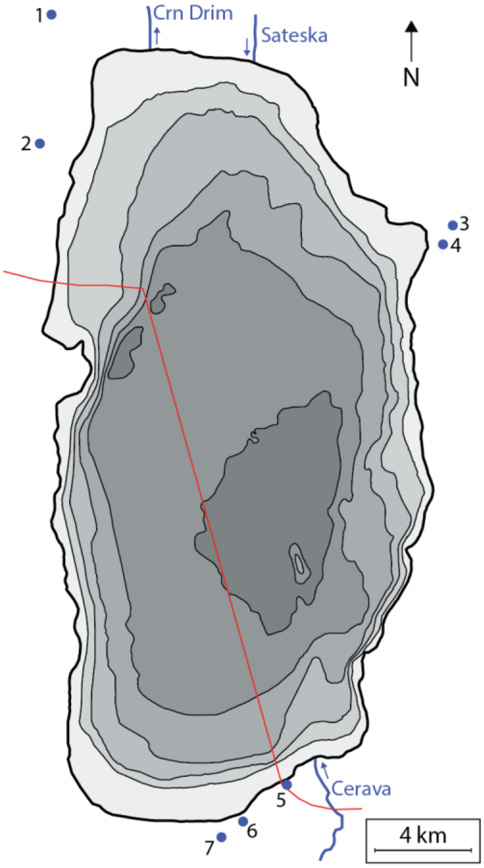

Figure 2.4 *Map of Lake Ohrid showing bathymetry (50 m isolines), major rivers with flow direction (blue lines), international border (red line) and the location of springs (1) Sum, (2) Dobra Voda, (3) Bej Bunar, (4) Biljana, (5) St. Naum, (6) Tushemisht, and (7) Zagorican (spring locations: Albrecht and Wilke, 2008, their figure 3; map: Vogel et al., 2010a, their figure 2b).*

Lake Ohrid has a long hydraulic residence time of roughly 70-80 years due to a relatively small drainage basin and large volume (Matzinger et al., 2006a; Popovska and Bonacci, 2007). The lake water volume and low nutrient supply support oligotrophic conditions (Stankovic, 1960; Matzinger et al., 2007; Vogel et al., 2010a), with an average Secchi depth of approximately 14 m (Matzinger et al., 2006b). The upper 150-200 m of the lake water column becomes thermally stratified in summer months and is mixed during winter (Matzinger et al., 2007), below this mixing depth a partially isolated water body is formed that is stratified by salinity (Albrecht and Wilke, 2008; Wagner et al., 2008a). Complete overturn is irregular and occurs around every 7 years (Hadzisce, 1966), which leads to a de-stratification of the complete water column during deep convective winter mixing (Matzinger et al., 2006b). Due to the partial and intermittent mixing, nutrient re-suspension from the sediment-water interface is limited and so further supports an oligotrophic environment (Vogel et al., 2010a).

2.2 Geology and tectonics

The Lake Ohrid basin is a tectonic graben that formed in the Dinaride-Albanide mountain chain most probably during the Tortonian-Messinian (ca. 5-8 Ma; Dumurdzanov et al., 2004), and has a basin and range-like geodynamic setting (Hoffmann et al., 2010). Numerous sedimentary basins in the southern Balkans were developed in association with Cenozoic tectonics that began in the Late Cretaceous-Palaeogene subsequent to the final closure of the Vardar Ocean (Figure 2.5; Burchfiel et al., 2008).

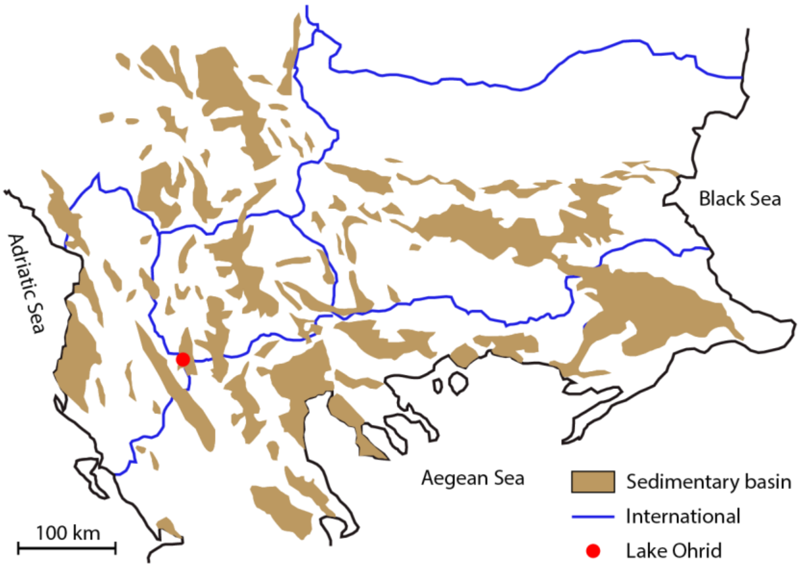

Figure 2.5 *Cenozoic sedimentary basins formed on the Balkan Peninsula principally relating to extensional tectonics (after Burchfiel et al., 2008, their figure 2).*

The Ohrid graben is located on the contact between the Mirdata Ophiolite Zone (an internal zone of the Albanides) and the Korabi Zone (part of the Western Macedonian Zone) (Hoffmann et al., 2010), aligned along a N-S striking fault zone that extends into Albania and Greece (Dumurdzanov et al., 2004). The Mirdata Zone to the west consists of obducted ophiolites of Jurassic age unconformably overlain by a thin succession of Upper Cretaceous transgressive carbonates (Figure 2.6; Channell and

Kozur, 1997; Robertson, 2004; Hoffmann et al., 2010). The Korabi Zone to the east comprises Palaeozoic metamorphic and magmatic rocks superposed by Triassic-Lower Jurassic carbonates and clastics (Figure 2.6; Reicherter et al., 2011).

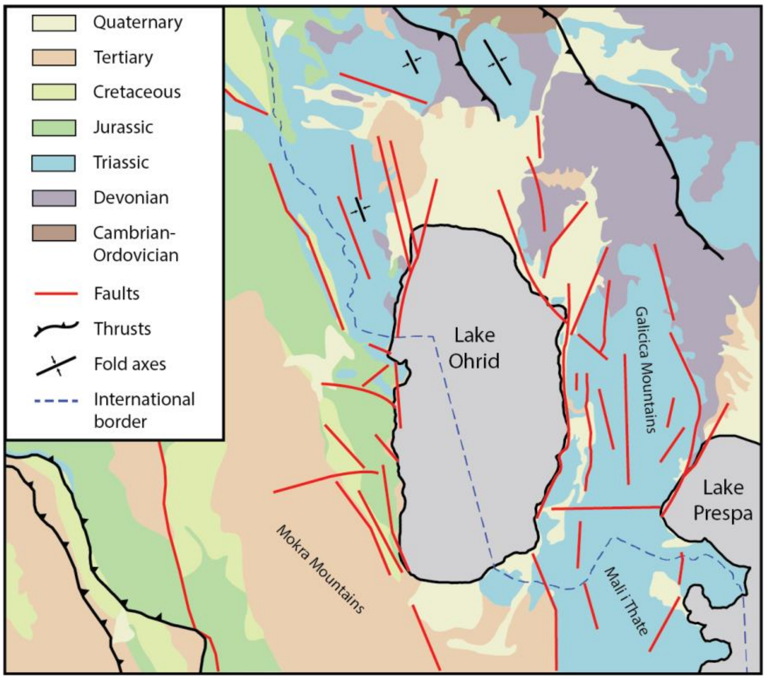

Figure 2.6 *Geological map of the Lake Ohrid basin, showing main geological units and structural elements (after Hoffmann et al., 2010; their figure 4).*

Cenozoic sedimentation occurred during two cycles separated by a depositional hiatus and is overlain by Quaternary sediments. The Miocene Piskupstina Formation contains gravel, sandstone, and clay-siltstone, and the succeeding Pliocene Solnje Formation consists of gravel and sandstone (Dumurdzanov et al., 2004). The Quaternary strata include fine-grained sediment indicant of remnant shallow lake areas to the south of the Ohrid basin, along with gravel and sand strata from river deltas and alluvial fans to the north of the lake (Hoffmann et al., 2010), where local peat deposits are also present (Dumurdzanov et al., 2004).

The basin has only been subjected to extensional deformation since formation and its sediments are either horizontal or fault-tilted, none are folded (Dumurdzanov et al., 2004). Lake Ohrid is located in an active seismic region and over the last few centuries several moderate earthquakes have been reported, the last major event to be recorded was in 1911 (magnitude 6.7, 15 km depth) (Muço et al., 2002; Reicherter et al., 2011). Comprehensive on- and offshore geomorphological and neotectonic investigations suggest the basin to be tectonically active (Hoffmann et al., 2010; Reicherter et al., 2011; Lindhorst et al., 2015), which is corroborated by recent earthquake activity within the last decade (USGS, 2015).

2.3 Climate

The Mediterranean is located within a transitional zone between the humid European temperate domain and the dry African sub-tropical region, providing a complex and sensitive climatology (Magny et al., 2013). In general, the climate is influenced by the sub-tropical anticyclone in summer and mid-latitude westerlies during winter, which leads to a pronounced precipitation seasonality characterised by hot, dry summers and mild, wet winters. This seasonal cycle is controlled by the northward migration of the Intertropical Convergence Zone (ITCZ) during summer, in response to interhemispheric temperature gradient changes (Tzedakis et al., 2009). In winter the ITCZ moves southward allowing the influence of westerlies to be established and the development of cyclogenesis across the whole Mediterranean (Figure 2.7; Tzedakis et al., 2009).

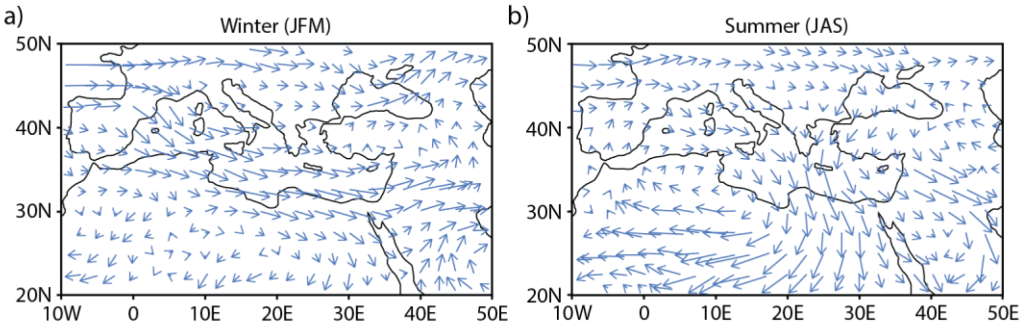

***Figure 2.7** Wind climatologies over the Mediterranean basin at 850 hPa for winter (JFM; a) and summer (JAS; b) (Raicich et al., 2003, their figure 1), showing the differences as a result of ITCZ movement.*

Hydrological conditions within the Mediterranean are strongly influenced by atmospheric circulation mechanisms, responsible for contrasting temperature and precipitation patterns in the region (Magny et al., 2013). The most prominent mode of variability is the North Atlantic Oscillation (NAO; Hurrell, 1995), particularly during boreal winter when the atmosphere is most dynamic, which is associated with a pressure contrast between the Icelandic low and the Azores high (Figure 2.8; Hurrell et al., 2002).

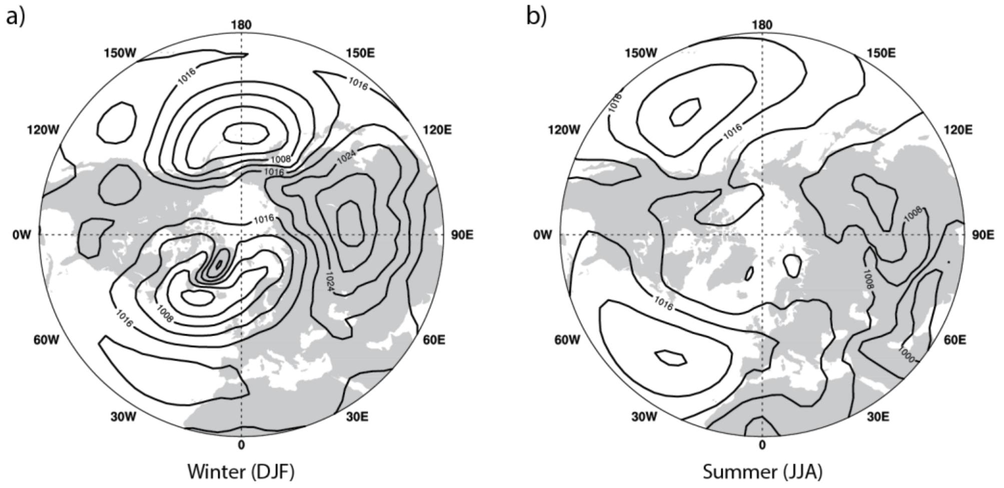

Figure 2.8 *Mean sea level pressure for (a) boreal winter and (b) boreal summer, the contour increment is 4 hPa (Hurrell et al., 2003, their figure 1).*

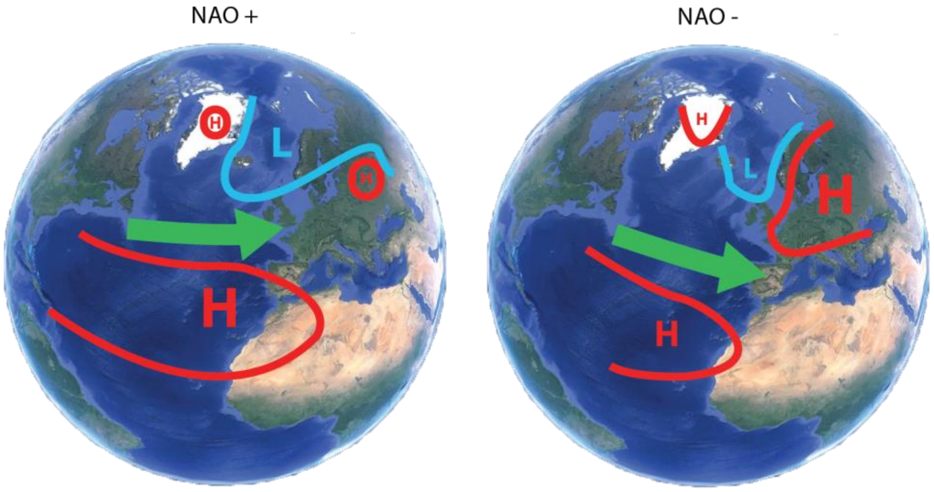

Figure 2.9 *Schematic NAO positive and negative phases, showing high (H; red) and low (L; blue) pressure centres and the direction of westerlies (map: Google Earth, 2013) (after Wanner et al., 2001, their figure 9).*

This pressure difference produces large changes in both the speed and direction of westerly winds, and in the related transport of heat and moisture across the North Atlantic and European continents (Figure 2.9; Hurrell et al., 2003). When there is a high pressure gradient between the two sites (high index or positive NAO), westerly winds are strengthened and have a more northerly flow direction transporting mild, moist air across north-western Europe (Hurrell et al., 2002). When Atlantic storm tracks shift northwards during a positive NAO phase, moisture delivery is reduced to southern Europe and the Mediterranean resulting in the development of widespread dry conditions (Magny et al., 2013).

Conversely, when the Azores high and Icelandic low pressure centres are weaker, the gradient is reduced (low index or negative NAO) and the westerlies can move southward bringing more frequent storm activity and precipitation to mid-European latitudes and the Mediterranean (Bout-Roumazeilles et al., 2007; Hurrell and Deser, 2009). NAO variability and winter temperatures are significantly correlated across wide regions of the northern hemisphere (Hurrell and Dickson, 2005), and during a positive (negative) NAO phase the Mediterranean experiences cooler (warmer) temperatures than normal (Hurrell, 1996; Mann, 2002; Trigo et al., 2002; Xoplaki, 2002).

Local orography modifies the path of the westerlies at surface level (Raicich et al., 2003), producing climatic sub-zones that have variable precipitation and temperature distributions (Zanchetta et al., 2007a). Based on the traditional classification scheme (Köppen, 1900), the Mediterranean climate is defined as mid-latitude temperate with hot or warm and dry summers (Lionello et al., 2012). However, this classification does not apply to a large proportion of the region and in Macedonia a diversity of climate exists due to secondary modification of Mediterranean influences predominantly by topography (Figure 2.10). The climate of Lake Ohrid and its watershed is therefore controlled by both sub-Mediterranean and continental influences (Panagiotopoulos et al., 2013), owing to the lake’s location in a deep valley sheltered by mountains and its proximity to the Adriatic Sea (Vogel et al., 2010a).

Mean air temperatures range between −6°C (January) and 32°C (June), measured between 1960-1991 at a meteorological station in the town of Ohrid, with an average annual air temperature of 11°C (Figure 2.11; Popovska and Bonacci, 2007). Unlike neighbouring Lake Prespa, the water in Lake Ohrid never freezes and surface water temperatures remain between 6°C and 26°C, and bottom water temperature stays relatively constant between 5°C and 6°C (Popovska and Bonacci, 2007). The Lake Ohrid watershed has an average annual rainfall of around 900 mm (Figure 2.11; Popovska and Bonacci, 2007), slightly elevated above the national average of approximately 730 mm/year (Tančev and Petkovski, 2006). The prevailing wind direction predominantly traces the Ohrid valley along its north-south axis, with northerly winds during autumn-winter and southerly winds in spring-summer (Stankovic, 1960).

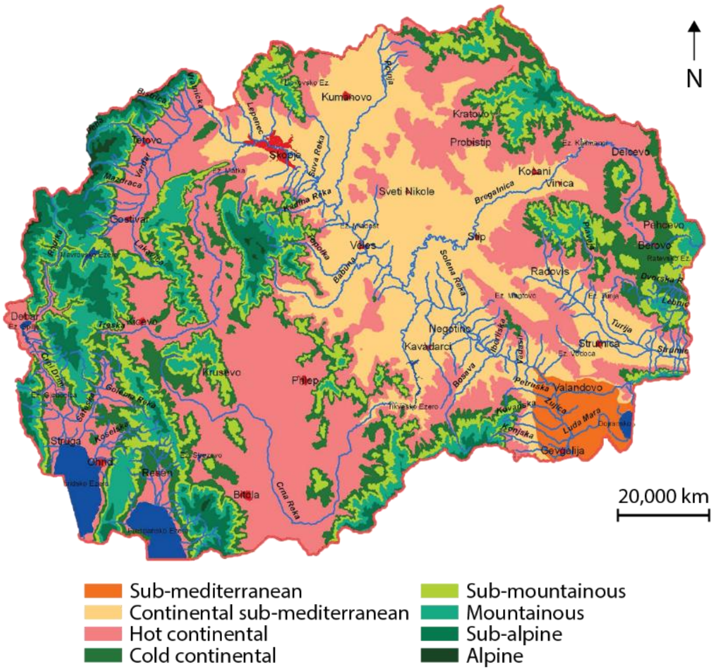

Figure 2.10 *Macedonian climate types defined by altitude and annual cycle of temperature and precipitation (Glavinov, 2012; their figure 2).*

The Mediterranean has been identified as a prominent hot-spot in future climate change predictions (Giorgi, 2006), having a forecast warming of up to 0.46°C per decade (Lelieveld et al., 2012; Lionello et al., 2012). Since 1960 mean summer heat wave intensity, duration and quantity have increased by up to 8% in central and eastern areas (Kuglitsch et al., 2010) and annual precipitation is shown to have a significant negative trend between 1901-2009 (Philandras et al., 2011). In Macedonia, over the second half of the 20th century annual mean temperatures have increased by roughly 0.2°C and precipitation has considerably decreased by around 100 mm (Figure 2.12a; Lambevska, 2011). Future projections for the middle and end 21st century suggest these trends are set to continue, by 2100 average temperatures in Macedonia may be 4-5°C higher when compared to 1961-1990 and precipitation could potentially be reduced by up to 25% (Figure 2.12b).

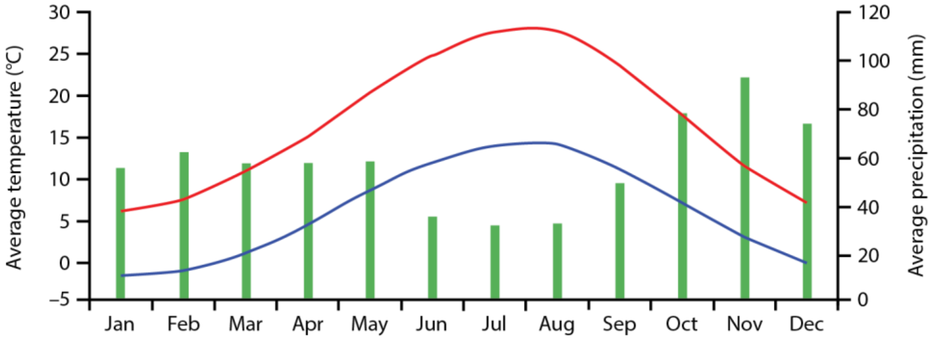

Figure 2.11 *Climate data from the town of Ohrid, showing monthly averages for precipitation (green) and maximum (red) and minimum (blue) temperature over a 30-year period (data: WMO, 2015).*

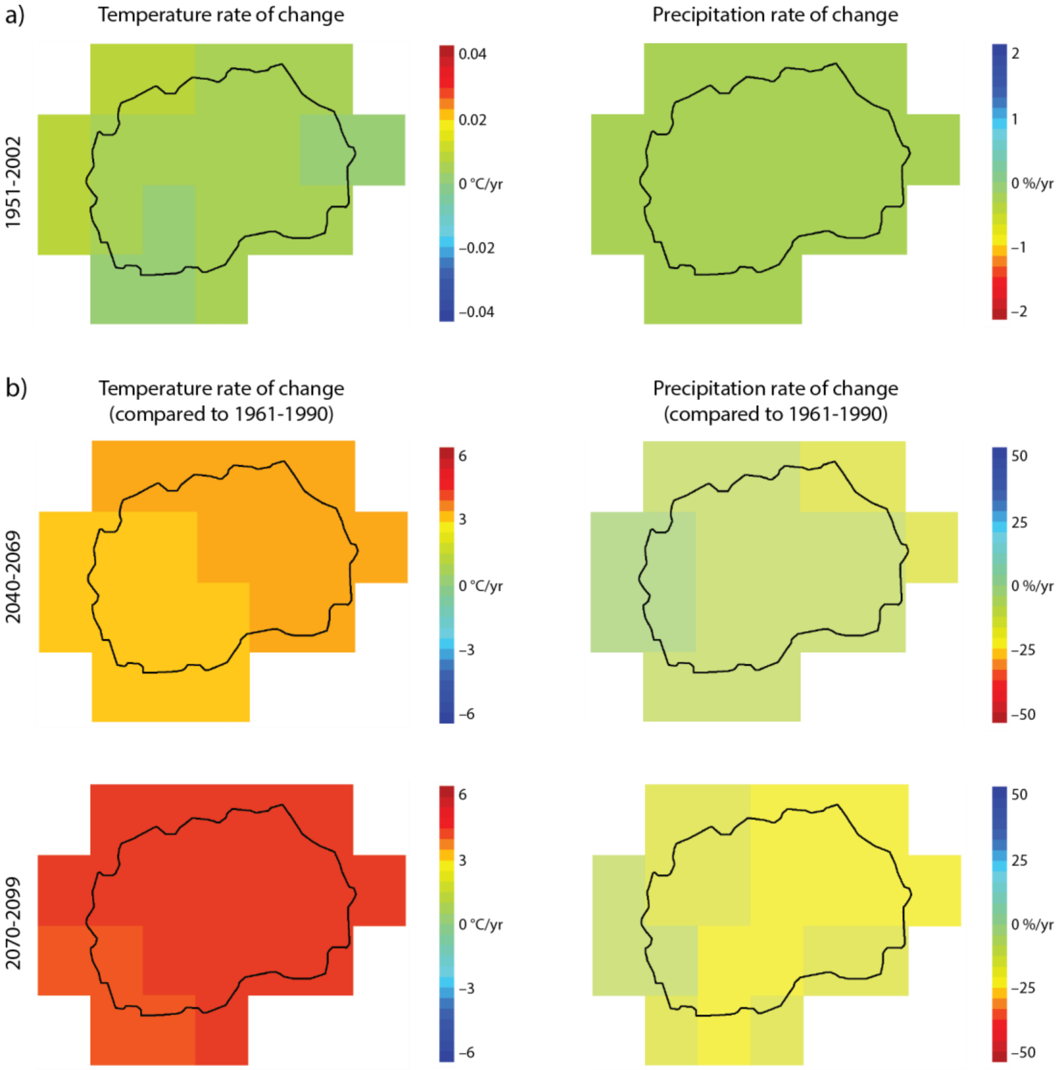

Figure 2.12 *(a) Rates of temperature and precipitation change 1951-2002, and (b) projected (UKMO-HadCM3; SRES A2 scenario) temperature and precipitation change 2040-2069 and 2070-2099 compared to 1961-1990 (maps: CW, 2015).*

2.4 Previous work at Lake Ohrid

2.4.1 Early studies

Lake Ohrid has long been associated with an extraordinary degree of endemic biodiversity and a detailed primary research history is given by Albrecht and Wilke (2008). In summary, some of the earliest work on Ohrid was conducted by two Viennese zoologists, Franz Stein-Dachner and Rudolf Sturany, who first visited the lake in 1891 and reported endemic fish and mollusc species (Steindachner, 1892; Sturany, 1894). A large proportion of the current knowledge of Ohrid and its basin rests on exploratory geological, geomorphological and limnological investigations by Jovan Cvijić (1865-1927; e.g. Cvijić, 1906, 1911). However, systematic research on endemic faunas only began following the end of World War I and with the opening of the Hydrobiological Station Ohrid by Sinisa Stankovic (1892-1974) in 1935, which published its own periodicals giving rise to a plethora of scientific studies. The findings from these early studies on Lake Ohrid are collated within the extensive monograph by Stankovic (1960). After a period of regional political instability, rejuvenated scientific interest over the past two decades has led to a substantial advance in research in multiple fields, including limnology and hydrology (Anovski et al., 1991; Spirkovski et al., 2001; Matzinger et al., 2006a; Matzinger et al., 2006b; Popovska and Bonacci, 2007), geology and tectonics (Dumurdzanov et al., 2004; Dumurdzanov et al., 2005; Hoffmann et al., 2010; Reicherter et al., 2011), biodiversity and evolution (Albrecht and Wilke, 2008 and references therein), and environmental conservation and anthropogenic impacts (Watzin et al., 2002; Matzinger et al., 2007; Kostoski et al., 2010).

2.4.2 Sedimentary records

There have been several sedimentary cores recovered from Lake Ohrid since 1973 (Figure 2.13; e.g. Roelofs and Kilham, 1983; Wagner et al., 2009a; Lézine et al., 2010; Vogel et al., 2010a), which are up to 15 m long and span the past 140,000 years (with hiatuses). Several shorter cores have also been taken from marginal locations specifically to study features such as lake level fluctuations and faunal changes (e.g. Albrecht et al., 2010; Lindhorst et al., 2010). These sequences provide information on climate, environmental and geological changes over the last glacial-interglacial cycle utilising a variety of different proxies (Table 2.2), and highlight the potential of Lake Ohrid for longer-term reconstructions.

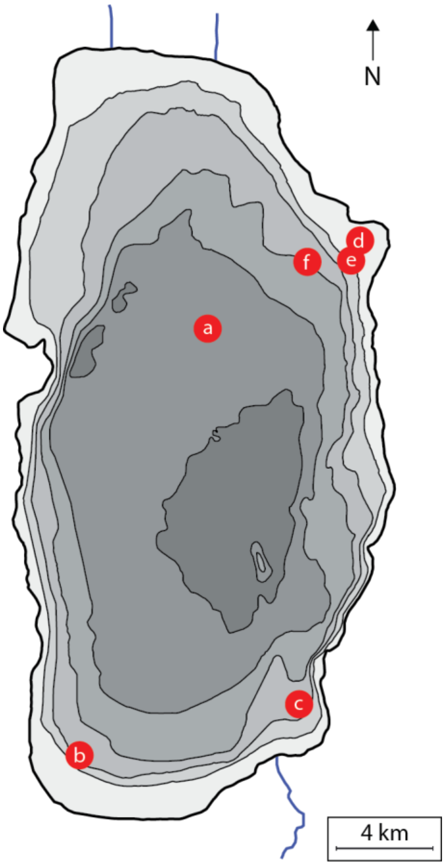

Figure 2.13 *Map of Lake Ohrid bathymetry (50 m isolines) showing drill sites for cores (a) Core 9, (b) Jo2004-1, (c) Lz1120, (d) Co1200, (e) Co1201, and (f) Co1202 (map: Vogel et al., 2010a).*

The first long sediment sequence recovered from Lake Ohrid in 1973 (Core 9) was investigated for water, organic, $CaCO_3$ and diatom content (Roelofs and Kilham, 1983), however inconsistencies with the age model (extrapolated using linear regression to 30 ka) complicate the interpretation of the proxy record. Subsequently, eight near-surface sediment samples (up to 120 cm depth) were taken between 2002 and 2005 and analysed for physical properties, grain size and biogeochemistry, alongside a shallow hydro-acoustic seismic survey comprising over 280 km of sub-bottom profiles (Wagner et al., 2008a). Further coring sites (Lz1120, Co1202, JO2004-1; Figure 2.13) were selected based on the hydro-acoustic data, at locations where parallel reflectors and planar bedding indicated undisturbed sediment successions to be present (Belmecheri et al., 2009; Wagner et al., 2009a; Vogel et al., 2010a). Multiple sediment cores have also been recovered from nearby Lake Prespa (Co1204, Co1215; Wagner et al., 2010; Wagner et al., 2012a), which affords the opportunity to study contemporaneous changes in hydrology and chemistry between the two lakes (Wagner and Wilke, 2011). The results from previous cores and seismic investigations indicate that Lake Ohrid (and Lake Prespa) contains an extensive sediment sequence that documents both long and short term climate and environmental change since the penultimate glacial stage.

Table 2.1 *Previous sedimentary records from Lake Ohrid (coring locations are shown in Figure 2.14).*

Core	Length (m)	Age (ka)	Analyses	Reference
Core9 (a; 1973)	8.85	30	Diatoms, biogeochemistry	(Roelofs and Kilham, 1983)
Jo2004-1 (b; 2004)	10.00	140	Ostracods, pollen, tephra, biogenic isotopes, XRD, Mag-Sus	(Belmecheri et al., 2009; Belmecheri et al., 2010; Caron et al., 2010; Lézine et al., 2010)
Lz1120 (c; 2005)	10.75	40	Geophysical, granulometric, biogeochemistry, bulk isotopes, diatoms, ostracods, pollen, biomarkers, FTIRS	(Vogel et al., 2008; Wagner et al., 2008b; Wagner et al., 2009a; Holtvoeth et al., 2010; Leng et al., 2010a; Sulpizio et al., 2010b)
Co1200 (d; 2007)	2.60	130	XRF, biogeochemistry, tephra, mollusc shells	(Albrecht et al., 2010; Lindhorst et al., 2010)
Co1201 (e; 2007)	6.00	140	XRF, biogeochemistry, tephra	(Lindhorst et al., 2010)
Co1202 (f; 2007)	14.94	136	Biogeochemistry, bulk isotopes, XRF, granulometric, tephra, FTIRS, diatoms, biomarkers	(Holtvoeth et al., 2010; Leng et al., 2010a; Reed et al., 2010; Sulpizio et al., 2010b; Vogel et al., 2010a; Vogel et al., 2010c; Wagner et al., 2010)

Holocene and interglacial sediments are characterised by high carbonate, organic matter and diatom content, and low clastic detritus (Wagner et al., 2009a; Leng et al., 2010a), concomitant with a dense catchment vegetation dominated by deciduous trees (Figure 2.14; Panagiotopoulos et al., 2014), overall implying higher temperatures and moisture availability. Abrupt variations in the biogeochemical composition of interglacial sediments are most likely related to climatically-induced changes in aquatic productivity and hydrology (Vogel et al., 2010a).

Conversely, glacial sediments contain negligible carbonate and organic matter, and variable amounts of coarse silt to fine sand grade clastic material (Vogel et al., 2010a). Catchment vegetation during glacial periods was distinguished by steppe taxa and pine-dominated open landscapes, indicative of colder conditions and lower moisture availability (Panagiotopoulos et al., 2014). The lake experienced greater mixing and water column oxygenation related to increased wind activity and changes in catchment dynamics (Wagner et al., 2009a; Vogel et al., 2010a).

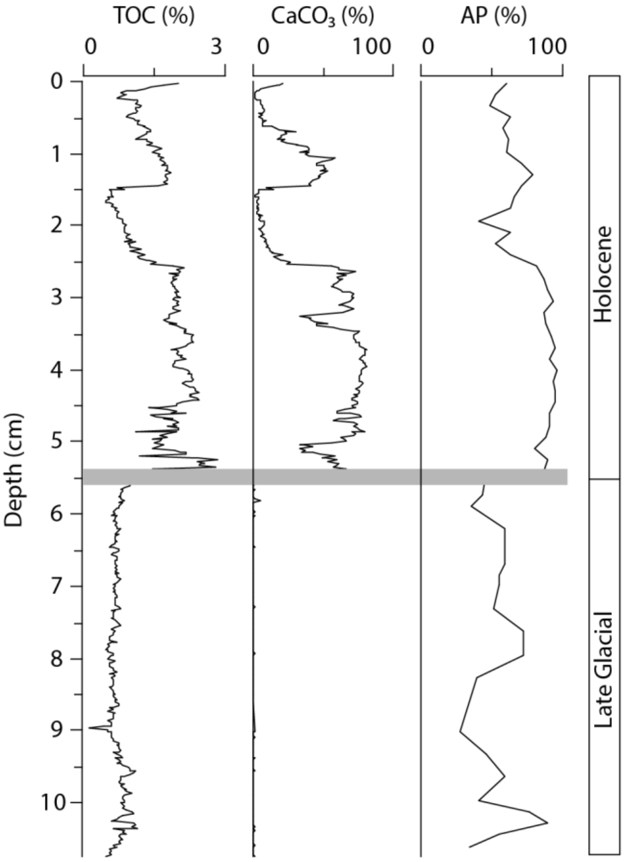

Figure 2.14 *Geochemical and pollen data from Lake Ohrid core Lz1120 (Wagner et al., 2009a), including TOC, $CaCO_3$ and arboreal pollen (AP) percentage. Grey band indicates hiatus.*

In addition to recording a longer-term signature of climate change, short-term and rapid events are also documented in both Pleistocene and Holocene sediments. During the Last Glacial, maxima in the concentration of fine-sand sized material and Cr-Zr/Ti ratios along with minima in arboreal pollen are tentatively correlated to North Atlantic Heinrich events inferring cold, dry conditions and increased aeolian activity driving enhanced lake water mixing (Wagner et al., 2009a; Vogel et al., 2010a; Wagner et al., 2010). Rapid climate shifts during the Holocene are also observed and mark the impact of the 8.2 ka and 4.2 ka events (ca. 5.1 m and 3.5 m in Lz1120, respectively), and the Medieval Warm Period and Little Ice Age (Wagner et al., 2009a; Holtvoeth et al., 2010).

To aid dating of these sedimentary sequences multiple cores from Lake Ohrid have been examined for tephra layers and cryptotephra to produce a regional tephrostratigraphic framework (Wagner et al., 2008b; Sulpizio et al., 2010b; Vogel et al., 2010c). Cores were found to contain up to 12 tephra layers and cryptotephra indicating Ohrid to be a distal archive of Italian volcanic activity and ash dispersal (Figure 2.15), allowing for the construction of robust chronologies through cross-correlation of geochemical fingerprints (e.g. Caron et al., 2010; Sulpizio et al., 2010b; Vogel et al., 2010c). The framework includes one tephra from the Middle Pleistocene at 131 ka (P-11), seven from the Upper Pleistocene between 107 and 30 ka (X-6, X-5, C-20, Y-6, Y-5, Taurano and Y-3) and three from the Holocene (Mercato, FL and AD 472/512) (Sulpizio et al., 2010b).

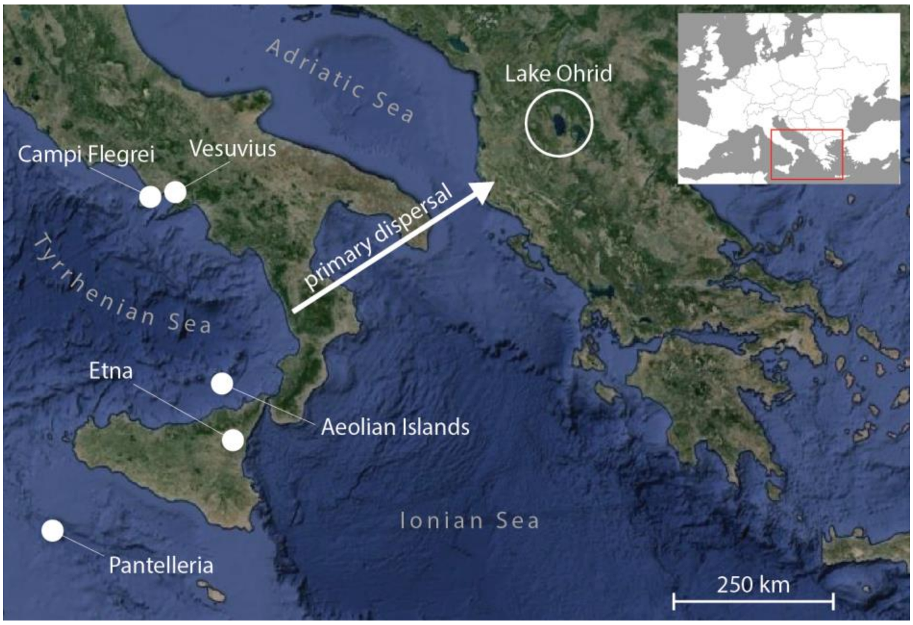

Figure 2.15 *Location map of major Quaternary Italian volcanoes (modified from Giaccio et al., 2008).*

2.5 Summary

Lake Ohrid is a transboundary lake on the Balkan Peninsula formed within a Neogene tectonic graben that is still seismically active today. The lake has a large water volume and long residence time, and receives a proportion of its water input from neighbouring Lake Prespa through a network of karst aquifers.

The Balkan Peninsula is located at the confluence between humid European and dry African climates, providing a complex and seasonal climatology influenced by the sub-tropical anticyclone in summer and mid-latitude westerlies during winter. Over the past half century precipitation and temperature have decreased and increased respectively, and climate models identify the Mediterranean region as a prominent hot-spot for substantial climate change over the next 100 years.

Results from previous work indicate Lake Ohrid to be highly sensitive to global-scale climatic and environmental changes over the last glacial-interglacial cycle, proving its potential for longer-term reconstructions and confirming the lake to be a world class site for the application of stable isotope techniques to recover an extended palaeoclimate record through the Quaternary.

CHAPTER 3 | THEORETICAL FRAMEWORK

3.1 Stable isotopes in palaeoenvironmental research

Stable isotope techniques have long been applied to lake systems to characterise the impact of environmental change (e.g. using authigenic carbonates; Stuiver, 1970; Fritz et al., 1975; Eicher and Siegenthaler, 1976), and are an essential proxy in palaeolimnology to identify the effects of global climate change (as reviewed by Ito, 2001; Schwalb, 2003; Leng and Marshall, 2004). Stable isotope records from lacustrine carbonates are now widely available (at least for the current interglacial), and have been used to not only reconstruct local climate and hydrology (e.g. Rosqvist et al., 2007; Zanchetta et al., 2007a), but also give spatial context to environmental change by assessing regional datasets (e.g. Roberts et al., 2008; Roberts et al., 2011b; Magny et al., 2013). However, as the physical and chemical composition of lake sediments is controlled by a wide range of both internal and external variables (Cohen, 2003), it is important to understand these processes to determine the significance of changes in the isotope composition of carbonate for palaeoclimate reconstructions. Further, additional information on the influence of climate change can be acquired by integrating isotope data with other lines of multi-proxy evidence (Schwalb, 2003), such as organic geochemistry. This chapter will therefore review stable isotope systematics and controls on the composition of lacustrine deposits.

3.2 Theory, notation and standards

A chemical element contains a characteristic number of protons that determines its place in the periodic table; however, different forms of the same element can occur when their nuclei comprise different numbers of neutrons (an isotope). This will impart a new atomic weight to the isotope as neutrons have a mass of 1.6749×10^{-27} kg, which, can produce significant differences in behaviour during chemical, physical and biological processes in nature (Bowen, 1991). The resultant effects are generally associated with a partitioning (fractionation) of isotopes (Hoefs, 1980), which can be produced during isotope exchange reactions, a form of chemical equilibrium where the net concentration of reactants and products remains constant with time, or by kinetic processes that separate isotopes during unidirectional reactions (Hoefs, 2009).

Measureable fractionations are produced by lighter elements as the relative mass difference between individual isotopes is large, and when combined with higher abundances in hydrological, geological and biological systems, certain elements (e.g. H, C, N, O, and S) are more integral for use as environmental tracers (Clark and Fritz, 1997).

Stable isotope (i.e. non-radioactive) abundances are measured from the gaseous phase of a substance on a mass spectrometer as the apparent ratio of the two most abundant isotopes of an individual element (Clark and Fritz, 1997). Typically in a lacustrine environment this may include $^{2}H/^{1}H$, $^{13}C/^{12}C$, $^{15}N/^{14}N$, and $^{18}O/^{16}O$, depending on the constitution of the deposit (Leng et al., 2006). The apparent (or relative) isotope ratio of a sample is substituted in place of the true (or absolute) ratio as the concentration variation imparted by fractionation is small; hence a higher precision can be gained from the relative variation in isotope abundance whilst utilising more straightforward analytical techniques (Clark and Fritz, 1997). The isotope ratio of a measured sample (R_{sample}) is compared to a known laboratory reference calibrated to an international standard ($R_{standard}$) and reported as the relative difference between the sample and standard (δ) in parts per mille (‰; Equation 3.1).

The relative difference is termed to be ‘positive’ or ‘heavier’ when R_{sample} is greater than $R_{standard}$, and termed ‘negative’ or ‘lighter’ when less. The global standard used as a benchmark for the isotope composition of water samples (H and O) is Vienna Standard Mean Ocean Water (VSMOW) and for the isotope composition of carbonate and organic matter (C) is Vienna Pee Dee Belemnite (VPDB).

$$\delta_{sample}\ (‰) = \frac{R_{sample} - R_{standard}}{R_{standard}} \times 1000 \tag{3.1}$$

3.3 Stable isotopes in lake sediments

3.3.1 Controls on $\delta^{18}O$ in lake water

The oxygen isotope composition of lake water ($\delta^{18}O_{lakewater}$) is determined by 1) the isotope composition of the precipitation received by the lake ($\delta^{18}O_{precipitation}$), and 2) any subsequent modification to the signal by catchment and intra-lake processes that are typically dependent on hydrology (Leng and Marshall, 2004). In lake systems with a natural outflow and short residence time (i.e. hydrologically open lakes) changes in the isotope composition of lake water will principally be driven by variations in $\delta^{18}O_{precipitation}$, which in turn is a function of several extra-lake controls at both regional (e.g. temperature, source, continentality) and local (e.g. altitude, amount, seasonality) scales.

The inceptive forcing on $\delta^{18}O_{precipitation}$ occurs at the moisture source, which is generally the oceans (the largest water reservoir on Earth) as the main supplier of atmospheric moisture (Cohen, 2003). At this initial stage the main regulators of $\delta^{18}O_{precipitation}$ are the isotope composition of surface water, temperature, relative humidity, and wind regime, where evaporation results in the ocean source becoming isotopically enriched and the resultant vapour depleted (Clark and Fritz, 1997; Darling et al., 2006). Following this primary fractionation, further depletion occurs during moisture transport due to partial condensation (‘rainout’) and the loss of heavier water molecules ($^{1}H^{2}H^{16}O$ and $^{1}H^{1}H^{18}O$) through a Rayleigh-type distillation process. As an air mass cools its moisture carrying capacity is reduced and water vapour will condense to maintain equilibrium conditions (Clark and Fritz, 1997). Precipitation in higher latitudes therefore tends to have a more negative isotope composition and an increasingly steep $\delta^{18}O$-temperature gradient as the area is both colder and towards the end of the ‘rainout’ process. The mean isotope-temperature gradient is reported to be approximately 0.2 to 0.7‰/°C (outside of the tropics), and have an average coefficient over mid- and high-latitudes of around 0.6‰/°C (Dansgaard, 1964; Rozanski et al., 1992, 1993). The continentality and altitude of a site will also broadly correlate with $\delta^{18}O_{precipitation}$ as the fractionation is temperature-dependent, so that precipitation becomes lighter with increasing distance from the coast and at higher altitudes (e.g. Bowen and Wilkinson, 2002). Continental sites can also experience large seasonal variations in temperature, which will consequently produce a greater annual range of $\delta^{18}O_{precipitation}$ (Clark and Fritz, 1997).

Following condensation a raindrop will continually re-equilibrate with surrounding moisture as it moves towards the surface, and so have a final isotope composition reflecting that of near-ground water vapour (Darling et al., 2006). In certain regions this can lead to an ‘amount’ effect, first recognised by Dansgaard (1964), which describes the strong inverse relationship between $\delta^{18}O_{precipitation}$ and the amount of precipitation. If precipitation is low and a dry air column persists then rainfall can be subject to kinetic fractionation and lose moisture through evaporation before reaching the ground. Conversely, higher amounts of rainfall can have an opposing effect and cause atmospheric moisture to take on a more negative value and preserve low $\delta^{18}O$ (the in-cloud signature) at ground level (Rozanski et al., 1993).

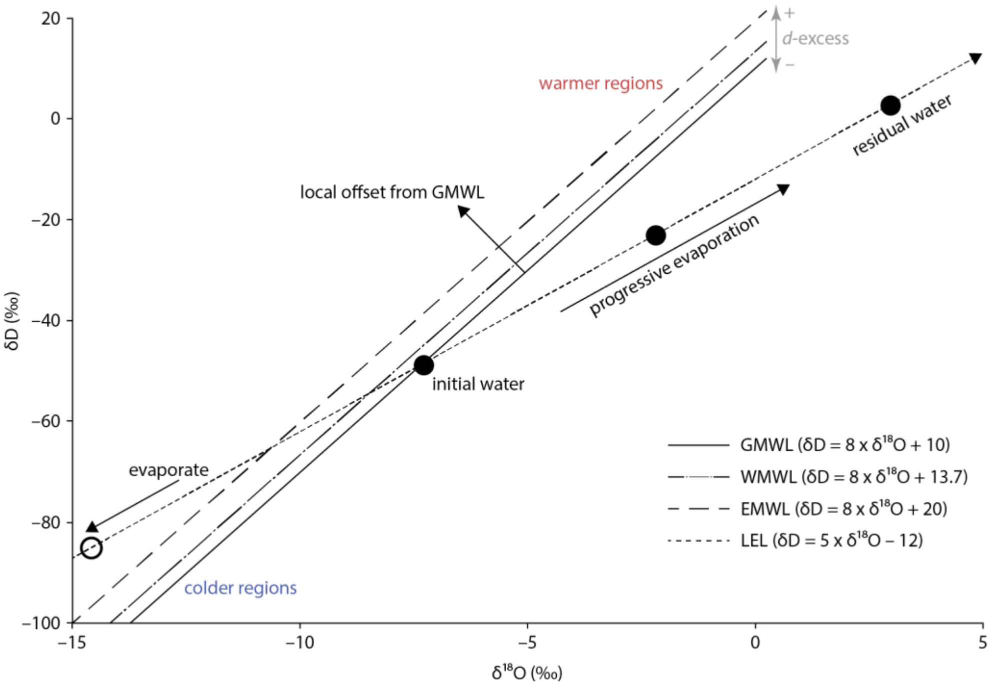

Figure 3.1 *The global meteoric water line (GMWL) is offset from local meteoric water lines (LWML), including western and eastern Mediterranean meteoric water lines (WMWL, EMWL), and a hypothetical local evaporation line (LEL) showing the evolution of an evaporating body of water (modified from Leng and Marshall, 2004; Jasechko et al., 2014).*

Empirical evidence demonstrates that $\delta^{18}O$ and δD are closely correlated on a global scale and define a GMWL (Equation 3.2; Craig, 1961). However, the isotope composition of precipitation significantly varies at a local scale producing a region-specific LMWL. Local changes in the ratio of equilibrium fractionation factors for ^{18}O and ^{2}H determine the variance in gradient from the GMWL (evaporation <8, condensation >8) and intercept values are driven by modification to primary evaporation in moisture source areas (Dansgaard, 1964). For example, the observed meteoric water lines for the western Mediterranean (WMWL, Equation 3.3; Celle-Jeanton et al., 2004) and average eastern Mediterranean (EMWL, Equation 3.4;

Dotsika et al., 2010, and references therein) have similar gradients but a different intercept, indicative of precipitation formation under different equilibrium conditions. As well as being influenced by global, regional and local factors, further alteration to the isotope composition of waters can take place after being incorporated into a lacustrine system.

$$\delta D = (8 \times \delta^{18}O) + 10 \quad (GMWL) \tag{3.2}$$

$$\delta D = (8 \times \delta^{18}O) + 13.7 \quad (WMWL) \tag{3.3}$$

$$\delta D = (8 \times \delta^{18}O) + 20 \quad (EMWL) \tag{3.4}$$

Following transfer to a lacustrine system any subsequent modification to the isotope composition of precipitation is typically driven by evaporative enrichment, although contributions from surface and groundwater inputs may also have an effect, and the degree of evaporative influence is strongly associated with lake hydrology (Cohen, 2003).

In open-basin, short residence time lakes this influence is generally negligible, and the isotope composition of lake water will predominantly reflect that of the meteoric precipitation received by the lake and plot on (or near to) the LMWL (Leng et al., 2006). Open lakes with very short residence times (typically smaller lakes) may not reflect mean annual precipitation and will instead respond to seasonal changes in the isotope composition of precipitation (Leng and Marshall, 2004). Summer and winter rainfall, each having a characteristic isotope composition, can also be homogenised in well-mixed open lakes if the residence time exceeds 1 year and thereby dampen the amplitude of any seasonal signal. However, overall lake size notwithstanding, if lake water becomes stratified during summer months the isotope composition of surface waters may reflect summer rainfall rather than the annual average (Leng et al., 2006), as there will be little exchange between the epilimnion and hypolimnion (Stuiver, 1970). Alternatively, surface waters may reflect winter precipitation if a density contrast exists between lake water and spring snowmelt facilitating the formation of a freshwater lid (Dean et al., 2013).

In closed-basin (or terminal) lakes, particularly those in dry or low latitude regions with long residence times, evaporation can have a much greater impact on the isotope composition of lake water (Leng and Marshall, 2004). In these settings $\delta^{18}O_{lakewater}$ is primarily dependent on the balance between hydrological inputs and outputs (Leng et al., 2006) and any primary fractionation influence (e.g. temperature, source) is generally only of secondary importance and can be masked by evaporative concentration and residence-related effects (Talbot, 1990, and references therein). Evaporation is a kinetic fractionation that depends on the transitional velocity of different isotopes, which acts to remove lighter oxygen (^{16}O) at a rate controlled by wind speed, relative humidity and temperature (Ito, 2001), resulting in elevated $\delta^{18}O_{lakewater}$ above that of background precipitation (Leng et al., 2006, and references therein). The amount of evaporative influence is therefore dependent on the residence time of a lake, as the longer a standing body of water remains in place, the greater exposure it has to evaporation and so there is a higher potential for fractionation. In this situation lake water is offset from its initial composition (GMWL/LMWL), and progresses along a LEL where the residual water composition is determined by the extent of evaporation and isotope value of the evaporating water (Figure 3.1). Where residence time extends over tens to hundreds of years, lake water can become homogenised to the extent that short-term changes in either climate or hydrology have little effect and the overall evaporated (^{18}O-enriched) signal becomes buffered to high frequency variations (see further discussion in Chapter 5; Leng et al., 2006).

3.3.2 *Controls on $\delta^{18}O$ in lake carbonates*

Lake sediments comprise different fractions incorporating autochthonous and allochthonous components, where the carbonate fraction may consist of primary (authigenic or endogenic) and biogenic mineral precipitates, detrital grains or the products of diagenesis (Ito, 2001). It is therefore vital to discriminate between primary and detrital components as a prerequisite to isotope analysis, to ensure accurate information on palaeoclimate can be ascertained (Leng et al., 2010b). Further, it is also important to assess the mineralogy of a sample as there are a number of types of carbonate that precipitate in lakes (e.g. calcite, aragonite, dolomite, siderite, mostly dependent on lake water chemistry), which have different mineral-water fractionations (Leng et al., 2006, and references therein) and may form under different environmental conditions (Leng et al., 2013). Endogenic carbonate precipitation in the water column is generally concomitant with maximum phytoplankton activity due to the photosynthetic uptake of dissolved CO_2 or can also be associated with the evaporative removal of CO_2 (Ito, 2001), both of which will drive calcium carbonate ($CaCO_3$) supersaturation in the water column (Leng and Marshall, 2004). If additional CO_2 is incorporated into the system, primarily by means of respiration and decomposition of organic matter, the reaction is reversed causing $CaCO_3$ dissolution; the formation or removal of $CaCO_3$ is therefore directly driven by the availability of CO_2 (Figure 3.2; Cohen, 2003).

The isotope composition of a carbonate mineral precipitated under thermodynamic equilibrium is exclusively controlled by the temperature and isotope composition of the lake water in which it formed (Figure 3.3; Leng and Marshall, 2004). The controls on lake water have been discussed in section 3.4, however a temperature-dependent fractionation during precipitation must also be considered.

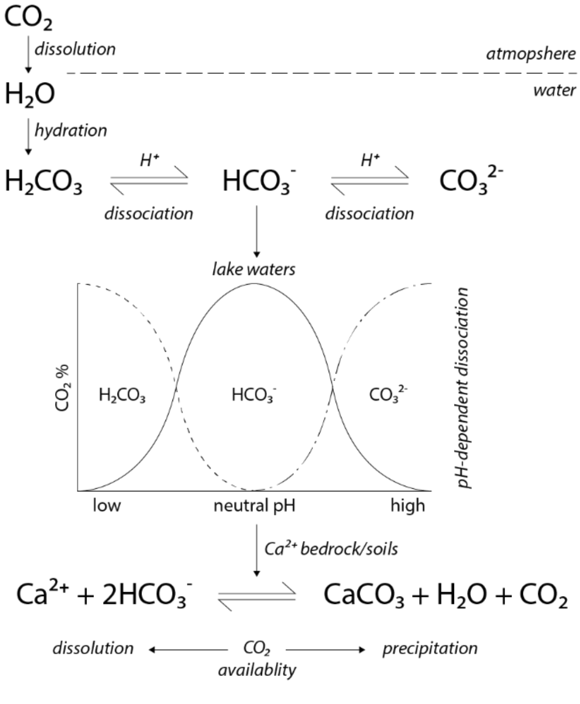

Figure 3.2 *Inorganic carbon in a lake system and the formation of calcium carbonate (after Wetzel, 1983; Cohen, 2003). Dissolved inorganic carbon (DIC) hydrates to form carbonic acid (low pH) and depending on pH will dissociate to form bicarbonate (neutral pH) or carbonate (high pH). When* CO_2 *is lost (biological assimilation or degassing) calcium carbonate will precipitate to re-establish equilibrium through the formation of* CO_2*.*

Elevated temperatures lead to a decreased fractionation between lake water and mineral due to higher associated energy states, where for carbonates precipitated in equilibrium a decrease of −0.24‰ is observed for every 1°C increase in temperature (Stuiver, 1970). However, this fractionation will be inconstant if the reaction does not take place under equilibrium conditions. Common disequilibrium effects (or vital effects for biogenic carbonates) in lacustrine environments include variations in precipitation rate, pH changes, and growth in microenvironments (Leng and Marshall, 2004).

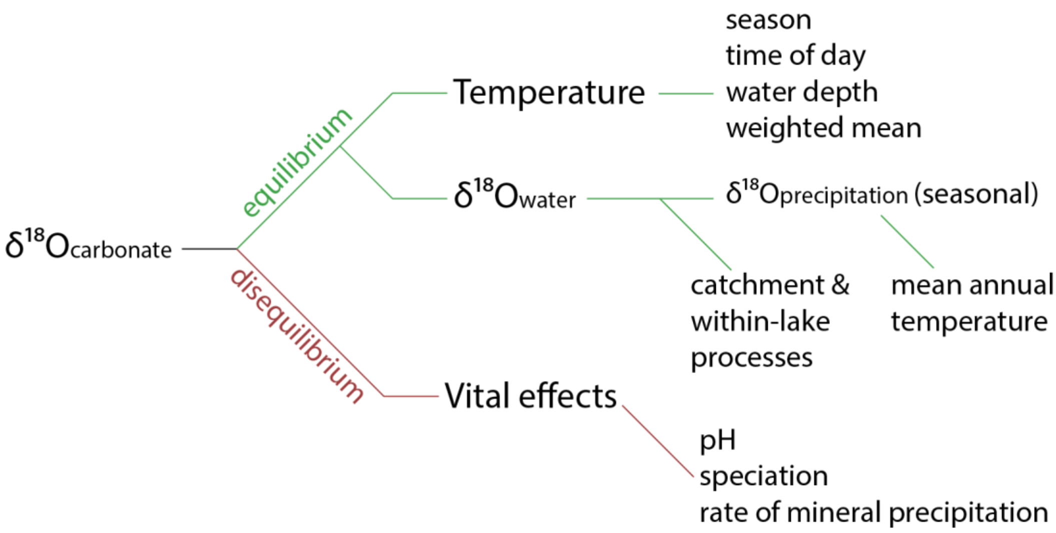

Figure 3.3 *Controls on $\delta^{18}O$ in lake carbonates (modified from Leng and Marshall, 2004).*

If a carbonate mineral forms under isotope equilibrium, the fractionation of oxygen is dependent on temperature and the relationship can be defined empirically using fractionation (or palaeotemperature) equations. Although several fractionation relationships and palaeotemperature equations have been derived (e.g. Epstein et al., 1953; Craig, 1965; O’Neil et al., 1969), the most precise associations have been generated through laboratory experiments for individual carbonate mineralogies, such as that proposed by Kim and O'Neil (1997) for calcite (Equation 3.5). In this equation temperature (T) is measured in Kelvin (i.e. °C + 273.18) and α is the mineral-water fractionation (i.e. $[^{18}O/^{16}O]_{calcite}/[^{18}O/^{16}O]_{lakewater}$).

$$1000 \ln \alpha_{(calcite-water)} = 18.03(10^3 T^{-1}) - 32.42 \tag{3.5}$$

Equation 3.5 has been reexpressed in a more practical form by Leng and Marshall (2004), so that δc represents $\delta^{18}O_{PDB}$ of the carbonate and δw is $\delta^{18}O_{SMOW}$ of the lake water (Equation 3.6).

$$T°C = 13.8 - 4.58(\delta c - \delta w) + 0.08(\delta c - \delta w)^2 \tag{3.6}$$

In freshwater environments calcite is normally precipitated, however under more evaporated conditions other types of carbonate may form (e.g. aragonite and dolomite) that have different mineral-water fractionation factors altering the resultant carbonate isotope composition. For example, aragonite and dolomite precipitated at equilibrium have a positive fractionation with respect to calcite of +0.8‰ and +2.6‰ (Vasconcelos et al., 2005; Kim et al., 2007). If analysing bulk sediment it is therefore important to constrain what carbonate mineralogies are present to ensure that stratigraphic variations in isotope composition are truly a product of environmental change, rather than fluctuations in the relative abundance of individual sediment components (e.g. Dean et al., 2015).

If it can be shown that a systematic relationship is present between temperature and the mineral-water isotope compositions in the modern environment, and assuming equilibrium precipitation occurs, oxygen isotope data can be quantitatively interpreted in terms of palaeotemperature. There are two temperature effects to consider, the first is imparted by the isotope-temperature gradient during precipitation (+0.6‰/°C; section 3.3.1) and secondly the carbonate-water fractionation (−0.24‰/°C; discussed above). If a lake is controlled by $\delta^{18}O_{precipitation}$, any change imparted by the isotope composition of precipitation will be opposed by the mineral-water fractionation to produce an overall covariance of +0.36‰/°C (after Eicher and Siegenthaler, 1976; Leng and Marshall, 2004). However, although a temperature-dependent fractionation may well be present, it is a magnitude smaller than that imparted through evaporative processes (potentially >10‰; e.g. Leng et al., 1999; Eastwood et al., 2007), and so has lesser significance for short residence time, closed-basin lakes.

3.3.3 Controls on $\delta^{13}C$ in lake carbonates

When carbonates precipitate, as with $\delta^{18}O$, they also capture $\delta^{13}C$ of the dissolved inorganic carbonate of the lake water in which they form. The total dissolved inorganic carbon (TDIC) can for most lakes (neutral pH) be approximated to HCO_3^-. There is only a small offset between TDIC and carbonate mineral during equilibrium precipitation, for example $\delta^{13}C_{calcite}$ is only 1‰ more positive than $\delta^{13}C_{TDIC}$ at 16°C (Romanek et al., 1992), and hence in lake sediment records $\delta^{13}C_{calcite}$ can provide information on past variations in $\delta^{13}C_{TDIC}$ and associated carbon-cycle transitions (Leng and Marshall, 2004). Unlike $\delta^{18}O$, there are multiple reservoirs that can contribute to the overall carbon budget of a lake (Figure 3.4), and the complexity of carbon pathways does not allow for simple assumptions regarding fractionation to be made (Cohen, 2003).

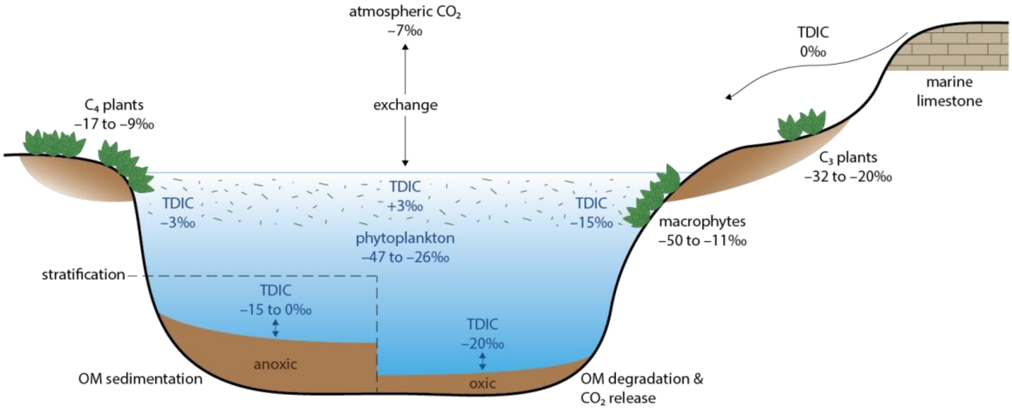

Figure 3.4 *Major sources of lacustrine carbon and respective $\delta^{13}C$ values, the resultant $\delta^{13}C_{TDIC}$ is also indicated (after Leng and Marshall, 2004).*

In aquatic environments $\delta^{13}C_{TDIC}$ is controlled by several factors including the isotope composition of inflowing waters and by two important fractionation effects: 1) the chemical exchange between atmospheric CO_2 and dissolved HCO_3^- leading to higher $\delta^{13}C$ in the bicarbonate, and 2) kinetic processes during the non-equilibrium metabolic reduction of carbon that partitions ^{12}C into the resultant organic matter (lower $\delta^{13}C$; Hoefs, 1980; McKenzie, 1985).

Inflowing waters can provide a significant proportion of a lake's carbon budget, and this carbon may originate from multiple sources. Ground and river waters typically have low $\delta^{13}C_{TDIC}$, as they contain a large amount of isotopically light carbon liberated during the decay of organic matter. When organisms utilise atmospheric CO_2 during photosythesis, a substantial carbon fractionation occurs through the diffusion, carboxylation, and subsequent conversion of CO_2 to carbohydrate, resulting in 5 to 25‰ lower $\delta^{13}C$ (Clark and Fritz, 1997). The extent of carbon fractionation depends on the photosynthetic pathway followed, which may be through the C_3 (Calvin), C_4 (Hatch-Slack) or CAM (Crassulacean acid metabolism) cycle. Terrestrial ecosystems are generally dominated by C_3 plants that typically have average $\delta^{13}C \approx -27‰$ (range = −32 to −20‰; Figure 3.5). In environments characterised by higher temperatures, dry conditions and low CO_2:O_2, C_4 plants are more common that have average $\delta^{13}C \approx -12‰$ (range = −17 to −9‰). CAM plants are normally found in desert regions and comprise an intermediary range of values between those of C_3 and C_4 plants.

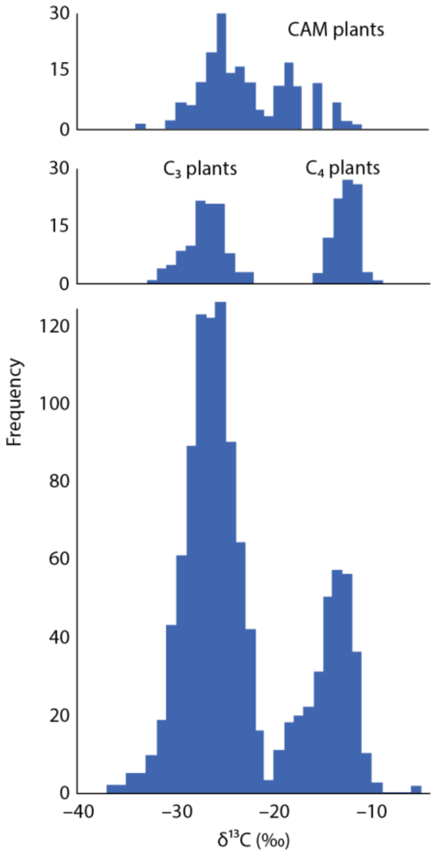

Figure 3.5 *Resultant carbon isotope composition of different photosynthetic pathways (after Deines, 1980, Figure 9.3), showing the values for terrestrial plants (bottom), known C3 and C4 plants (middle) and CAM plants (top).*

Over time deceased organic matter accumulates in soils and isotopically light CO_2 is produced by aerobic bacterial action with a negligible fractionation during decay (Sharp, 2007), following which it is able to enter superficial waters by dissolution. The reaction then follows a similar route as shown in Figure 3.2, where the CO_2 is hydrated to produce carbonic acid that will dissociate to become bicarbonate, carbonate and hydrogen ions. The dominant carbonate species at neutral (≈ 7 to 10) pH is bicarbonate (Figure 3.2), which has a fractionation factor of ≈ +10‰ when in equilibrium with CO_2 gas (Equation 3.7; Mook et al., 1974). Therefore the carbon isotope composition of bicarbonate derived exclusively from C_3 soil CO_2 should have $\delta^{13}C$ between −22‰ and −10‰, and for C_4 soils between −7‰ and +1‰; as mentioned previously, the carbonate precipitated from TDIC would have average values 1‰ higher than this.

$$1000 \ln \alpha^{13}\mathrm{C}_{HCO_3-CO_{2(g)}} = (9.483 \pm 0.22) \times (10^3 T^{-1}) - (23.89 \pm 0.75) \qquad (3.7)$$

If a lake's inflow passes through carbonate (karst) aquifers the local surface and groundwater chemistry will be dominated by Ca^{2+} and HCO_3^- ions (Cohen, 2003), following the enhanced dissolution of the aquifer rocks due to the incorporation of additional CO_2 from soils (Figure 3.2; Clark and Fritz, 1997). Limestones usually comprise ancient marine carbonates that have an average $\delta^{13}C$ of around 0‰ (Hudson, 1977; Jin et al., 2009), and typically range between −3‰ and +3‰ (Andrews et al., 1993; Hammarlund et al., 1997; Leng et al., 1999), meaning subsequent to dissolution more ^{13}C is incorporated into inflowing waters and $\delta^{13}C_{TDIC}$ will be higher.

In certain localities maximum $\delta^{13}C_{TDIC}$ can equal or exceed that of the average $\delta^{13}C$ of catchment geology (e.g. Andrews et al., 1993; Leng et al., 2010a), and other mechanisms are required to produce such isotopically heavy values. One such mechanism can be attributed to isotopic exchange between TDIC and atmospheric CO_2, which is more likely to occur in a standing body of water (i.e. in closed lakes). Experimental data shows that if enough time is available the exchange process will tend toward equilibrium (Usdowski and Hoefs, 1990), and so would not be expected in open lake systems due to their associated shorter residence times. The carbon isotope composition becomes heavier as $^{12}CO_2$ reacts more quickly with water than $^{13}CO_2$, and the fractionation during outgassing leaves the water body with higher $\delta^{13}C$ (Usdowski and Hoefs, 1990). Atmospheric CO_2 has $\delta^{13}C$ ≈ −7‰ (Craig, 1953; Craig and Keeling, 1963), and so equilibrium exchange with lake water will produce aqueous TDIC (HCO_3^-) with $\delta^{13}C$ ≈ +3‰ (Equation 3.7). Therefore higher $\delta^{13}C_{TDIC}$ values may reflect variable degrees of equilibration between atmospheric CO_2 and aqueous HCO_3^- (Andrews et al., 1993).

Evaporative drawdown in closed-basin lakes will also affect the oxygen isotope composition of lake water. The preferential loss of ^{16}O during evaporation can drive extreme ^{18}O-enrichment resulting in covariance between oxygen and carbon isotope values (Talbot, 1990), potentially the product of unidirectional or cyclic transitions between humid and dry climate states (Drummond et al., 1995). The degree of covariance in a closed lake can depend on several factors, including hydrological balance (dilutionary effects), stability of lake volume, vapour exchange and evaporation (Li and Ku, 1997). Ultimately the covariance signal will be recorded in primary lacustrine carbonates and can therefore potentially be used to determine the extent of past hydrological closure (Talbot, 1990). However, when the spatial coherency of lake sediment records is assessed, for example across the Mediterranean, it is found that controls are not temporally consistent between lakes and that for some regions covariance may offer little insight into palaeohydrological closure (Roberts et al., 2008).

In addition to the controls on covariance stated above, the correlation between $\delta^{18}O$ and $\delta^{13}C$ can also be decoupled by post-depositional processes, such as methanogenesis (Leng et al., 1999). The metabolic pathway used by bacteria during the reduction of organic matter strongly favours ^{12}C, which, for isotopic mass balance, produces isotopically light methane and proportionally enriches the bicarbonate ion in ^{13}C up to +35‰ (Equation 3.8; Curry et al., 1997).

$$CH_3COO^- + H_2O \rightarrow CH_4 + HCO_3^- \qquad (3.8)$$

The methane is removed by ebullition or by emission through the stems of aquatic macrophytes, and the enriched bicarbonate is incorporated into TDIC (Curry et al., 1997). Methanogenesis-derived bicarbonate is consequently another potential source for isotopically heavy carbonates that may have $\delta^{13}C$ in excess of +20‰ (Hudson, 1977, Figure 1).

A further mechanism for producing heavier carbon isotope compositions can be related to the effects of increased aquatic productivity. Phytoplankton and other planktonic organisms utilise dissolved CO_2 (or in some cases HCO_3^-, see below) during photosynthesis and preferentially incorporate ^{12}C, thus leaving TDIC isotopically heavy. In winter to early spring $\delta^{13}C_{TDIC}$ will remain generally constant through the water column as photosynthetic activity is low, however in late spring to summer overturn supplies fresh nutrients to surface waters and blooms cause $\delta^{13}C_{TDIC}$ to become significantly enriched with respect to ^{13}C (McKenzie, 1985). Stratification in summer months will drive a vertical isotope gradient with high $\delta^{13}C$ in the epilimnion, in contrast to hypolimnetic low $\delta^{13}C$ due to dissolution of settling particulate organic matter and the subsequent release of ^{12}C (Cohen, 2003). During periods of enhanced photosynthetic activity the CO_2 content of surface waters can be reduced to such an extent that they become supersaturated in calcium carbonate (Figure 3.2), and as there is direct relationship between TDIC and carbonate (+1‰; Romanek et al., 1992), changes to TDIC will be reflected by a comparable shift in the precipitated carbonate mineral. Lake sediment $\delta^{13}C_{calcite}$ stratigraphies are therefore able to provide information on past change in aquatic productivity and the extent of respiration (McKenzie, 1985).

3.4 Organic matter in lake sediments

Organic matter (OM) is a dynamic biogeochemical component of lake sediments that originates from a complex mixture of organic material that primarily originates from organisms that have lived both within a lake and in its surrounding watershed (Meyers and Teranes, 2001). The majority of OM derives from the particulate detritus of plant material, which can be divided into two groups based on its biochemical composition: 1) non-vascular lower plants (e.g. algae) that are nitrogen-rich due to an abundance of proteins and nucleic acids, and 2) vascular higher plants (e.g. grasses, trees) that are lignin- and cellulose-rich but nitrogen-poor (Talbot and Johannessen, 1992; Meyers and Ishiwatari, 1993). In most lakes the autochthonous detritus of single-celled phytoplankton is the dominant source of OM to sediments (Cohen, 2003), however the contribution from land plants can also be important and the interplay between the two sources is strongly influenced by productivity and transport processes (Meyers, 1997).

Only a minor fraction (<10%) of the biosynthesised OM produced escapes remineralisation and degradation to reach the sediment surface, as prior to burial early diagenesis in the photic zone continues during sinking and intensifies through bioturbation within the benthos (Meyers, 1994), hence initial source proportions may not be exported to the sedimentary record (Meyers and Ishiwatari, 1993). Consequently, it is important for palaeoenvironmental reconstructions to know to what degree the composition of sediment OM reflects that of the original source material and to assess the extent of alteration and degradation (Meyers and Teranes, 2001). Specific components of OM are more susceptible to degradation than others, however the bulk parameters C/N and $\delta^{13}C_{organic}$ are thought to retain source information, in spite of the known decreases associated with sedimenting OM (Meyers, 1994).

3.4.1 TOC and C/N

Total organic carbon (TOC) concentration is commonly thought to be proportional to the amount of biomass exported to the sedimentary record, and is influenced by initial productivity rates and subsequent degradation (Cohen, 2003). TOC is expressed as a weight/weight ratio and therefore can be diluted or concentrated by variations in the quantity other sediment components (Meyers and Teranes, 2001).

The source of OM in lake sediments can be partially distinguished by the C/N ratio, which is directly influenced by the presence or absence of cellulose in the original plant material (Figure 3.6; Meyers and Ishiwatari, 1993). Non-vascular algal organic matter typically has low C/N values between 4 and 10, whereas vascular land plants have higher values in excess of 20 due to larger quantities of cellulose (Meyers and Teranes, 2001). A combination of lacustrine and terrestrial sources will commonly produce sediment OM with intermediary values around 13-14 (Meyers and Ishiwatari, 1993). Elemental compositions are readily altered during early diagenesis that may increase or decrease C/N ratios of OM through the selective degradation of carbon- or nitrogen-rich components, however this is generally does not produce a large enough change to override the fundamental differences in original OM source compositions (Meyers, 2003).

In oligotrophic lakes, as OM degrades in sediments C/N ratios frequently decrease with depth due to anaerobic utilisation of organic carbon (lowering TOC), and the release of ammonium (NH_4^+) which can be absorbed by clay minerals (fixed N; Meyers and Lallier-Verges, 1999). This is also observed in soils where the retention of ammonia as a product of OM decomposition and the loss of carbon yields lower

C/N values (Meyers, 1994). Sediment grain size also has a role in determining the C/N ratio of OM, controlled by the type of organic material and mineral composition, where in general C/N is lower in finer sediments. Coarser sediments are able to contain more intact cellulose-rich terrestrial detritus, and finer sediments have a larger proportion of clay minerals to retain ammonia, thus hydrodynamic sorting of sediments can bias source signals and influence C/N (Meyers, 1997).

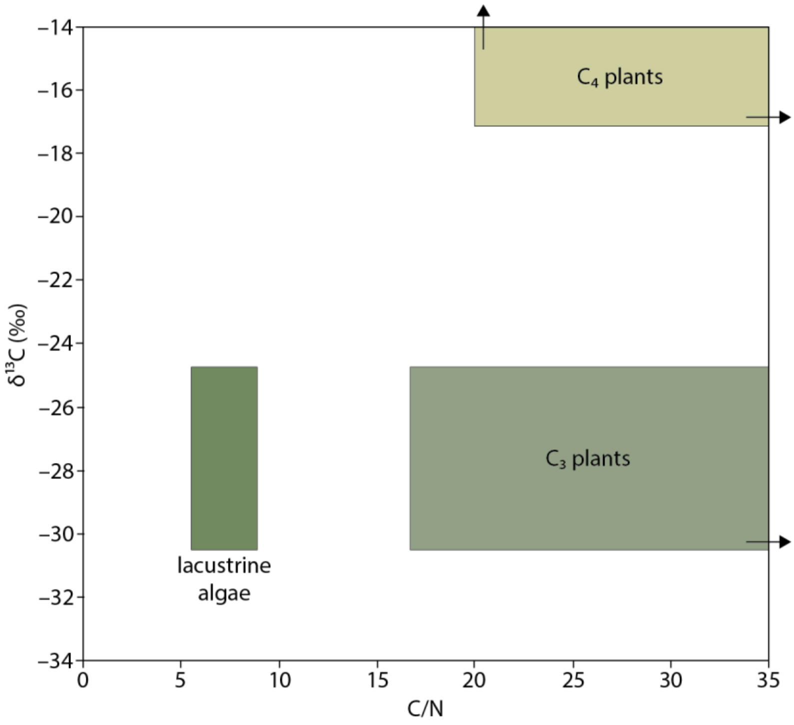

Figure 3.6 *Typical elemental (C/N) and carbon isotope composition ($\delta^{13}C$) ranges of lacustrine organic inputs, including algae, C_3 plants and C_4 plants (after Meyers and Teranes, 2001).*

3.4.2 Organic carbon isotopes

Sources of sediment OM can further be assessed by using $\delta^{13}C_{organic}$, which also can provide information on past productivity rates and reflects the dynamics of fractionation during photosynthesis and the $\delta^{13}C$ of source material (Figure 3.7; Meyers, 1997). The majority of plants fix carbon using the C_3 photosynthetic pathway that strongly fractionates carbon isotopes in favour of ^{12}C producing an approximate −20‰ shift from the inorganic carbon source (Meyers and Ishiwatari, 1993). C4 plants impart a lesser shift between −6‰ and −4‰. For land plants utilising atmospheric CO_2

($\delta^{13}C \approx -7‰$), the resultant OM will therefore roughly have average $\delta^{13}C_{organic} \approx -27‰$ and $-12‰$ for C_3 and C_4 plants, respectively (Figure 3.4).

The phytoplankton OM (C_3 algae) produced within a lake will normally be indistinguishable from that produced by terrestrial plants, if using CO_2 in isotopic equilibrium with the atmosphere (Meyers and Teranes, 2001). However, when there is a severe reduction in total CO_2 concentration in a lake, photosynthetic aquatic organisms may utilise HCO_3^- in its place (Wetzel, 1983). In some organisms this change in metabolism is pH dependent and is likely to be considerably important in lacustrine settings where pH is greater than 8.5 (Talbot and Johannessen, 1992, and references therein). Algal OM produced from assimilation of HCO_3^- will have around 10‰ higher $\delta^{13}C$ compared to its CO_2 equivalent ($\alpha^{13}C_{HCO_3-CO_2}$; Equation 3.7), leading to OM $\delta^{13}C_{organic}$ in the range of C_4 plants (Meyers and Teranes, 2001). Alternately, during periods of enhanced surface run-off (due to higher rainfall, forest clearance for instance) greater delivery of isotopically light soil-derived CO_2 will drive lower $\delta^{13}C_{organic}$ values for algal OM. In addition to the formation of inorganic carbon within a lake, the TDIC pool is also utilised by plants and therefore changes to TDIC can have a significant effect on $\delta^{13}C_{organic}$ (Leng et al., 2006).

As phytoplankton preferentially utilise ^{12}C during photosynthesis, the sedimentation of algal OM exports this carbon and removes it from the surface TDIC pool. Over time newly produced OM will have progressively heavier $\delta^{13}C_{organic}$, assuming the exported carbon is buried and not released. Algal productivity is a primary factor in the determination of sediment $\delta^{13}C_{organic}$ values, as the most common form of lacustrine OM is allochthonous, however pH, nutrient limitation and growth rate will also affect isotope compositions (Meyers and Teranes, 2001).

Although post-burial diagenesis may alter the $\delta^{13}C_{organic}$ of sediment OM, it has been demonstrated that the diagenetic effect is minimal (Hodell and Schelske, 1998), and the effect of selective diagenesis is likely to be <2‰ (Meyers, 1997).

3.4.3 Rock-Eval pyrolysis

Rock-Eval pyrolysis is conventionally associated with determining the hydrocarbon potential of petroleum source rocks (Espitalie et al., 1977), however more recently the technique has been applied in both marine and terrestrial settings to characterise sedimentary OM and differentiate source areas in several palaeoenvironmental studies (e.g. Steinmann et al., 2003; Lojka et al., 2009; Zocatelli et al., 2012; Sebag et al., 2013; Hare et al., 2014). Rock-Eval parameters can be used to indicate the source of OM as different organisms incorporate hydrogen in variable proportions; proteins and lipids (e.g. algal remains) contain abundant hydrogen, whereas cellulose and lignin (e.g. terrestrial plants) contain little hydrogen (Cohen, 2003). Additionally, the concentration of hydrogen in hydrocarbons (organic H-compounds) is influenced by redox conditions in the depositional environment, whereby under anoxic conditions H-abundance is higher as hydrocarbons are commonly volatile when in the presence of oxygen (Cohen, 2003). Rock-Eval datasets can therefore also provide evidence on the geochemical quality and degradation history of sediment OM.

The Rock-Eval procedure involves progressively heating a sediment sample to give a temporal quantification of hydrocarbon release over a given temperature range of typically between 300°C and 650°C (see Section 4.3). Analysis produces several outputs, including S1 (volatile hydrocarbons), S2 (hydrocarbon components produced due to thermal cracking of kerogen), S3 (CO_2 released during pyrolysis), and TOC (pyrolysed + residual organic carbon) (Meyers, 1997). Two parameters that can be derived from S1, S2 and TOC data, the Hydrogen Index (HI) and Oxygen Index (OI) are particularly useful in the interpretation of limnological sediment records. HI represents the hydrocarbons generated as a proportion of the total OM (Equation 3.9), and OI approximately represents the amount of oxygen with respect to total OM (Equation 3.10).

$$Hydrogen\,Index\,(HI) = \frac{S2}{TOC} \times 100 \cong \frac{H}{C} \tag{3.9}$$

$$Oxygen\,Index\,(OI) = \frac{S3}{TOC} \times 100 \cong \frac{O}{C} \tag{3.10}$$

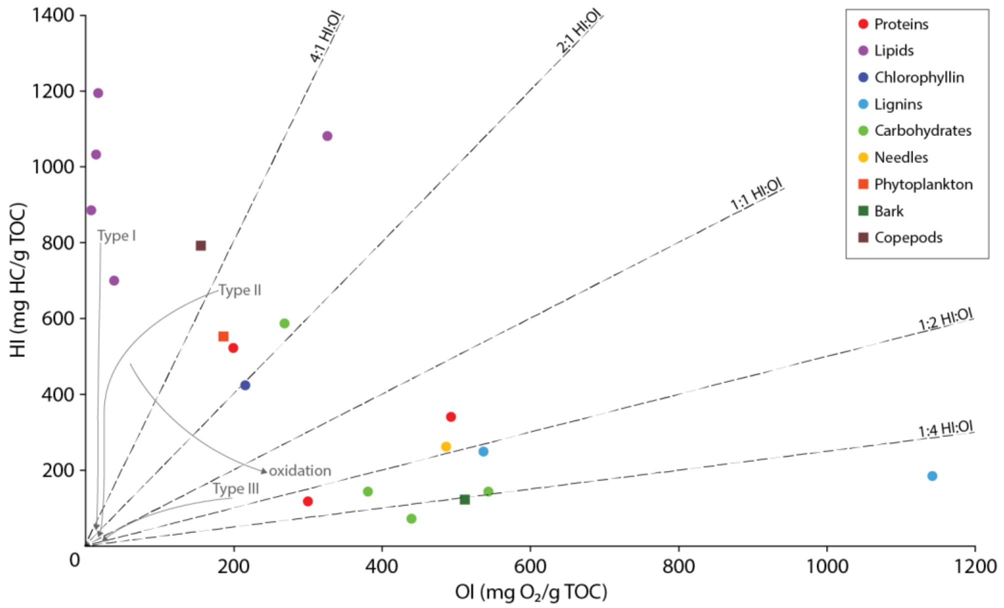

Figure 3.7 *Modified van Krevelen diagram for sedimentary OM, showing HI-OI values derived from chemical and biological standards (Carrie et al., 2012, Table 1a, Figure 4), alteration pathways of Types I, II, and III OM (grey lines; Meyers and Teranes, 2001), and selected HI:OI ratios (dashed lines).*

The parameters HI and OI are normally interpreted as proxies for H/C and O/C, which is advantageous considering the analytical requirement to produce the ratios with actual elemental analysis (Meyers and Teranes, 2001). The fractions comprise several different compounds that reflect the composition and diagenesis of the original OM (Carrie et al., 2012), and to illustrate the origin of hydrocarbon compounds, as well as degradation pathways, modified van Krevelen diagrams (HI vs. OI) can be used that identify three main categories of OM (Figure 3.7).

Type I OM consists of hydrocarbon-rich material that originates from microbial biomass or the waxy coatings of terrestrial plants, Type II OM has moderate concentrations of hydrocarbons that are derived from algae (or a mixed source), and Type III is from carbohydrate-rich, hydrocarbon-poor material commonly associated with vascular woody plant matter (Meyers and Teranes, 2001). When assessing van Krevelen-type plots it is important to consider the effects of degradation, as alteration processes can modify the elemental content of sediment OM. If Type I or II material is oxidised the concentration of hydrocarbons will decrease, whilst oxygen content increases, thus imposing Type III characteristics and obscuring the primary compositional signal (Meyers and Lallier-Verges, 1999).

As TOC is thought to represent the quantity of OM transferred to the sedimentary record, it follows that enhanced aquatic productivity will be traced by a parallel increase in both TOC and HI (S2) due to the incorporation of hydrocarbon-rich algal material. Covariance between these two parameters may therefore be used to indicate variations in primary production and organic deposition across periods of environmental change (Figure 3.8; Meyers, 2003).

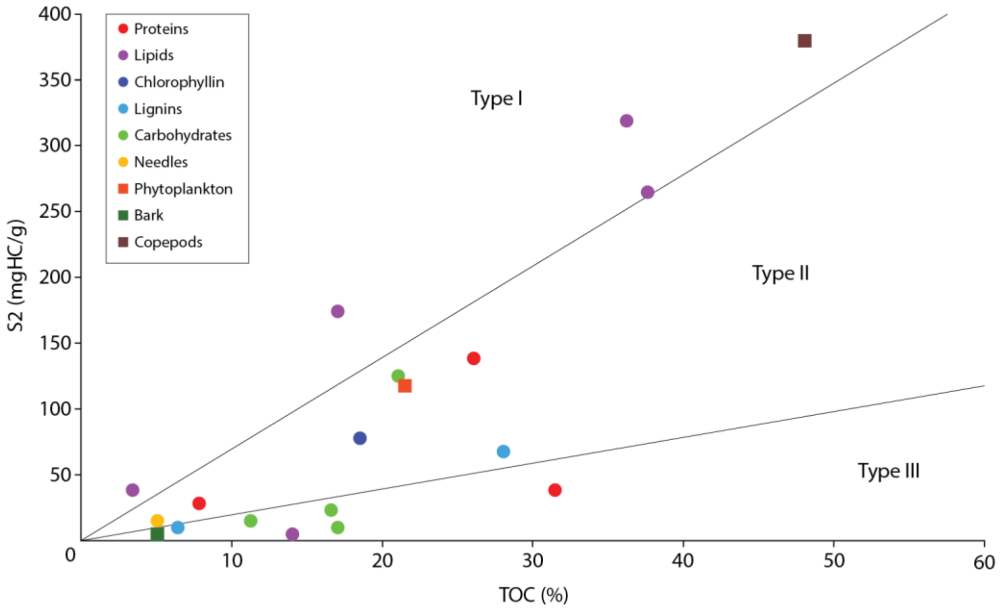

Figure 3.8 *Pseudo van Krevelen diagram for sedimentary OM, showing S2-TOC values from chemical and biological standards and their respective Type I, II or III category assignment (Carrie et al., 2012, Table 1b, Figure 2).*

If there is an abundance of clay minerals in the matrix of a sample, a proportion of the hydrocarbon yield can be retained through adsorption during the thermal cracking process and lead to anomalously low S2 and HI values (Ariztegui et al., 2001). This is resolved using the x-intercept of a regression line fitted to a S2 vs. TOC plot, where a positive intercept suggests that a matrix effect is present and indicates the concentration of OM present with no petroleum potential (Ramanampisoe and Disnar, 1994). The gradient of the regression line provides an estimate of the amount of pyrolisable hydrocarbons present in TOC when multiplied by a factor of 10 (Langford and Blanc-Valleron, 1990), which is useful to assess different OM S2-TOC groupings and their associated degrees of palaeoproductivity. Degradation of OM can also alter TOC and HI (S2) values (Meyers and Lallier-Verges, 1999), which might be suggested by a downcore covariant reduction in TOC and HI (S2) that is negatively correlated to OI as OM is progressively oxidised during methanogenetic diagenesis (Patience et al., 1996).

3.5 Summary

Lake sediment archives consist of various inorganic and organic components that are produced both within a lake and transferred from the surrounding catchment. Analysis of these constituents for various geochemical parameters can yield information on past changes in climate and environment, however care must be taken to investigate possible degradation or reworking to minimise the possibility of an overprinted or disturbed signal. The modern lake setting should be studied to fully understand and calibrate contemporary systematics, to enable more accurate assumptions to be made about past conditions and thus allow for inferences regarding historical and geological departures from present conditions.

Oxygen isotope data from lacustrine carbonate is a function of the temperature and isotope composition of the lake water in which it formed, and can be used to reconstruct past variations in climate; although records are subject to a number of controls primarily dependent on lake hydrology. In open lake systems the isotope composition of lake water is largely determined by the isotope composition of precipitation, which in turn is the product of several effects, including moisture source, temperature, continentality, altitude, amount and seasonality. Alternatively, in closed-basin lakes the isotope composition of lake water is driven by evaporative processes and is a function of the balance between hydrological inputs and outputs. In lakes with extended residence times and little through flow isotope values can approach a steady state, thereby buffering isotope compositions to higher frequency variations in climate.

Carbon pathways in lakes are complex, potentially being associated with inputs from many different reservoirs, and are subject to multiple controlling factors such as the isotope composition of inflowing waters, gaseous exchange with the atmosphere, and aquatic productivity. Interplay between these factors determines the TDIC content of lake waters and the isotope composition of inorganic lake carbonate can provide information on past variations in TDIC. Sources of organic carbon can be differentiated between autochthonous and allochthonous origins using proxies such as C/N, $\delta^{13}C_{organic}$, and Rock-Eval pyrolysis. A significant proportion of organic matter is lost during settling and sedimentation through degradation, however primary source signals are thought to be preserved in both bulk sediments and in molecular proxies.

CHAPTER 4 | ANALYTICAL METHODS

Sediment from a ca. 10 m core and the upper ca. 248 m of a 569 m composite profile recovered during separate fieldwork campaigns to Lake Ohrid were analysed using the methods outlined in this chapter, including stable isotope analysis of carbonates and organic matter, organic geochemistry, Rock-Eval pyrolysis, and thin section techniques. The individual drill campaigns and sediment sampling techniques specific to each core are discussed in Chapter 6 and Chapter 7. Any data generated by international collaborators as part of the wider SCOPSCO project, for example lithology, chronology, geochemistry (TIC, TOC), utilised in the thesis are also discussed (and referenced) in the relevant subsequent chapters.

All preparation work for stable isotope and organic analyses were carried out at the University of Leicester or at the Stable Isotope Facility (SIF) at the British Geological Survey (BGS) in Keyworth. Scanning electron microscopy and X-ray diffraction was also carried out at the BGS. The author conducted a large proportion of preparatory and analytical work, however SIF/BGS staff assisted with some of the preparation and analyses (footnotes indicate where this was the case).

4.1 Stable isotope analysis of carbonates

4.1.1 Calcite-bearing samples

Sediment aliquots containing predominantly calcite (interglacial samples assessed using XRD and SEM, see Sections 4.4 and 4.6) were processed by disaggregating around 250-500 mg of core sample in a 500 ml glass beaker containing 100 ml of 5% sodium hypochlorite (NaClO) solution for 24 hours to oxidise any reactive organic matter (OM), which may lead to erroneous final measurements[1]. Following this, samples were passed through a 64 μm sieve using a fine brush and deionised water to remove any potential biogenic carbonate (e.g. shell fragments). The <64 μm fraction was then diluted to 500 ml and rinsed three times with deionised water to remove any remaining NaClO or oxidised OM. After carefully tipping off the majority of deionised

---

[1] Where possible samples were prepared and analysed for isotopes by the author. SIF staff helped with isotope training and also prepared and analysed a proportion of the Lake Ohrid samples.

water from the final rinse (<50 ml), the samples were dried at 40°C and subsequently powdered and homogenised in an agate pestle and mortar.

Prior to analysis samples were weighed to contain 10 mg of $CaCO_3$ (i.e. a sample that contains 100% calcite would be weighed to 10 mg) using TIC data provided by Dr. Bernd Wagner at the University of Cologne, Germany[2]. As the carbonate content of Lake Ohrid sediments is known to fluctuate through time (see Section 2.4, Figure 2.15), the quantity of each sample required to produce a sufficient CO_2 yield for analysis must be calculated on a per sample basis. TIC data was assumed to mainly represent $CaCO_3$ (Wagner et al., 2008a). The $CaCO_3$ proportion of total sediment weight was calculated using Equation 4.1.

$$CaCO_3(\%) = TIC(\%) \times 8.33 \qquad (4.1)$$

TIC only represents the carbon atoms in the $CaCO_3$ compound and so to calculate the sediment proportion of $CaCO_3$ a factor of 100.09/12.01 = 8.33 must be applied, where the atomic mass of $CaCO_3$ = 100.09 and of carbon = 12.01. The samples will also not contain 100% $CaCO_3$ (due to other inclusions, e.g. inert clastic material), therefore, the final sample weight required for analysis must be calculated to contain 10 mg of $CaCO_3$ by means of Equation 4.2. This provided a conservative estimate as OM was removed prior to analysis.

$$Sample\ weight\ (mg) = \frac{100\ \%}{carbonate\ \%} \times 10\ mg \qquad (4.2)$$

Each carbonate sample was weighed into a glass vial and placed in a reaction vessel containing anhydrous phosphoric acid (H_3PO_4), which was then pumped to create a vacuum (Figure 4.1). Once a sufficient vacuum had been achieved ($< 8*10^{-5}$ mbar), the vessels were sealed and transferred to a water bath at 25°C to equilibrate for 15 minutes. The vessels were then overturned so that the sample tipped out and reacted with the phosphoric acid (Equation 4.3). The vessels were returned to the water bath

---

[2] Total Carbon (TC), TIC and TOC were measured at the University of Cologne using a DIMATOC 100 carbon analyser. An aliquot of sample was dispersed in deionised water. TC was determined by the quantity of CO_2 released after combustion at 900°C. TIC was determined by the quantity of CO_2 released after treating the sample with phosphoric acid and combustion at 160°C. TOC was calculated as the difference between TC and TIC.

and left to react for at least 16 hours at a constant 25°C (McCrea, 1950; Craig, 1957; Swart et al., 1991). After allowing enough time for a complete reaction, any remaining water vapour was removed from the liberated CO_2 by passing the gas through a cold trap held at −90°C. The purified CO_2 was then transferred and frozen in collection vessels submerged in liquid nitrogen (CO_2 sublimation point = −78.5°C) and pumped to a vacuum ($< 2*10^{-5}$ mbar) to remove any other gaseous fraction.

$$3CaCO_{3(s)} + 2H_3PO_{4(aq)} \rightarrow Ca_3(PO_4)_{2(aq)} + 3CO_{2(g)} + 3H_2O_{(l)} \qquad (4.3)$$

The evolved CO_2 was analysed using a VG Optima dual inlet mass spectrometer, where stable isotope measurements were made on CO_2 from the both the sample and a within-run carbonate standard (internal standard at SIF is MCS). The mass spectrometer measures three mass fractions (44, 45, 46), where it is assumed that these correspond to 44 = $^{12}C^{16}O_2$, 45 = $^{13}C^{16}O_2$, and 46 = $^{12}C^{16}O^{18}O$. The mass ratios of 45/44 ($\delta^{13}C$) and 46/44 ($\delta^{18}O$) were calculated relative to the Vienna Pee Dee Belemnite (VPDB) international standard (see Section 3.2, Equation 3.1), and corrected to account for the contribution of ^{17}O species (Craig, 1957).

Figure 4.1 *A) reaction vessel (1) containing the sample to be analysed (2) in glass vial (3) with phosphoric acid (4), and B) carbonate line at SIF, top line reaction vessels (5) are outgassing prior to the sample being reacted and bottom line CO_2 from reacted vessels (6) is being extracted using water trap (7) and liquid nitrogen cooled collection vessels (8).*

A fractionation factor must also be applied to $\delta^{18}O$ as although all of the carbon is transferred to the evolved CO_2 gas during reaction with phosphoric acid, only twothirds of the oxygen is collected (Equation 4.3; Sharp, 2007). The 'acid fractionation factor' is constant in this case as the oxygen fractionation between the evolved CO_2 and original mineral is temperature-dependent (here the reaction was controlled at 25°C). The fractionation factor (α) between CO_2 and calcite during reaction with phosphoric acid at 25°C is 1.01025 (Friedman and O'Neil, 1977). Using $\alpha_{CO_2-calcite}$ the $\delta^{18}O$ value of the original calcite can then be calculated using Equation 4.4 (Sharp, 2007).

$$1.01025 = \frac{1000 + \delta_{CO_2}}{1000 + \delta_{calcite}} \tag{4.4}$$

The analytical reproducibility calculated from the standard deviation (1σ) of the within-run laboratory standards was <0.1‰ for both $\delta^{18}O$ and $\delta^{13}C$.

4.1.2 Siderite-bearing samples

A proportion of the samples (mainly glacial samples) used in this study contained siderite ($FeCO_3$), which is chemically more resilient than calcite and requires a modified preparation technique to liberate CO_2 for analysis and avoid isotopic fractionation as the result of a partial reaction[3]. Where a full reaction (>99%) between calcite and anhydrous phosphoric acid at 25°C only takes a number of hours (McCrea, 1950), siderite may need several weeks or even months to produce a complete yield at this temperature (Figure 4.2; Rosenbaum and Sheppard, 1986).

Recent experimental work conducted at SIF into the procedure for the preparation of siderite-bearing material for isotope analysis found that sedimentary samples should be left for 4 days at 100°C to ensure a full reaction (Collins-Pearson, 2013). This study tested several variables, such as grainsize, treatment method, temperature, reaction time, and siderite chemistry, and the procedural conclusions are aligned with previous observations (Figure 4.2; Rosenbaum and Sheppard, 1986). Further, the work importantly highlighted that the NaClO treatment typically applied to samples to remove reactive organic matter can be used without any large oxidative effect on the siderite.

---

[3] Samples for siderite isotope analysis were prepared and run by SIF staff.

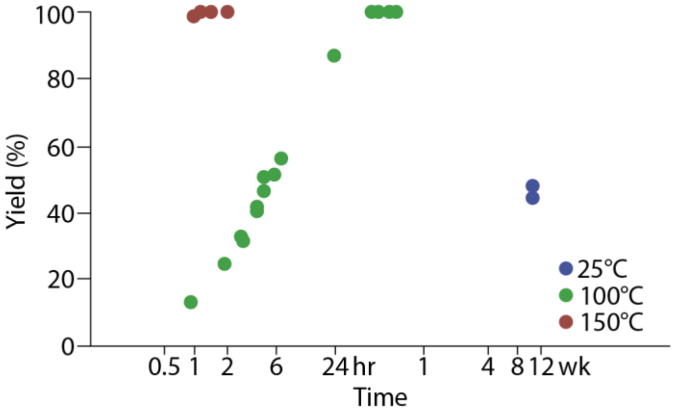

Figure 4.2 *CO_2 yield as a function of time for the reaction of siderite with phosphoric acid at temperatures of 25°C, 100°C and 150°C (Rosenbaum and Sheppard, 1986).*

The siderite samples were weighed into glass vials to give 10 mg of $FeCO_3$. The $FeCO_3$ proportion of total sediment weight was calculated from TIC data using Equation 4.5 (115.85/12.0107 = 9.65, atomic mass of $FeCO_3$ = 115.85 and C = 12.0107) and Equation 4.2. TIC was assumed to predominantly comprise siderite for these horizons and it was also assumed that the siderite was relatively pure (i.e. no isomorphous substitution), which is common for siderites precipitated in fresh water environments (Mozley, 1989).

$$FeCO_3(\%) = TIC(\%) \times 9.65 \tag{4.5}$$

The siderite-bearing sample and anhydrous phosphoric acid were reacted in collection vessels under vacuum at 100°C for 4 days to ensure a complete reaction took place. The evolved CO_2 gas was extracted and measured for isotopes using the same method previously outlined for calcite in Section 4.1.1. The fractionation factor used for siderite was 1.00881 (Rosenbaum and Sheppard, 1986). The analytical reproducibility calculated from the standard deviation (1σ) of the within-run laboratory standards was <0.1‰ for both $\delta^{18}O$ and $\delta^{13}C$.

4.2 Stable isotope and TOC/TN analysis of organic carbon

To remove carbonate for organic matter analysis, around 1 g of sediment sample was placed into a 500 ml glass beaker and disaggregated in approximately 100 ml of 5% hydrochloric acid (HCl) and left to react for 24 hours. Following this, the mixture was diluted to 500 ml with deionised water and subsequently rinsed three times to neutral pH, leaving the residual sample to settle between each rinse. The deionised water was then tipped off (<50 ml) and the beaker placed in a drying cabinet at 40°C. An agate pestle and mortar was used to grind and homogenise the dried sample, before being transferred to a vial[4].

As C and N measurements are presented as weight percentage, it is important that the total weight of the sample be accurately recorded prior to analysis. The weight required is determined by the amount of organic carbon present. Here, TOC values had been previously measured on bulk sediment at the University of Cologne and were provided by Dr. Bernd Wagner (see Section 4.1.1). Samples were weighed into tin capsules to provide 0.5 mg of organic carbon for analysis, which equated to between 5 and 70 mg of sample (TOC range 0.75-10.07%; Equation 4.6). The weight was measured to within 1 µg.

$$Sample\ weight\ (mg) = \frac{100\ \%}{TOC\ \%} \times 0.5\ mg \tag{4.6}$$

The tin capsules were sealed and analysed by flash (or Dumas) combustion using an online system comprised of a Costech ECS4010 elemental analyser (C and N) and a VG Optima mass spectrometer ($\delta^{13}C_{organic}$). Each sample was sequentially dropped from a pre-loaded carousel (auto-sampler) into a furnace heated to 1020°C. A short burst of oxygen was injected when the capsule entered and the exothermic reaction of tin at high temperatures resulted in a combustion temperature of 1400°C, which facilitated complete and instantaneous oxidation of all material (including any thermally resistant substances). The sample was fully combusted to produce CO_2, N, NO_x, S and H_2O (and typically excess O_2). A continuous flow of helium (carrier gas) moved the combustion products through the apparatus. The combustion tube (oxidation column) was packed with quartz wool, silvered cobaltous oxide, and chromium oxide, where chromium oxide (Cr_2O_3) acted as a secondary source of oxygen to aid combustion, sulphur-bearing compounds were removed through reaction with the silver coating, and halides reacted with the cobaltous oxide. The remaining gases (CO_2, N, NO_x, H_2O, and O_2) flowed through a reduction column,

---

[4] Samples were prepared and weighed for analysis by the author. Analytical work was observed by the author but conducted by SIF staff who also provided training.

which was packed with quartz wool and a mixture of copper wires and silica chips. Nitrous oxides and excess O_2 were reduced by reaction with the copper to form copper oxide. Subsequently, water was removed by passage through magnesium perchlorate and the remaining CO_2 and N flowed through a gas chromatographic column (GC). The GC separated CO_2 and N as each has a variable rate of progression determined by compound size (retention time).

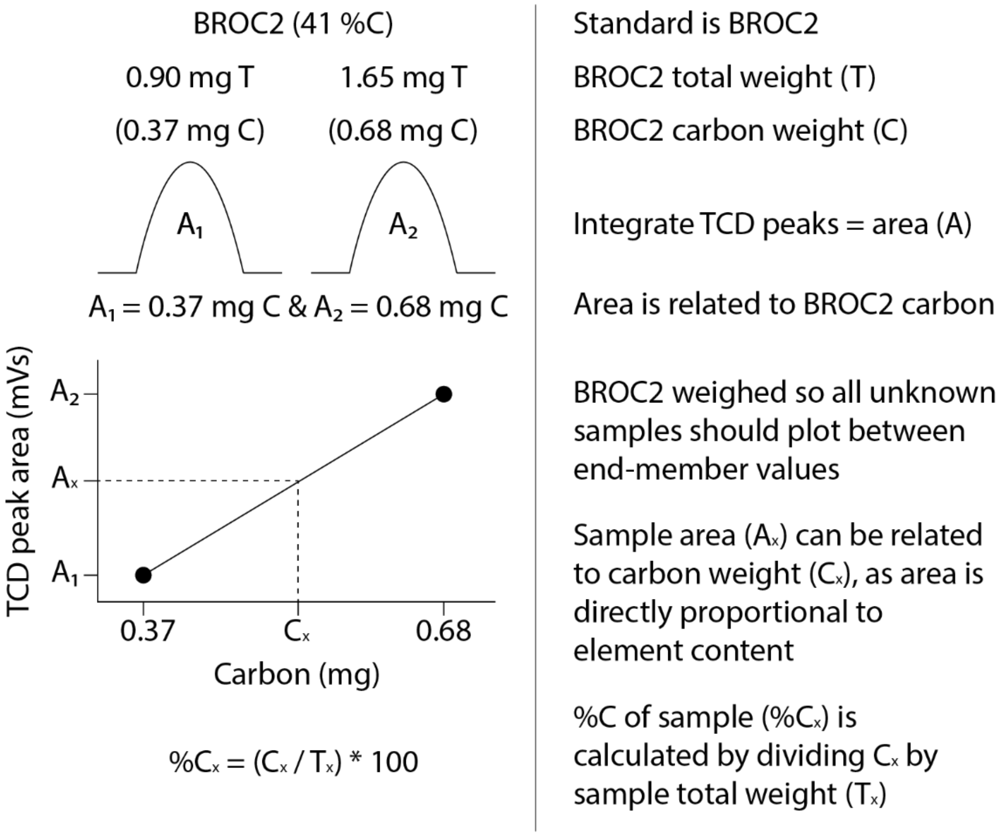

Standard is BROC2

BROC2 total weight (T)

BROC2 carbon weight (C)

Integrate TCD peaks = area (A)

Area is related to BROC2 carbon

BROC2 weighed so all unknown samples should plot between end-member values

Sample area (A_x) can be related to carbon weight (C_x), as area is directly proportional to element content

%C of sample (%C_x) is calculated by dividing C_x by sample total weight (T_x)

Figure 4.3 *Simplified example of how %C is calculated using standards.*

Upon exiting the GC a thermal conductivity detector (TCD) consecutively identified N and CO_2 and generated an electrical signal (mV) proportional to the concentration of each gas relative to the background helium stream. C and N elemental peaks were quantified by calibration to within-run standards of a known composition (Figure 4.3) and the quotient between the two weight percentages provides the C/N mass ratio (all C/N data in this thesis are given as mass ratio values). This can be converted to an atomic ratio by multiplying by 1.167 (atomic weight nitrogen/carbon; Meyers and Teranes, 2001).

The gaseous mixture (He, CO_2, N) was carried to the mass spectrometer system and initially passed through an acetone trap to remove any additional excess water, followed by a triple trap cooled by liquid nitrogen, which froze the CO_2 whilst all other gases present (He, N) were removed under vacuum. The trap was heated and the CO_2 transferred to the mass spectrometer inlet for analysis. $\delta^{13}C_{organic}$ values were calculated relative to VPDB (similar as for calcite and siderite, Section 4.1). Analytical reproducibility for the within-run standards was <0.1‰ for $\delta^{13}C$, and <1% for C and N.

4.3 Rock-Eval pyrolysis of organic matter

Rock-Eval pyrolysis was performed on a Rock-Eval 6 analyser (RE6; Vinci Technologies) in standard mode (pyrolysis and oxidation as a sequential process) using freeze-dried, homogenised, and then powered sediment samples (approximately 60 mg/dry weight)[5]. Each sample was heated at 25°C min^{-1} in an inert atmosphere of N_2 from 300°C up to 650°C. The residual carbon was then oxidised at 20°C min^{-1} (hold 5 min) from 300°C up to 850°C. A flame ionisation detector measured the release of hydrocarbons during the two stage pyrolysis and an infrared cell monitored CO and CO_2 release during thermal cracking of the bound organic matter. The performance of the RE6 apparatus was checked every 10 samples against the accepted values of the Institut Français du Pétrole (IFP) standard (IFP 160 000, S/N15-081840). Classical parameters generated by Rock-Eval analysis (S2, S3, TOC) and their calculated derivations (HI, OI) are discussed in Section 3.4.3. Here, the HI and OI are primarily used for which the analytical reproducibility of the within-run standards was ±16 for HI and ±3 for OI.

4.4 X-ray diffraction

The constituent mineralogy of sediment samples was investigated using X-Ray Diffraction (XRD) at the British Geological Survey, Keyworth[6]. Silicon crystal substrate XRD ‘zero-background’ mounts were used for samples in place of standard

---

[5] Dr. Christopher Vane and staff conducted all Rock-Eval analyses at the British Geological Survey, Keyworth, and kindly provided the methodology.

[6] Sample preparation was carried out by the author and Doris Wagner at the British Geological Survey. All analytical work was carried out by Doris Wagner, who kindly provided the methodology.

cavity mounts as the amount of material available for analysis was small. The samples were hand ground (<15μm) in an agate pestle and mortar and 30-50 mg was deposited onto the surface of silicon discs using 2 drops of acetone to give a thin even coverage of random orientation, and allowed to dry.

XRD analysis was conducted on a PANalytical X'Pert Pro series powder diffractometer, with Cobalt Kα_1 radiation over the scan range 4.5-85°2θ and a step size of 2.06°2θ min^{-1}. Phase identification for the diffraction data was conducted using PANalytical HighScore Plus version 4.0 analytical software interfaced with the latest version of the International Centre for Diffraction Data (ICDD) database.

4.5 Polished thin sections

Cores were sub-sampled for thin section material at the University of Cologne, Germany, using trays constructed from thin aluminium sheeting (after Francus and Asikainen, 2001)[7]. The trays were approximately 20 mm wide by 60 mm long and 5 mm deep with holes cut into the base to aid the resin impregnation processes. The trays were positioned on the sediment surface of a working core half, both in parallel (for textures) and perpendicular (for layers) to core length, and pushed in by hand. A piece of thin plastic wire was pushed in beneath one end of the tray and pulled along its length to slice the sediment. Trays were carefully removed to prevent any major disturbance to the core and the section material, then wrapped in plastic film and stored at 4°C.

The sediment was later freeze-dried under vacuum (still in the aluminium tray) and afterward warmed in a low temperature (40°C) oven overnight. Epoxy-resin was poured over the trays to consolidate the sediment and returned to the oven to dry[8]. The resin sediment block was then removed from the aluminium tray and hand ground on a glass plate with 15 μm aluminium oxide and propanol. A surface coat of resin was added to the polished side and returned to the oven to dry overnight. The sediment

---

[7] Sub-sampling was carried out by the author and Dr. Alexander Francke at the University of Cologne. The aluminium trays were constructed by Ascelina Hasberg.

[8] Thin section preparation was carried out by John Fletcher at the British Geological Survey Thin Section Department.

block was bonded to a glass slide using a colourless epoxy-resin and then cut using a circular saw. The cut edge was coarsely polished using aluminium oxide and propanol on an automated rotating base plate. A fine polish was achieved using successive grades of polycrystalline diamond pastes (15/6/3/1 μm) at around 35-40 minutes per grade.

4.6 Scanning electron microscopy with energy dispersive X-ray spectroscopy

Scanning electron microscopy (SEM) was carried out on thin sections (Section 4.5) using a FEI Quanta 600 environmental SEM in backscatter mode (BSEM) equipped with a fully-integrated Oxford Instruments INCA 450 energy dispersive X-ray spectroscopy (EDX) analysis system[9]. The SEM was operated in conventional high vacuum mode ($<1*10^{-4}$ torr), using an accelerating voltage of between 12.5-20 kV. Phase identification was conducted on selected features of interest using micro-chemical information obtained from semi-quantitative EDX spectra. Digital EDX element maps were also produced from selected areas of interest by the summation of data recorded from 30 frame scans recorded over a period of approximately 45 minutes. EDX spectra and digital element maps were processed using the Oxford Instruments INCA Suite software package, and the maps were digitally processed to show relative element concentrations (a ‘rainbow’ colour scheme was applied, so that blue = zero background, green/yellow/orange = low-intermediate concentration, red/white = high concentration).

4.7 Summary

In summary, sediments from a ca. 10 m core (Co1262) and a 248 m composite profile (5045-1) recovered from Lake Ohrid were analysed for stable isotopes of carbonate. Stable isotopes of organic matter, organic geochemistry and Rock-Eval pyrolysis were also used to investigate Co1262 to support the isotope data and provide a robust calibration for the long core. Thin sections, SEM-EDX and XRD techniques were also employed to ascertain the nature of carbonate species and morphology. The results of these analyses are presented in Chapter 6 (Co1262) and Chapter 7 (5045-1).

---

[9] SEM analysis was carried out by the author under the supervision of Antoni Milodowski at the British Geological Survey.

CHAPTER 5 | MODERN ISOTOPE HYDROLOGY

Understanding how the isotope composition measured from a mineral precipitate relates to the isotope composition of lake water is fundamental in resolving the systematics of how past climate variation is recorded in lacustrine sediment records (Leng and Marshall, 2004). The isotope composition of present-day waters from Lake Ohrid and the surrounding springs and river inflows have been previously investigated (e.g. Eftimi and Zoto, 1997; Anovski et al., 2001; Matzinger et al., 2006a; Leng et al., 2010a; Leng et al., 2013). The dataset covers water samples collected between 1984 to 2011 (Figure 5.1), showing that modern waters from Lake Ohrid fall on a Local Evaporation Line (LEL) away from the Local Meteoric Water Line (LMWL) inferring that they have undergone kinetic fractionation (Leng and Marshall, 2004).

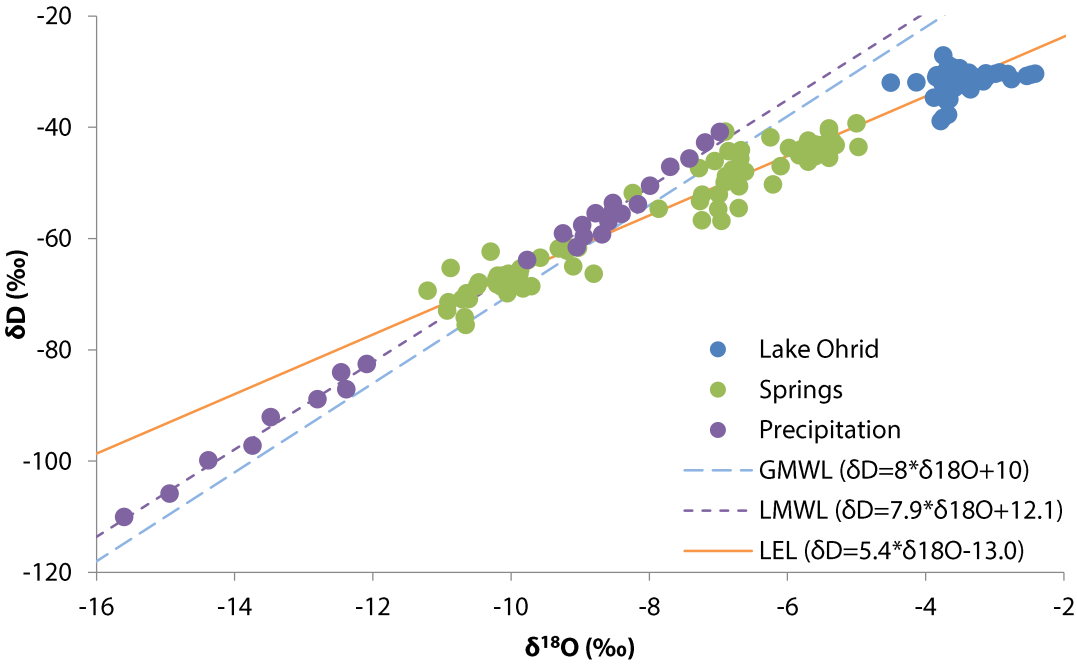

Figure 5.1 *Modern isotope composition (δ^{18}O and δD) of waters from Lake Ohrid, springs and local direct/catchment rainfall (Anovski et al., 1980; Anovski et al., 1991; Eftimi and Zoto, 1997; Anovski, 2001; Matzinger, 2006; Jordanoska et al., 2010; Leng et al., 2010a). The GMWL (Craig, 1961), LMWL (Anovski et al., 1991; Eftimi and Zoto, 1997) and calculated LEL are given.*

However, previous studies rely on simple linear regression models to describe the contemporary isotope hydrology and do not utilise the available data to provide a complete calibration for sediment cores taken from Lake Ohrid (e.g. Belmecheri et al., 2010; Leng et al., 2010a). A better, quantitative, understanding of the modern isotope system is needed as a prerequisite for interpreting isotope data from the new Ohrid cores discussed as part of this thesis (cores Co1262, 5045-1). In this chapter, the modern hydrology and isotope data from Lake Ohrid is therefore reviewed and a new lake mass balance model using modern isotope data is presented and discussed.

5.1 Water mass balance

The water mass balance of a lake can be described in general terms as the change in lake volume per unit time (dV/dT), which is a function of the sum of the water inputs (I) and outputs (Q) from the lake system (Equation 5.1; Steinman et al., 2010).

$$\frac{dV}{dt} = \sum I - \sum Q \qquad (5.1)$$

Specifically, water inputs comprise direct precipitation on the lake (P) and surface and groundwater inflows (I), and water outputs include evaporation (E) and surface and groundwater outflows (Q) (Equation 5.2; Jones et al., 2015b).

$$\frac{dV}{dt} = P + I - E - Q \qquad (5.2)$$

A number of previous studies have investigated the modern hydrology of Lake Ohrid (e.g. Watzin et al., 2002; Matzinger et al., 2006b), including the construction of preliminary water balance models, and the following contemporary data are available for Lake Ohrid.

5.1.1 Precipitation

The average quantity of precipitation recorded at meteorological stations in the Lake Ohrid catchment varies between 703 and 1445 mm year^{-1}, however for stations directly at the lake's shoreline the average is 773 mm year^{-1} (Table 5.1; Watzin et al., 2002).

Table 5.1 *Average annual precipitation around the shoreline of Lake Ohrid (Watzin et al., 2002).*

Station	Precipitation (mm)
Ohrid	703
Struga	794
Saint Naum	889
Pestani	729
Pogradec	748
Average	773

Given Lake Ohrid has a surface area of 358 km^2, the amount of precipitation falling over the entire lake area is 276*10^6 m^3 yr^{-1}, or 8.8 m^3 s^{-1}.

5.1.2 Surface inflow

The primary surface inflow to Lake Ohrid is the River Sateska, which has an average discharge of 5.5 m^3 s^{-1}. Following high winter precipitation (Figure 2.11), river runoff can be up to 12.9 m^3 s^{-1} during spring months and in dry summers as low as 0.3 m^3 s^{-1} (Figure 5.2; Matzinger et al., 2006b). The distribution of runoff suggests a large proportion of spring snowmelt. Prior to 1962, the Sateska was a direct tributary of Ohrid's main outflow (River Crn Drim) but was diverted to provide hydro-electric power and reduce the sediment load of Crn Drim (Watzin et al., 2002). Other inflowing tributaries are less significant and have smaller discharges (for example the Pogradec, Koselka and Verdova rivers) and produce a total runoff around 3.4 m^3 s^{-1} (Matzinger et al., 2006b).

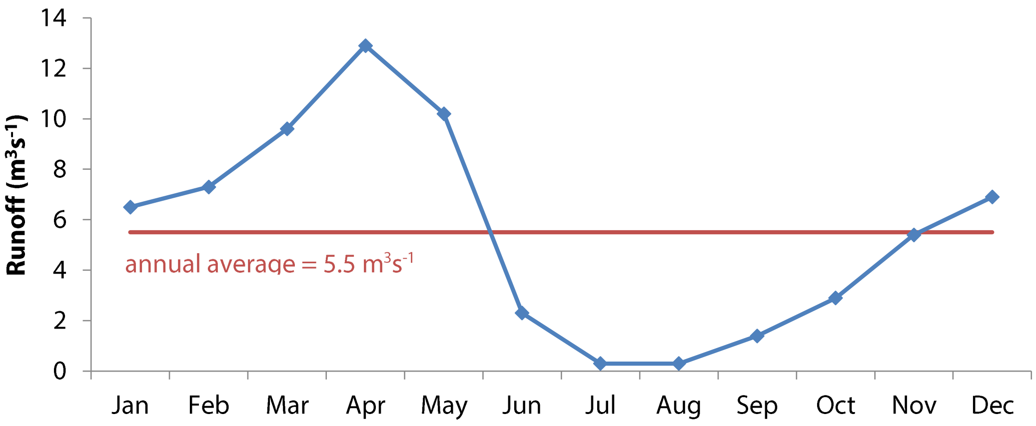

Figure 5.2 *Seasonal discharge of the River Sateska, the main riverine inflow to Lake Ohrid (Matzinger et al., 2006b and references therein).*

5.1.3 Groundwater inflow

The main groundwater inflow to Lake Ohrid is through a network of karst springs, which appear both above and below the present water line. The surface springs consist of three main complexes to the south and north-east of the lake shoreline. The largest is found to the south of the lake, where a collection of 15 springs at St. Naum yield between 4.6 to 11.24 $m^3 s^{-1}$ with an average annual discharge of 7.5 $m^3 s^{-1}$ (Popovska and Bonacci, 2007). To the west of St. Naum near the village Tushemisht, a second large zone consisting of 80 springs has an annual yield of approximately 2.5 $m^3 s^{-1}$ (Watzin et al., 2002) and the Biljana springs to the north-east of Lake Ohrid have a discharge reported to be around 0.26 $m^3 s^{-1}$ (Watzin et al., 2002).

It has been established using artificial and environmental tracers (Sulphorhodamine G dye and modern isotope data) that some spring water does not originate from a single source, but rather a proportion of water is delivered through underground karst channels from Lake Prespa (Amataj et al., 2007; Eftimi et al., 2007). Two groupings of springs are clearly resolved in δ^{18}O-δD space (Figure 5.3).

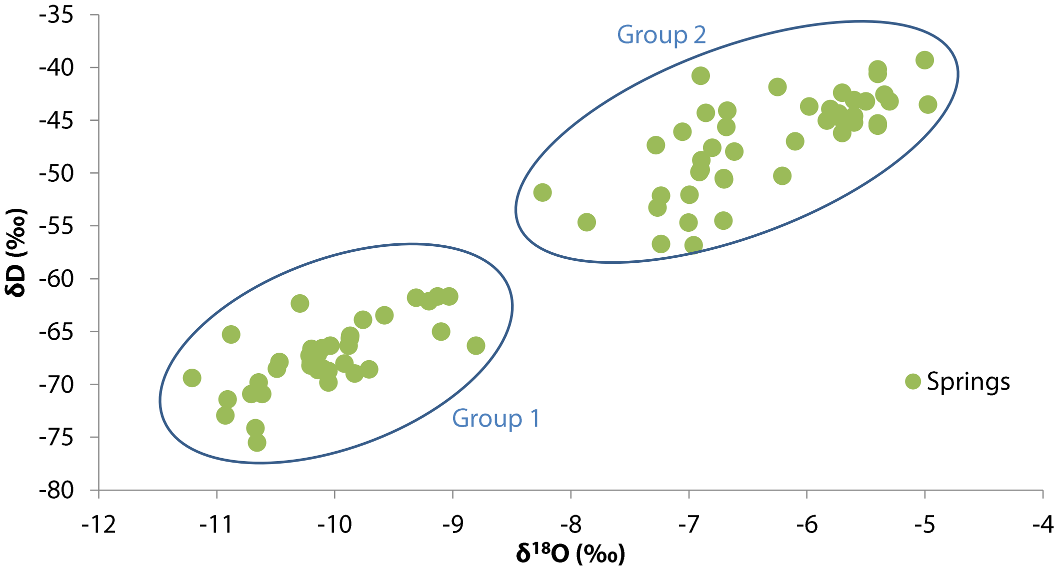

Figure 5.3 *Spring water isotope data showing two distinct groupings (Anovski et al., 1980; Anovski et al., 1991; Eftimi and Zoto, 1997; Anovski et al., 2001; Matzinger et al., 2006b; Jordanoska et al., 2010; Leng et al., 2010a).*

Two-component mixing analysis conducted using stable isotope and Cl^- data suggests that the ratio of water originating from Lake Prespa, in comparison to meteoric precipitation, is around 53% at the Tushemisht springs and 42% at St. Naum (Table 5.2; Anovski et al., 1991; Eftimi and Zoto, 1997; Anovski et al., 2001; Eftimi et al., 2001; Matzinger et al., 2006a). The Biljana springs are only fed by water derived from meteoric precipitation (Eftimi et al., 2007).

Table 5.2 *Component mixing between waters from local precipitation and Lake Prespa at the main spring inflows to Lake Ohrid (Anovski et al., 1991; Watzin et al., 2002; Amataj et al., 2007; Eftimi et al., 2007).*

Springs	Local precipitation-fed (m^3s^{-1})	Prespa-fed (m^3s^{-1})
St. Naum	4.3 (58%)	3.2 (42%)
Tushemisht	1.2 (47%)	1.3 (53%)
Biljana	0.3 (100%)	0 (0%)
Total	5.8 (56%)	4.5 (44%)

Lake Prespa has a reduced surface area to volume ratio in comparison to Ohrid, and therefore is more sensitive to seasonal variations in water balance (Leng et al., 2010a), hence its waters fall high on the LEL (average $\delta^{18}O = -1.5‰$ and $\delta D = -20.5‰$; Figure 5.4).

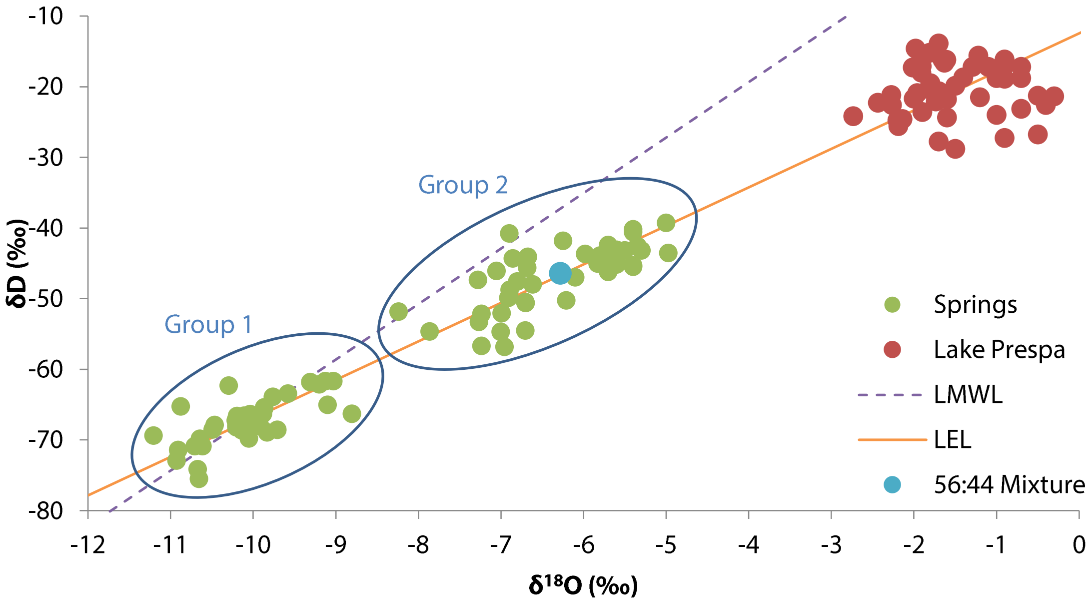

Figure 5.4 *Plot showing the influence of water derived from Lake Prespa on the isotope composition of spring water delivered to Lake Ohrid. The blue dot (56:44 Mixture) indicates the theoretical location of a water mass comprising 44% water from Lake Prespa and 56% meteoric precipitation (Table 5.3).*

If spring waters are derived from a mixed source, for example in the proportions given in Table 5.2 (i.e. 56:44), then the theoretical isotope composition for a combination of water from Lake Prespa and meteoric sources is around $\delta^{18}O = -6.3‰$ and $\delta D =$

−46.4‰ (Figure 5.4). This assumes that the average water isotope composition from Lake Prespa is directly transferred to Ohrid, and that the LMWL-LEL intersect (δ^{18}O = −10.04‰ and δD = −66.74‰) defines the isotope composition of meteoric-derived waters, as calculated by simultaneously evaluating the equations for the LMWL and LEL (Equations 5.3 and 5.4, respectively, as calculated from modern data).

$$\delta D = (7.86 \times \delta^{18}O) + 12.11 \quad \text{(LMWL)} \tag{5.3}$$

$$\delta D = (5.35 \times \delta^{18}O) - 13.02 \quad \text{(LEL)} \tag{5.4}$$

The theoretical water mixture sits within group 2 (Figure 5.4), and has a value very similar to that of the average for group 2 (δ^{18}O = −6.3‰ and δD = −47.0‰). Variation within group 2 can be explained by the spread of data within group 1 and measurements from Lake Prespa (apart from the two lowermost values, suggesting these had a higher component of precipitation-derived water). The data therefore suggest that 56:44 (Table 5.2) is a realistic annual average mixing coefficient and that there is probably a continuum of mixing for spring waters, where lower isotope values are primarily derived from meteoric precipitation and higher values have a variable component delivered from Lake Prespa.

The surface springs of Lake Ohrid receive approximately 4.5 $m^3 s^{-1}$ of water from Lake Prespa (Table 5.2), however the total water outflow from Lake Prespa into the underground karst system is estimated to total around 7.7 $m^3 s^{-1}$ (Anovski, 2001). The remaining 3.2 $m^3 s^{-1}$ of outflow from Lake Prespa is most likely transferred to Lake Ohrid through the sublacustrine network of springs along its eastern margin (Matzinger et al., 2006a). A precise value for the overall discharge from these springs is currently unknown. Precipitation infiltration rates for the karst massif are thought to be around 5.5 $m^3 s^{-1}$ for the southern Galičica (340 km^2; Anovski, 2001), which when scaled to the entire mountain range between Ohrid and Prespa (810 km^2) may potentially be as high as 13.1 $m^3 s^{-1}$. This assumes an effective karst infiltration of 55% and an average annual precipitation value of 980 mm (Anovski, 2001). However, Matzinger et al. (2006b) adopts a value of 9.9 $m^3 s^{-1}$ for total sublacustrine spring inflow, thereby implying a meteoric component of 6.7 $m^3 s^{-1}$ when the Prespa contribution is taken into account, although the value was calculated by closing the balance rather than being a direct measure of flowrate.

5.1.4 Evaporation

Evaporation is normally calculated using one of several equations (e.g. Penman, 1948; Valiantzas, 2006) dependent on the meteorological information available from a site (Jones et al., 2015a). Watzin et al. (2002) calculated the annual evaporation from the surface of Lake Ohrid to be 1145 mm (or 13 $m^3 s^{-1}$) using the Penman formula for open water evaporation and data from the meteorological station at Pogradec (south coast).

5.1.5 Surface outflow

The only surface outflow from Lake Ohrid is the River Crn Drim (northern margin), which has an average discharge of 24.9 $m^3 s^{-1}$ (Matzinger et al., 2006b). It is important to note however that before the diversion of the River Sateska in 1962, water input to Lake Ohrid would have been significantly reduced. It is probable that the lower inflow to Ohrid resulted in a concomitant decrease in outflow through Crn Drim, which may therefore have had a maximum runoff of 19.4 $m^3 s^{-1}$ prior to 1962.

5.1.6 Groundwater outflow

Groundwater outflow has not been observed to date (Wagner et al., 2008a) and is absent from previous water balance models (Watzin et al., 2002; Matzinger et al., 2006b). However, as Triassic limestone crops out along the western margin of Lake Ohrid and the basin is characterised by active faulting, groundwater outflow should not be excluded.

5.1.7 Water mass balance model

A revised water balance for Lake Ohrid, based on data from previous work outlined above (after Matzinger et al., 2006b), is shown in Table 5.3. The parameters G_iX and G_oY are substituted for the unknown quantity of groundwater inflow sourced from meteoric infiltration and potential groundwater outflow, respectively. Lake Ohrid is assumed to have reached a steady state (Popovska and Bonacci, 2007), such that no change in lake volume is observed over a given period of time (Equation 5.5) and thus the sum of water inputs is equal to sum of outputs (Equation 5.6).

Table 5.3 *Revised water balance of Lake Ohrid (after Anovski, 2001; Watzin et al., 2002; Matzinger et al., 2006b).*

Source	Flow rate ($m^3 s^{-1}$)
Inputs	
Precipitation (P)	8.8
Rivers (R)	8.9
Springs: Prespa-fed (S_{PR})	7.7
Springs: local precipitation-fed (S_{LP})	$5.8 + G_iX$
Total	$31.2 + G_iX$
Outputs	
Evaporation (E)	13.0
River outflow (S_Q)	24.9
Groundwater outflow (G_Q)	G_QY
Total	$37.9 + G_QY$

$$\frac{dV}{dt} = 0 \tag{5.5}$$

$$P + R + S_{PR} + S_{LP} = E + S_Q + G_Q \tag{5.6}$$

Using the values presented in Table 5.3, the water mass balance for Lake Ohrid can therefore be represented by Equation 5.7, which rearranged gives Equation 5.8.

$$31.2 + G_iX = 37.9 + G_QY \tag{5.7}$$

$$G_iX - G_QY = 6.7\ (m^3\ s^{-1}) \tag{5.8}$$

5.2 Isotope mass balance

The isotope mass balance of a lake can be represented by Equation 5.9 (Jones et al., 2015b), which is defined as the sum of the products of water flux (P, I, E, Q) and the isotope composition of the inflows (δ_P, δ_I) and outflows (δ_E, δ_Q).

$$\frac{dV\delta_L}{dt} = P\delta_P + I\delta_I - E\delta_E - Q\delta_Q \tag{5.9}$$

Using the parameters from Table 5.3, Equation 5.9 can be reexpressed for Lake Ohrid (Equation 5.10).

$$\frac{dV\delta_L}{dt} = P\delta_P + R\delta_R + S_{PR}\delta_{S_{PR}} + S_{LP}\delta_{S_{LP}} - E\delta_E - Q\delta_Q - G_QY\delta_{G_QY} \qquad (5.10)$$

The river input to Lake Ohrid is assumed to directly originate from precipitative waters over the catchment (C_{LP}) that will have a similar average annual value as the infiltrated component of spring water, such that $\delta_R = \delta_{S_{LP}} = \delta_{C_{LP}}$. Any water outflow through the River Crn Drim or potential groundwater flux is assumed to have the same average isotope composition as the measured lake water, so $\delta_Q = \delta_{G_QY} = \delta_L$ (assuming Lake Ohrid is well mixed; see Matzinger et al., 2006b). Taking these assumptions into account, and given the lake is thought to be in a steady state ($dV\delta_L/dt = 0$), Equation 5.10 can be re-expressed (Equation 5.11).

$$P\delta_P + (R + S_{LP} + G_iX)\delta_{C_{LP}} + S_{PR}\delta_{S_{PR}} = E\delta_E + (Q + G_QY)\delta_L \qquad (5.11)$$

A proportion of the hydrological values in Equation 5.11 (P, R, S_{LP}, S_{PR}, E, and Q) are already known from the measurements summarised in Table 5.3, where the only unknown parameters are G_iX and G_QY.

The isotope composition of precipitation falling directly on the lake's surface (δ_P) was measured as part of an IAEA Regional Project (RER/8/008) at the St. Naum spring complex, where $\delta^{18}O = -8.4‰$ and $\delta D = -52.9‰$ (mean weighted value, 1986; Anovski, 2001). In contrast, isotope measurements for local rivers and surface springs (δ_{CLP}) that are thought to have a main component of their water provided by local precipitation typically show lower average values $\delta^{18}O = -10.1‰$ and $\delta D = -67.4‰$ (Anovski et al., 1980; Anovski et al., 1991; Eftimi and Zoto, 1997; Leng et al., 2010a). This suggests that infiltration is fed by precipitation at a much higher altitude (Anovski, 2001), and probably contains a component of snowfall. Snow is characterised as having much lower isotope values than rain, as it reflects fractionation at lower temperatures at within-cloud conditions (Darling et al., 2006; Dean et al., 2013). Snowfall is thought to define the pattern of annual discharge of the River Sateska where maximum discharge occurs when snowfields start to melt in early spring (Figure 5.2; Matzinger et al., 2006b).

Lake water measured from Lake Prespa (δ_{SPR}) over the 30-year sampling period has average $\delta^{18}O = -1.5‰$ and $\delta D = -20.5‰$ (Figure 5.4), and it is assumed that this value is transferred directly to Ohrid through the underground karst network. Similar measurements conducted for Lake Ohrid (δ_L) show average $\delta^{18}O = -3.5‰$ and $\delta D = -31.7‰$ (Figure 5.1).

The isotope composition of evaporation (δ_E) is difficult to measure, and so is typically calculated using the Craig and Gordon (1965) evaporation model (Equation 5.12; Steinman et al., 2010).

$$\delta_E = \frac{(\alpha^{*} \times \delta_L) - (h \times \delta_A) - \varepsilon}{1 - h + (0.001 \times \varepsilon_K)} \qquad (5.12)$$

In Equation 5.12, α* is the reciprocal of the equilibrium isotopic fractionation factor (α) calculated for $\delta^{18}O$ (Equation 5.13) and δD (Equation 5.14) using the equations of (Horita and Wesolowski, 1994), where T_W is the temperature of lake surface water (in degree K), assumed to be 287.15°K (Stankovic, 1960).

$$\ln \alpha = 0.35041\left(\frac{10^6}{{T_W}^3}\right) - 1.6664\left(\frac{10^3}{{T_W}^2}\right) + 6.7123\left(\frac{1}{T_W}\right) - 7.685 \times 10^{-3} \qquad (5.13)$$

$$\ln \alpha = 1.1588\left(\frac{{T_W}^3}{10^9}\right) - 1.6201\left(\frac{{T_W}^2}{10^6}\right) + 0.79484\left(\frac{T_W}{10^3}\right) + 2.9992\left(\frac{10^6}{{T_W}^3}\right) - 161.04 \times 10^{-3} \qquad (5.14)$$

The normalised relative humidity (h) is the quotient of the saturation vapour pressure of the overlying air ($e_{s\text{-}a}$) and the saturation vapour pressure at the surface water temperature ($e_{s\text{-}w}$) (Equation 5.15 and 5.16; Steinman et al., 2010), which relates the measured relative humidity (RH; 69.6%) to the temperature (T) of the air (11.53°C) or lake water (14.00°C).

$$h = RH \times \frac{e_{s-a}}{e_{s-w}} \qquad (5.15)$$

$$e_{s-a\ \&\ s-w} = 6.108 \times e^{\frac{17.27 \times T}{T + 237.7}} \qquad (5.16)$$

The isotope composition of atmospheric moisture (δ_A) is assumed to be in equilibrium with precipitation (Equation 5.17), where ε* (Equation 5.18) is the per mil equilibrium separation of oxygen and hydrogen (Gibson et al., 2002).

$$\delta_A = \delta_P - \varepsilon^* \tag{5.17}$$

$$\varepsilon^* = 1000 \times (1 - \alpha^*) \tag{5.18}$$

The total isotopic separation factor (ε; Equation 5.19) comprises both equilibrium (ε*) and kinetic (ε_K; Equation 5.20 and 5.21) components (Gibson et al., 2002).

$$\varepsilon = \varepsilon^* + \varepsilon_K \tag{5.19}$$

$$\varepsilon_K = 14.2 \times (1 - h) \quad \text{(for } \delta^{18}\text{O)} \tag{5.20}$$

$$\varepsilon_K = 12.5 \times (1 - h) \quad \text{(for } \delta\text{D)} \tag{5.21}$$

In particularly large lakes, such as Ohrid, evaporation can have a significant influence on the overlying atmosphere producing a moisture feedback, and it is therefore important to consider the effects on kinetic fractionation (Equation 5.22). As lake water evaporates, the fraction (*f*) of evaporate incorporated in the overlying atmosphere modifies δ_A by the addition of δ_E to form δ'_A (Gibson et al., 2015).

$$\delta'_A = (1 - f)\delta_A + f\delta_E \tag{5.22}$$

In a feedback system, the modified isotope composition of evaporation is therefore defined by Equation 5.23 (Gibson et al., 2015).

$$\delta'_E = \frac{(\alpha^* \times \delta_L) - (h \times \delta'_A) - \varepsilon}{1 - h + (0.001 \times \varepsilon_K)} \tag{5.23}$$

Equations 5.22 and 5.23 are solved iteratively so that for isotope mass balance δ^{18}O and δD are equal. This is achieved using a variable *f* and simultaneously evaluating Equations 5.8 and 5.11.

The iterative calculation suggests that G_QY equals 6.0 m^3 s^{-1} and G_iX equals 12.7 m^{3}s^{-1}. For conservation of isotope mass balance the fraction of evaporate incorporated into the atmosphere overlying Lake Ohrid is approximately 37%, which is consistent with other larger lakes, such as Lake Superior (40%), Lake Michigan

(33%), and Lake Ontario (27%) (Jasechko et al., 2014). Given all the above, a new water balance model based on the initial summary balance of Matzinger et al. (2006b) and incorporating the new calculated parameters is given in Table 5.4.

Table 5.4 *A new water balance for Lake Ohrid.*

Source	Flow rate ($m^3 s^{-1}$)	Flow rate (%)
Inputs		
Precipitation	8.8	20
Rivers	8.9	20
Springs	26.2	60
(Prespa-fed)	(7.7)	(18)
(Precipitation-fed)	(18.5)	(42)
Total	43.9	
Outputs		
Evaporation	13.0	30
River outflow	24.9	57
Groundwater outflow	6.0	13
Total	43.9	

A larger proportion of the hydrological inflow budget can therefore be ostensibly attributed to the underground karst aquifer network. In addition, although not previously described, a component of groundwater outflow must also be present for isotope mass balance (based on the calculations and assumptions outlined above).

5.3 Implications for palaeo-records from Lake Ohrid

Lake Ohrid is shown to receive a proportion of its inflowing water from Lake Prespa, which has lake water evaporated beyond that of Ohrid (Figure 5.4). If all water input is derived from meteoric sources, the intersect between the LEL and LMWL defines the average annual isotope composition of inflowing water. However, as Lake Ohrid receives a component of evaporated water from Lake Prespa, the average annual isotope composition of total water input will be located away from the LEL and LMWL intersect. In addition, direct rainfall on the lakes surface is suggested to have a higher isotope composition than that delivered to Ohrid through river and spring inflows due to elevation. Taking these different sources and their respective isotope compositions into account, the calculated average weighted inflow to Lake Ohrid is $\delta^{18}O = -8.3‰$ and $\delta D = -56.3‰$ (Figure 5.5).

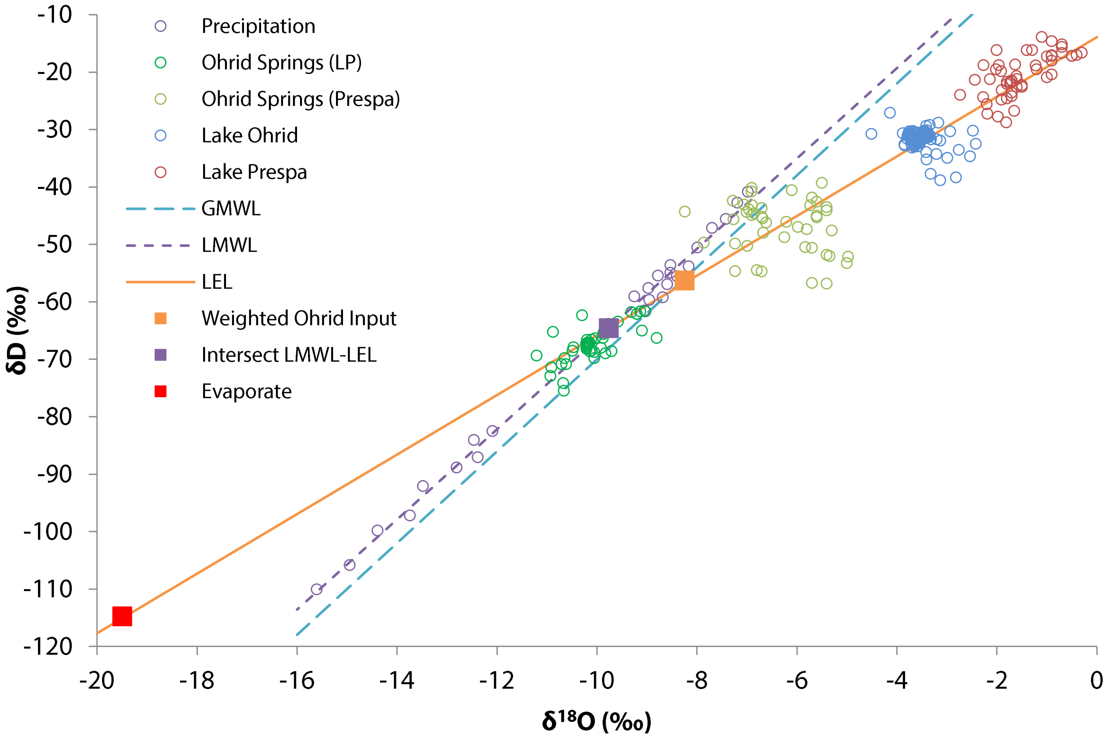

***Figure 5.5** Summary modern isotope composition of waters from Lake Ohrid and its inflows, including calculated average inflow and isotope composition of evaporate.*

The average weighted input for Lake Ohrid suggests that the amount of water delivered by direct precipitation, runoff and groundwater sources, to an extent, counteracts the addition of evaporated water from Lake Prespa. However, if the underground connection to Lake Prespa was shut off, for example due to tectonic processes or a water level drop in Lake Prespa prohibiting outflow, the isotope composition of water input to Lake Ohrid in response would transition to lower values ($\delta^{18}O = -9.7‰$ and $\delta D = -63.9‰$). Thus, short-term variations in the isotope composition of water in Lake Prespa probably have little bearing on the isotope composition of water in Lake Ohrid, although variations in flowrate may account for a greater change in Ohrid lake water $\delta^{18}O$.

In terms of interpreting past lake water balance from $\delta^{18}O$ of carbonates from Lake Ohrid cores, a generally uniform isotope composition over the 30-year sampling period of modern lake waters suggests Lake Ohrid has reached a steady state due to its large water volume and 70-year residence time. Variation in $\delta^{18}O$ of carbonates will therefore most likely represent low frequency changes in water balance as a direct function of climate. The majority of inflow is from surface and sublacustrine springs

(60%), however water input will ultimately be controlled by the amount of precipitation received at the lake and over the catchment. At present, surface water inflow is predominantly driven by spring snowmelt, and so changes in seasonality and winter season length could impact the timing and magnitude of water balance and isotope variations. The position of lake water on the LEL (Figure 5.5) will predominantly vary depending on the amount of precipitation and extent of evaporation (i.e. P/E ratio), however given that evaporation accounts for 30% of water output overall changes in precipitation input may have a greater influence on lake water $\delta^{18}O$.

5.4 Summary

5.4.1 Contemporary hydrological balance

The isotope composition of contemporary waters from Lake Ohrid shows the lake to be an evaporative system, where the measured modern isotope data fall on a LEL away from the LMWL. Hydrological input is derived from direct precipitation, river inflow and springs; the latter are found to be compositionally different depending on the level of mixing with waters derived from Lake Prespa. Hydrological output in previous water balance models has been ascribed to evaporation and river outflow, however for isotope mass balance a component of groundwater outflow is necessary. Calculations based on Lake Ohrid being a feedback system, whereby 37% of the overlying atmosphere comprises evaporate, indicate that groundwater outflow is approximately equal to 6.0 $m^3 s^{-1}$. In addition, the precipitation-fed component of sub-lacustrine springs is estimated to have a flowrate of 12.7 $m^3 s^{-1}$. The new hydrological balance described in this chapter is summarised in Figure 5.6.

5.4.2 Implications for interpretation of $\delta^{18}O$

The calculated modern water balance for Lake Ohrid indicates a complex hydrology, which is possibly influenced by multiple drivers and partly dependent on the connection to other nearby lake systems. A low $\delta^{18}O$ range in modern lake water implies that Lake Ohrid has reached a steady state and the position of modern lake water on a LEL suggests lake water $\delta^{18}O$ is driven by water balance, representing slow, centennial-millennial changes in climate. However, evaporation only accounts for 30% of water output, therefore the predominant driver of lake water $\delta^{18}O$ is most likely the amount of water inflow as a function of changes in precipitation (rather than being intrinsically link to the P/E ratio).

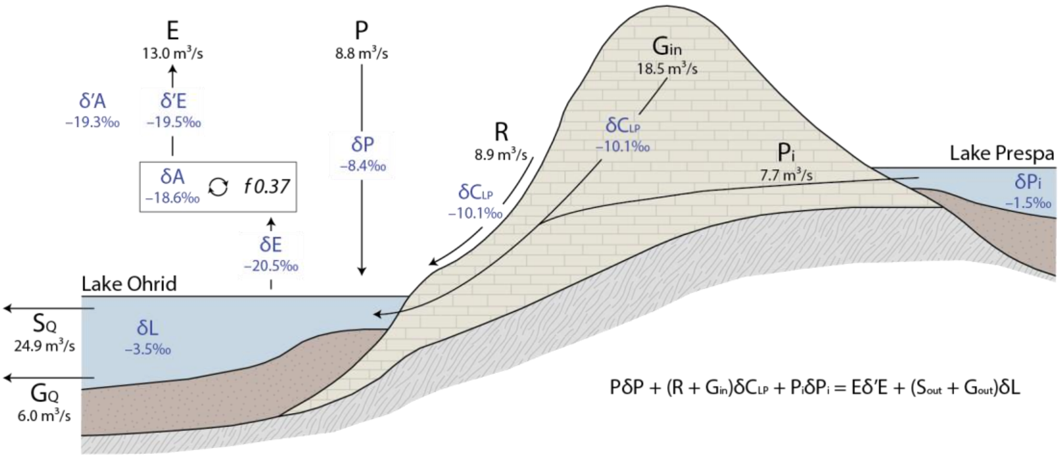

Figure 5.6 *Summary of modern hydrological and isotope mass balance for Lake Ohrid on a schematic cross-section through the Galičica mountain range, showing inputs including precipitation (P), surface inflows (R), groundwater inflow comprising a precipitation-fed component (G_{in}) and outflow from Lake Prespa (P_i), and outputs including evaporation (E), surface outflow (S_Q) and groundwater outflow (G_Q). The isotope composition of inputs and outputs includes precipitation over the lake (δP) and catchment (δC_{LP}), Prespa lake water (δP_i), Ohrid lake water (δL), atmospheric moisture (δA), and evaporation (δE). A fraction (f) of the overlying atmosphere comprises water evaporated from Lake Ohrid, modifying to isotope composition of δA ($\delta' A$) and δE (δ\`E). The isotope mass balance equation for Lake Ohrid is also given.*

CHAPTER 6 | LINI CO1262

This chapter is based on the publication: Lacey, J. H., Francke, A., Leng, M. J., Vane, C. H. & Wagner, B. 2015. A high-resolution Late Glacial to Holocene record of environmental change in the Mediterranean from Lake Ohrid (Macedonia/Albania). International Journal of Earth Sciences, 104 (6), 1623-1638.

6.1 Introduction

The "Lini" site is located approximately 2 km to the east of the Lini Peninsula in 260 m water depth, adjacent to the western shore of Lake Ohrid (41°03'56.9"N, 020°40'21.9"E; Figure 5.1). The locality was primarily selected as part of the SCOPSCO project to investigate the tectonic activity of faults bounding the western basin and sub-lacustrine landslides. Information on the sedimentary architecture of the location was obtained through hydro-acoustic and multichannel seismic surveys conducted during the period 2004 to 2009 (Reicherter et al., 2011; Lindhorst et al., 2015).

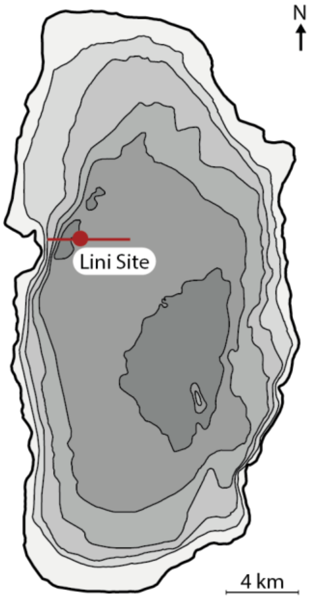

Figure 6.1 *Bathymetric map of Lake Ohrid (50 m isolines) showing the location of the 'Lini' coring site (red dot) and the path of the seismic profile in Figure 5.2 (red line).*

The multichannel seismic investigations revealed prominent high-angle normal faults and half-graben structures in front of the peninsula, in conjunction with a sedimentary infill of well-stratified layers interbedded between several Mass-Wasting Deposits

(MWD, Figure 6.2; Reicherter et al., 2011). Higher-resolution parametric echosounder profiles also indicate these structures to be present in front of the Lini Peninsula (Wagner et al., 2012b).

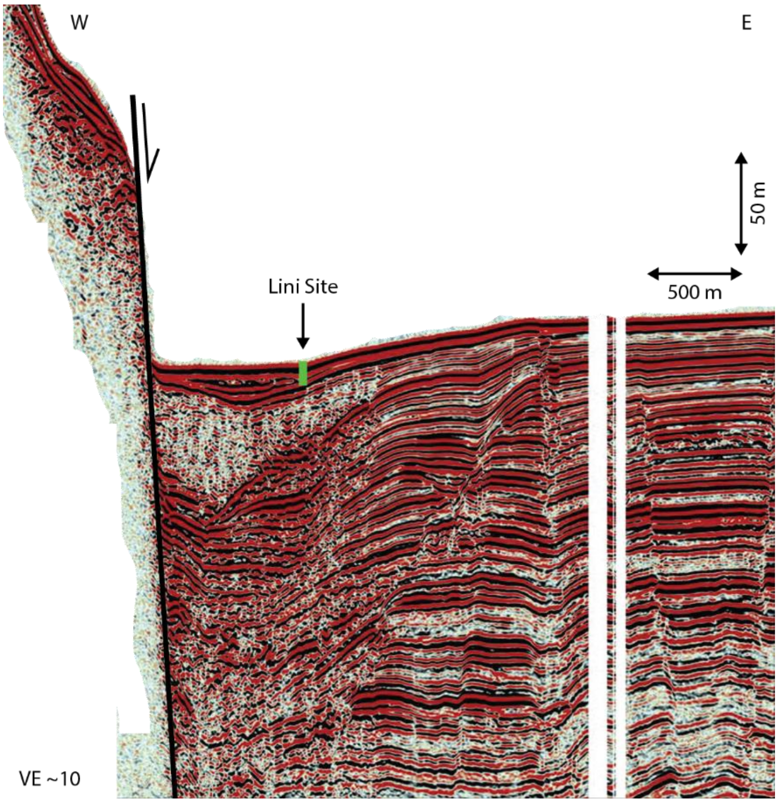

Figure 6.2 *Seismic profile taken in front of the Lini Peninsula (vertical exaggeration VE ≈ 10), showing the coring location, depth of core Co1262 (green line), the Lini fault and the sedimentary succession of horizontally-bedded sediments and several MWD (modified from Wagner et al., 2014, their figure 4).*

6.2 Core recovery

In June 2011 a ca. 10 m sediment core (Co1262) was recovered from the Lini site in 2 m long sections using a UWITEC coring system (www.uwitec.at/), operated by a team from the University of Cologne. The cores were taken from a floating platform using a gravity corer to recover undisturbed surface sediments and a percussion piston corer for deeper sediments. Core recovery approached 100% and any disturbance or loss of sediment between the individual sections is thought to be minimal (<6 cm; Wagner et al., 2014). Following recovery, the cores were split into roughly 1 m long sections and stored in darkness at 4°C. The core sections were then subsequently opened and halved lengthwise, after which one half was described macroscopically and analysed using high-resolution X-Ray Fluorescence (XRF) on an ITRAX core scanner at 2 mm resolution (Wagner et al., 2012b). The other half was divided into 2 cm segments, freeze dried and each 2 cm portion was homogenised. The Lini core was analysed for total inorganic carbon (TIC) and total organic carbon (TOC) using a DIMATOC 200, and total sulphur (TS) and total nitrogen (TN) using an elemental analyser (Wagner et al., 2012b).

6.3 Sampling

Aliquots from core Co1262 were taken in June 2012 for the analysis of the carbon isotope composition of organic matter ($\delta^{13}C_{organic}$), TOC, TN, and Rock-Eval pyrolysis (RE) from the surface to 1.19 m at every 2 cm, beneath which a 2.02 m thick MWD occurs (Wagner et al., 2012b). Aliquots were then taken at 2 cm intervals from 3.21 to 9.63 m to a second MWD (0.18 m thick), and below 9.81 m sampling continued to the base of the core at 10.05 m. The MWD material is homogenous with no significant changes in TIC or TOC content (Wagner et al., 2012b) and was not included in sampling as the horizons represent short-term events that are considered to be instantaneous. The composite sequence of undisturbed sediment is 7.85 m long.

The sediments of Co1262 were sampled for the oxygen and carbon isotope composition of calcite ($\delta^{18}O_{calcite}$ and $\delta^{13}C_{calcite}$, respectively) at the same resolution as the organic samples to 7.29 m, beneath which TIC content decreases to <0.1% (Wagner et al., 2012b), and so could not be analysed for isotopes. Aliquots were taken from a subsequent zone of higher TIC between 7.75 and 8.13 m at 2 cm resolution.

6.4 Chronology

The age model for Co1262 is based on 6 radiocarbon ages, 3 tephras and cross-correlation with previously published records from Lake Ohrid and nearby Lake Prespa. Radiocarbon dating, tephra analysis and correlation were carried out by Wagner et al. (2012b), the age model was calculated and published by Lacey et al. (2015a)[10].

---

[10] Age model was produced by Dr Bernd Wagner and Dr Alexander Francke, University of Cologne.

Radiocarbon dating has been conducted on terrestrial plant material (5 samples) and fish remains (1 sample) using accelerated mass spectrometry (AMS) at the University of Cologne Centre for AMS (Table 6.1; Wagner et al., 2012b).

Table 6.1 *Radiocarbon and calendar ages from Co1262 (Wagner et al., 2012b).*

AMS Lab ID	Depth (m)	Material	C weight (mg)	^{14}C age (yr BP)	Calendar age (cal yr BP)
COL 1251.1.1	0.17	terrestrial plant	1.00	164±20	140±145
COL 1735.1.1	4.42	terrestrial plant	0.74	2176±46	2190±140
COL 1736.1.1	5.20	terrestrial plant	0.99	3280±45	3510±110
COL 1737.1.1	5.37	terrestrial plant	0.93	3581±40	3850±130
COL 1738.1.1	5.74	terrestrial plant	1.00	4370±44	5030±190
COL 1243.1.1	7.54	fish bone	0.53	10492±37	12400±190

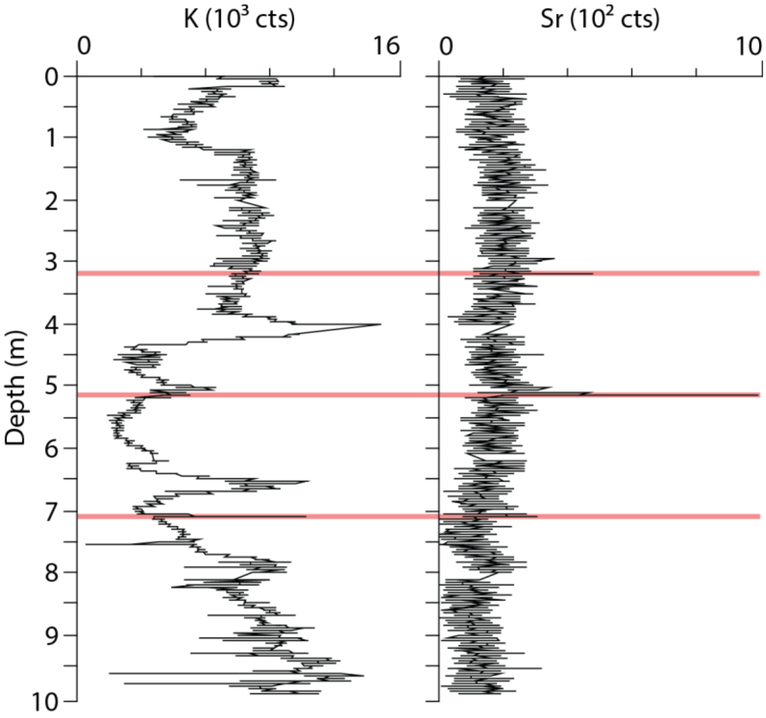

Figure 6.3 *Location of tephra in Co1262 (red bars) based on K and Sr XRF profiles (Wagner et al., 2012b).*

Conventional radiocarbon ages were converted to calendar ages (cal yr BP) using CALIB 6.1.1 (Stuiver and Reimer, 1993) and the IntCal09 dataset (Reimer et al., 2009) with an uncertainty level of 2σ. Radiocarbon dating was not applied to bulk organic matter as a reservoir effect of >1,500 years has been documented in previous Lake

Ohrid cores (Wagner et al., 2008a; Vogel et al., 2010a), due to the incorporation of old carbon (likely derived from local geological sources) that was not in equilibrium with atmospheric $^{14}CO_2$ at the time of sedimentation. In contrast to bulk measurements, terrestrial sources of organic matter are considered to provide a more robust estimate of sediment age as they are not overly influenced by the incorporation of aquatic carbon (Cohen, 2003). Tephrostratigraphic work was carried out on samples from three horizons defined by peaks in XRF data (K and Sr; Figure 6.3), and the geochemical composition of each sample was defined using energy-dispersive spectrometry (EDS) on glass shards and micro-pumice fragments (Wagner et al., 2012b).

The geochemical composition of glass shards at 7.09 m plotted on a total alkali-silica (TAS) diagram show a dominant phonolitic composition and have relatively high silica contents (>57%; Figure 6.4). A homogenous phonolitic chemistry of the glass shards indicates a correlation with the Mercato eruption from Somma Vesuvius, which was produced during its Plinian phase (Santacroce et al., 2008) and the tephra products had a predominant eastward dispersal pattern (Figure 6.5; Sulpizio et al., 2010b). This was the only central Mediterranean eruption during the Holocene and Late Pleistocene that shows this characteristic phonolitic composition (Santacroce et al., 2008).

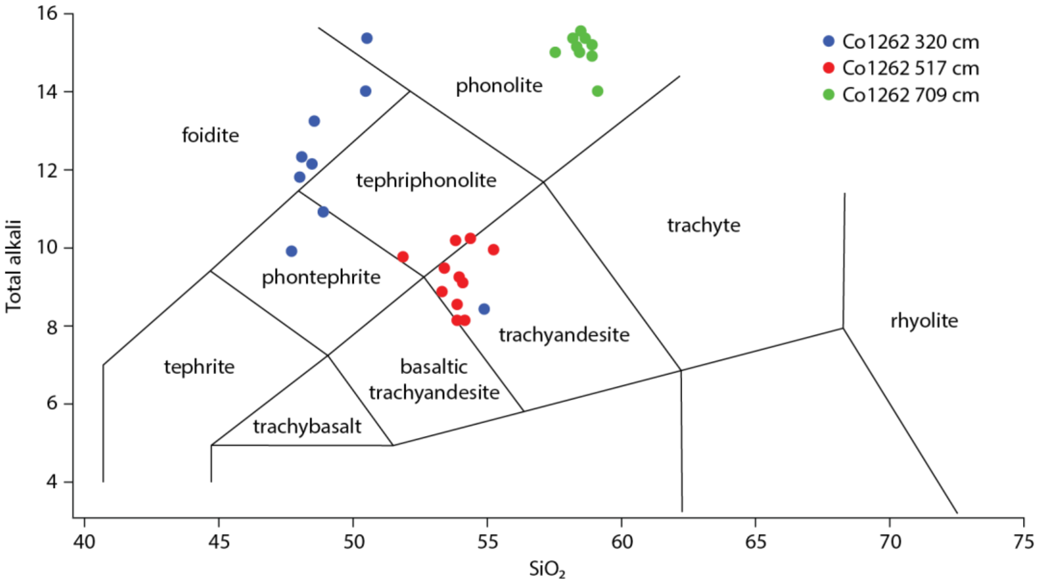

Figure 6.4 *Total alkali-silica diagram (TAS; Le Bas et al., 1986) used to classify the tephra and crypto-tephra identified in core Co1262 (after Wagner et al., 2012b).*

The tephra shows similarities to cryptotephra OT0702-3 from Ohrid core Co1202 (Vogel et al., 2010c) and to tephra PT0915-2 from Prespa core Co1215 (Damaschke et al., 2013). Radiocarbon dates have been obtained for the Mercato eruption from soil organic fractions suggesting a maximum age of 8890±90 cal yr BP (Santacroce et al., 2008), whereas Zanchetta et al. (2011) report an age of 8540±50 cal yr BP using charcoal from the base of the proximal fallout deposit. Taking into account bounding radiocarbon dates from Lake Prespa core Co1215, Damaschke et al. (2013) suggest that 8890±90 cal yr BP is perhaps a more favourable estimate for the Mercato eruption.

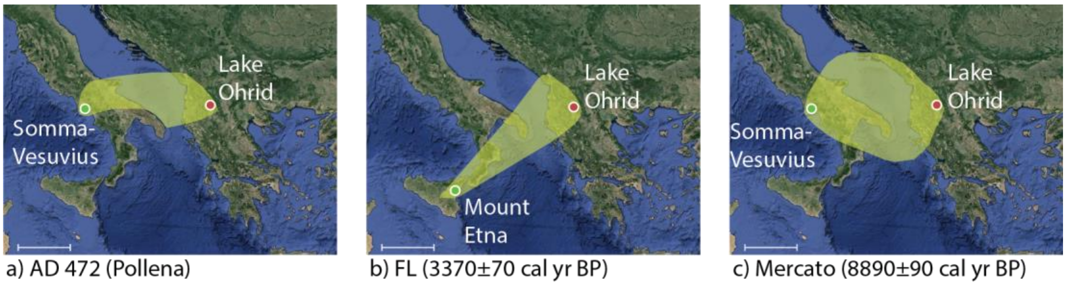

a) AD 472 (Pollena) b) FL (3370±70 cal yr BP) c) Mercato (8890±90 cal yr BP)

Figure 6.5 *Dispersal maps for the tephra layers recognised in core Co1262 (modified from Sulpizio et al., 2010b). Green dot = origin volcano, red dot = Lake Ohrid, yellow area = dispersal pattern defined by the occurrence of tephra in sediment (marine and lacustrine) records, white bar = 250 km.*

Glass shards found at 5.17 m in core Co1262 plot predominantly within the trachyandesite field on the TAS diagram (Figure 6.4). This composition is solely characteristic of fallout deposits from Mount Etna, as the volcano is the only known active source of this magma type in the central Mediterranean during the Holocene (Coltelli et al., 2000). The geochemistry can be correlated to a previously recognised tephra in Lake Ohrid core Lz1120 between 3.10-3.15 m (Wagner et al., 2008b) and cryptotephra OT0702-2 in core Co1202 (Vogel et al., 2010c), and has also been recognised in nearby Lake Shkodra (Sulpizio et al., 2010a). According to the relative age and composition of this tephra, it can be correlated to the deposits of the FL eruption of Mount Etna (NE dispersal direction; Figure 6.5) that has been radiometrically dated using charred material to 3370±70 cal yr BP (3150±60 ^{14}C yr BP; Coltelli et al., 2000).

The stratigraphically youngest tephra found in Co1262 at 3.20 m has a continuous compositional variation between phonolite and phonotephrite when plotted on the

TAS diagram (Figure 6.4). Given ^{14}C dates measured below this tephra layer, the only known source of undersaturated fallout deposits during this period in the central Mediterranean is the Somma-Vesuvius volcano (Ayusoa et al., 1998; Santacroce et al., 2008). Geochemical analysis suggests a compositional overlap between this tephra and volcanic material produced during the AD 472 (1478 cal yr BP) and AD 512 (1438 cal yr BP) eruptions (Figure 6.6; Sulpizio et al., 2005; Sulpizio et al., 2010b). The AD 472 eruption was radiometrically dated using carbonised wood from within pyroclastic material and palaeosoil beneath the flow deposits (Rosi and Santacroce, 1983), and the AD 512 eruption age is based on historical accounts (Cioni et al., 2008). The geochemistry of the two eruptions is relatively similar due to a short (40 year) age separation and having been erupted from the same magma chamber, however the geochemical composition of the AD 512 succession overlaps the mafic "tail" of the AD 472 magma (Figure 6.7; Santacroce et al., 2008).

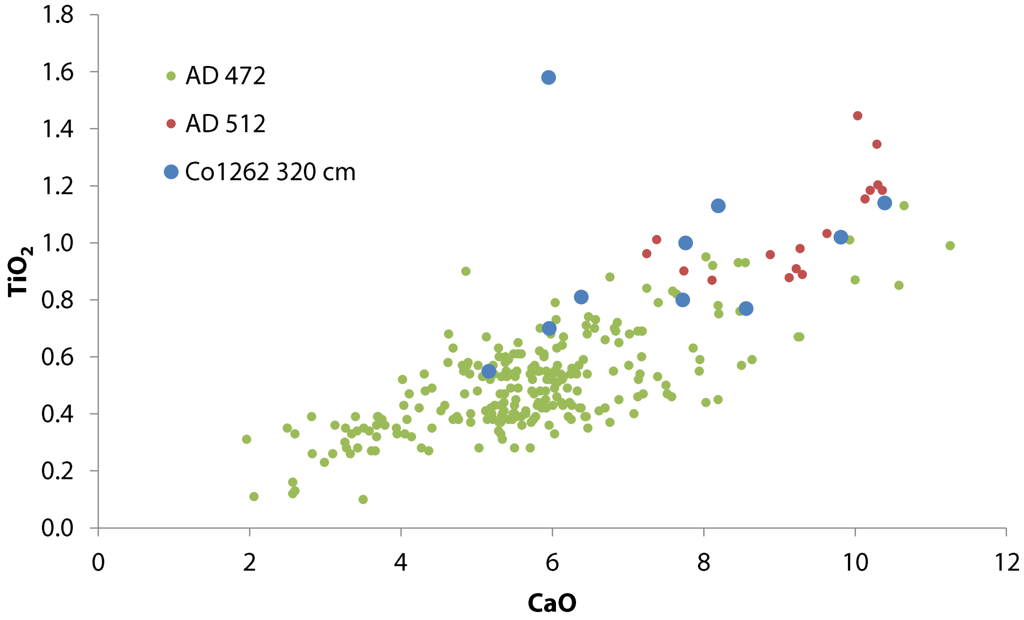

Figure 6.6 *TiO_2-CaO plot showing geochemical overlap between the 320 cm tephra in Co1262 and glass composition of proximal deposits from AD 472 and AD 512 eruptions (Santacroce et al., 2008).*

The overlap between the tephra layer in Co1262 at 3.20 m and proximal data from both the AD 472 and AD 512 successions suggests that it is not possible to discern a particular affinity to either eruption (Figure 6.7). Although a distinct eruptive source can be characterised for nearby Lake Shkodra (160 km northwest of Lake Ohrid,

Figure 6.7; Sulpizio et al., 2010a), considering the relatively low sedimentation rate in Lake Ohrid and the short time between eruptions, a mixed deposit containing both AD 472 and AD 512 tephra has been proposed for Lake Ohrid (Vogel et al., 2010c; Wagner et al., 2012b; Damaschke et al., 2013).

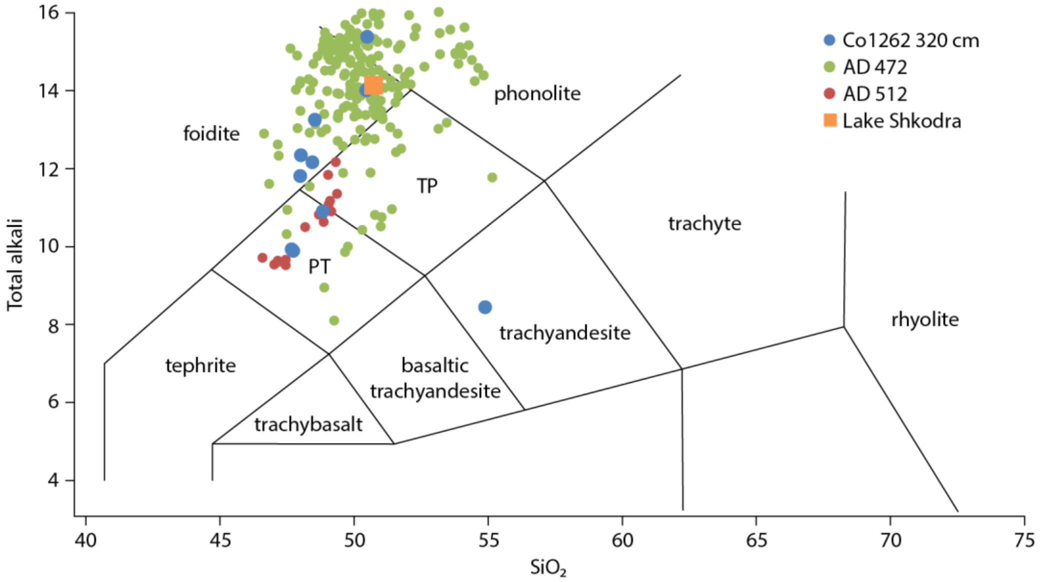

Figure 6.7 *TAS plot showing the compositional difference between AD 472 and AD 512 proximal deposits (Santacroce et al., 2008), and the relationship to the Co1262 320 cm tephra layer. The average geochemical composition of comparable tephra from Lake Shkodra clearly identify the AD 472 eruption (Sulpizio et al., 2010a).*

In previous studies of Lake Ohrid (cores Lz1120, Co1202) and Lake Prespa (cores Co1204, Co1215), TIC and TOC were shown to be highly sensitive to climate and environmental variations during the Late Glacial to Holocene (Wagner et al., 2009a; Vogel et al., 2010a; Wagner et al., 2010; Aufgebauer et al., 2012). Therefore, significant changes in these proxies can be used to correlate between sediment records and provide additional chronological control (Figure 6.8). A TOC increase in Co1262 between 9.50 m and 9.00 m is most likely coincident with the first significant TOC rise in cores Co1204 and Co1215 from Lake Prespa, which occurred at the onset of the Holocene around 11.6 ka (Wagner et al., 2010; Wagner et al., 2012a).

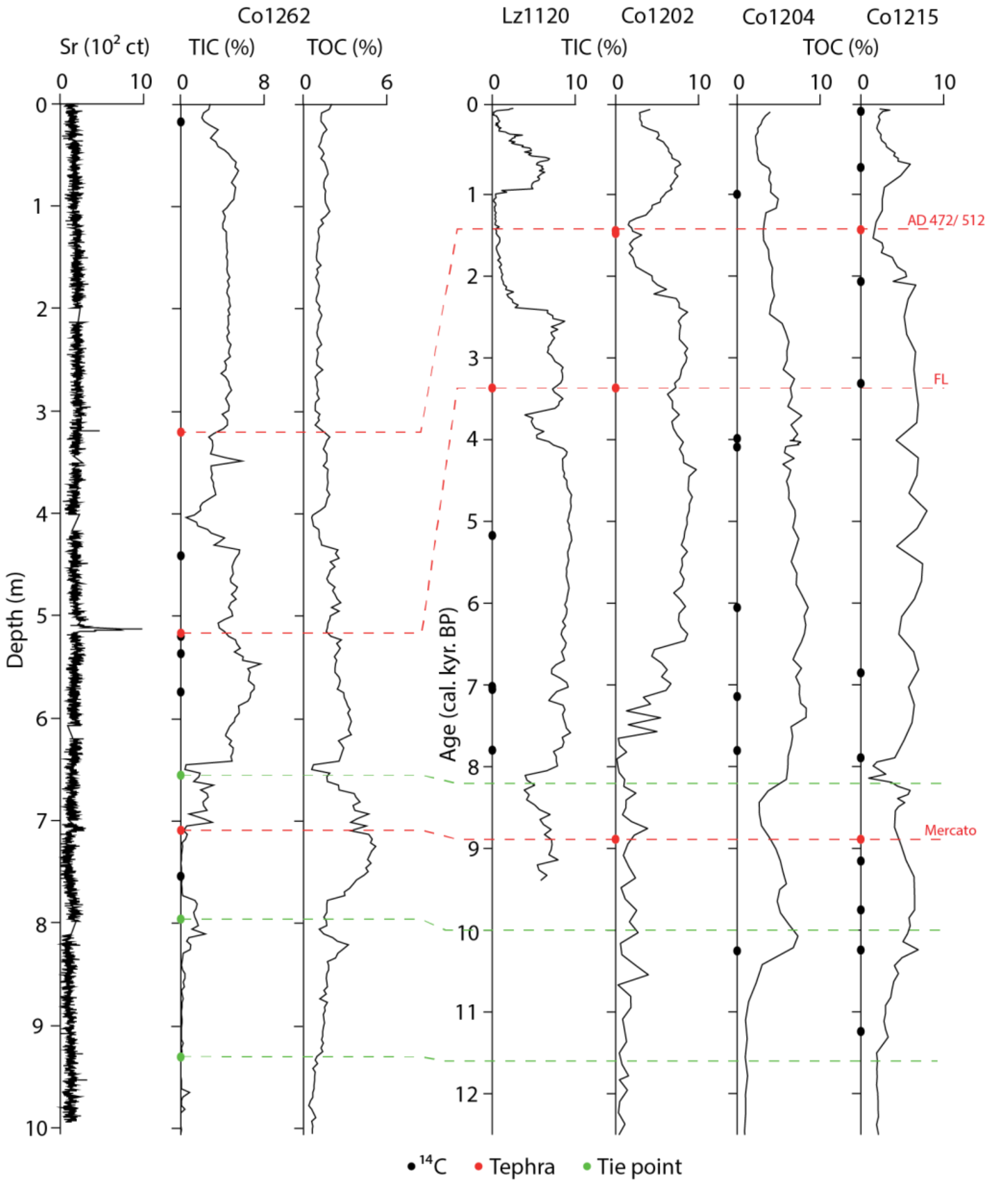

Figure 6.8 *Co1262 XRF (strontium), TIC and TOC data plotted with radiocarbon dates, tephras and cross-correlation tie points to other Lake Ohrid (Lz1120, Co1202) and Lake Prespa (Co1204, Co1215) cores (adapted from Wagner et al., 2012b).*

A peak in TIC and minimum TOC at approximately 8.00 m in Co1262 corresponds to similar variations in Lake Prespa during the period 10.5 ka to 9.5 ka (Aufgebauer et al., 2012), which is contemporaneous with a minimum in winter precipitation reconstructed from a pollen record at nearby Lake Maliq (Bordon et al., 2009). The significant decrease in both TIC and TOC (Figure 6.8), and the sharp increase in K content (Figure 6.3), around 6.55 m are most probably linked to similar fluctuations in cores Lz1120 and Co1202 from Lake Ohrid (Vogel et al., 2010a; Wagner et al., 2010) and cores Co1204 and Co1215 from Lake Prespa (Wagner et al., 2010; Aufgebauer et al., 2012). The variations observed in TIC and TOC data from these cores were correlated to the 8.2 ka cooling event, which is also assumed for core Co1262 and is chronologically consistent with the occurrence of the Mercato tephra layer at 7.09 m dated to 8.9 ka (see above).

Table 6.2 *Summary of radiocarbon dates, tephra and cross-correlation tie points used in the age model for core Co1262.*

Depth (m)	Material	^{14}C age (yr BP)	Age (cal yr BP)
0.00	Surface	-	–61.5
0.17	Terrestrial plant	164 ± 20	-
3.20	AD 472 tephra	-	1478
3.20	AD 512 tephra	-	1438
4.42	Terrestrial plant	2176 ± 46	-
5.17	FL tephra	-	3,370 ± 70
5.20	Terrestrial plant	3280 ± 45	-
5.37	Terrestrial plant	3581 ± 40	-
5.74	Terrestrial plant	4370 ± 44	-
6.55	Tie point	-	8,200
7.09	Mercato tephra	-	8,890 ± 90
7.54	Fish bone	10492 ± 37	-
7.96	Tie point	-	10,000
9.30	Tie point	-	11,600
10.05	Bottom of core	-	-

The age model was calculated using the software package CLAM v.2.2. (Blaauw, 2010), operating with the IntCal 13 calibration curve (Reimer et al., 2013), and interpolated between the radiocarbon ages, tephras and cross-correlation points using a smooth spline function (smoothing = 0.1; Figure 6.9). A smooth spline polynomial function was selected for age depth model calculations as the chronological data indicated a variable sedimentation rate is present (Table 6.2), which means simple point-to-point interpolation or linear regression is not suitable (Cohen, 2003).

MWD identified in Co1262 by Wagner et al. (2012b) are observed to be transparent and chaotic units in parametric sediment echosounder profiles and as homogenous zones in geochemical data (121.6-319.6 cm, 346-350 cm, 545-549 cm, 960-980 cm). The MWD are assumed to be instantaneous events for age model calculations and so are subtracted from the composite profile (shown as grey bars in Figure 6.9).

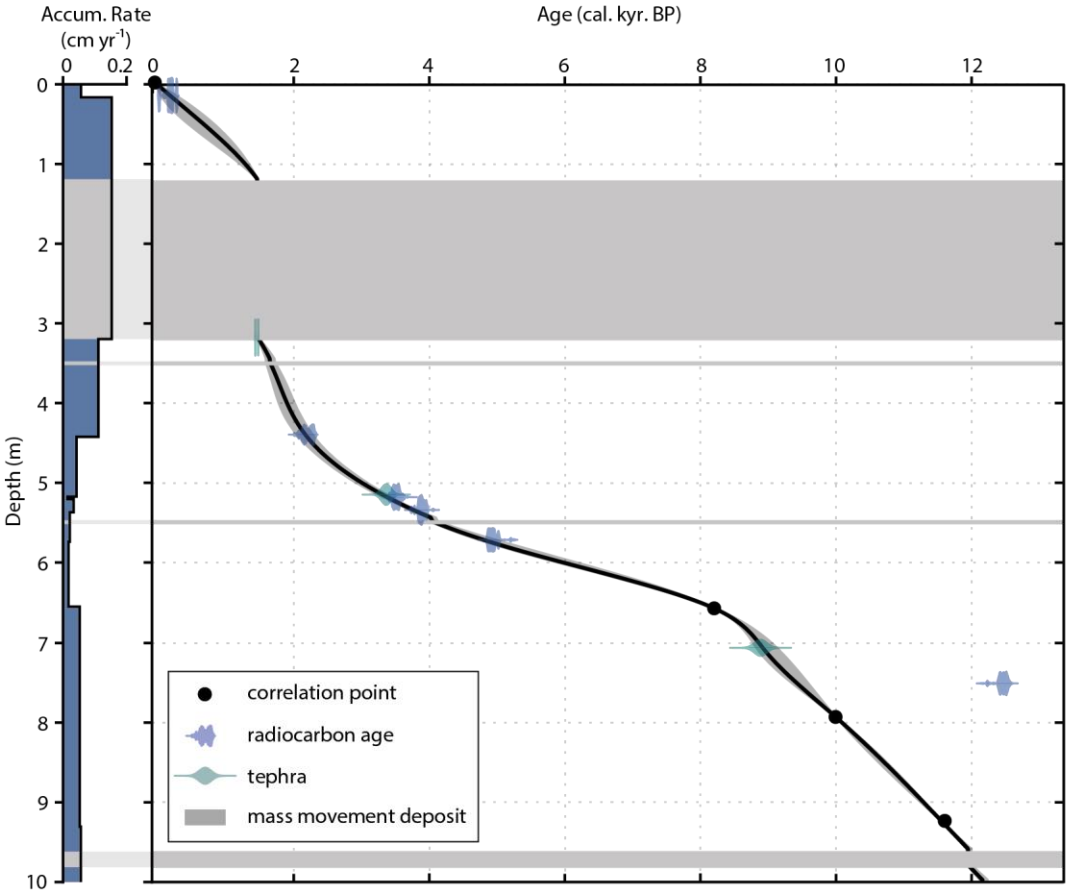

Figure 6.9 *Age-depth model for core Co1262 based on 3 tephra geochemical correlations, 6 calibrated radiocarbon ages derived from terrestrial plant and fish material, and cross-correlation of physical parameters (TIC and TOC) with previous Lake Ohrid (Lz1120, Co1202) and Lake Prespa (Co1204, Co1215) cores. Accumulation rate (cm year^{-1}) was calculated between known dates using correlated core depths. Blue radiocarbon curves represent the most probable distribution of calibrated ages. Green tephra markers display a Gaussian distribution of calibrated age error. MWD found at 1.21-3.19, 3.46-3.50, 5.45-5.49 and 9.60-9.80 cm are shown as light grey bands.*

Fish remains found at 7.54 m have a radiocarbon age of approximately 12.4 ka, which reflect an older date than expected given the Mercato tephra layer above and chronological tie points below. Such a discrepancy is most likely due to a reservoir effect, measured on bulk sediment in previous cores to be around 1.5 ka (Wagner et al., 2008a; Vogel et al., 2010a), and/or re-deposition (Wagner et al., 2012b).

The age model for core Co1262 shows a tripartite sedimentation regime, with a higher accumulation rate in the lower and upper sections (0.10 and 0.12 cm year^{-1} respectively), and reducing between 4.40 and 6.85 m to 0.05 cm year^{-1} (Figure 6.9). As accumulation rate changes through the core the continuous sample size of 2 cm will incorporate a variable temporal signal, providing a resolution (per centimetre) of roughly 20 to 40 years when sedimentation is lower, and 10 to 20 years when higher. However, any annual-scale signal is most likely overridden by bioturbation, which is prevalent in Co1262 (Wagner et al., 2012b) and is also observed in several other cores from Lake Ohrid (Wagner et al., 2009a; Vogel et al., 2010a).

6.5 Results

A total of 393 samples were analysed from core Co1262 for $\delta^{13}C_{organic}$, TOC, TN, and RE on bulk organic matter, using the methods described in Sections 4.2 and 4.3 from the sediment horizons detailed in Section 6.3. Stable isotopes from inorganic material could not be measured on samples with TIC <0.5%, therefore 280 samples were analysed for $\delta^{18}O_{calcite}$ and $\delta^{13}C_{calcite}$ using the method described in Section 4.1 on the sediment horizons defined in Section 6.3. Utilising the age model outlined above, a date has been interpolated for each individual sample depth (i.e. every 2 cm) in CLAM v.2.2 and data from core Co1262 can therefore be shown as a time series plot. Zonation of the dataset was carried out using constrained hierarchical clustering (CONISS) in R version 3.1.2 (Team, 2015) operating with the 'rioja' package (Juggins, 2015) on the results from organic analyses. The number of significant zones recognised in the sequence was determined by comparing the dispersion of the hierarchical classification to a broken-stick model using the 'bstick' function in R (Juggins, 2015), which suggests that there are 11 significant zones (Figure 6.10).

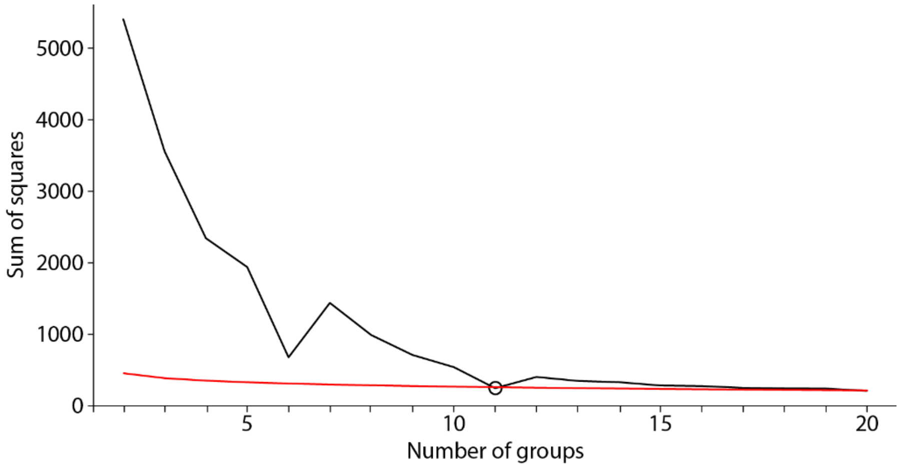

Figure 6.10 *Graphical representation of the number of significant zones in core Co1262 (circle = 11), calculated using the 'bstick' function in R operating with the 'rioja' package. The black line represents the observed data, and the red line the expected values obtained from the broken-stick model.*

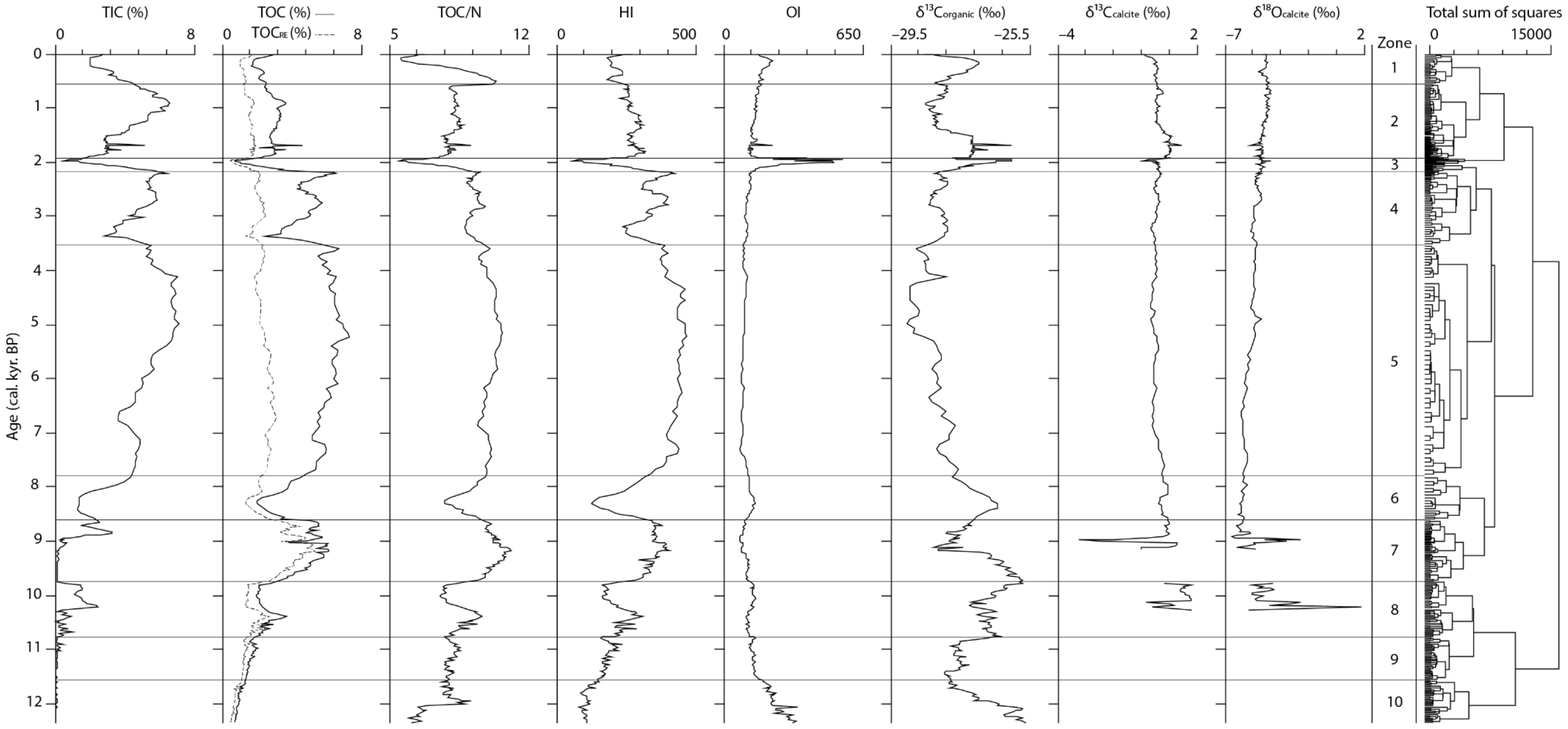

Figure 6.11 *Multi-proxy data from Co1262, including TIC, TOC (TIC-adjusted), TOC$_{RE}$ (bulk), TOC/TN, Hydrogen Index (HI), Oxygen Index (OI), $\delta^{13}C_{organic}$, $\delta^{13}C_{calcite}$, and $\delta^{18}O_{calcite}$.*

Table 6.3 *Covariation statistics for Figure 6.11 showing Pearson's correlation coefficient (bottom left section) and p-value (top right section) for each proxy, calculated using PAST 3.03 (Hammer et al., 2001). Bold values indicate a strong (>0.6) or very strong (>0.8) correlation, and red exceed the 0.1% significance level (i.e. no linear correlation is present).*

	TIC	TOC	TOC_{RE}	TOC/TN	HI	OI	$\delta^{13}C_{organic}$	$\delta^{13}C_{calcite}$	$\delta^{18}O_{calcite}$
TIC		0.000	0.530	0.000	0.000	0.000	0.000	0.001	0.937
TOC	**0.60**		0.000	0.000	0.000	0.000	0.000	0.000	0.000
TOC_{RE}	0.03	**0.75**		0.000	0.000	0.000	0.013	0.019	0.000
TOC/TN	0.33	**0.83**	**0.78**		0.000	0.000	0.000	0.000	0.000
HI	**0.63**	**0.96**	**0.71**	**0.80**		0.000	0.000	0.000	0.000
OI	-0.28	**-0.64**	**-0.62**	**-0.71**	**-0.69**		0.000	0.736	0.000
$\delta^{13}C_{organic}$	**-0.73**	-0.54	-0.13	-0.42	-0.58	0.40		0.000	0.345
$\delta^{13}C_{calcite}$	-0.21	-0.25	-0.14	-0.22	-0.25	0.02	0.46		0.011
$\delta^{18}O_{calcite}$	0.00	-0.43	-0.45	-0.39	-0.36	0.27	0.06	-0.15	

Figure 6.11 shows the multi-proxy data from Co1262 plotted against age, including TIC, TOC (TIC-adjusted), TOC_{RE} (bulk), TOC/TN, HI, OI, $\delta^{13}C_{organic}$, $\delta^{13}C_{calcite}$, and $\delta^{18}O_{calcite}$. The dendrogram resulting from the clustering analysis is plotted alongside the significant zones (two short-interval zones around 2 ka have been combined to form Zone 3 and hence there are 10 zones in total).

6.5.1 Zone 10 (12.3 ka − 11.5 ka)

Zone 10 is defined by the lowest average TOC and TIC of the record, where TIC is negligible ($\bar{x}$ = 0.1±0.0%) and TOC remains <1.4%. TOC/TN is very low (<7) until ca. 12.0 ka, after which there is a rapid (23-year) increase to values >8. HI is low throughout the zone ($\bar{x}$ = 110.7±17.8) and starts to increase toward the upper boundary with Zone 9 and OI is initially high ($\bar{x}$ = 246.3±45.0) but steadily decreases over the zone. $\delta^{13}C_{organic}$ is high for the first ca. 0.3 ka of Zone 10 (>−26.3‰) and then decreases through to 11.5 ka (<−27.8‰). The lack of calcite in this zone is prohibitive for stable isotope analysis, meaning $^{18}O/^{16}O$ and $^{13}C/^{12}C$ could not be measured.

6.5.2 Zone 9 (11.5 ka − 10.8 ka)

TIC remains low throughout Zone 9 ($\bar{x}$ = 0.1±0.1%) and TOC increases through the zone from 1.3 to 1.7% ($\bar{x}$ = 1.6±0.2%). Following the sharp increase in TOC/TN in Zone 10, values stay reasonably constant through Zone 9 ($\bar{x}$ = 8.1±0.3%) apart from a small decrease nearing the upper boundary after 10.9 ka. HI increases through the zone to a maximum of 240 at 10.9 ka, after which a short-term decrease occurs as with TOC/TN. OI continues to decrease after the boundary with Zone 10, and in opposition to HI and TOC/TN increases slightly at the boundary with Zone 9. $\delta^{13}C_{organic}$ shows relatively low values through the zone ($\bar{x} = -27.6\pm0.2$‰), however there is a large increase at the boundary with Zone 9 to values approaching those seen prior to ca. 12.0 ka. As TIC remains negligible, $\delta^{18}O_{calcite}$ and $\delta^{13}C_{calcite}$ could not be measured for Zone 9.

6.5.3 Zone 8 (10.8 ka − 9.7 ka)

A small increase in TIC after 10.8 ka is followed at 10.2 ka by a transition to higher values (up to 2.5%) for ca. 0.5 ka, and then a return to very low TIC at the boundary with Zone 7 around 9.7 ka. A simultaneous increase in TOC, TOC/TN and HI occurs between 10.8 ka and 10.4 ka, after which values decrease through to 9.8 ka. These proxies then show a rapid increase across the boundary with Zone 7. OI remains fairly constant ($\bar{x} = 126.0\pm13.5$) and shows a slight increase between 10.3 ka and 9.7 ka. $\delta^{13}C_{organic}$ is around −26.7‰ until ca. 10 ka and then transitions to more positive values, reaching a maximum (−25.7‰) at the Zone 8/7 boundary at 9.7 ka. The preservation of TIC between 10.2 ka and 9.7 ka allowed for stable isotope analysis of calcite. $\delta^{18}O_{calcite}$ and $\delta^{13}C_{calcite}$ show the highest average values of the record ($\bar{x} = -4.0\pm1.7$‰ and $\bar{x} = 1.2\pm0.6$‰, respectively), and there is a distinct spike to higher $\delta^{18}O_{calcite}$ and lower $\delta^{13}C_{calcite}$ centred around 10.2 ka.

6.5.4 Zone 7 (9.7 ka − 8.6 ka)

TIC is low until around 9.1 ka, at which point there is a significant increase up to values of 3.3%. TOC increases from Zone 8 and remains relatively high throughout Zone 7 ($\bar{x} = 5.1\pm0.8$%), reaching a maximum peak of 6.1% between 9.2 ka and 9.1 ka. TOC/C and HI follow a similar trend to TOC, with values increasing to a peak after 9.2 ka (11.2 and 405.0, respectively), after which TOC/TN and HI decrease toward 8.6 ka and the boundary with Zone 6. OI remains very low ($\bar{x} = 98.1\pm13.8$) throughout the zone. $\delta^{13}C_{organic}$ decreases to a minimum at 9.1 ka (−28.3‰) and subsequently increases toward the upper boundary at 8.6 ka. A prominent rapid excursion to higher

$\delta^{18}O_{calcite}$ and lower $\delta^{13}C_{calcite}$ occurs around ca. 9.0 ka, following which both proxies show less variability and more consistent values.

6.5.5 Zone 6 (8.6 ka − 7.8 ka)

Zone 6 is characterised by an excursion centred on 8.2 ka to lower values across TIC, TOC, TOC/TN, and HI, and to higher values in OI and $\delta^{13}C_{organic}$. Following this minimum point (or maximum for OI and $\delta^{13}C_{organic}$), all proxies show the opposite trend to that proceeding 8.2 ka. $\delta^{18}O_{calcite}$ and $\delta^{13}C_{calcite}$ remain stable and similar to values seen at the end of Zone 7 ($\bar{x}$ = −5.9±0.1‰ and $\bar{x}$ = 0.6±0.1‰, respectively).

6.5.6 Zone 5 (7.8 ka − 3.5 ka)

Subsequent to 7.8 ka, TIC, TOC, TOC/TN and HI are all high and reach a maximum between 5.4 ka and 4.0 ka, whereas OI and $\delta^{13}C_{organic}$ are both low and reach a concurrent minimum. TIC, TOC, and HI show maximum average values for the whole record, and OI and $\delta^{13}C_{organic}$ show minimum average values. A reversal to lower values, or higher values for OI and $\delta^{13}C_{organic}$, occurs after 4.0 ka where proxies decrease (or increase) to the boundary between Zone 5/4. $\delta^{18}O_{calcite}$ and $\delta^{13}C_{calcite}$ show a steady transition to higher and lower values through Zone 5, respectively, and there is a short-term transition to lower $\delta^{13}C_{calcite}$ and higher $\delta^{18}O_{calcite}$ between 5.0 ka and 4.8 ka.

6.5.7 Zone 4 (3.5 ka − 2.2 ka)

A pronounced excursion to lower values in TIC, TOC, TOC/TN, and HI occurs around 3.3 ka, which is concomitant with a transition to higher $\delta^{13}C_{organic}$. Following 3.3 ka, TIC, TOC, TOC/TN and HI increase and $\delta^{13}C_{organic}$ decreases through to 2.7 ka, after which there is a second, lesser magnitude excursion to lower values (higher for $\delta^{13}C_{organic}$) centred around 2.5 ka. There is a subsequent increase in TIC, TOC, TOC/TN and HI, and decrease in $\delta^{13}C_{organic}$ toward the boundary with Zone 3. OI remains low but increases through Zone 4 ($\bar{x}$ = 114.9±10.1), from 95 at 3.5 ka to ca. >125 after 2.5 ka, with minor peaks at 3.3 ka and 2.5 ka. $\delta^{18}O_{calcite}$ and $\delta^{13}C_{calcite}$ remain stable through Zone 4 ($\bar{x}$ = −5.0±0.2‰ and $\bar{x}$ = 0.3±0.1‰, respectively), however there is a distinctive transition to higher $\delta^{18}O_{calcite}$ after 2.8 ka with a peak of ca. −4.6‰ between 2.7 ka and 2.6 ka. A similar trend is also observed in $\delta^{13}C_{calcite}$, which has a transition to marginally lower values at 2.5 ka, before reaching a peak of +0.5‰ at 2.2 ka.

6.5.8 Zone 3 (2.2 ka − 1.9 ka)

Zone 3 is defined by a major excursion across all organic proxies to values that appear to be consistent with those occurring within Zone 10. The excursion in centred around 2.0 ka, at which point TIC, TOC, TOC/TN and HI show minimum values after a decline from the boundary with Zone 4 at 2.2 ka. OI displays a more complex pattern of variation by having three distinct peaks between 2.0 ka and 1.9 ka, although the highest peak is coincident with minima in TIC, TOC, TOC/TN and HI. $\delta^{13}C_{organic}$ shows a distinct transition to higher values until 2.0 ka, after which there is a sharp decline back to lower values. $\delta^{13}C_{calcite}$ is inversely correlated with $\delta^{13}C_{organic}$, and shows little variation until a decrease to lower values just after 2.0 ka. There is a short-term peak to higher $\delta^{18}O_{calcite}$ immediately following 2.0 ka.

6.5.9 Zone 2 (1.9 ka − 0.5 ka)

Following an increase from the end of Zone 3, TIC is constant around 2.9% between 1.8 ka and 1.5 ka (apart from two spikes that are most likely associated with MWD) and then increases to a peak of 6.6% at 0.9 ka. TOC shows a similar trend to TIC, however does not display the same magnitude of variability, only increasing to a minor peak at 0.9 ka. TOC/TN show little variation in Zone 2 ($\bar{x}$ = 8.2±0.4), staying constant at 8 until 1.5 ka, increasing slightly to 8.3 between 1.5 ka and 0.7 ka, and increasingly rapidly to >10 at the border with Zone 1. Two increases in HI centred around 1.8 ka and between 1.4 ka to 1.1 ka are followed by lower values (ca. 255) until the border with Zone 1. OI increases through Zone 2 from ca. 115 at 1.8 ka to ca. 180 at 0.5 ka, with a prominent spike to higher values (>230) at 1.7 ka. $\delta^{13}C_{organic}$ shows little variation until 1.5 ka (apart from the two spikes also seen in TIC data) having a value around −27.0‰, and then decreases to around −28.0‰ between 1.4 ka and 0.5 ka. The same pattern of variation is also seen in $\delta^{13}C_{calcite}$, with a transition from values around 0.8‰ until 1.5 ka, to values around 0.3‰ between 1.4 ka and 0.5 ka. $\delta^{18}O_{calcite}$ has high average values in Zone 2 ($\bar{x}$ = −4.4±0.3‰) and shows a gradual transition from around −4.7‰ at 1.9 ka up to −4.1‰ at 0.5 ka (apart from a spike to lower values at 1.7 ka).

6.5.10 Zone 1 (0.5 ka − Present)

TIC and TOC decrease in the initial 0.3 ka of Zone 1 to reach a minimum (2.0% and 1.7%, respectively) between 0.2 ka and 0.1 ka, and then begin to increase (TOC > TIC) over the last 100 years. TOC/TN follows a similar trend, however decreases to a minimum of 5.6 nearer to 0.1 ka and then starts to increase in the last 100 years. HI decreases to a minimum of 180 between 0.5 ka and 0.4 ka, increases to a peak of 241 between 0.4 ka and 0.3 ka, and shows a recent increase similar to TIC and TOC. OI and $\delta^{13}C_{organic}$ increase steadily between 0.5 ka and 0.1 ka, and then decrease more rapidly over the last 100 years. $\delta^{13}C_{calcite}$ shows little variation between 0.5 ka and 0.1 ka, and then decreases to present, whereas $\delta^{18}O_{calcite}$ shows a distinct decline to lower values between 0.4 ka and 0.3 ka.

6.6 Discussion

6.6.1 Sources of organic matter in the Lake Ohrid sedimentary record

The OM contained within lake sediments represents past changes in productivity, catchment vegetation, and the amount of particulate and dissolved material transferred to the lake, as well as degradation and dilution effects resulting from differing abundances of inorganic components (Section 3.4; Meyers and Teranes, 2001). OM consists of a compound mixture of lipids, carbohydrates and proteins, amongst other constituents, produced by organisms that lived both within the lake and in the surrounding catchment (Meyers, 2003). The geochemical composition of sedimentary OM is a direct function of the environment of formation, which imparts a characteristic source signature that enables assessment of the aquatic and terrestrial contribution to sedimentary OM. Organic geochemical analysis, including TOC/TN, RE, and $\delta^{13}C_{organic}$ are used here to estimate the origin of OM and ultimately establish the environmental significance of changes in organic sedimentation (Talbot and Livingstone, 1989; Meyers and Teranes, 2001).

6.6.1.1 TOC, TN, and TOC/TN

TOC/TN ratios of bulk OM are frequently used to distinguish the primary source of OM to lake sediments, typically differentiated by the characteristic composition of vascular and non-vascular plants (Section 3.4). In general, aquatic plants have low

TOC/TN (<10) and terrestrial plants high TOC/TN (>20) (Meyers and Teranes, 2001), with macrophytes occupying intermediate values (13-18, measured at Lake Ohrid; Holtvoeth et al., 2015). TOC/TN for Co1262 is low overall (mass ratio x̄ = 8.8±1.2), ranging from 5.5 to 11.2 (weight ratio x̄ = 10.2±1.4, range 6.5 to 13.0), which suggests a predominantly algal OM source (Meyers and Teranes, 2001). Therefore, higher TOC and overall low TOC/TN most likely reflect periods of enhanced primary productivity in Lake Ohrid (Francke et al., 2015), which are observed to correspond to high biogenic silica contents (Vogel et al., 2010a) and an increase in the amount of diatom frustules (Wagner et al., 2009a; Zhang et al., 2015). Higher TOC and productivity require elevated temperatures and a sufficient nutrient supply to surface waters, which are delivered by river and karst inflows, as well as by nutrient recycling at the lake bottom (Matzinger et al., 2006b). Greater OM accumulation in sediments could also be due to enhanced preservation and less oxidation at the sediment surface as a result of reduced mixing of the water column encouraging the onset of anoxic conditions (Wagner et al., 2009a). Conversely, low aquatic OM accumulation may be promoted by improved lake water mixing and oxic bottom water conditions, which limit phosphorous recycling from surface sediments and promote bacterial activity and OM decomposition (Wagner et al., 2009a; Francke et al., 2015).

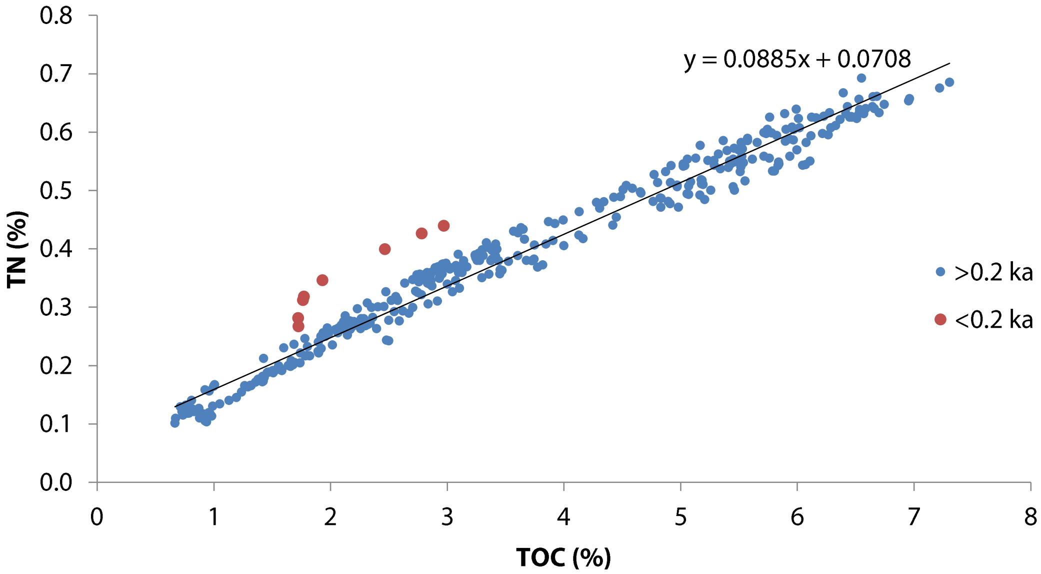

Figure 6.12 *Plot of TOC and TN, showing a linear trendline (r^2 = 0.98) and the equation of the regression line between 12.3 ka and 0.2 ka (blue dots). TOC and TN after 0.2 ka are indicated by red dots.*

A strong linear correlation exists between TOC and TN during 12.3 ka to 0.2 ka (r^2 = 0.98, p = <0.001, n = 369; Figure 6.12), which indicates that higher TN concentrations are a direct function of nitrogen-rich OM supply. After 0.2 ka, TOC and TN data fall above the linear regression line and concentrations of TN show a greater increase relative to TOC, most probably due to anthropogenic activity and recent eutrophication (Matzinger et al., 2007). The positive intercept of the regression line with the TN axis at 0.07% (where TOC = 0%; Figure 6.12) suggests that, in the absence of OM, a fraction of inorganic nitrogen (N_{in}) must be present.

The most likely source of N_{in} to the sediments of Co1262 is from the clay fraction of mineral soils, as ammonium (NH_4^+), in particular, can bind to clay minerals (Section 3.4.1; Meyers, 1994). Soil OM measured to the southeast of Lake Ohrid is reported to have low TOC/TN of around 11-12, which is likely due to enhanced NH_4^+ levels (Holtvoeth et al., 2015). Moreover, given the deep location of the Lini site away from any major inlets, the location may have received a greater quantity of finer material with a larger proportion of high N_{in} (lower TOC/TN) clay minerals due to hydrodynamic sorting (Meyers, 1997).

Hence, in Lake Ohrid, higher TOC, TN, overall low TOC/TN are most likely a function of enhanced aquatic productivity and/or restricted lake water mixing promoting anoxic bottom water conditions and less oxidation of OM. During periods of enhanced mixing, low TOC/TN may also result from higher N_{in} concentrations due to enhanced clay-bound NH_4^+ supply from the catchment, which is supported by K intensity data obtained from high resolution XRF scanning (Figure 6.13; Wagner et al., 2012b).

Variations in the clastic matter content of sediments is thought to be related to K intensities, where high K typically correlates to enhanced clastic matter supply (Cohen, 2003), and can therefore provide information on past variations in sedimentological composition and catchment denudation rates (Francke et al., 2015). High K content in the Co1262 sediments has a broad negative correlation to TOC/TN, and generally occurs where the sediments contain very little OM or $CaCO_3$ (Figure 6.13), suggesting clastic supply is typically higher when within-lake productivity is low and/or when there is more frequent lake water overturn, mixing, and bottom water oxidation.

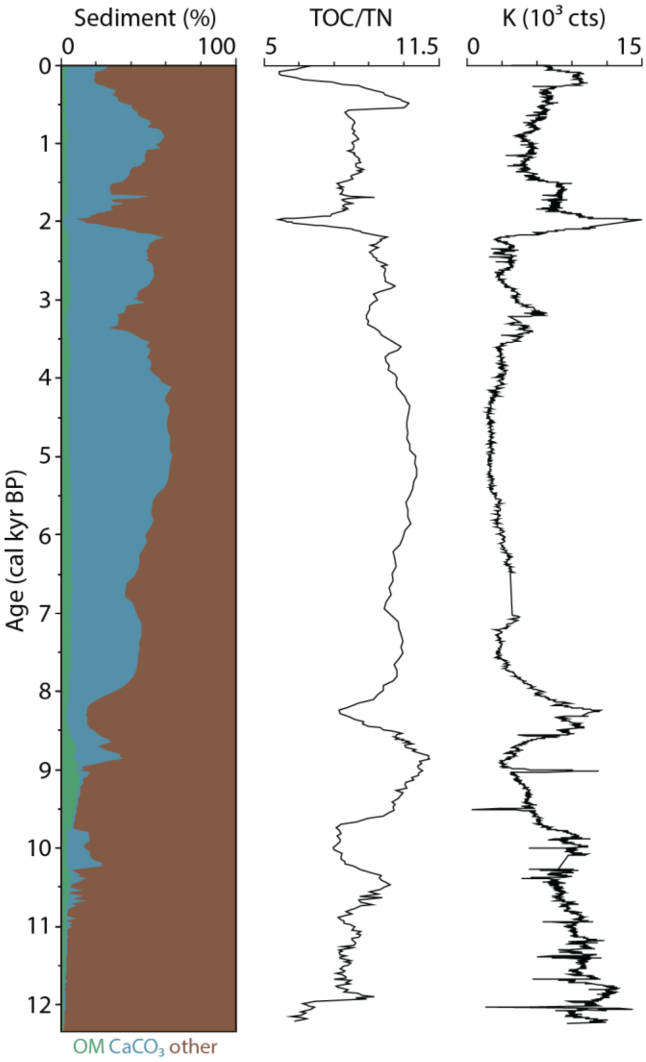

***Figure 6.13** Sediment composition of Lini Co1262 (OM calculated from TOC*2, $CaCO_3$ calculated from TIC*8.33, ‘other’ calculated as the resultant fraction), TOC/TN and K.*

6.6.1.2 Rock-Eval Pyrolysis

The relative contribution of aquatic and terrigenous material to lacustrine sediments can also be evaluated using RE, which separates OM into carbon fractions based on differences in thermal lability (see Section 3.4.3; Hare et al., 2014). The proportion of pyrolisable carbon (PC; or labile OM) comprises three major fractions: S1 (free volatile hydrocarbons), S2 (hydrocarbons produced during thermal cracking of OM) and S3 (CO and CO_2 released during thermal cracking of oxygen-bearing OM) (Sanei et al., 2005). A residual carbon (RC) fraction typically contains resistant and refractory compounds mainly derived from terrigenous plant material (Carrie et al., 2012). These primary fractions can be combined with TOC_{RE} to determine the Hydrogen Index (HI; $S2/TOC_{RE}*100$) and Oxygen Index (OI; $S3/TOC_{RE}*100$), which correlate with H/C and O/C ratios and thus provide important evidence for the elemental composition of OM (Espitalie et al., 1985; Disnar et al., 2003).

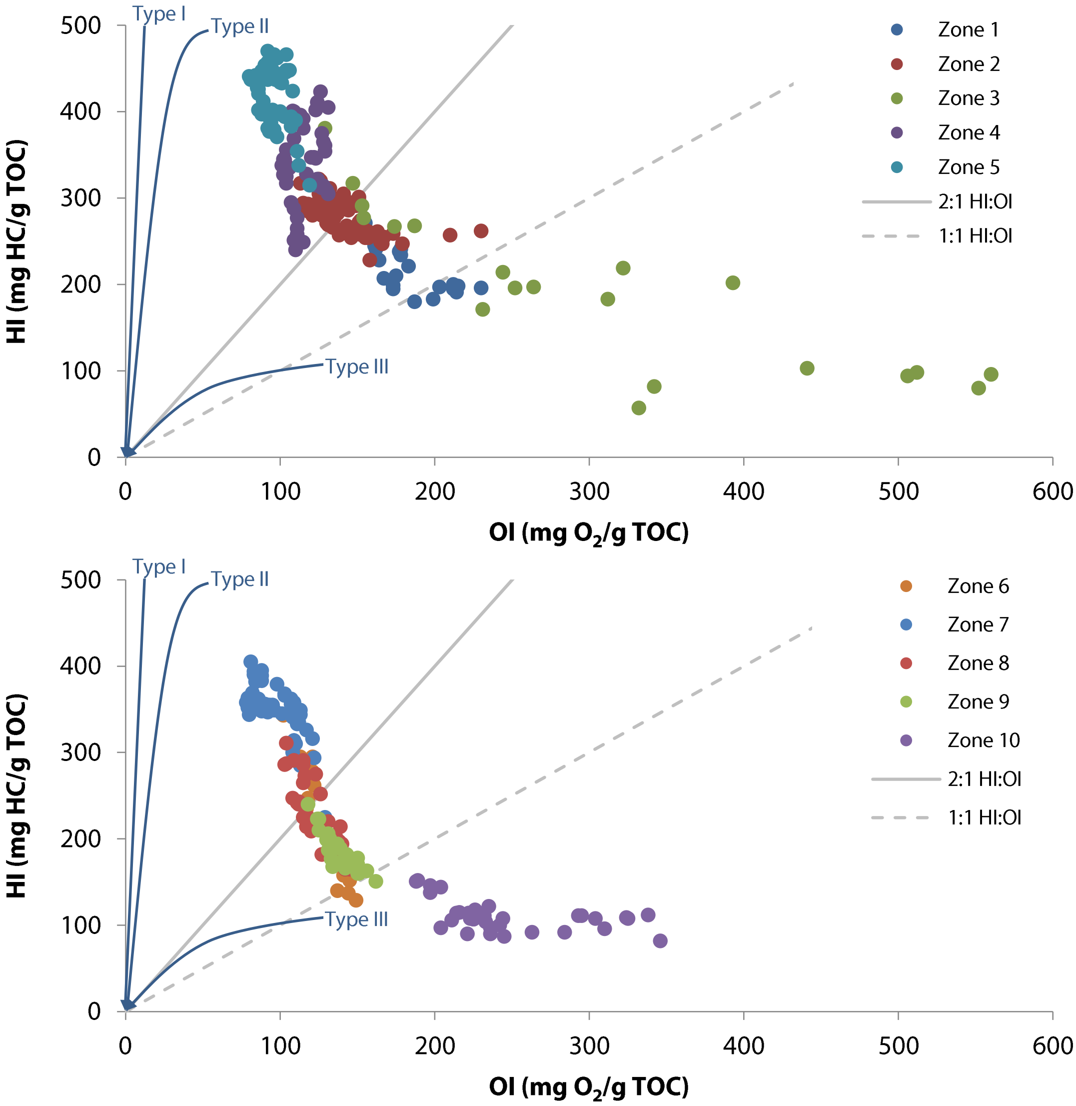

Figure 6.14 *Rock-Eval modified van Krevelen diagram of HI and OI for all Co1262 zones, showing HI/OI = 2 and HI/OI = 1 and thermal alteration pathways for OM Types I, II, and III.*

Three main types of OM are distinguished using a HI-OI van Krevelen-type diagram (Types I, II, III), where Type I sediments are characterised by hydrocarbon-rich material from microbial biomass or waxy land plants, Type II are typically derived from algal OM, and Type III from woody plant material (Meyers and Teranes, 2001). The data from Co1262 predominantly show Type II OM, which fall on a curve of changing OI towards lower HI and higher OI (Type III) suggesting a differential amount of oxidation either as a product of source changes and/or degradation (Figure 6.14). Although the majority of the data can be ascribed to Type II OM, there are evidently down-core variations as each zone is partially offset from the previous. There is a clear and well constrained transition from Zone 10 through to Zone 7, going from high OI-low HI to high HI-low OI sediments. A reverse pattern is observed for Zones 5 to 1, with a transition back to ‘Zone 10-type’ sediments in Zone 3.

The ratio of HI:OI, >2 associated with fresh aquatic material (Carrie et al., 2012) and <2 with fresh terrigenous plant litter (Disnar et al., 2003), suggests where HI is greater than ca. 240 the sediments mainly comprise aquatic OM (Figure 6.14). High HI:OI (>2) is observed over much of the Co1262 sequence (Figure 6.15). Significant excursions to lower HI:OI may potentially be linked to periods of enhanced terrestrial input from either OM with originally low HI:OI and/or degraded material.

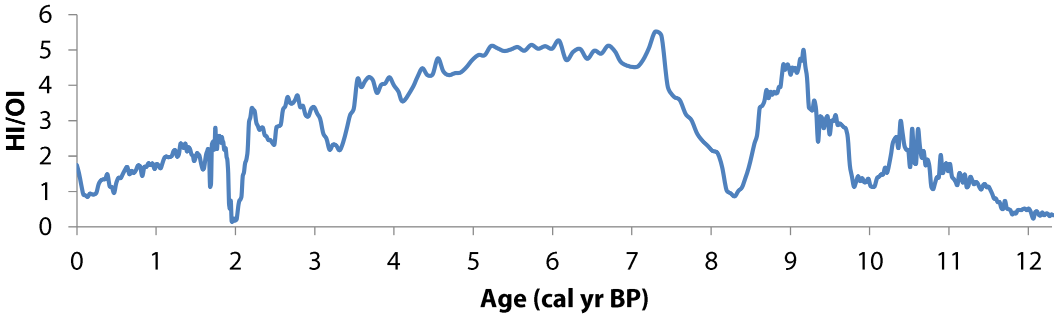

Figure 6.15 *Ratio of HI:OI plotted against age.*

In addition, analysis of soil OM from a variety of ecosystems has shown that HI decreases whilst OI increases under greater degradation and with longer residence times prior to deposition (Disnar et al., 2003), inferring that periods of enhanced soil input may also be partly responsible for zones of low HI:OI (for example at ca. 10, 8, 2 ka; Figure 6.15). The variation of HI:OI shows a strong positive covariation ($r^2 = 0.69$, $p < 0.001$) with TOC/TN (Figure 6.16), suggesting the zones of potential terrigenous input comprise lower TOC/TN. Figure 6.16 also highlights Zone 1, in accordance with Figure 6.12, to fall away from the general trend line and show low HI:OI and greater variation in TOC/TN.

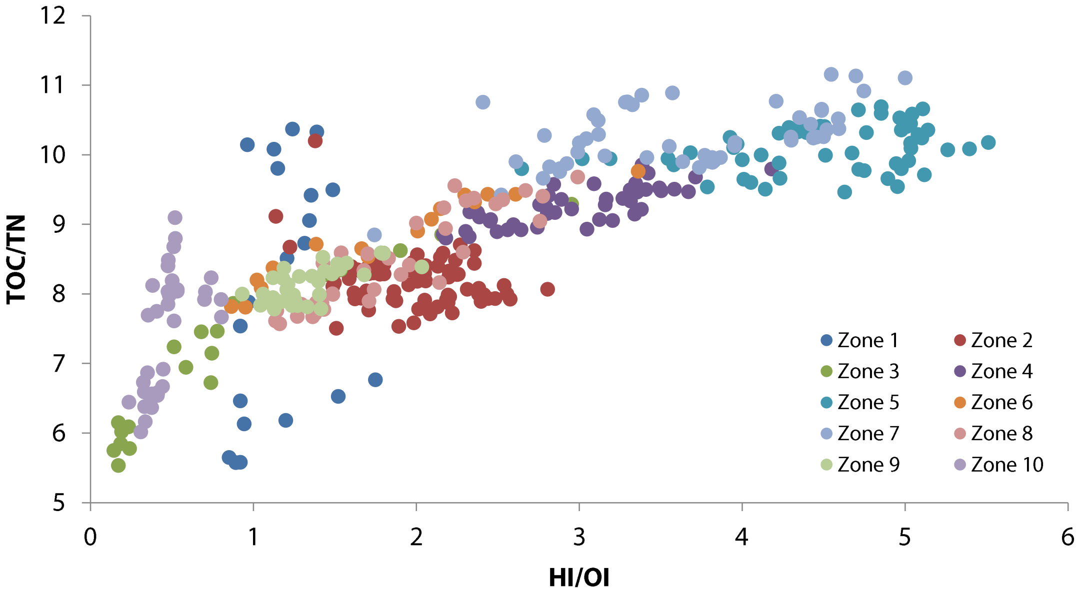

Figure 6.16 *Plot of TOC/TN and HI/OI showing ratios for each Co1262 zone.*

HI values can be subject to a matrix-effect, especially in clay-rich samples (due to highly reactive surfaces and associated adsortion; Ariztegui et al., 2001), whereby a proportion of the hydrocarbons generated during thermal cracking are retained by the matrix (Langford and Blanc-Valleron, 1990). This process leads to lower S2 values and therefore can directly influence HI (S2 normalised to TOC content). A graph of S2 against TOC_{RE} can potentially eliminate this problem and can be used to evaluate and classify OM components (Langford and Blanc-Valleron, 1990; Ariztegui et al., 2001). When S2:TOC_{RE} is plotted the samples define a linear regression line with a very strong positive correlation ($r^2 = 0.93$, $p < 0.001$; Figure 6.17). The boundaries between organic matter types in Figure 6.17 are defined as HI = 700 (70 wt. % hydrocarbon) for between I/II and as HI = 200 (20 wt. % hydrocarbon) for II/III (after Langford and Blanc-Valleron, 1990).

The majority of the Co1262 samples can be characterised as Type II OM, as with the HI:OI diagram (Figure 6.14), and zones 6, 9, 10 can be characterised as Type III OM (Figure 6.18). A transition from Type II to III OM is observed to only occur at low TOC_{RE} and S2 values (<1.8%; Figure 6.18), which suggests periods of low TOC are either accompanied by a change to hydrocarbon-poor sediments or dominated by degradation (or retention) processes.

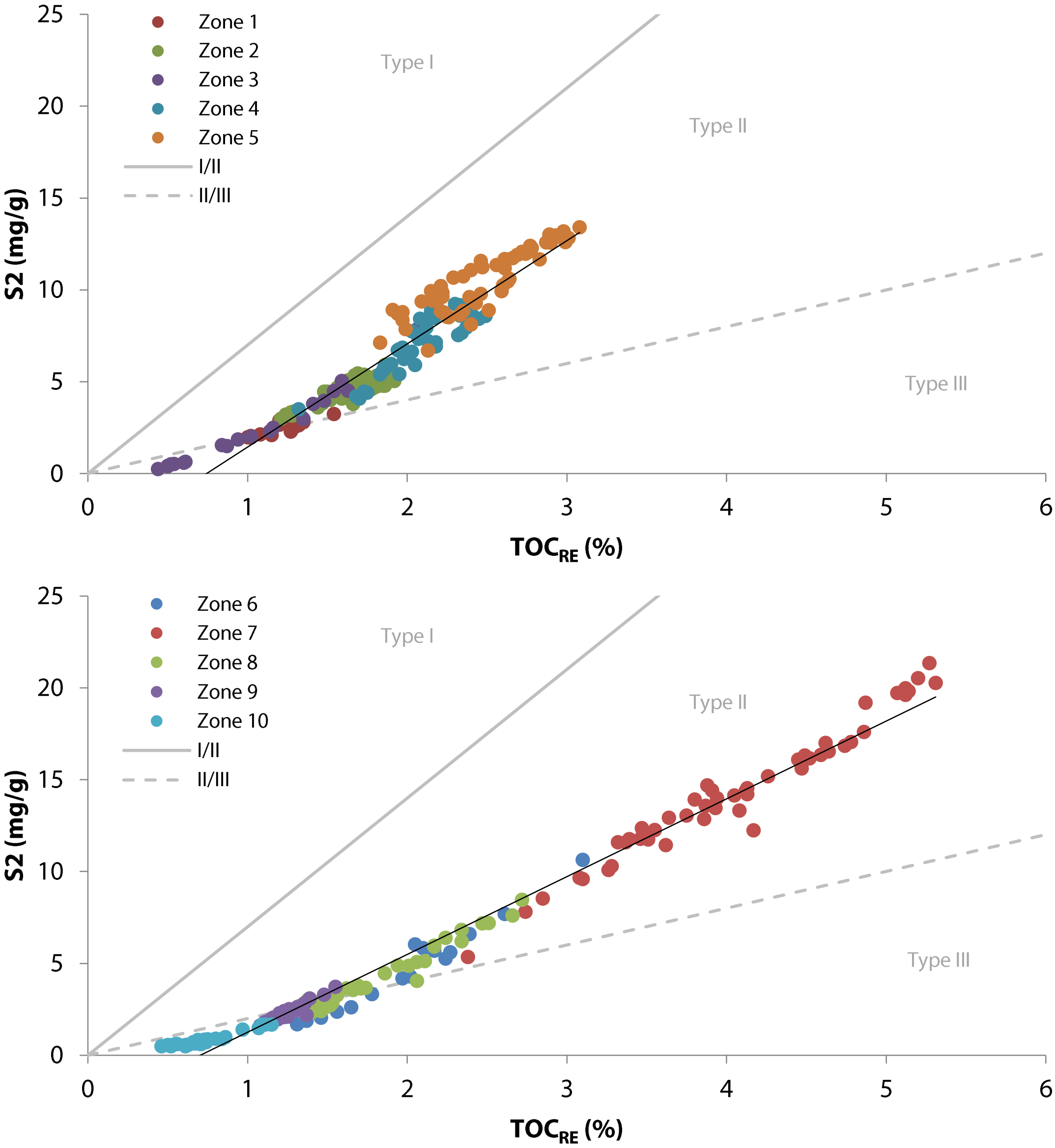

***Figure 6.17** Rock-Eval modified van Krevelen diagram of S2 and TOCRE for Co1262, showing the boundaries of OM types (grey lines; see text) and the linear regression for each group of included zones (black lines).*

A regression line fitted to the S2:TOCRE data should intercept at the origin (i.e. 0,0), as a minor concertation of hydrocarbons should be contained within OM even when low TOC concentrations are present. If there is a positive x-axis intercept, a threshold of OM (with a given HI) must be exceeded before hydrocarbons are released during pyrolysis due to the matrix effect and the position of the intercept provides a measure of the amount adsorption (Langford and Blanc-Valleron, 1990).

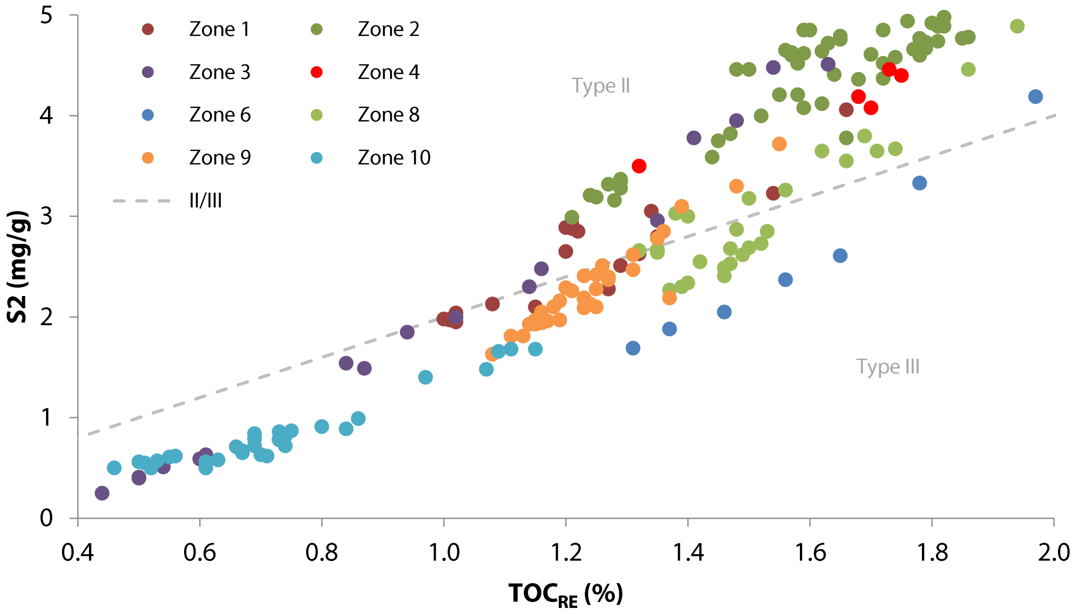

Figure 6.18 *Rock-Eval modified van Krevelen diagram of S2 and TOC$_{RE}$ for Co1262, showing the transition from Type III- to Type II-dominated sediments.*

The regression line equation and calculated x-intercept (at S2 = 0) for each zone from Co1262 are given in Table 6.4. When considering the entire record the regression line intercepts the x-axis at 0.6% TOC, which suggests this is the amount of OM that must be present to overcome the matrix effect and obtain hydrocarbon release during pyrolysis (Ariztegui et al., 2001). The y-intercept may also be used to determine the extent of adsorption and may be more useful than the x-intercept given that, in comparison to TOC, S2 is less dependent on the nature of the OM (Langford and Blanc-Valleron, 1990). The y-intercept for all the S2 data is −2.5; in general therefore the adsorptive capacity of 1 g of sediment is equivalent to 2.5 mg of pyrolisable hydrocarbons (PHc).

Table 6.4 *The fitted regression line, calculated x-intercept and % pyrolisable hydrocarbons (see text) for each zone of Co1262.*

Zone	S2 v. TOC$_{RE}$ Regression	x-intercept	% PHc
All	$y = 4.35x - 2.45$	0.6	43.5
1	$y = 3.21x - 1.31$	0.4	32.1
2	$y = 3.19x - 0.68$	0.2	31.9
3	$y = 4.17x - 1.95$	0.5	41.7
4	$y = 5.80x - 4.88$	0.8	58.0
5	$y = 4.65x - 1.05$	0.2	46.5
6	$y = 5.00x - 5.28$	1.1	50.0
7	$y = 4.84x - 5.33$	1.1	48.4
8	$y = 4.19x - 3.36$	0.8	41.9
9	$y = 4.06x - 2.75$	0.7	40.6
10	$y = 1.86x - 0.53$	0.3	18.6

The slope of the linear regression line for S2:TOC$_{RE}$ data is likely related to the %PHc, calculated as ten times the regression gradient (Langford and Blanc-Valleron, 1990). When considering the Co1262 sequence, a gradient of 4.35 suggests that PHc in the TOC is approximately equal to 43.5% (Table 6.4). Taking into account the average %PHc for each zone (Table 6.4), the quantity of PHc is observed to be generally high between zones 4-9 (maximum in Zone 4), moderately reduced in zones 1-3 and at a minimum in Zone 10 (Figure 6.19).

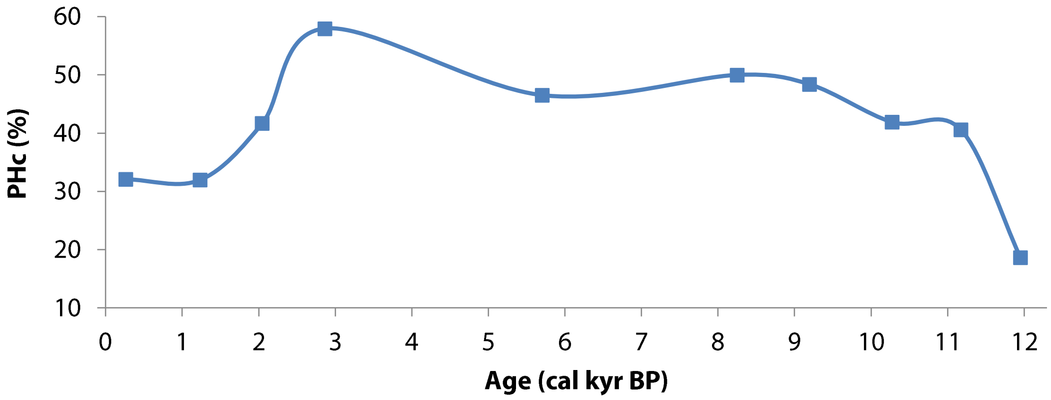

Figure 6.19 *Percent of pyrolisable hydrocarbons (see text) plotted against age, squares indicate mid-point age of each zone.*

During RE pyrolysis a sediment sample is heated to 650°C (releasing PC) and any OM remaining is termed RC (Section 4.3). In experiments conducted on fresh OM, the main constituents of RC was shown to be lignin and cellulosic material, however other components (e.g. phytoplankton and lipids) may undergo a relative increase following degradation and remineralisation processes (Carrie et al., 2012). The proportion of RC in OM (RC/TOC$_{RE}$) from Co1262 shows a very strong negative correlation to HI (r^2 = 0.95, p <0.001) (Figure 6.20), suggesting that where the RC component of OM decreases the HI value increases. Further, this implies that higher HI values strongly correlate with the presence of either less cellulosic and lignin-bearing material or a lower content of degraded/remineralised material. The plot of RC/TOC$_{RE}$ and OI reveals an overall non-linear relationship, although between OI = 80 to 200 a moderate positive correlation exists between the two variables (Figure 6.20). However, for some samples above OI = 200 and RC/TOC$_{RE}$ = 0.7, a small increase in RC/TOC$_{RE}$ relates to a large increase in OI. This suggests that as material becomes progressively more degraded it becomes more oxidised (higher OI) and more resistant (higher

RC/TOC_{RE}), and for high RC/TOC_{RE} content there is either a OM source change or environmental conditions that promote enhanced degradation.

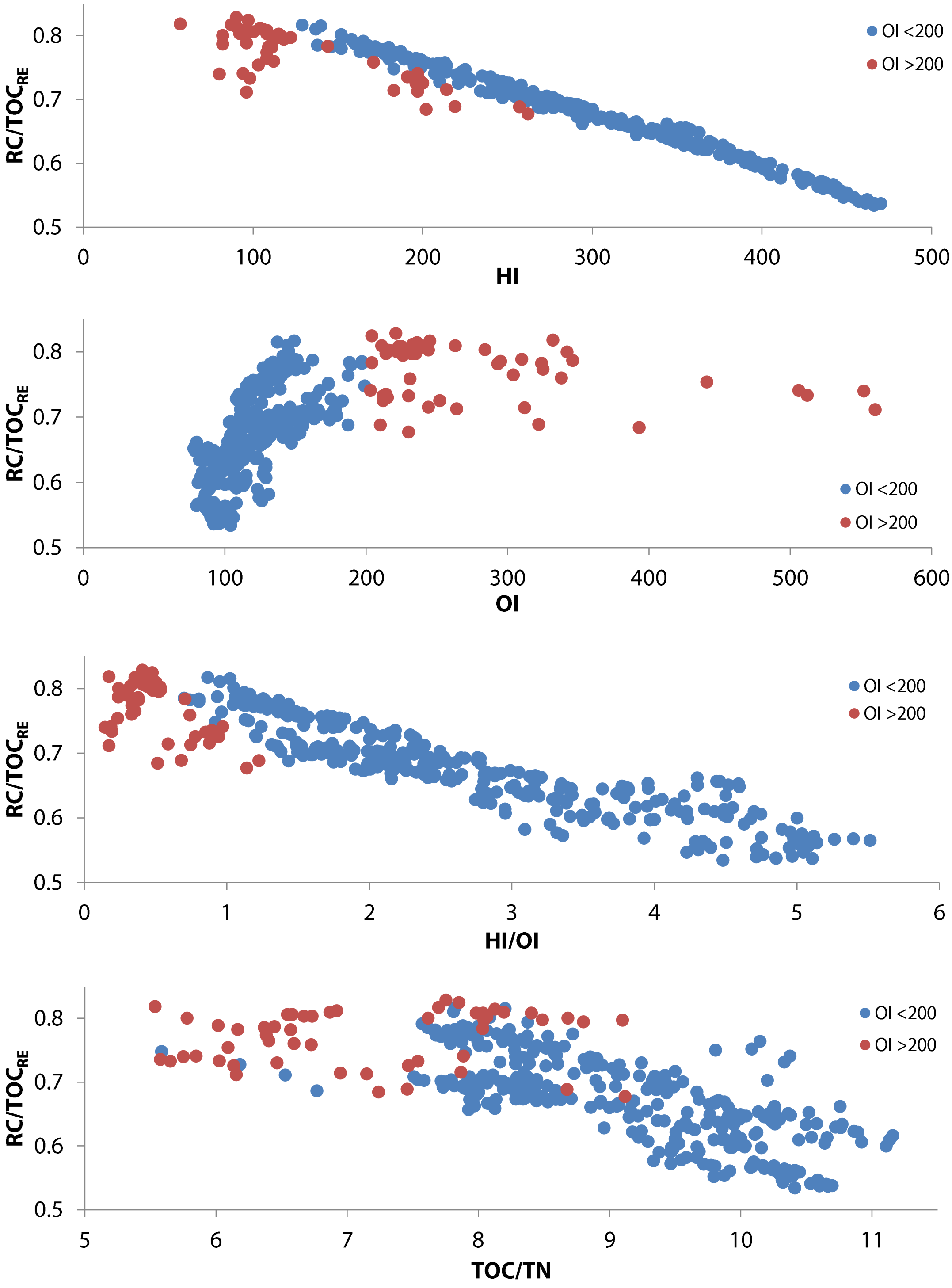

Figure 6.20 *Residual carbon component of OM plotted against HI, OI, HI:OI and TOC:TN, differentiated for OI below 200 and OI above 200.*

The relationship between RC/TOC$_{RE}$ and HI:OI is illustrated in Figure 6.20. As for Figure 6.15, a low HI:OI ratio (<2) suggests the composition is potentially related to greater terrigenous input and/or degradation and Figure 6.20 infers that these sediments also are characterised by high RC/TOC$_{RE}$. In addition, this material generally shows the lowest TOC/TN values (Figure 6.20). The data for OI >200 incorporates the transitional phases around large excursions and thus a spread is present into higher HI, lower OI and higher TOC/TN regions. The lowest HI, HI:OI and TOC/TN grouping is temporally located prior to 11.6 ka in Zone 10 and around 2 ka in Zone 3, suggesting these zones in particular may have enhanced terrestrial input and/or the greatest extent of degradation.

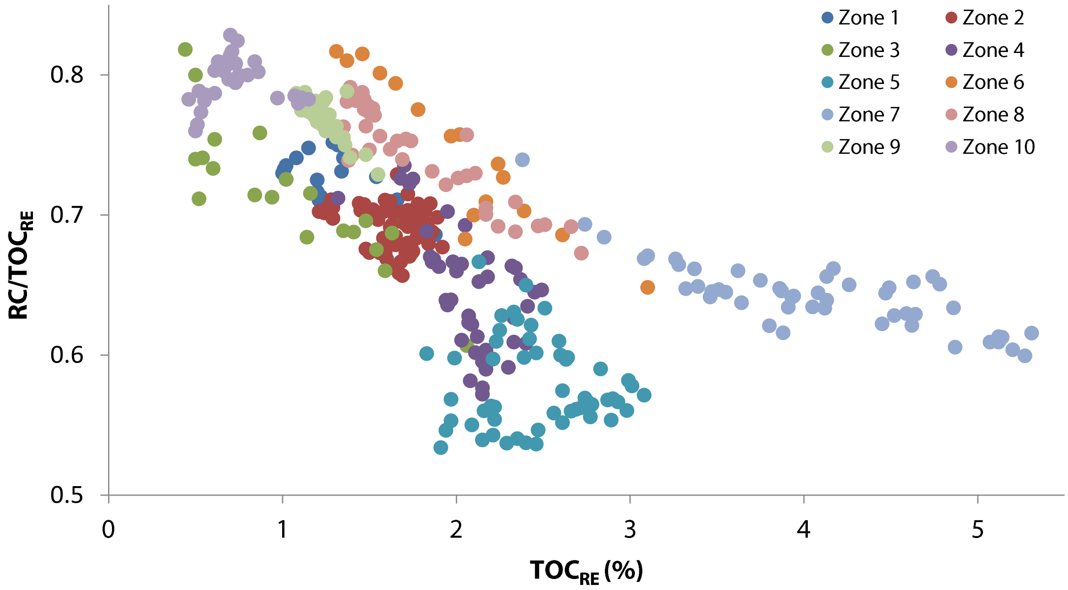

***Figure 6.21** Residual carbon component of OM plotted against total OM.*

A comparison of TOC$_{RE}$ with respect to the RC component of TOC$_{RE}$ is shown in Figure 6.21. An overall negative correlation between the two variables is observed, inferring that where TOC$_{RE}$ is low, the RC component of TOC$_{RE}$ increases. This suggests that the presence of RC, a product of terrestrial input or degradational processes, is a direct function of the amount of TOC$_{RE}$ present. Although this may imply zones of overall low TOC$_{RE}$ are dominated by terrigenous material, the continuum from low to high TOC$_{RE}$ infers that this is in fact more likely a product of differential amounts of OM degradation. Where degradation is high, the removal of labile OM in the first instance will reduce overall TOC and increase the proportion of RC in TOC.

Importantly, an additional observation from Figure 6.21 is that two main groupings of data are present, one with a progression from Zones 10-6 and a second from Zones 5-1 (also illustrated in the generalised plot of S2 against TOC_{RE}; Figure 6.22). The two groups are directly related to inorganic carbonate precipitation in the lake, where during periods of higher TIC the proportion of TOC in sediment reduces and therefore so does the proportion of PC (i.e. S2 also reduces).

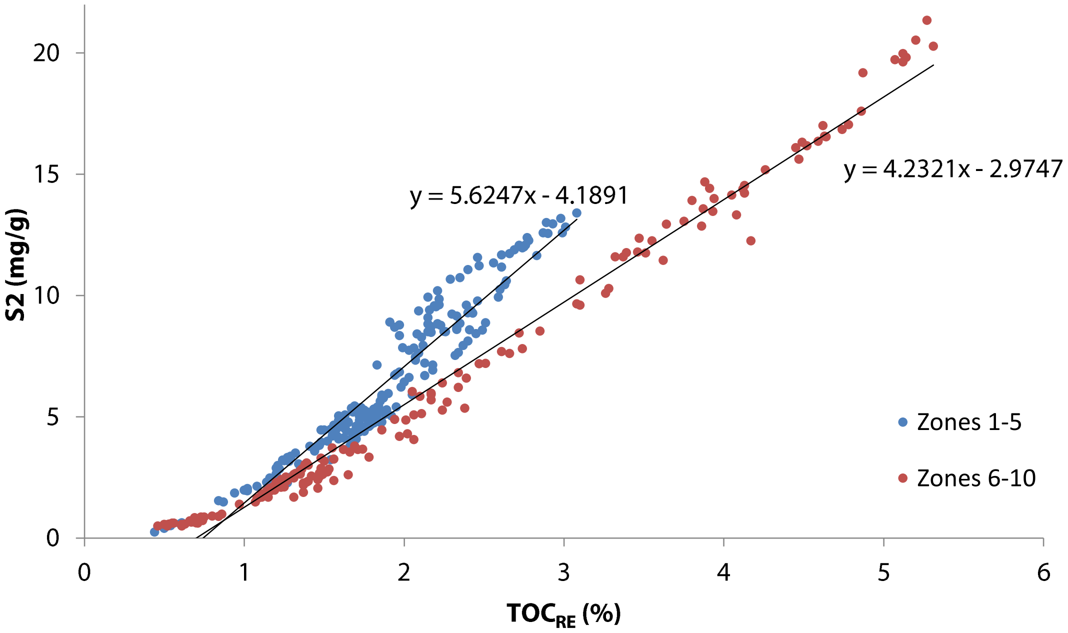

Figure 6.22 *Plot of S2 and TOC_{RE} showing two data groups with individual linear regression lines.*

The sediments of Zone 5 should most likely occupy the same approximate S2:TOC_{RE} space as those of Zone 7 (Figure 6.17), however TIC effectively reduces the extent of TOC_{RE} and S2 variation. Figure 6.23 shows the difference in z-score (value minus the mean, divided by the standard deviation) for TOC_{RE} and TIC over the Co1262 sequence. Prior to the Zone 6-5 boundary, there is generally a positive difference between the z-scores indicating that quantity of TOC_{RE} in a sediment sample is greater than TIC. However, after this boundary the opposite is true and TIC becomes the larger constituent. Although this does not take into account the other sedimentary components present (which have not been quantified), if their proportion changed both TIC and TOC_{RE} would be expected to show a concomitant reduction in concentration. Assuming all of the data should plot on the same regression line (negating the influence of TIC), the steeper gradient defined by Zones 1-5 in Figure 6.22 suggests that the decrease in TOC_{RE} as a percentage of sediment composition exerts a greater influence TOC_{RE} values than it does on S2 values. In addition, this perhaps implies that during times of greater TIC production, the TOC_{RE} component of sediments comprises a greater proportion of hydrocarbon-rich material (high S2) and thus most likely derives from algal (Type II) OM. This is corroborated by the PHc estimate from each group, being 56.3% for Zones 1-5 and 42.3% for zones 6-10 (calculated from the regression lines in Figure 6.22; Langford and Blanc-Valleron, 1990) and implies that higher TOC (Figure 6.11) is driven by algal productivity.

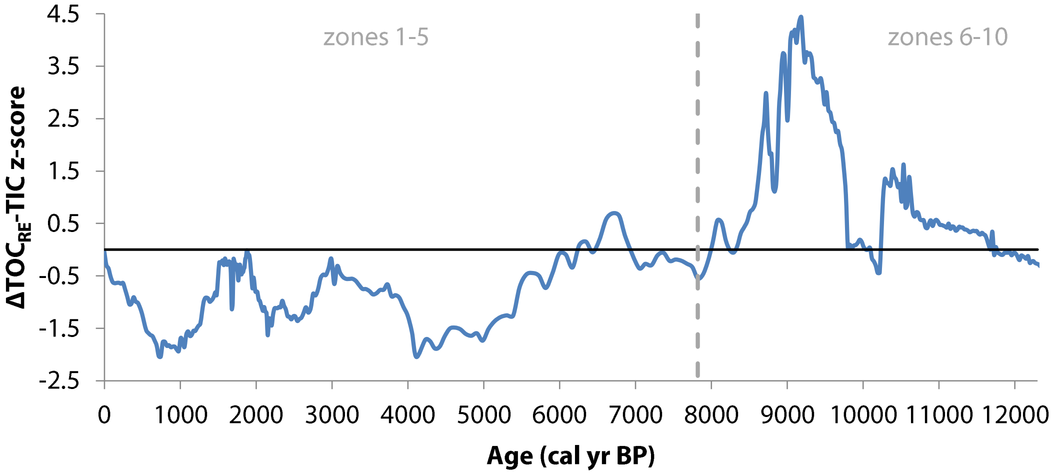

Figure 6.23 *Difference in z-score for TOC_{RE} and TIC through Co1262, showing the boundary between zones 6 and 5, and the zero line (where TOC_{RE} and TIC are in equal proportions).*

6.6.2 Carbon isotope composition of organic matter and calcite

The relative contribution of aquatic and terrestrial sources to sedimentary OM can be further assessed using the carbon isotope composition of OM ($\delta^{13}C_{organic}$). A plot of C/N against $\delta^{13}C_{organic}$ indicates that most of the OM in Lake Ohrid is sourced from autochthonous algal production (Figure 6.24), which is also observed in RE van Krevelen diagrams that show Type II sediments typically derived from algal detritus (Figure 6.14 and 6.17; Meyers and Teranes, 2001). This suggests that $\delta^{13}C_{organic}$ will most likely act as a tracer of past changes in the aquatic carbon cycle, rather than being primarily determined by variations in OM source, providing there was limited post depositional change (Leng et al., 2010a). However, even if degradational processes reduce overall TOC accumulation and selective diagenesis occurs, bulk sediments are thought to retain their primary isotope signature and preserve relative isotope variations (Meyers et al., 1995; Hodell and Schelske, 1998).

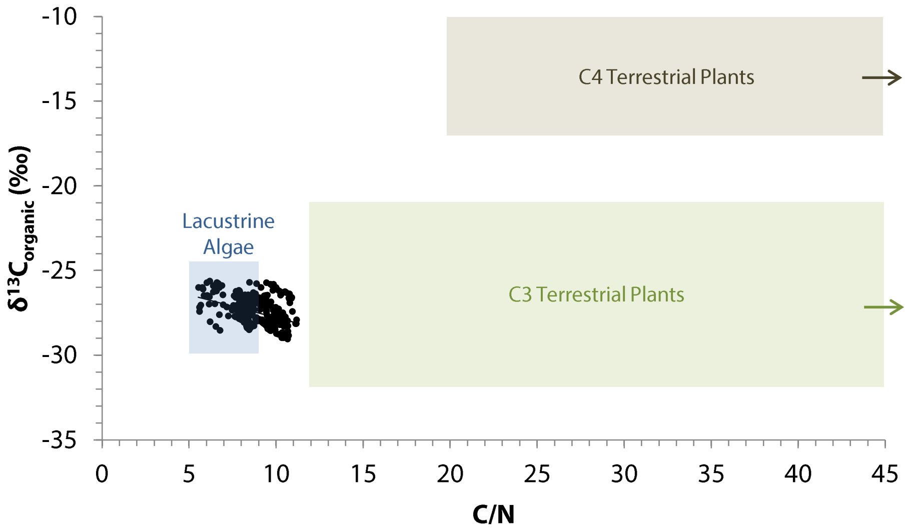

Figure 6.24 *$\delta^{13}C_{organic}$ and TOC/TN for Co1262 (black dots) and generalised zones characterising the major sources of plant OM to lacustrine sediments (after Meyers, 1994).*

Lake Ohrid is an alkaline lake with a pH of between 8.0 and 8.9 in pelagic waters (measured 2004-2006; Tasevska et al., 2012), which have an ionic composition dominated by calcium (Ca) and bicarbonate (HCO_3^-) (Stankovic, 1960). In hard water lakes, such as Lake Ohrid, algae utilise dissolved HCO_3^- (approximates total dissolved inorganic carbon, TDIC, at pH 7-9) and therefore $\delta^{13}C_{organic}$ will most likely reflect changes in the isotope composition of the dissolved HCO_3^- pool ($\delta^{13}C_{TDIC}$). Similarly, when endogenic carbonate precipitates it captures lake water $\delta^{13}C_{TDIC}$ (Section 3.3.3) and thus both $\delta^{13}C_{calcite}$ and $\delta^{13}C_{organic}$ should record past changes in $\delta^{13}C_{TDIC}$. Although $\delta^{13}C_{calcite}$ is not available for the whole core (due to low TIC in areas), Figure 6.25 shows that there is a moderately strong covariant relationship between $\delta^{13}C_{calcite}$ and $\delta^{13}C_{organic}$ ($r = 0.69$, $p < 0.001$) and infers that TDIC is the main source of carbon for both OM and calcite. Moreover this suggests that $\delta^{13}C_{organic}$ variations are unlikely to be a function of OM source changes throughout much of Co1262. However, during periods where $\delta^{13}C_{calcite}$ and $\delta^{13}C_{organic}$ are decoupled, variations in $\delta^{13}C_{organic}$ may be related to greater allochthonous input.

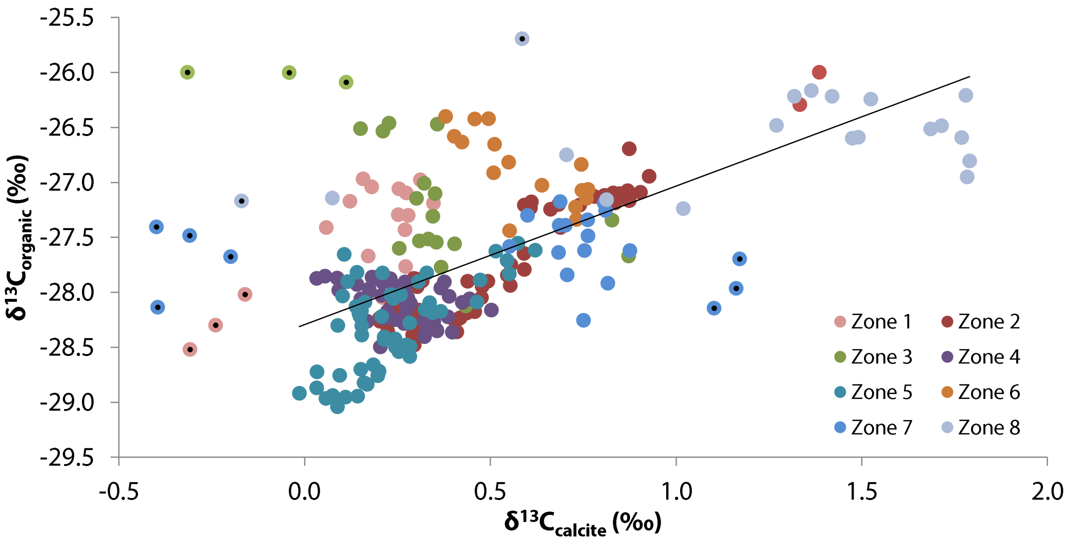

Figure 6.25 *Carbon isotope composition of organic matter and calcite, black dots suggest potential zones of decoupling.*

The isotope composition of TDIC in a lake is primarily a function of the source of carbon (atmospheric, lithospheric, or organogenic) and is also subject to further modification by in-lake processes (atmospheric exchange, photosynthesis and respiration) which are themselves influenced by water balance (Section 3.3.3; Mayer and Schwark, 1999). Given that Lake Ohrid receives a large proportion of its incoming water from karst springs (Chapter 5), the dissolution of catchment rocks most likely provides a large amount of bicarbonate to the lake. Geological sources of bicarbonate have high $\delta^{13}C$ as they comprise ancient marine carbonates that, typically range between −3 and +3‰ (Andrews et al., 1993; Hammarlund et al., 1997). Measured values for several of the geological units in the Ohrid catchment give an average $\delta^{13}C$ = +1.1‰ (Figure 6.26; Leng et al., 2010a), and confirm that $\delta^{13}C_{TDIC}$ of lake water will most probably be high (currently there are no $\delta^{13}C_{TDIC}$ data from Ohrid itself).

In opposition to geological sources of high $\delta^{13}C$ bicarbonate, a major source of carbon in ground and river water typically originates from isotopically light CO_2 liberated during the decay of terrestrial organic matter (Section 3.4). Low $\delta^{13}C$ values are shown in isotope data from spring and river inflows to Lake Prespa that have average $\delta^{13}C$ = −11.5‰ (Figure 6.26; Leng et al., 2013), which is consistent with the upper calculated range for a soil CO_2 bicarbonate source (−22 to −10‰ for C3 plants; Leng and Marshall, 2004). If it is assumed that geological (+1.1‰) and soil CO_2 (−22 to

−11.5‰) bicarbonate sources form two end members comprising inflow $\delta^{13}C$ (−11.5‰), then a mixing model can be established (Table 6.5). The mixing model suggests that the soil CO_2 component is most probably of overall greater significance (at least during the current interglacial) in determining inflow $\delta^{13}C$ for Lake Prespa. However, geologically-sourced bicarbonate could be of roughly equal importance if catchment vegetation has particularly low $\delta^{13}C$ either due to comprising C3 plants with $\delta^{13}C$ nearing or exceeding −32‰ or where there is a significant decrease in the contribution from C4 plants ($\delta^{13}C$ = −7 to +1‰).

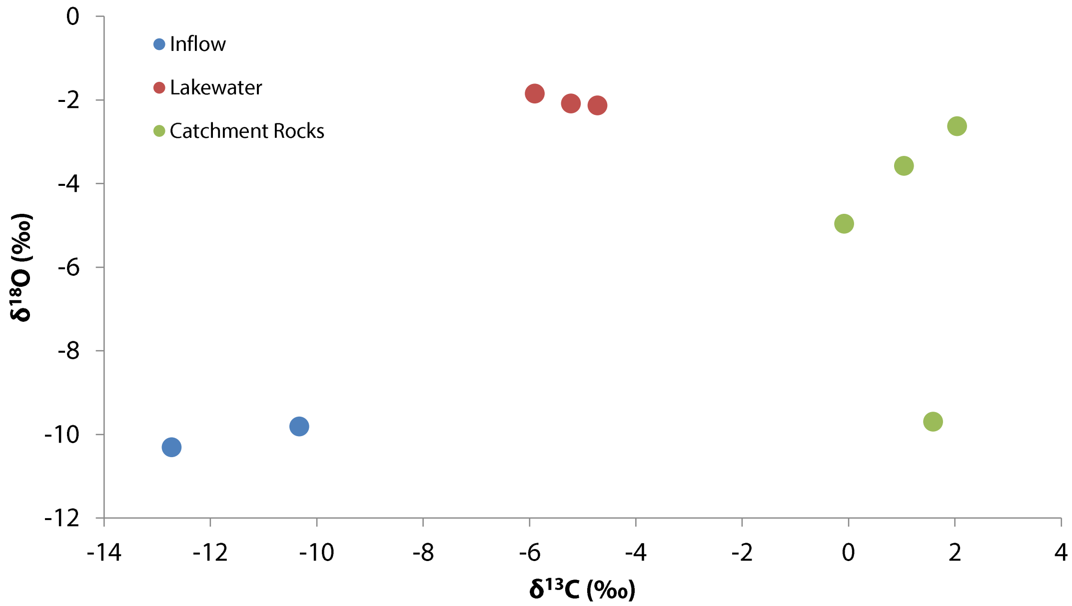

Figure 6.26 *Oxygen and carbon isotope composition of catchment rocks, and inflows and lake water from Lake Prespa (Leng et al., 2010a; Leng et al., 2013).*

Lake Prespa receives over 90% of its water from direct precipitation (35%) and surface run off (56%) (Anovski, 2001), and so geological sources of carbon may be only of a minor significance in determining $\delta^{13}C_{TDIC}$. Conversely, Lake Ohrid receives 60% of its water input from springs that flow through karst aquifers (Chapter 5, Table 5.4) and so it is most likely that $\delta^{13}C_{TDIC}$ is primarily influenced by the isotope composition of dissolved catchment carbonates. Dissolution processes will be more pervasive alongside enhanced incorporation of soil-derived CO_2 and the associated drop in pH. Hence, even when the proportion of lower $\delta^{13}C$ from soil CO_2 is greater, the amount of bicarbonate derived from higher $\delta^{13}C$ geological sources is concomitantly increased. This suggests that in wetter/warmer periods, where vegetation and soils are more developed, the influx of lower $\delta^{13}C$ from enhanced soil development will not excessively influence $\delta^{13}C_{TDIC}$, and overall inflow $\delta^{13}C_{TDIC}$ should still predominantly reflect that of the original geological carbon reservoir bicarbonate source.

***Table 6.5** Mixing model defining the relative importance of geological and soil CO_2 sources of bicarbonate in the inflowing water to Lake Prespa.*

C3 $\delta^{13}C_{HCO3-}$ (‰)	Soil CO_2 source	Geological source
−11.5	100%	0%
−22	54.5%	45.5%

Once inflowing waters reach the lake the bicarbonate pool may be modified by internal processes, the most prevalent being atmospheric exchange and variations in aquatic productivity. Internal processes are known to exert a control on the bicarbonate pool in Lake Prespa as modern lake water $\delta^{13}C = -5.3‰$, which is +6.2‰ higher than the average $\delta^{13}C$ of inflowing waters (Figure 6.26) and thought to be related to both exchange and productivity (Leng et al., 2013). Under equilibrium exchange with atmospheric CO_2 ($\delta^{13}C = -7‰$) lake water has a $\delta^{13}C_{TDIC}$ of approximately between +0 and +3‰, as there is a temperature-dependent fractionation between CO_2 and dissolved HCO_3^- of around 10‰ at 0°C and 7‰ at 30°C (Section 3.3.3; Mook et al., 1974). Lake Ohrid has a large surface area and long residence time, which makes exchange with the atmosphere more likely to occur. High and stable $\delta^{13}C_{calcite}$ in Co1262 (average = +0.42±0.48‰) suggests $\delta^{13}C_{TDIC}$ may have been dominated by atmospheric equilibration. Given the overall stability of $\delta^{13}C_{calcite}$, and in $\delta^{13}C_{organic}$ (average = −27.45±0.77‰), a proportion of the variance could well be driven by changes in temperature. For instance, a 5°C increase would reduce the fractionation between CO_2-HCO_3^- by 0.5‰ and could therefore result in lower $\delta^{13}C_{TDIC}$ (assuming inflow $\delta^{13}C_{TDIC}$ did not change). As average $\delta^{13}C_{calcite}$ is ca. +0.4‰, average $\delta^{13}C_{TDIC}$ would be ca. −0.6‰ (due to a 1‰ offset; Section 3.3.3), which would require temperatures in excess of 35°C to drive lower fractionation, assuming complete exchange with atmospheric CO_2 occurred. Local temperatures are known to generally not exceed 30°C (Figure 2.12) and so total equilibration must not occur. Therefore, in addition to temperature changes, the degree of equilibration with atmospheric CO_2 (as a modifier of inflow $\delta^{13}C_{TDIC}$) may also be an important driver of lake water $\delta^{13}C_{TDIC}$.

Unlike atmospheric CO_2 exchange, which is likely to be a key driver of $\delta^{13}C_{TDIC}$ in Lake Ohrid, within-lake productivity changes most likely do not overly influence the isotope composition of lake waters. As a lake becomes more productive and phytoplankton preferentially utilise ^{12}C, the death and subsequent burial of algae exports lighter carbon to the lake floor (i.e. biological pump effect) and surface water becomes progressively enriched in ^{13}C. If productivity had an overriding impact, periods of high aquatic production (i.e. high $\delta^{13}C_{TDIC}$) should correlate with increased OM export to sediments, greater HI values and assumedly enhanced carbonate production. However, as $\delta^{13}C_{calcite}$ and $\delta^{13}C_{organic}$ always show a weak-moderate negative correlation with TIC, TOC and HI (Table 6.3, Figure 6.27), the export of OM and associated ^{13}C-enrichment of surface waters does not influence $\delta^{13}C_{TDIC}$, at least not within the sampling resolution. The negative correlation suggests that low $\delta^{13}C_{TDIC}$ can be associated with periods of enhanced aquatic OM export to sediments and greater carbonate production.

Over extended timescales (centennial-millennial), the source and isotope composition of bicarbonate, as well as in-lake processes, are likely to be significantly influenced by water balance variations (Mayer and Schwark, 1999). Periods that are characterised by overall wetter conditions will have greater delivery of lower $\delta^{13}C$ from inflowing waters, as lake water has likely been subject to atmospheric exchange (higher $\delta^{13}C$). Wetter and warmer climates also promote a densely vegetated catchment, thereby improving soil development and lowering inflow $\delta^{13}C$ due to a greater C3 component. Furthermore, enhanced water inflow to Lake Ohrid is likely to result in greater outflow, which reduces lake water residence time and the potential for atmospheric exchange thereby lowering $\delta^{13}C$. A faster inflow rate may also lead to a reduction in residence time for spring waters within the karst aquifer system, thereby limiting carbonate dissolution (however this could arguably be counteracted by a decreased pH from an increased soil CO_2 concentration). In addition, generally warmer temperatures would lead to a reduction in fractionation between atmospheric CO_2 and bicarbonate in surface waters, thereby lowering $\delta^{13}C_{TDIC}$.

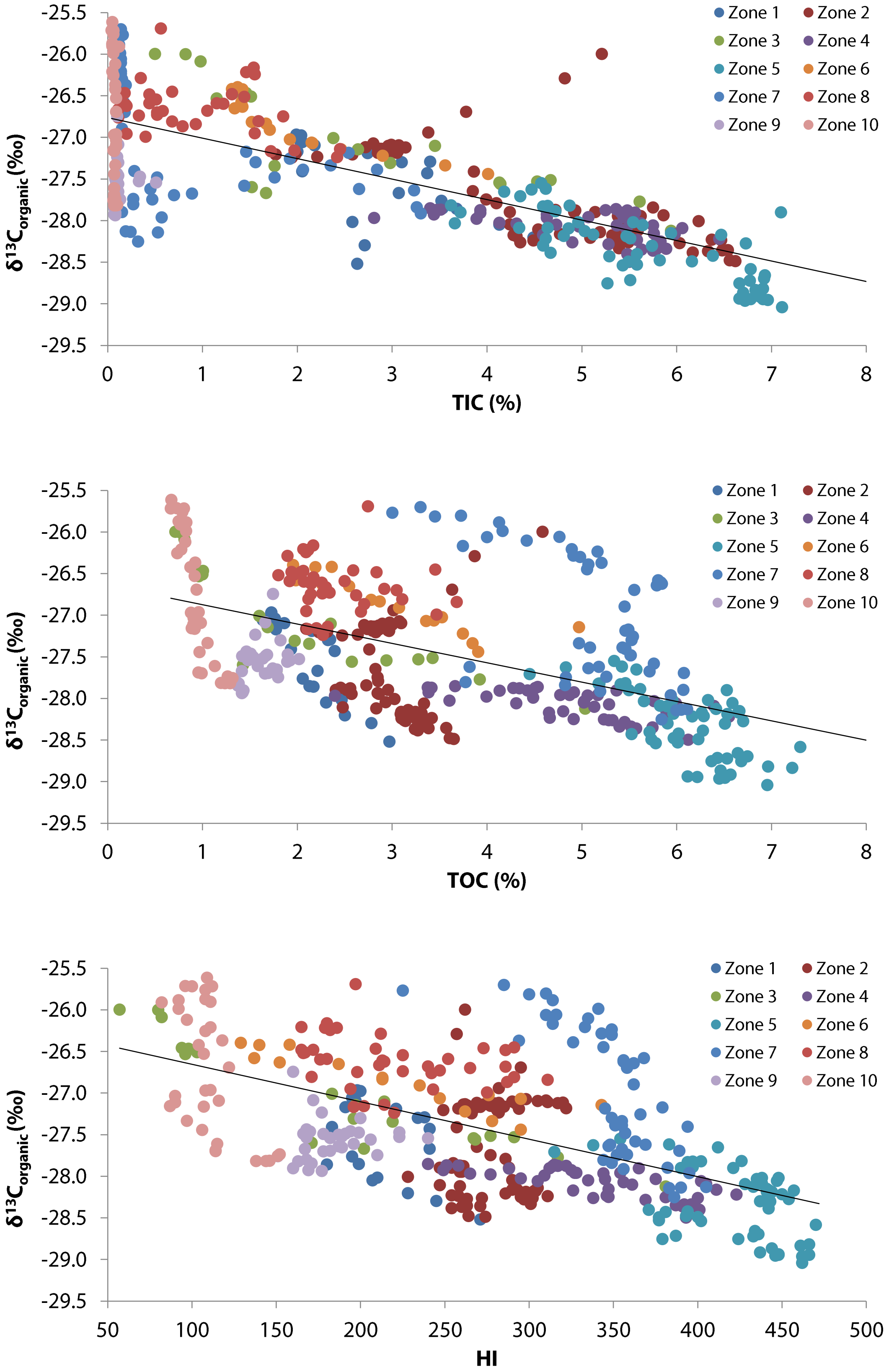

Figure 6.27 *Carbon isotope composition of organic matter plotted against TIC, TOC and HI, showing linear regression of the whole dataset.*

6.6.3 Carbonate precipitation and the oxygen isotope composition of calcite

Endogenic calcite is precipitated within the epilimnion during summer months in response to higher temperatures and enhanced photosynthetic activity (Section 3.3.2; Wagner et al., 2008a; Leng et al., 2010a), which has been observed in both deep and shallow sediment trap studies (Matzinger et al., 2006b; Matter et al., 2010). This requires an adequate supply of Ca^{2+} and HCO_3^- ions, which in Lake Ohrid are principally derived from the karst aquifer system (Matzinger et al., 2006a). The concentration of Ca^{2+} and HCO_3^- ions in lake water will be increased during periods of enhanced chemical weathering of catchment limestones and due to higher evaporation rates (Vogel et al., 2010a; Francke et al., 2015). Sediment trap studies in Lake Ohrid indicate that summer calcite precipitation is up to three times that produced during winter, and verify a concomitant increase in productivity by phytoplankton counts and chlorophyll-α measurements (Matzinger et al., 2007). The production of calcite is typically higher in coastal zones compared to deeper areas of the basin, and is strongly correlated to areas of higher productivity (Figure 6.28; Vogel et al., 2010b).

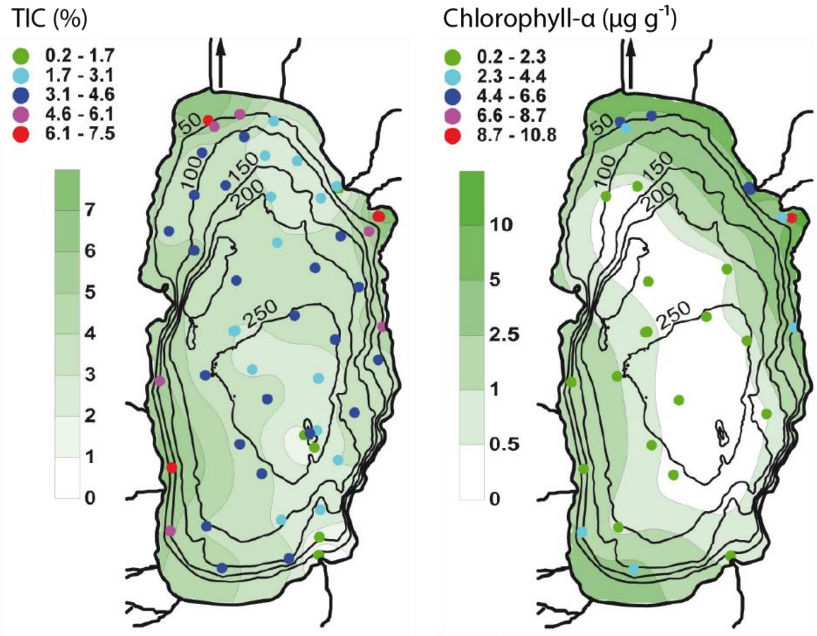

Figure 6.28 *Interpolated spatial distribution maps showing the concentration of TIC and chlorophyll-α (from Vogel et al., 2010b).*

Conversely, a lower calcite abundance is observed in areas with greater river inflow either due to a reduction in Ca^{2+} and HCO_3^- due to the rivers draining a carbonate-free catchment area and/or increased clastic supply reducing the proportion of carbonates in the sediment (Vogel et al., 2010b). Calcite concentration will also be a function of preservation, where, in the presence of oxygen, OM decomposition and the subsequent release of H_2CO_3 lowers bottom water pH and leads to the dissolution of calcite (Figure 3.2; Vogel et al., 2010a; Francke et al., 2015).

Calcite crystals precipitated in the water column or those found in surface sediments are relatively pristine, with individual idiomorphic crystals reaching up to 20 µm and crystal clusters up to 150 µm (Matter et al., 2010). Matter et al. (2010) identified regular ca. 1µm diametre holes in the calcite crystals from both sediment traps and surface cores (Figure 6.29a), which may be related to organic (picoplankton) nucleation sites that have since been degraded and lost. Further, this hypothesis was supported by very high measured concentrations of picocyanobacteria cells in Ohrid lake water. Similar holes in calcite crystals were observed by Wagner et al. (2008a) and are also present in calcite crystals from Lini site sediments (Figure 6.29b).

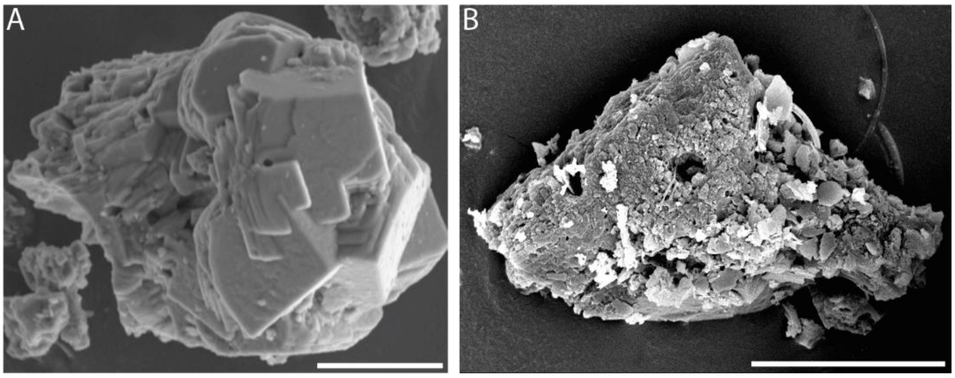

***Figure 6.29** SEM images of calcite crystals a) large idiomorphic crystal cluster from surface sediments (15 cm core depth; from Matter et al., 2010), and b) crystal cluster from Lini core at 4.2 ka, both showing characteristic picoplankton holes (scale bars = 20 µm).*

Lake Ohrid has precipitated endogenic calcite throughout much of the Holocene, reaching up to 7.1% TIC (60% $CaCO_3$ at 5.0 ka), however toward the base of the core TIC becomes negligible (Figure 6.11). As TIC content is thought to be related to aquatic productivity (Figure 6.28), it is likely the periods of low TIC relate to overall colder conditions that inhibit primary productivity. Further, periods of low TIC can be correlated to low TOC and TOC/TN (Section 6.6.1), which also occurs during the Last Glacial (Wagner et al., 2009a; Vogel et al., 2010a). This suggests that in addition to a reduction in productivity due to colder climate conditions, the degradation of OM was also enhanced. Very low TOC/TN precludes an OM source change and infers that TIC dissolution was likely associated with improved mixing conditions and a more oxygenated water column, leading to OM oxidation and lower bottom water pH (Francke et al., 2015). In the transition from colder to warmer periods (i.e. glacial terminations) there appears to be an environmental threshold that needs to be surpassed before calcite is preserved in the Lake Ohrid sediments. Focusing on the period 12.3 ka to 10.5 ka in core Co1262, TIC is observed to be negligible until ca. 11.1 ka, however TOC_{RE} increases from the very base of the core at 12.3 ka (Figure 6.30). Increasing accumulation (and preservation) of OM suggests both warmer conditions driving greater primary productivity and also reduced lake water mixing leading to lower rates of OM degradation. Consequently, at times when TOC is lower than ca. 1.2%, environmental conditions are inferred to be potentially unfavourable to calcite precipitation and preservation.

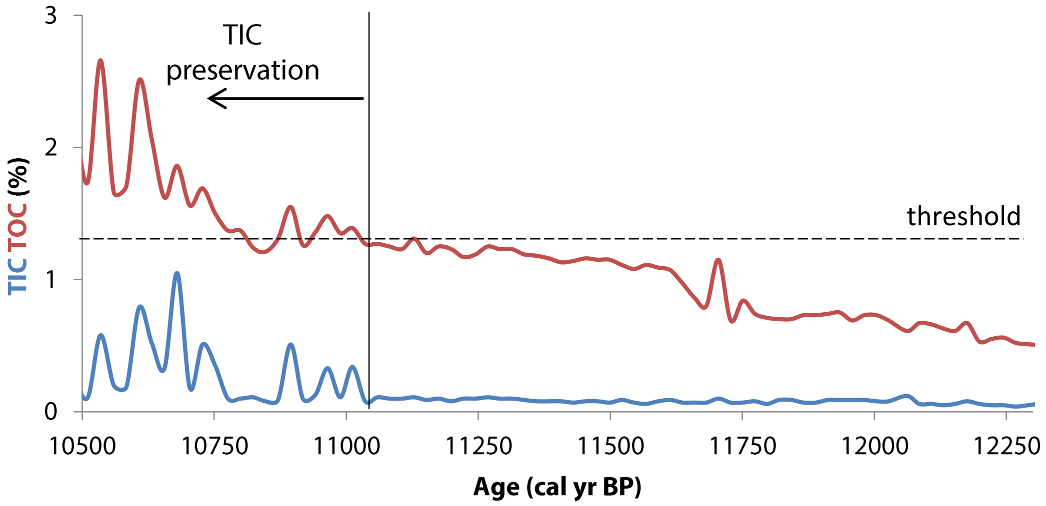

Figure 6.30 *TIC and TOC_{RE} plot against age, suggesting a threshold (dashed line) must be surpassed before calcite is preserved in sediments.*

Assuming the endogenic calcite precipitated in isotopic equilibrium with the lake water, $\delta^{18}\text{O}_{\text{calcite}}$ is solely a function of $\delta^{18}\text{O}_{\text{lakewater}}$ and the lake water temperature at the time of formation (Leng and Marshall, 2004). This interdependence can be summarised by a fractionation equation for oxygen relating calcite, water and temperature, for example $T°C = 13.8 - 4.58(\delta c - \delta w) + 0.08(\delta c - \delta w)^2$ (Equation 3.6, Section 3.3.2; Leng and Marshall, 2004). If the average temperature of the photic zone during summer months is approximately 18°C (0-20 m water depth average temperature between June-August; Stankovic, 1960), and using the average measured modern $\delta^{18}O_{lakewater}$ (ca. −3.5‰, Chapter 5), the calculated $\delta^{18}O_{calcite}$ of contemporary calcite precipitation should be approximately −4.4‰ using the Leng and Marshall (2004) expression of Kim and O'Neil (1997). This is equal to $\delta^{18}O_{calcite}$ from Co1262 core top sediments, suggesting that calcite is precipitated in equilibrium with lake water and associated with summer conditions.

The modern oxygen isotope data indicate a clear disparity between measured $\delta^{18}O_{lakewater}$ and the average weighted isotope composition of meteoric and groundwater inflow ($\delta^{18}O$ = −8.3‰, Chapter 5). Using the mean summer lake water temperature of 18°C, and the weighted $\delta^{18}O$ of inflowing water, calcite precipitated from a hypothetical, non-evaporated lake water source would have $\delta^{18}O_{calcite}$ = −9.2‰ (using Leng and Marshall, 2004). Similarly, low $\delta^{18}O_{calcite}$ values were not found in Co1262 (minimum $\delta^{18}O_{calcite}$ = −6.5‰ at 8.9 ka), or observed in any previous isotope data from Lake Ohrid (Leng et al., 2010a), which indicates that lake water has probably been subject to evaporative (kinetic) fractionation throughout the Holocene. This assumes that changes in temperature and $\delta^{18}O_{precipitation}$ do not largely influence $\delta^{18}O_{lakewater}$, and that $\delta^{18}O_{lakewater}$ is primarily a function of changes in water balance (i.e. variations in inflow vs. outflow). If, however, temperature was a dominant influence, the approximate linear $\delta^{18}O_{calcite}$ change observed between modern (−4.5‰) and early Holocene (−6.5‰) values in Co1262 (Figure 6.31) would require a decrease of over 5°C from that of present day (as the measured carbonate will covary with temperature by +0.36‰ $°C^{-1}$, Section 3.3.2; Leng and Marshall, 2004). Palynological evidence suggests that the early Holocene is characterised by the presence of thermophilous arboreal taxa within the catchment (Panagiotopoulos et al., 2013), and overall stable, warm climate conditions are also inferred (Bordon et al., 2009), indicating that such a significant drop in average temperature is unlikely and that temperature is not a primary driver of $\delta^{18}O_{lakeewater}$.

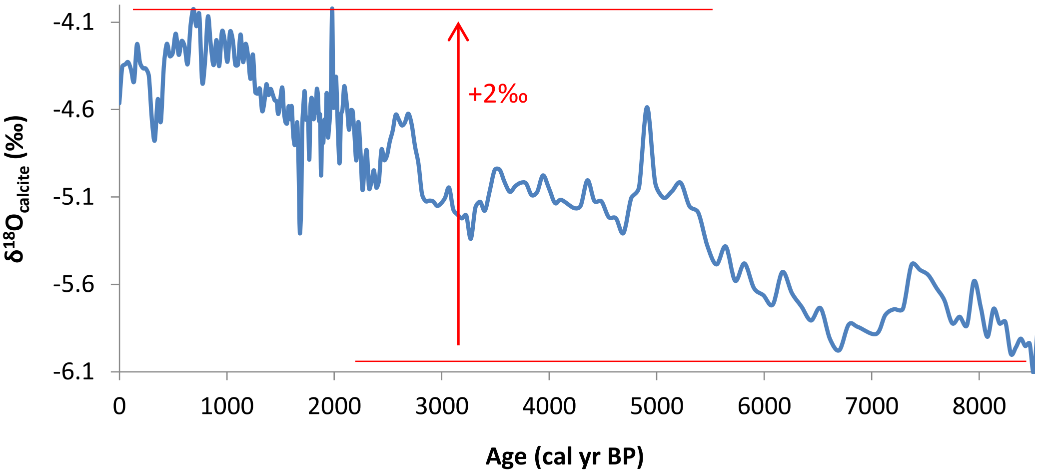

***Figure 6.31** Oxygen isotope composition of calcite from 8.5 ka to present, showing an overall +2‰ increase.*

As calcite is thought to precipitate in equilibrium with lake water, and given that temperature effects are not a primary influence on $\delta^{18}O_{calcite}$ or $\delta^{18}O_{lakewater}$, changes in $\delta^{18}O_{lakewater}$ must be driven by an alternative mechanism. This could potentially be due to variations in $\delta^{18}O$ of source waters. Modern precipitation data measured at Lake Ohrid plot on a local meteoric water line, which indicates a *d*-excess of +12‰ ($\delta D=7.86*\delta^{18}O+12.11$, Equation 5.3, Figure 6.32).

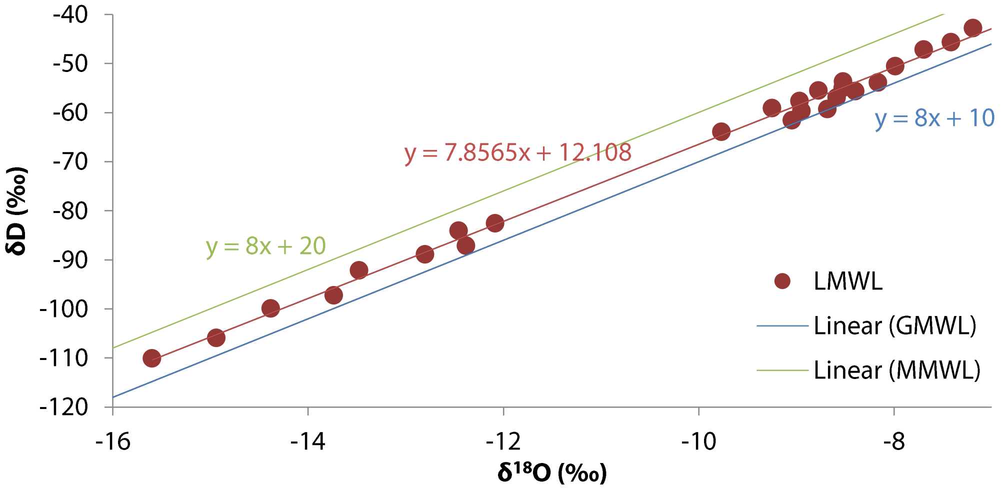

***Figure 6.32** Isotope composition of local precipitation (Anovski et al., 1991), which defines a LMWL (red) offset from the GMWL (blue) to a lesser extent than the MMWL (green).*

Subsequent to evaporation from an ocean source, the *d*-excess of a water mass does not significantly change during modification within an evolving air mass as $\delta^{18}O$ and δD typically vary proportionally (Sharp, 2007; Fernández-Chacón et al., 2010). The average *d*-excess for global marine waters (GMWL) is +10‰ (Section 3.3.1; Dansgaard, 1964), however this can fluctuate regionally due to differences in wind speed, humidity and sea surface temperatures (Clark and Fritz, 1997), and is in excess of +20‰ for the eastern Mediterranean (MMWL; Dotsika et al., 2010, and references therein).

This suggests that the predominance of water delivered to Lake Ohrid, at least recently, is largely sourced from air masses derived from the North Atlantic as the measured *d*-excess is closer to that of mean ocean water than of partially evaporated Mediterranean water (Gat et al., 2003; Dotsika et al., 2010). The isotope composition of water in the Mediterranean Sea is observed to be progressively enriched eastward (Figure 6.33), and so any increase (decrease) in local contribution in addition to the North Atlantic source will lead to higher (lower) $\delta^{18}O_{precipitation}$. Changes to the source of precipitation may well exert a minor influence $\delta^{18}O_{lakewater}$, however $\delta^{18}O$ variation between Atlantic and Mediterranean-derived water is not considered a primary determinate of $\delta^{18}O_{lakewater}$. However, the magnitude of variation between the two source areas could produce a component of the high frequency fluctuations observed in $\delta^{18}O_{lakewater}$ at the centennial-scale.

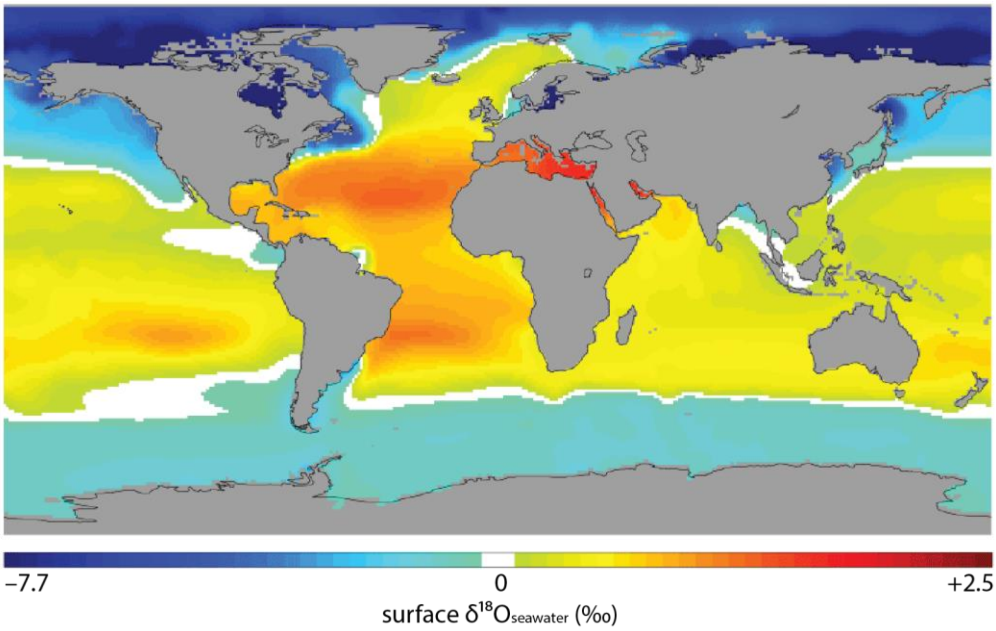

***Figure 6.33** Gridded dataset of surface $\delta^{18}O_{seawater}$ measurements since 1950 compiled by Schmidt et al. (1999) (from LeGrande and Schmidt, 2006).*

Assuming the source of precipitation is constant, variations in the isotope composition of an individual source must also be considered. Over glacial-interglacial timescales the isotope composition of mean $\delta^{18}O_{seawater}$ are reported to be +1.0±0.1‰ higher at the Last Glacial Maximum (LGM) than present due to the expansion of global ice volume (Schrag et al., 2002). In comparison, the Mediterranean is thought to have been +1.2±0.1‰ enriched at the LGM due to local evaporative enrichment (Paul et al., 2001). These changes suggest that the overall magnitude of variation at each location is small, and considering these changes occur over extended timeframes, the change within an interglacial (for example the Holocene) is most likely insignificant in determining $\delta^{18}O_{lakewater}$.

Given that changes in temperature and the source of precipitation can perhaps only account for minor variations in $\delta^{18}O_{lakewater}$, the main driver of $\delta^{18}O_{lakewater}$ is expected to be water balance (Chapter 5). As the oxygen isotope composition of modern lake water is evaporated with respect to average weighted inflow, in general between +4 and +6‰, within-lake processes must have a direct influence on $\delta^{18}O_{lakewater}$. Overall enriched $\delta^{18}O$ suggest that evaporation is continuous and prevalent, at least over the last ca. 10 ka (where continuous isotope data are available). If the water balance of the lake is considered, the volume of input to Lake Ohrid is solely dependent on the amount of precipitation (including the Prespa component; Chapter 5), and the average weighted input will always have a lower $\delta^{18}O$ than lake water as it has always been evaporated (at least through the Holocene, see calculation above). Therefore, when there is more precipitation (and/or less evaporation) $\delta^{18}O_{lakewater}$ will be lower and when there is less precipitation (and/or more evaporation) $\delta^{18}O_{lakewater}$ will be higher. In addition, during periods of greater water input, water output is likely to also increase and so the residence time of the lake will decrease, resulting in the lake being less able to buffer shorter-term variations in water balance.

$\delta^{18}O_{lakewater}$ has remained relatively constant over the last 30-year sampling period (−3.5±0.3‰; Section 5.2), suggesting that decadal- to centennial- scale changes may be buffered due to the overall long residence time and large water volume. As accumulation rates vary between 0.02 and 0.25 cm yr^{-1}, the amount of climate signal captured by endogenic calcite will change through the core, being as low as 10 years and up to 90 years per 2 cm sample interval. However, even with variations in the integrated climate signal, the overall trend observed in $\delta^{18}O_{calcite}$ does not change over the last 8.9 ka (Figure 6.34), which confirms that residence time and lake volume efficiently buffer changes in $\delta^{18}O_{lakewater}$ beyond centennial-scale variations.

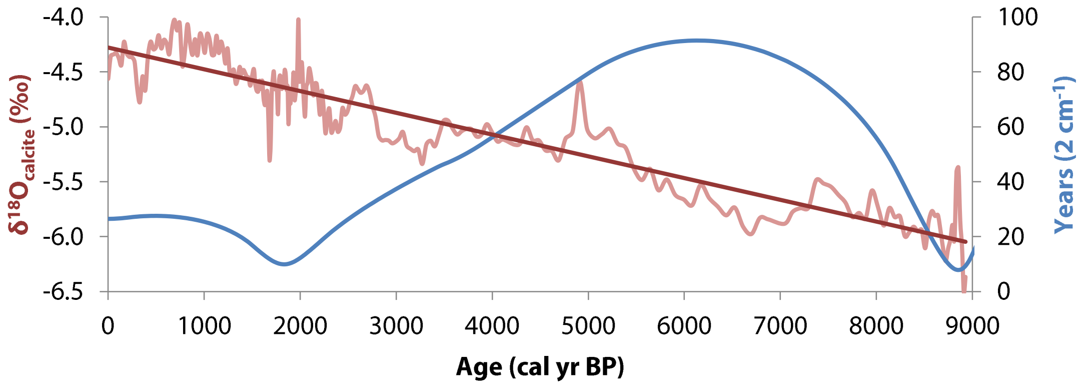

Figure 6.34 *The oxygen isotope composition of calcite over the last 8.9 ka plotted against the temporal amount of climate signal integrated within the selected sample size (i.e. 2 cm).*

Prior to 8.9 ka larger-scale fluctuations are observed in the Co1262 record, which may be due to a higher sedimentation rate and overall shorter residence time thereby integrating high frequency variations. The general trend of Holocene $\delta^{18}O_{calcite}$ advocates that Lake Ohrid has most likely reached a stable state and suggests that $\delta^{18}O_{calcite}$ (and by proxy $\delta^{18}O_{lakewater}$) reflects long-term variations in water balance (P/E) primarily driven by millennial-scale climate change.

Although calcite is preserved throughout most of the Holocene, a component of detrital carbonate could be present during phases when a higher proportion of clastic material enters the lake. These periods are associated with higher K in XRF data and constrained in Co1262 to the lower and upper parts of the core (Figure 6.13). Detrital carbonates commonly have a different isotope composition when compared to the endogenic fraction in lake sediments (Leng et al., 2010b), however in Lake Ohrid the catchment geology was measured to have $\delta^{18}O$ between −9.7 and −2.6‰ (Figure 6.26; Leng et al., 2010a). The lowest catchment values are not seen in the $\delta^{18}O_{calcite}$ record but the higher values do overlap with isotope measurements from the core.

While it is not possible to discern between endogenic and allogenic carbonates based on isotope data alone, SEM investigations suggest the carbonate is typical of endogenic precipitation (Belmecheri et al., 2009; Lézine et al., 2010; Matter et al., 2010), and XRD confirms that (interglacial) carbonate is calcite (Leng et al., 2010a), indicating that the amount of detrital calcite is likely negligible (Matzinger et al., 2007; Wagner et al., 2008a; Vogel et al., 2010a). As Lake Ohrid is located in a karstic area a proportion of detrital carbonate might be expected in the sediments, however the main river inputs drain a broadly carbonate free catchment (Vogel et al., 2010b) and other inputs comprise direct precipitation or groundwater inflow (Chapter 5). The highest rates of clastic input and catchment denudation are thought to occur in glacial periods (Francke et al., 2015), which are seen to have a minor component of detrital dolomite (discussed in Chapter 7). Sourced from dolomitized catchment rocks (Reicherter et al., 2011), the detrital carbonate is limited to glacial input and is easily recognised under SEM as sparse large crystals (>20 μm) set within a finer matrix. The dolomite, if present at all, is only found in very low concentrations and so will not impact on $\delta^{18}O_{calcite}$, especially during interglacial periods.

6.6.4 Late Glacial to Holocene environmental variability at Lake Ohrid

6.6.4.1 Late Glacial (12.3 ka − 12.0 ka)

At the base of the core (ca. 12.3 − 12.0 ka) TIC, TOC, TOC/TN and HI are all low with high OI and $\delta^{13}C_{organic}$, which is commensurate with the presence of gravel-sized grains that most likely represent ice-rafted debris (IRD) implying that the lake was at least partially ice-covered during winter (Wagner et al., 2009a; Wagner et al., 2012b). Enhanced clastic supply is suggested by high K content (Figure 6.35) and given the elevated accumulation rate and OI alongside reduced autochthonous input (low TIC and TOC), allochthonous input may have been higher. Greater catchment erosion would have been promoted by an open landscape with stadial-like characteristics dominated by herbaceous vegetation signifying cold and dry conditions (Panagiotopoulos et al., 2013). Diatom data from Co1262 show a low-diversity assemblage dominated by *Cyclotella fottii* (Figure 6.35), which suggests low temperature-dependent productivity similar to the conditions during the Last Glacial (Zhang et al., 2015). Although external nutrient supply was likely high due to enhanced allochthonous input, the low-diversity diatom assemblage infers low temperatures may have restricted in-lake productivity (Zhang et al., 2015). Lake Ohrid is sensitive to surface cooling and reduced temperatures would trigger more frequent and complete deep convective mixing (Matzinger et al., 2006b). Currently the lake mixes roughly every ca. 7th winter (Hadzisce, 1966), however if the lake became monomictic or dimictic the water column would be better oxygenated and thus promote OM degradation and calcite dissolution, as observed in organic proxies.

The cold and dry phase is likely the Younger Dryas chronozone (Kotthoff et al., 2008a), which is defined by a return to glacial-like conditions (Rossignol-Strick, 1995). This time period correlates to a significant reduction in mean annual temperature (−9°C) and annual precipitation (−400 mm) reconstructed from pollen data at nearby Lake Maliq (Albania; Bordon et al., 2009), which is similar to observations from across the Mediterranean reflected in marine records from the Aegean (Kotthoff et al., 2011), Adriatic (Combourieu-Nebout et al., 2013) and Ionian (Emeis et al., 2000) basins, and in terrestrial records from Greece (Wilson et al., 2008), Italy (Allen et al., 2002) and Turkey (Jones et al., 2007). Steppic-pollen infer cold and dry conditions across the Mediterranean during the Younger Dryas (Desprat et al., 2013), and a reduction in precipitation of up to 50% (Kotthoff et al., 2011) would have likely led to a lower lake level, given that outflow may have remained comparatively high (Chapter 5). Shallower lake levels during the Younger Dryas are observed in other records from the central and eastern Mediterranean (Digerfeldt et al., 2000; Wick et al., 2003; Magny et al., 2007; Jones et al., 2013; Cvetkoska et al., 2014), and may be responsible for a hiatus in Lz1120 (Wagner et al., 2009a). A sparsely-vegetated catchment would preclude major soil development (Panagiotopoulos et al., 2013) and, in combination with less water throughput, the intensity of karst weathering and delivery of Ca^{2+} and HCO_3^- ions to the lake would have probably been greatly reduced. In addition, glacial activity and permafrost in the catchment due to lower temperatures would prohibit precipitation infiltration, thereby lowering inflow to the karst system and increasing surface runoff (Belmecheri et al., 2009; Ribolini et al., 2011), which is consistent with higher K content in the lower core. A reduction in delivery of Ca^{2+} and HCO_3^- ions, in addition to enhanced lake water mixing and dissolution potential, may create the basis for a threshold (Figure 6.30) before calcite is precipitated and preserved in sediments.

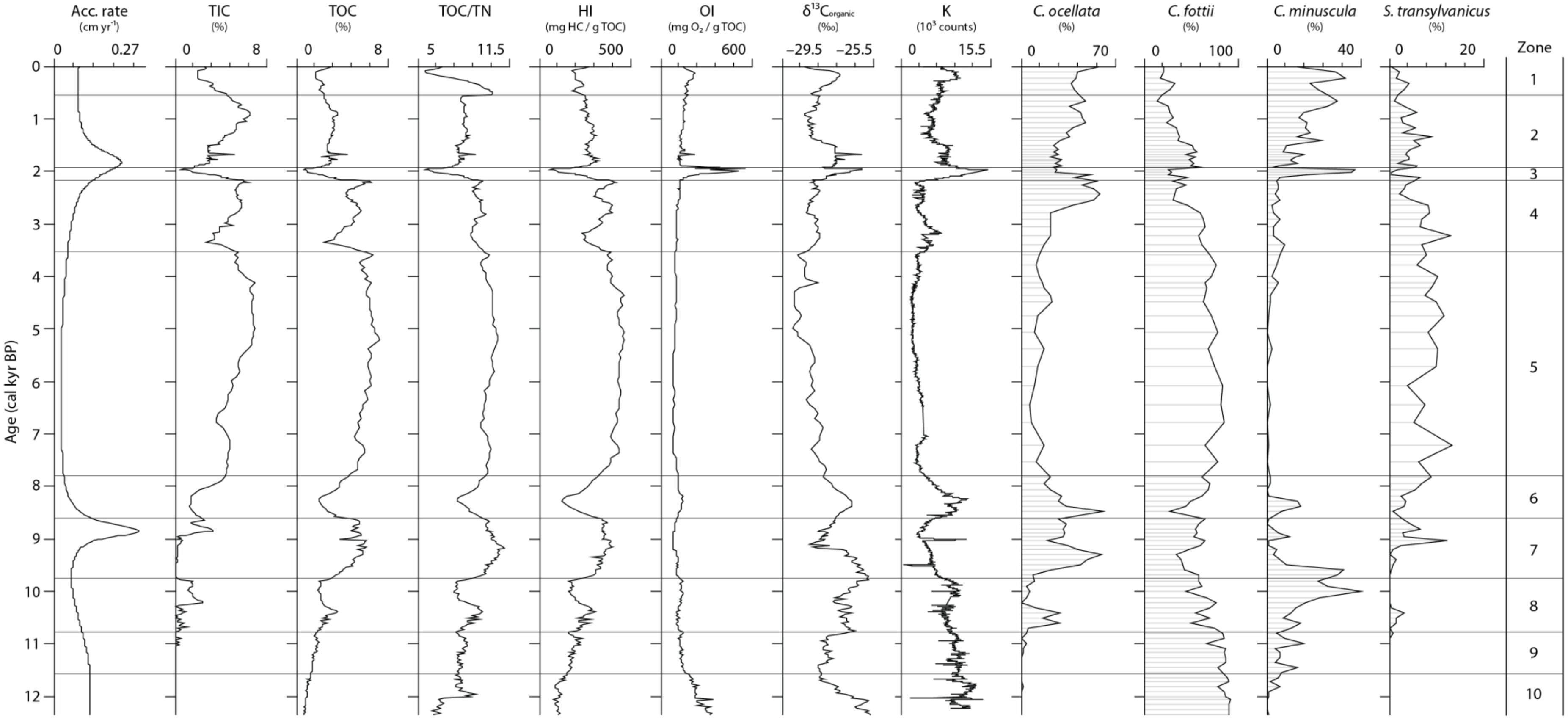

Figure 6.35 *Comparison of organic data with XRF (K; Wagner et al., 2012b) and diatom data (Zhang et al., 2015) from Co1262, showing the zones defined in Section 6.5.*

6.6.4.2 Earliest Holocene (12.0 − 10.3 ka)

The abrupt increase in TOC/TN after 12 ka and subtler increase in TOC and HI through to 10.4 ka provide the first signs of greater in-lake productivity and/or a decrease in lake water mixing leading to progressively less OM degradation (trend to lower OI). Enhanced thermal stratification and climate warming are also inferred from the increasing presence of *Cyclotella minuscula* (Figure 6.35; Zhang et al., 2015), and catchment pollen signals the gradual expansion of arboreal taxa at the expense of herbs (Panagiotopoulos et al., 2013). The Ohrid record suggests a much more subdued response to changing climate in comparison to the relatively rapid climate transition (ca. 150 years) suggested by reconstructions from Lake Maliq (Bordon et al., 2009) and the Aegean Sea (Kotthoff et al., 2011) (taking into account uncertainty in the age models; Figure 6.36).

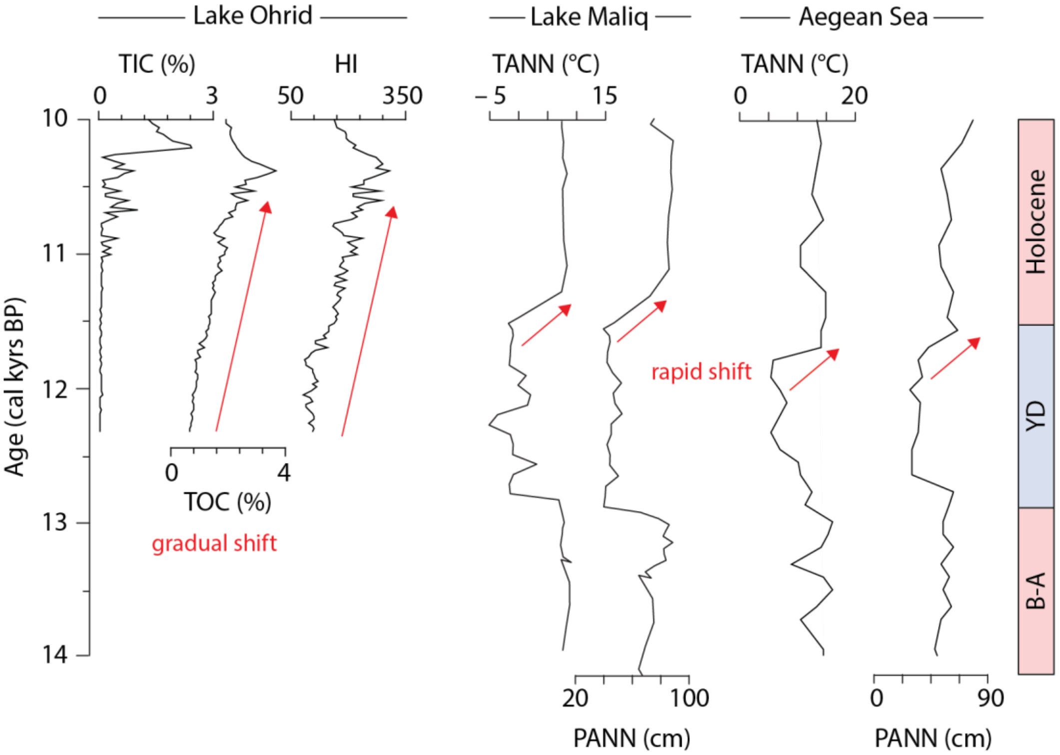

Figure 6.36 *Comparison between organic proxies from Lake Ohrid Co1262 and pollen-based annual temperature (TANN) and annual precipitation (PANN) reconstructions from Lake Maliq (Bordon et al., 2009) and the Aegean Sea (Kotthoff et al., 2011) plotted against individual age models.*

The lack of calcite in the sediment record implies that catchment soil development and precipitation were not high enough to deliver Ca^{2+} and HCO_3^- ions from dissolution of catchment rocks, and/or winter temperatures were still low enough for regular lake water mixing to occur. Overall low diatom concentrations indicate temperatures were still very low (Zhang et al., 2015), and an initial dominance of non-steppic herb taxa after the Younger Dryas across the region suggests that higher precipitation may not have supported extensive forest development (Zhang et al., 2014, and references therein). A lag in the expansion of woodland would have inhibited soil development and associated catchment karst dissolution, and therefore may be correlated to the overall low calcite content of sediments, which is also assumed for Lake Prespa (Aufgebauer et al., 2012). HI starts to increase after 11.8 ka, driven by an increase in S2 (Figure 6.37), concomitant with higher TOC, TOC/TN and lower $\delta^{13}C_{organic}$, OI, which is assumed to correlate with higher aquatic productivity and the onset of the Holocene.

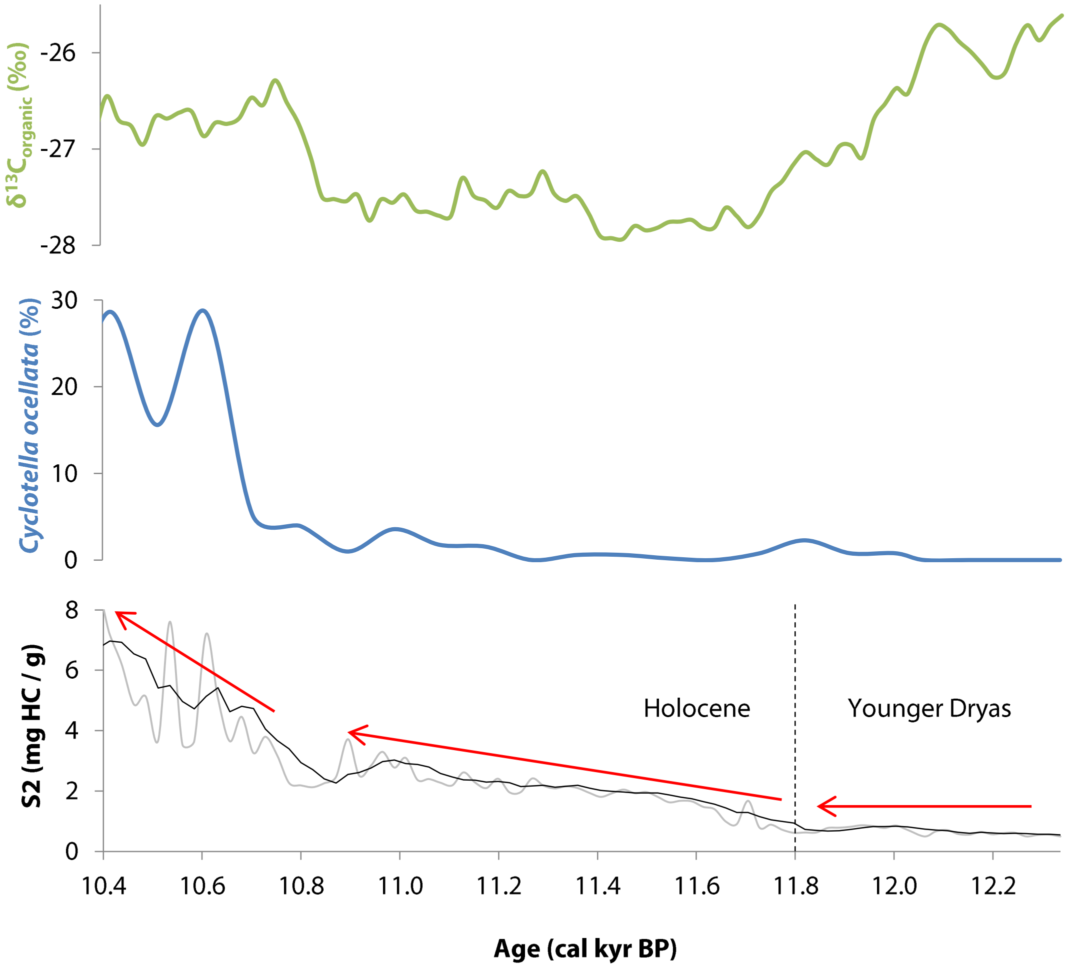

Figure 6.37 *Plot of $\delta^{13}C_{organic}$ (green),* Cyclotella ocellata *(blue; Zhang et al., 2015) and S2 between the base of the core and 10.4 ka, showing the raw data (grey line), 5-point moving average (black line) and the start of Holocene warming (dashed line).*

Ice-rafted debris is present until 11.3 ka (Wagner et al., 2012b), suggesting winters were still cold enough for partial ice cover but summers were becoming progressively warmer, corroborating a gradual transition from the Younger Dryas to the Holocene. A faster rate of S2 increase occurs after 10.8 ka alongside the abrupt introduction of epilimnetic diatom taxa, in particular *Cyclotella ocellata*, higher $\delta^{13}C_{organic}$ (Figure 6.37) and higher TIC (Figure 6.36). The synchronous change seen across these proxies suggests a rapid increase in aquatic productivity due to warmer climate conditions, as a high abundance of *Cyclotella ocellata* is indicative of high temperature-induced productivity (Reed et al., 2010; Zhang et al., 2015). The positive correlation observed between $\delta^{13}C_{organic}$ and S2 (also seen in TOC_{RE} and HI) after 10.8 ka is not present over the whole core (Figure 6.27), leading to the assertion that productivity does not typically drive changes in $\delta^{13}C_{organic}$ (Section 6.6.2). However, the change to higher $\delta^{13}C_{organic}$ alongside a clear increase in productivity suggests the export of ^{12}C to sediments raising epilimnetic $\delta^{13}C_{TDIC}$, and further, this also implies a reduction in lake water mixing and enhanced thermal stratification to facilitate ^{12}C-export and reduce OM recycling.

6.6.4.3 Early Holocene (10.3 − 7.8 ka)

After 10.3 ka, there is the first substantial calcite increase of the record (TIC values are up to 2.5%) and an apparent simultaneous decrease in organic productivity within the lake (lower TOC, TOC/TN, HI, S2) through until 9.8 ka. Although this ca. 500-year period could be ascribed to dilutionary effects (i.e. more calcite lowering the concentration of other sedimentary components), this is perhaps a too simplistic explanation as $\delta^{13}C_{organic}$ also increases by +1.6‰ through this interval. Epilimnetic nutrient availability was thought to be limited at this time, as suggested by low diatom concentration and a transition from *Cyclotella ocellata* dominance to *Cyclotella minuscula* (Figure 6.35), which Zhang et al. (2015) ascribe to nutrients being adsorbed onto precipitating calcite particles that are subsequently exported to sediments (Allen and Ocevski, 1977). However, this is somewhat contradictory if productivity is linked to calcite production (Matzinger et al., 2006b; Matter et al., 2010). The precipitation of calcite suggests that soils in the catchment must have developed to the extent that they are able to influence karst dissolution thereby increasing the concentration of Ca^{2+} and HCO_3^- ions in lake water. Increased water input from the karst system would also increase the geological-sourced component of TDIC pool, which would lead to higher $\delta^{13}C_{TDIC}$ and $\delta^{13}C_{organic}$ through this zone (Section 6.6.2). This infers that precipitation must have been high enough to facilitate groundwater flow through the spring network. However, a short-term reduction in annual precipitation is reconstructed from Lake Maliq combined with warm summer temperatures (Bordon et al., 2009). A dry climate (especially summer drought) during this period is further suggested by the stalling of forest development in the catchment and evidence for increased fire activity (Panagiotopoulos et al., 2013), which is also reported at Lake Van in Turkey (Wick et al., 2003). An open catchment more susceptible to erosion is inferred from an elevated K concentration, however this would increase nutrient delivery to the lake and be opposed to the observed low diatom abundance. If summer temperatures were high and a generally dry climate existed evaporation would increase and concentrate Ca^{2+} and HCO_3^- in surface waters (Vogel et al., 2010a), thus promoting calcite formation. Intense calcite precipitation could limit nutrient availability as suggested by Zhang et al. (2015) and warm summer temperatures and increased water column stratification may also limit nutrient recycling by decreasing the potential for OM degradation. This event may be linked to an early Holocene abrupt event observed at the Ioannina basin in Greece, where low lake levels and dry conditions are inferred from diatom and pollen data between 10.1 and 9.7 ka (Lawson et al., 2004; Wilson et al., 2008). Although the climate event is questioned by the lack of a response to the widespread ‘8.2 ka event’ (Alley et al., 1997) at Ioannina, Lake Ohrid indicates that two separate events are present (Figure 6.38; see discussion of 8.2 ka event below).

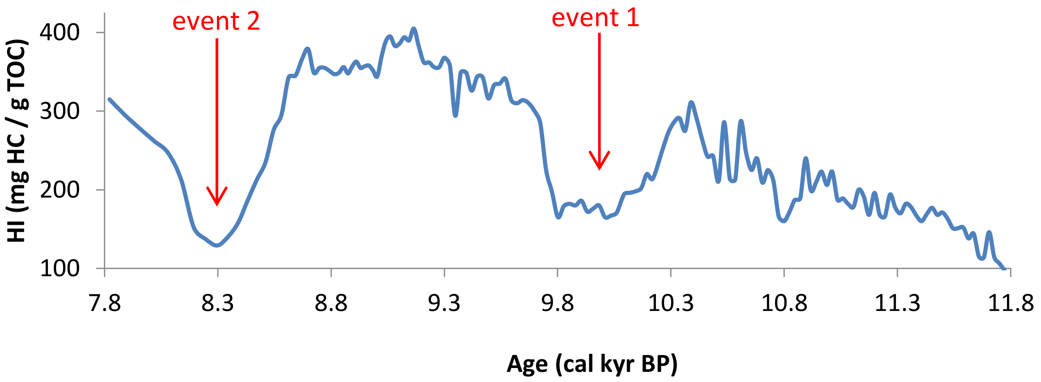

Figure 6.38 *HI against age, showing the response to two early Holocene events.*

A period of enhanced in-lake productivity is inferred by the organic data between 9.8-8.6 ka, where higher HI and S2 suggests a greater quantity of algal material in sediments. Although sedimentation rate increases from a minimum at ca. 9.8 ka to a maximum at ca. 8.8 ka, K content steadily decreases over this time interval (i.e. lower clastic supply) and calcite content is negligible until after 9 ka, inferring that higher sediment accumulation is driven by increasing aquatic productivity. This is also documented in diatom data from Co1262 that show an increasing abundance of *Cyclotella ocellata* and decreasing *Cyclotella minuscula* (Zhang et al., 2015), which is the opposite of 'event 1' (Figure 6.35 and 6.38) and implies high temperature-induced productivity. Given that nutrient supply must have been high to support the dominance of mesotrophic *Cyclotella ocellata* (Wagner et al., 2009a; Lorenschat et al., 2014), and internal nutrient cycling was likely low due to strong thermal stratification in response to warmer summer temperatures (Bordon et al., 2009), external nutrient supply must have been high. The catchment was characterised by a dense vegetation and soil formation (Aufgebauer et al., 2012; Panagiotopoulos et al., 2013), which is consistent with decreasing K content as a result of lower catchment erosion, but not necessarily with increased nutrient supply.

At this time many records from the Mediterranean region suggest a change in precipitation regime to an overall wetter climate (see Section 6.6.5; Roberts et al., 2008, and references therein), and evidence for increased lake levels are reported from several nearby sequences in Macedonia (Francke et al., 2013), Greece (Digerfeldt et al., 2000; Jones et al., 2013), and Italy (Zanchetta et al., 2007a; Joannin et al., 2012). Enhanced annual precipitation is thought to have been more evenly distributed (Panagiotopoulos et al., 2013), which could moderate summer evaporation and, along with increased inflow, may have led to more dilute lake water (with respect to Ca^{2+} and HCO_3^-) thus preventing calcite formation. Overall greater inflow and forest vegetation, alongside decreasing $\delta^{13}C_{organic}$ suggests that enhanced soil development and chemical weathering in the catchment delivered greater quantities of soil-derived carbon and nutrients to the lake (e.g. Zhang et al., 2014). This would support in-lake productivity and reduce water residence time in the karst system leading to the generally lower Ca^{2+} and HCO_3^- ion availability and reduce calcite precipitation.

Climate warming and in-lake productivity are thought to have occurred between 9.2 and 8.6 ka, characterised by maxima in TOC, TOC/TN and HI, and minima in OI and $\delta^{13}C_{organic}$, which is consistent with records from Lake Prespa (9.3-8.3 ka; Aufgebauer et al., 2012) and Lake Dojran (ca. 9 ka; Francke et al., 2013). High summer temperature likely persisted through until 8.6 ka, where after ca. 9 ka calcite is present in the core and corresponds to a maximum in sedimentation rate (Figure 6.35). Calcite precipitation is likely in response to greater productivity, substantiated by the parallel increase in abundance of the mesotrophic diatom *Stephanodiscus transylvanicus* (Figure 6.35; Wagner et al., 2009a; Zhang et al., 2015).

A distinct maxima in K concentration around 9 ka (7.09 m core depth; Figure 6.39) is thought to be caused by tephra deposit relating to the Mercato eruption of Mount Vesuvius (Section 6.4; Wagner et al., 2012b). The peak is synchronous with a reduction in TOC, TIC, and S2, however there is little change in TOC/TN, HI, OI and $\delta^{13}C_{organic}$. As ratio values do not show any fluctuation the tephra most likely had a dilutionary effect on sediments rather than a direct influence of productivity or climate, which is also implied by a lack of response in diatoms (Zhang et al., 2015).

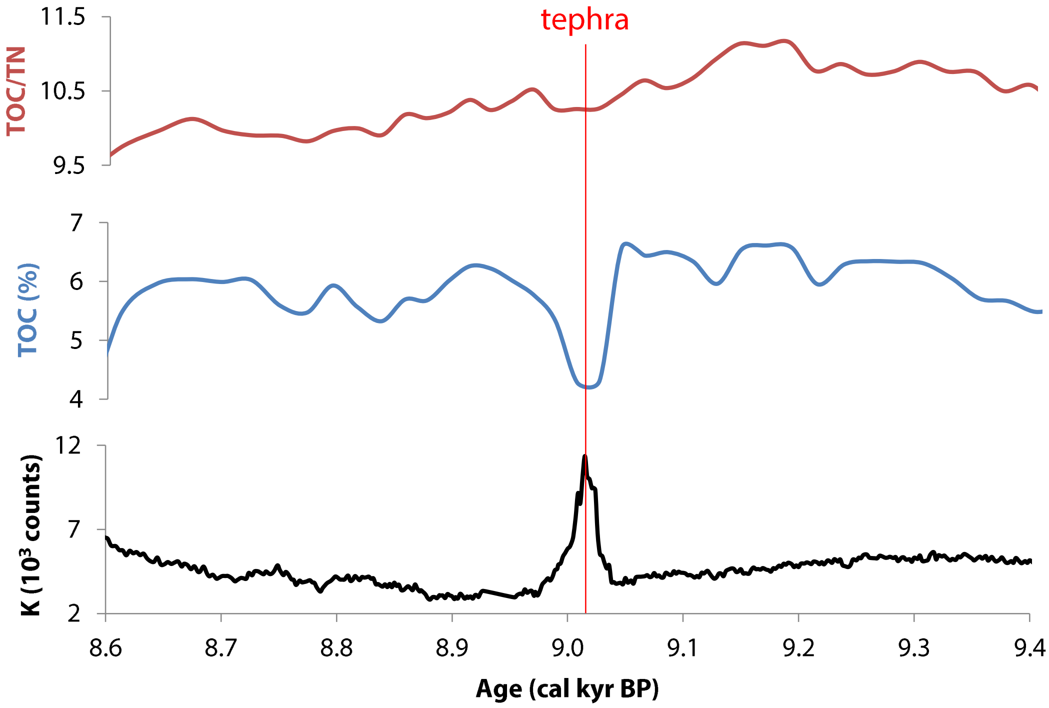

Figure 6.39 *Plot of K, TOC, and TOC/TN data, showing the position of the Mercato tephra layer.*

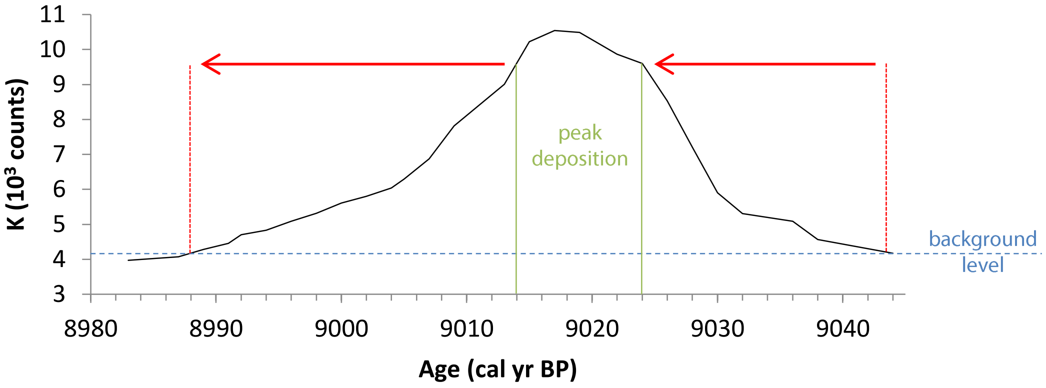

Figure 6.40 *Plot of K concentration (3-point moving average), showing the Mercato tephra deposition.*

Although the original volcanic eruption may have only lasted a short time (hours-days; Macedonio et al., 1988), the residence time during transport will be rapid in comparison to the observed distribution in sediments (Figure 6.40). The time between the first elevation above background levels of K and the period of peak distribution is 19 years, however the tail after deposition of the tephra is 26 years. Taking into account uncertainty in the age model, this suggests that not only was the tephra mixed with existing sediments (not an instantaneous peak), but also that greater redistribution occurred after deposition (tail is longer than rise). This qualifies how sedimentary processes and bioturbation in Ohrid can affect the resolution of short-term events and restrict the reconstruction of annual to decadal-scale environmental change. If it is assumed tephra deposition was confined to a period of less than one-year for this event, the minimum resolution attainable for Ohrid sediments is therefore approximately 50 years (irrespective of higher sedimentation rates).

The period between ca. 8.6-8.0 ka is characterised by distinct minima in TIC, TOC, TOC/TN, and HI and maxima in OI, $\delta^{13}C_{organic}$, and K concentration (Figure 6.41). Previous records from other sites in Lake Ohrid also record a distinct decrease in both TIC and TOC (Wagner et al., 2009a; Vogel et al., 2010a), which suggests a basin-wide response to a decrease in productivity and calcite formation, and/or more OM degradation and calcite dissolution due to enhanced lake water mixing. Lower winter temperatures and drier conditions are reconstructed from nearby Lake Maliq (Bordon et al., 2009), which is consistent with a decrease in catchment arboreal pollen percentages and a simultaneous increase in *Artemisia* suggesting an opening of the tree cover and reduction in soil development (Aufgebauer et al., 2012; Panagiotopoulos et al., 2013). Drier conditions and sparse soils would reduce karst dissolution, thereby raising lake water $\delta^{13}C_{TDIC}$ also producing the observed higher $\delta^{13}C_{organic}$. A drier climate is thought to have led to lower lake levels in both Ohrid (Holtvoeth et al., 2015) and Prespa (Aufgebauer et al., 2012), as well as in other central Mediterranean lake records (Magny et al., 2007; Heymann et al., 2013). This is most likely a response to the '8.2 ka event' (Johnsen et al., 1992), driven by a rapid cooling in the North Atlantic region reported to be around 6-7°C from Greenland ice cores (Alley et al., 1997; Leuenberger et al., 1999).

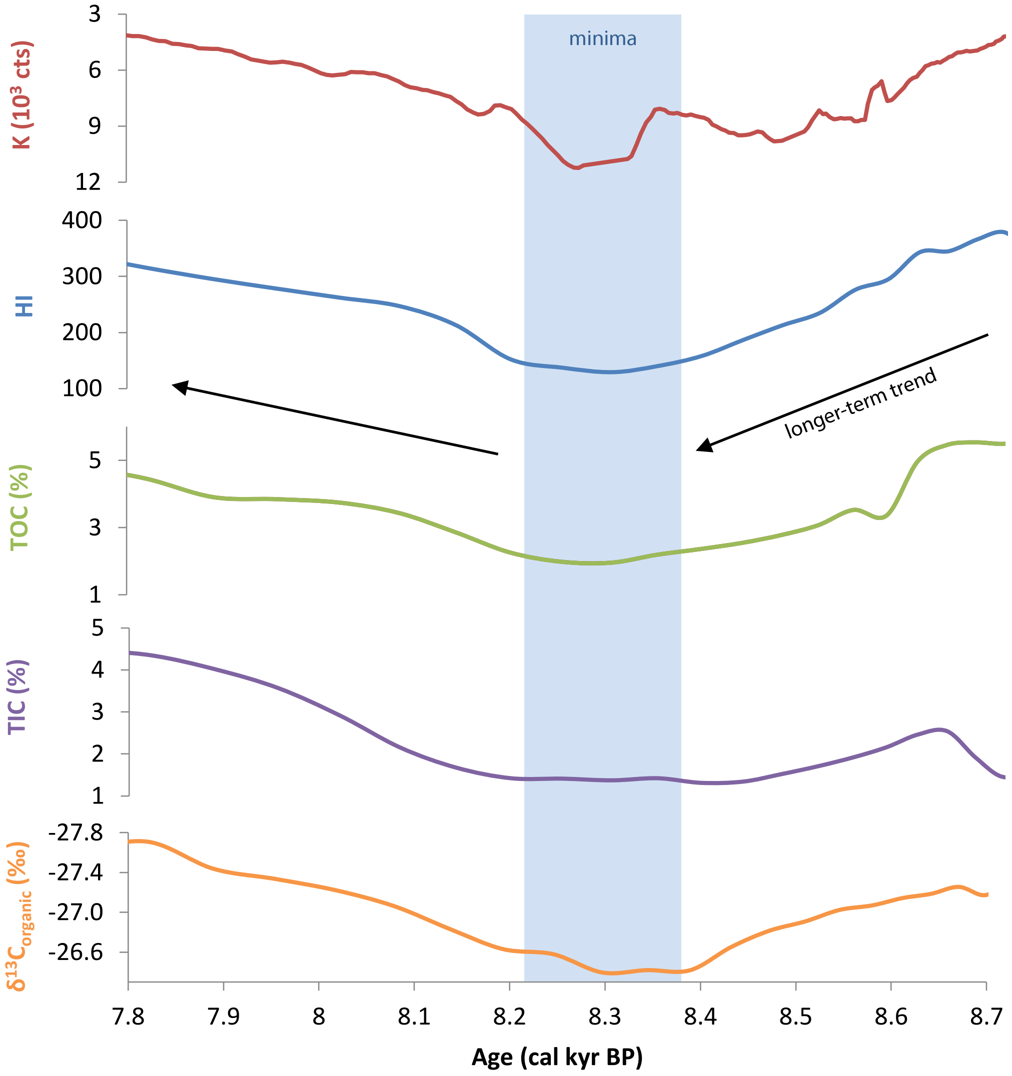

Figure 6.41 *Plot of $\delta^{13}C_{organic}$ (reversed axis), TIC, TOC, HI, and K concentration (revered axis) between 8.7 and 7.8 ka, showing a common perturbation.*

Although reconstructions suggest a rapid and synchronous response across the North Atlantic region to a ca. 150 year climate event (Thomas et al., 2007; Daley et al., 2011), records from Mediterranean sites generally imply that the abrupt event is superimposed on a longer-term cooling of up to around 500-600 years (Rohling and Palike, 2005; Berger and Guilaine, 2009; Dean et al., 2015). Moreover, temperature reconstructions from the Mediterranean region suggest a more subtle change of around 2-4°C from both marine and terrestrial records (Kotthoff et al., 2008b; Bordon et al., 2009; Marino et al., 2009; Pross et al., 2009; Peyron et al., 2011), however conditions were not uniform across Europe (Magny et al., 2007; Zanchetta et al., 2007b; Peyron et al., 2011). A hydrological tri-partition is thought to have existed in response to cooling, with mid-latitudes between 50° and 43° experiencing a wetter climate and latitudes outside of this zone drier conditions (Magny et al., 2003). The abrupt cold event around 8.2 ka and related climate anomalies are thought to have been triggered by a slowdown of North Atlantic thermohaline circulation (THC) induced by catastrophic meltwater release during the terminal demise of the Laurentide ice sheet (Alley et al., 1997; Barber et al., 1999; Hoffman et al., 2012; Lewis et al., 2012). A reduced THC favours increased sea-ice coverage of the Nordic Seas, which in turn abates the transfer of mild, humid Atlantic air masses across much of Europe (Pross et al., 2009; Peyron et al., 2011). A strong low-high latitude thermal gradient and southward displacement of westerlies would increase cyclonic activity over mid-latitudes, and bring dryness to more northern and southern latitudes (Renssen et al., 2002; Magny et al., 2003). This would have allowed the Siberian High to intensify and expand (sub)polar climate conditions over Eurasia (Rohling et al., 2002), leading to increased outbreaks air from higher to lower latitudes resulting in cold and dry winter-spring seasons (Renssen et al., 2002; Marino et al., 2009).

The Co1262 record supports a cold and dry event at this time, suggesting lower productivity and calcite production (and/or lower preservation; Figure 6.3). Maximum cool and dry conditions at Lake Ohrid are consistent with the proposed timing of meltwater introduction to the North Atlantic (8.49-8.04 ka; Lewis et al., 2012), however the duration of the event is observed to be more extended than suggested by records from the North Atlantic region (150±30 years; Daley et al., 2011). Although the exact timing and chronology of the event cannot be directly compared between records (as a tie point at 8.2 ka is used in the Co1262 age model, Section 6.4), the overall magnitude and duration can be considered. The high resolution nature of the Co1262 dataset provides good constraint to the overall magnitude of change and confidence in the structure of the excursion (Figure 6.42). A decrease in HI (assumed to be related to productivity and/or degradation, Section 6.6.1) immediately commences after 8.7 ka and continues to reach a minimum at 8.3 ka. This is followed by a period of rapid recovery up to 8.1 ka, after which a steady increase occurs over the next ca. 800 years suggesting the event lasted between ca. 600 (end of rapid recovery) and 1000 years (to return to pre-event levels, HI ≈ 350).

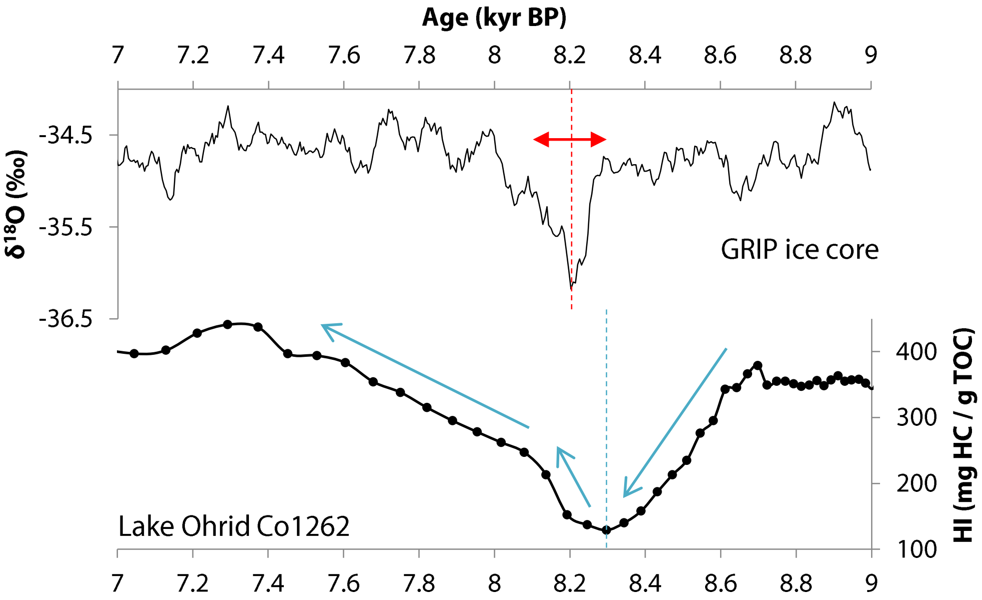

Figure 6.42 *Comparison of Lake Ohrid Co1262 HI with the δ^{18}O curve (11-point running average) from the Greenland Ice Core Project (GRIP) ice core, plotted on individual time scales.*

Events of a similar duration are reported from other Mediterranean records (Rohling et al., 2002; Kotthoff et al., 2008b; Francke et al., 2013; Dean et al., 2015). Given that this trend initiates prior to the earliest estimated timing of freshwater outburst in the North Atlantic (Lewis et al., 2012), the observed climate deterioration could instead be related to intervals of reduced solar output (Bond et al., 2001; Rohling and Palike, 2005). Solar variability is supported by three peaks in^{14}C production between 8.4 and 7.9 ka, suggesting that the longer-term cooling is concomitant with a phase of decreasing solar forcing (Muscheler et al., 2004; Muscheler et al., 2005). In all, the

Co1262 record suggests a multi-centennial period of climate deterioration around the 8.2 ka event, supporting the hypothesis that cooling started before 8.5 ka.

6.6.4.4 Middle Holocene (7.8 ka – 4.4 ka)

The period directly after the 8.2 ka event shows a steady increase in TOC followed shortly after by a more moderated increase in TIC (Figure 6.43), reinforcing the observation that a climate (or environmental) threshold must be passed before calcite is precipitated and/or preserved during the transition from cold-dry to warm-wet climate conditions (as in Figure 6.30).

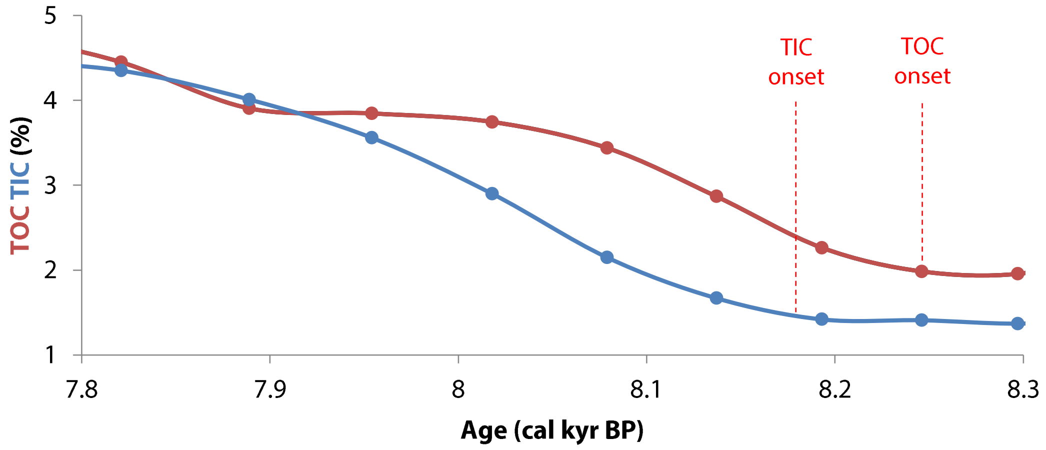

***Figure 6.43** Plot of TOC and TIC, showing a temporal offset between organic matter production and calcite precipitation.*

Following the transition from the 8.2 ka event a steady rise in TOC suggests more organic productivity (and/or preservation) in response to warmer temperatures. The delayed onset and gradual increase in calcite precipitation could be correlated to the slow decline in OI inferring lake water may still be well oxygenated, which is supported by a low Fe/Ti ratio assumed to indicate more oxidising conditions (Figure 6.44; after Aufgebauer et al., 2012). In addition, a stable decline in $\delta^{13}C_{organic}$ suggests that there may have been a slow increase in catchment soil development and the associated low availability of Ca^{2+} and HCO_3^- ions may also have limited calcite precipitation, perhaps explaining its lag behind enhanced in-lake productivity. The measured lowering of K concentration and OI (and increase in Fe/Ti) between ca. 8.3-7.6 ka may be due to the continued input of detrital clastic material inferring the catchment was still rather open and erosion could take place, supporting high aeolian activity the late development of soils (Figure 6.44).

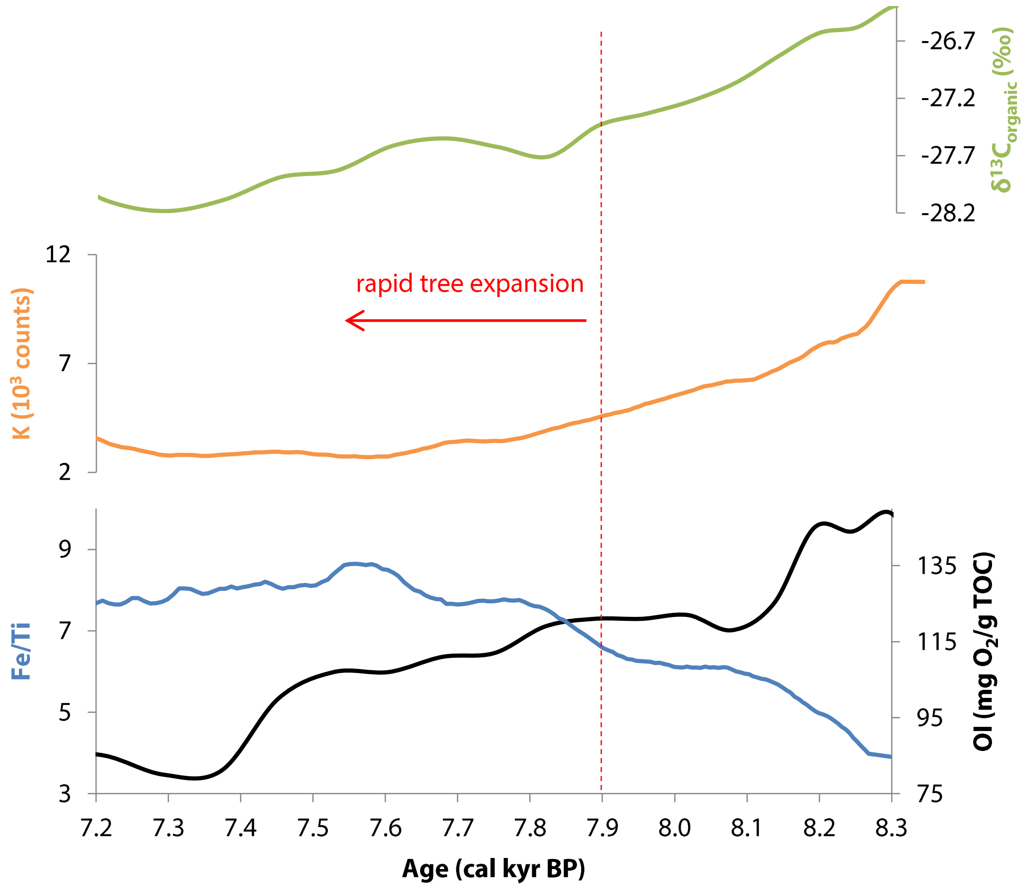

Figure 6.44 *Plot of* $\delta^{13}C_{organic}$*, K concentration (11-point running average), OI and Fe/Ti (11-point running average), showing the transition out of the 8.2 ka event and the timing of tree expansion in the catchment (Panagiotopoulos et al., 2013).*

The rise to higher TIC, TOC, TOC/TN and HI at around 7.4 ka (Figure 6.35) is coincident with minima in OI, K concentration and higher Fe/Ti, and follows a rapid expansion of thermophilous trees in the catchment after ca. 7.9 ka and the return of dense vegetation, which suggests relatively wet and mild conditions (Panagiotopoulos et al., 2013). A humid climate is also inferred at this time from Corchia cave in northern Italy, where peak rainfall was found between 7.9 and 7.4 ka (Zanchetta et al., 2007b), and most likely corresponds to the deposition of Sapropel 1 in the Mediterranean Sea (Kallel et al., 1997; Ariztegui et al., 2000).

A climate optimum is inferred between ca. 7.4-4.4 ka by elevated TIC, TOC, TOC/TN and HI in Co1262 suggesting high temperatures and in-lake productivity, which is supported by high calcite and OM content in cores Lz1120 and Co1202 (Wagner et al., 2009a; Vogel et al., 2010a). A basin-wide response to improved climate conditions is also implied by lower K concentration that in combination with maxima in arboreal pollen percentages (assemblages dominated by *Pinus* and *Quercus* deciduous type; Wagner et al., 2009a; Panagiotopoulos et al., 2013) suggests a catchment with well-developed forests and low erosion rates. A transition toward lower $\delta^{13}C_{organic}$ through the mid-Holocene follows the expansion of trees in the catchment and most likely corresponds to increased soil activity and perhaps relates to the growth of a C3-dominated vegetation system (i.e. lower $\delta^{13}C_{TDIC}$; Section 3.3.3). Greater soil development in the catchment would also enhance chemical weathering and karst dissolution providing a higher amount of Ca^{2+} and HCO_3^- ions to the lake promoting calcite precipitation. Strong thermal stratification in response to warmer temperatures during summer months and milder winters would reduce lake water mixing (Matzinger et al., 2006b) and give rise to reducing conditions (higher Fe/Ti and low OI) thus facilitating better OM and calcite preservation. In addition, reduced lake water circulation would limit mixing-induced upward nutrient supply and epilimnetic nutrient availability, which is implied by restricted diatom productivity as seen in the overall reduction of *Cyclotella ocellata* (Figure 6.35; Zhang et al., 2015).

Based on broad maxima in TIC, TOC and HI, and minima in $\delta^{13}C_{organic}$, OI, and K concentration, optimum conditions for calcite precipitation and OM preservation at Lake Ohrid were most likely reached between 5.3 ka and 4.4 ka. The highest proxy values are observed around 5 ka (Figure 6.35). This is consistent with mid-Holocene conditions at Lake Prespa (Wagner et al., 2010; Aufgebauer et al., 2012) and at Lake Dojran (Francke et al., 2013). The steady rise in calcite content (and also OM) observed in these lakes after the cool and dry climate of the 8.2 ka event suggests that improving conditions were spatially and temporally consistent across the Balkan Peninsula (Figure 6.45). However, the maximum in calcite and OM content at Lake Ohrid around ca. 5.0 ka occurs subsequent to the start of a climatic trend towards drier conditions from ca. 6 ka, observed in isotope data from lakes Ohrid, Prespa, Dojran and Van (Section 6.6.5; Wick et al., 2003; Leng et al., 2010a; Francke et al., 2013; Leng et al., 2013), and as lower reconstructed lake levels from lakes Pergusa, Preola and Trifoglietti (Sadori and Narcisi, 2001; Magny et al., 2011b; Joannin et al., 2012). This could be linked to the seasonality of precipitation, where a strong seasonal hydrological contrast in the early Holocene driven by a bias towards winter precipitation (Tzedakis, 2007) may have reduced, allowing for the combined scenario of lessening winter inflow (trend to higher $\delta^{18}O_{lakewater}$) and summer calcite precipitation (persistent warm summer temperatures). Regional-scale drivers of climate are discussed in further detail in Section 6.6.5.

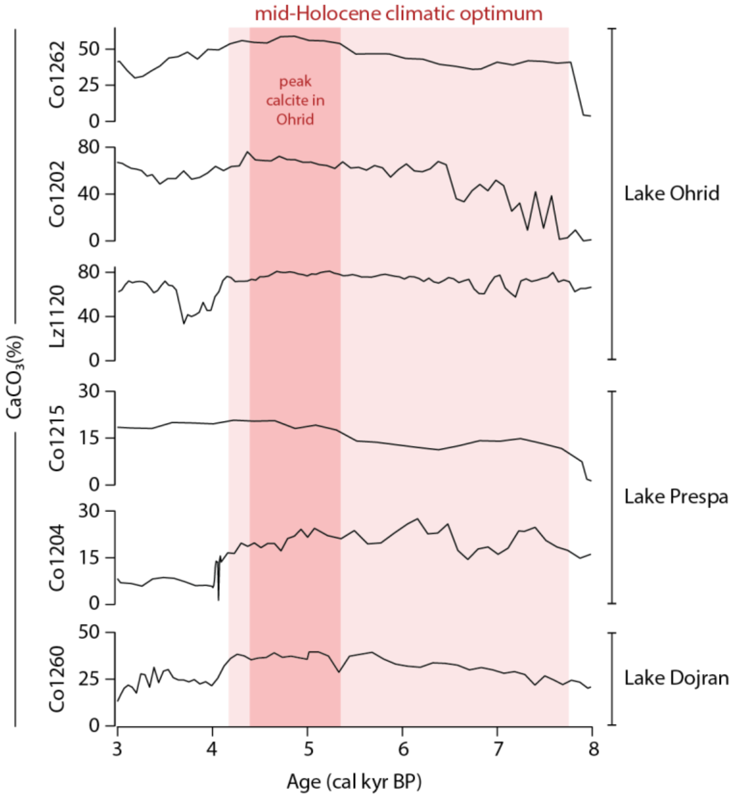

Figure 6.45 *Comparison of the calcite content ($CaCO_3$ %) of sediments from Lake Ohrid cores Co1262, Co1202 (Vogel et al., 2010a), Lz1120 (Wagner et al., 2009a), Lake Prespa cores Co1215 (Aufgebauer et al., 2012), Co1204 (Wagner et al., 2010), and Lake Dojran core Co1260 (Francke et al., 2013).*

6.6.4.5 Late Holocene (4.4 ka − Present)

The late Holocene from ca. 4.4 ka is characterised by higher variability in organic proxies, contrasting with the overall stable conditions observed during the middle Holocene period (Figure 6.35 and 6.45). After peak conditions (maxima in calcite and TOC at ca. 5 ka), TIC, TOC, TOC/TN, HI and Fe/Ti show a steady transition to lower values through to approximately 4.1 ka, suggesting cooler conditions with increased lake water mixing, subsequent to which the rate of decline increases. This trend is paralleled by increasing $\delta^{13}C_{organic}$ and OI. A gradual rise in K concentration from 4.1 ka suggests increasing clastic supply and catchment erosion, and further that decreasing organic productivity (lower TOC and HI) is not limited by nutrient supply, inferred by high *Cyclotella ocellata* abundance (Zhang et al., 2015). The increase in K concentration and concomitant trend to lower values in organic proxies could be related to changing environmental conditions and/or dilutionary effects, as well as increasing pressure from rising anthropogenic activity in the catchment (see later discussion; Roberts et al., 2011a; Sadori et al., 2011). An overall deterioration in environmental conditions is supported by lower arboreal pollen percentages at Lake Pergusa (Sadori and Narcisi, 2001), a negative water balance at Lake Trifoglietti (Joannin et al., 2012) and Nar Gölü (Dean et al., 2015), and lower sea surface temperature estimates from the Adriatic Sea (Sangiorgi et al., 2003) and Aegean Sea (Rohling et al., 2002). The observed trend may be linked to a climate oscillation between 4.3-3.8 ka (Magny et al., 2009), however the variation at Lake Ohrid is not so much a short-term event (centered on 4.2 ka in global reconstructions; Booth et al., 2005), but rather represents a longer-term phase of change between ca. 4.1 ka to 2.2 ka.

Centered on minima in TIC, TOC, and HI at around 3.4-3.2 ka, the potential climate oscillation is coincident with higher $\delta^{13}C_{organic}$ and K concentration and is also seen in core Lz1120 and Co1202 from Lake Ohrid (Wagner et al., 2009a; Vogel et al., 2010a). Good chronological constraint is provided throughout this interval of the core by the Etna FL tephra and three radiocarbon dates from terrestrial plant material (Figure 6.46; Section 6.4). A peak in Sr concentration clearly demarcates the Etna FL tephra, which corresponds to the sharp decrease in TIC and TOC most likely caused by the input of the tephra and a change in the relative abundance of sedimentary components. The upper radiocarbon date suggests that a decline in calcite production (or preservation) started around 400 years (20 cm) prior to tephra deposition, and so it is unlikely that the decline is solely a response to tephra input. Given the 2σ uncertainty on the upper and lower radiocarbon dates, the phase most likely lasted between 1400 and 1900 years.

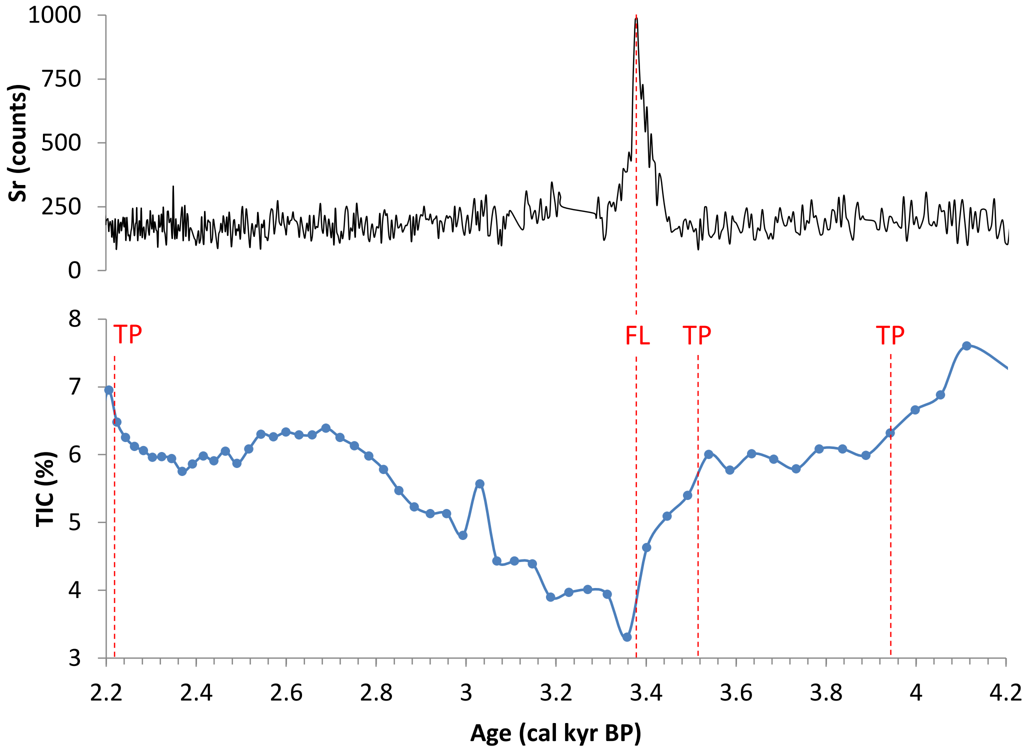

Figure 6.46 *Calcite content and Sr concentration, showing the location chronological control points including the Etna FL tephra (FL) and radiocarbon dates from terrestrial plant material (TP).*

The rise of calcite and OM content in the sediments is short-lived as after 2.2 ka a second excursion is observed across all proxies, characterised by low TIC, TOC, TOC/TN and HI, and the highest OI and K of the record (Figure 6.35). Similar to the previous event, the interval is chronologically well constrained by a terrestrial plant radiocarbon date (lowermost TP in Figure 6.46) and the AD 472/512 tephra (Section 6.4, Figure 6.47). A high sedimentation rate and K concentration through this zone imply an elevated supply of clastic material and high catchment erosion rates. Higher $\delta^{13}C_{organic}$, extremely high OI and low TOC/TN (which remained relatively high during 4.4-2.2 ka) suggests that this event could be related to a significant input of heavily oxidised and degraded terrestrial material. A peak in *Cyclotella minuscula* abundance coincident with the maxima in K concentration and minima in calcite (Figure 6.47) infers high epilimnetic productivity at this time and supports enhanced terrestrial input and delivery of nutrients (Zhang et al., 2015).

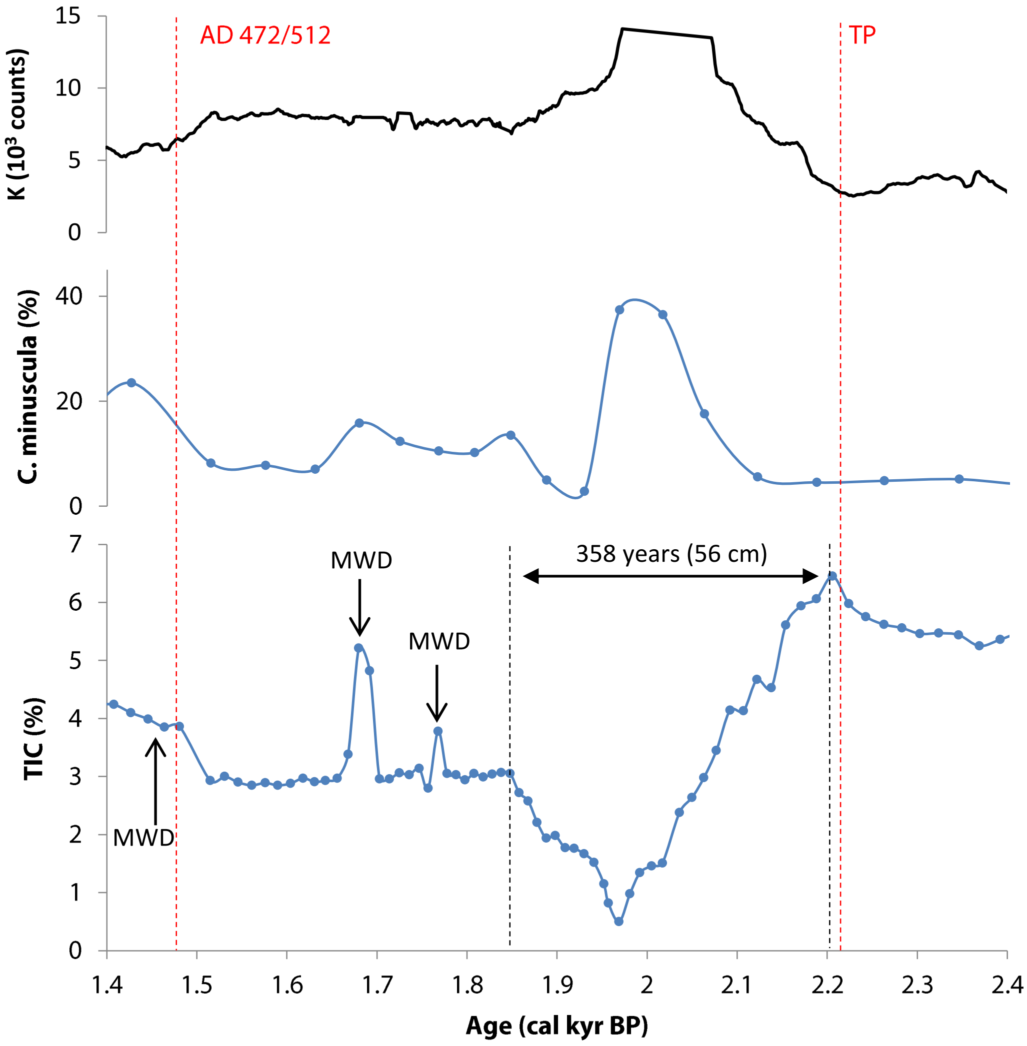

Figure 6.47 *Calcite and K concentration plotted with diatom abundance of* Cyclotella minuscula *(Zhang et al., 2015), showing the location of AD 472/512 tephra, radiocarbon date from terrestrial plant material (TP), and the locations of known mass wasting deposits (MWD).*

In the sediments directly above the ‘2.2-1.9 ka event’, several mass wasting deposits (MWD) are identified by homogenous sediments with a change in grainsize composition and can be correlated to a reduction in water content (Wagner et al., 2012b). The material for MWD likely originates from previously deposited sediments from shallower waters around the Lini Peninsula, which have higher carbonate content than in deeper areas (Figure 6.28). Therefore, in addition to a reduction in water content, MWD sourced from these locations should be characterised by higher calcite contents, as seen in the MWD between 320-121 cm and around 350 cm core depth

(Figure 6.48). An abrupt change to lower water content and higher Ca concentration at the base of the known MWD at 320 cm is distinct from the '2.2-1.9 ka event' (Figure 6.48), which has a more prolonged trend to lower calcite (TIC and Ca). However, the drop in water content at 404 cm is similar to within the MWD at 350 cm, so there could be a MWD toward the end of the event.

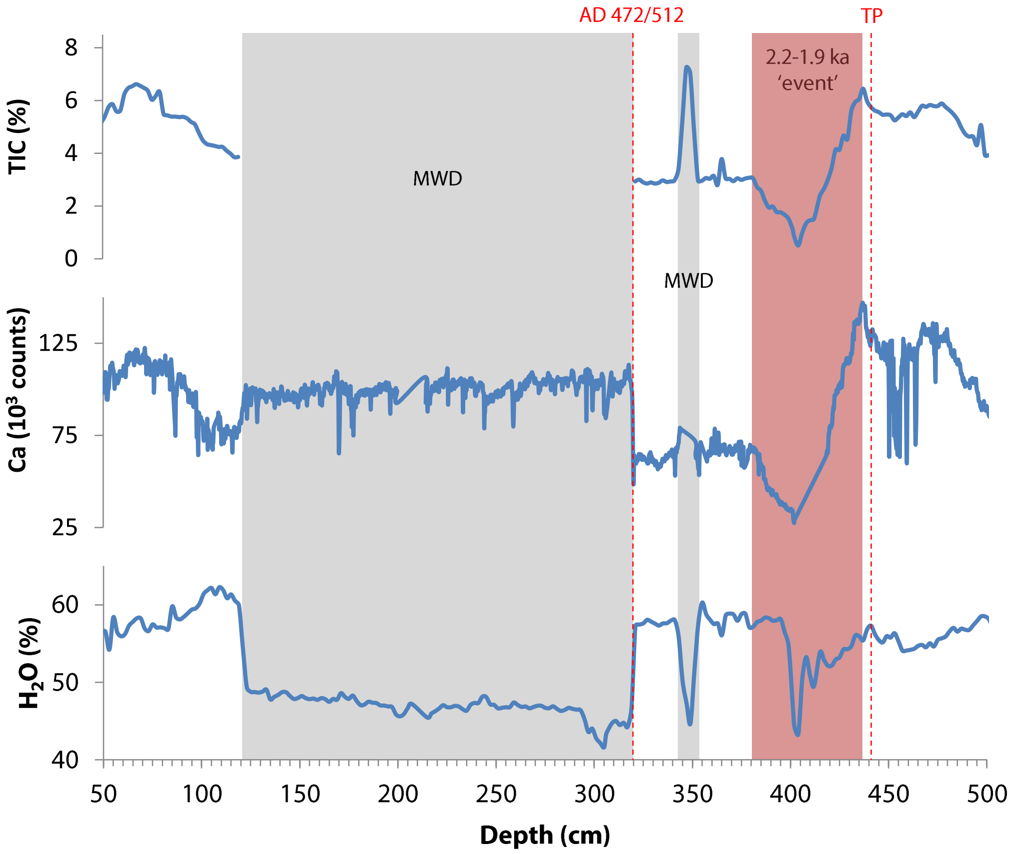

Figure 6.48 *Calcite content (TIC) plotted against Ca concentration and water content (Wagner et al., 2012b), showing the location of the AD 472/512 tephra, terrestrial plant radiocarbon age (TP), known mass wasting deposits (MWD) and the '2.2-1.9 ka event' described in Figure 6.47.*

A possible cause of greater erosion could be a lake level rise, where previously exposed shorelines are flooded and material can be transported downslope. The isotope record from Lake Ohrid is unlikely to record such abrupt changes given its large volume and residence time (see Section 6.6.5), however Lake Prespa is more sensitive to short-term (decadal) variations in water balance (Matzinger et al., 2006a; Leng et al., 2010a; Leng et al., 2013). Oxygen isotope data from Prespa imply an overall greater amount of precipitation (winter recharge) and a decreasing residence time around 2 ka (Figure 6.49; Leng et al., 2013). The overall wetter climate suggested by

Lake Prespa might have raised the water level of Ohrid and increased local erosion. Alternately (or in parallel), after 2 ka pollen data suggest that woodlands were receding and the landscape was becoming more open due to anthropogenic forest clearance, inferred from a substantial increase in crop trees and steppe taxa (Panagiotopoulos et al., 2013). Human-induced forest clearance could not only create a large amount of terrestrial organic detritus, but also would crucially enable a greater amount of surface run-off delivering both oxidised OM and nutrients to the lake. A climatically-induced period of relative humidity may therefore be super-imposed on a change in anthropogenic catchment land-use at this time.

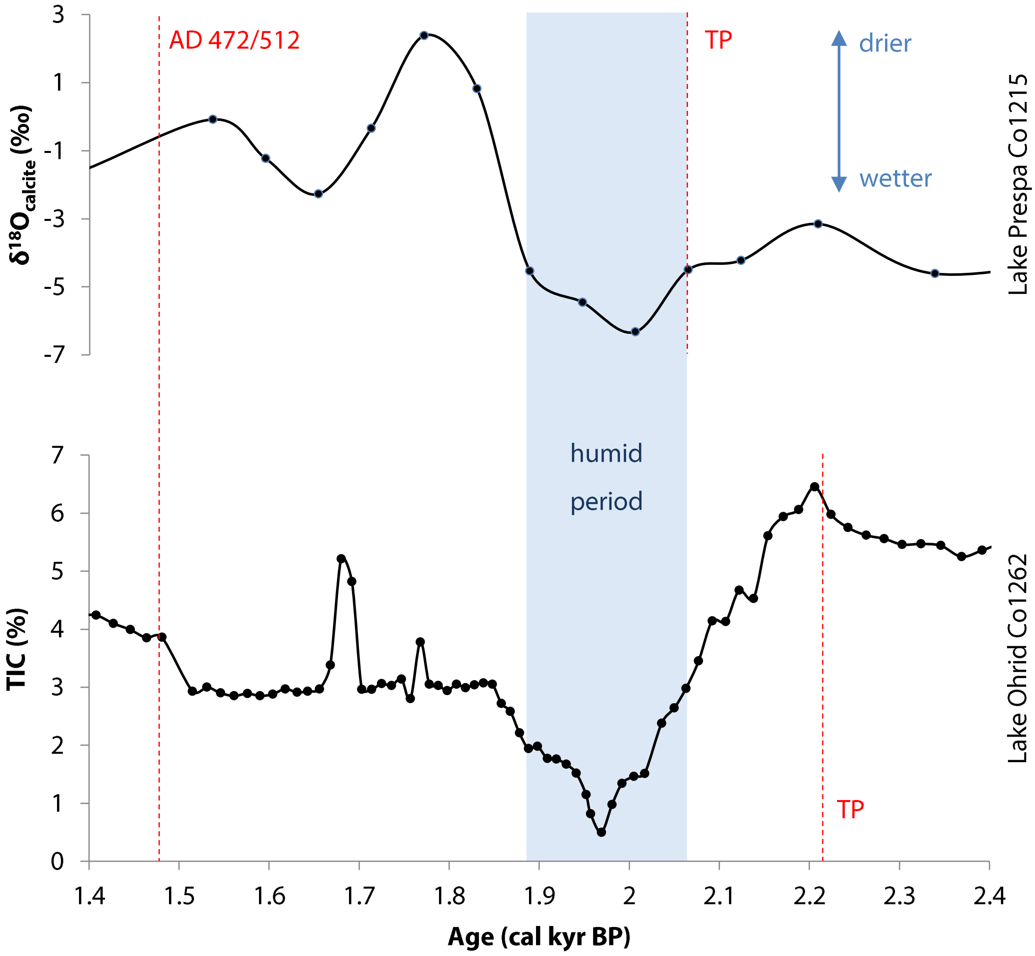

Figure 6.49 *Calcite from Lake Ohrid Co1262 plotted against* $\delta^{18}O_{calcite}$ *from Lake Prespa (Leng et al., 2013), showing the location of the AD 472/512 tephra and radiocarbon ages from terrestrial plants (TP).*

The large MWD between 320-121 cm directly overlies the AD 472/512 tephra, providing chronological constraint to the base of the deposit. Based on the mean sedimentation rate for this part of the core, Wagner et al. (2012b) suggest that the mass movement occurred < 20 years after tephra fallout and that the MWD is most likely related to an earthquake that destroyed the city of Ohrid in the early 6th century AD.

Over the last 1500 years, an increase in TIC and TOC between 500-1100 AD (Figure 6.50) is synchronous with a greater abundance of *Cyclotella ocellata* (Zhang et al., 2015), and a short-term reversal in the decline of arboreal pollen percentages (Wagner et al., 2009a; Aufgebauer et al., 2012; Panagiotopoulos et al., 2013). This suggests that epilimnetic nutrient availability and productivity were higher in response to warmer summer temperatures (Bordon et al., 2009; Kaniewski et al., 2011), most likely associated with the Medieval Warm Period (MWP; Crowley and Lowery, 2000). However, annual precipitation (summer and winter) are reconstructed as being reduced at this time (Bordon et al., 2009), and higher oxygen isotope values from both Ohrid and Prespa suggest that lake levels may have been lower than present (Section 6.6.5; Leng et al., 2013). A lower lake level is supported by archaeological findings of historical settlements dated to the 11th century below the modern water line at Lake Prespa (Matzinger et al., 2006a), and a high-resolution beach ridge record correlates this to a 10% reduction in winter-spring recharge (van der Schriek and Giannakopoulos, 2015). Warmer summer temperatures would promote a reduction in lake water mixing, and lower recharge would limit external nutrient supply (supported by lower K concentration, Figure 6.50), however this is counter to higher diatom abundance in Lake Ohrid. A reduction in Prespa lake level (10-15 m) can change its trophic state and increase the supply of bio-available phosphorus to Ohrid through the karst system (Matzinger et al., 2006a), thereby enhancing productivity at a time of overall drier climate conditions.

After a peak in TIC and TOC at 1100 AD, the values decline to a minimum between ca. 1800-1900 AD, which is confirmed by a radiocarbon date from terrestrial plant material at 1810 AD (Section 6.4; Figure 6.50). Maxima in OI, $\delta^{13}C_{organic}$, and K concentration imply enhanced lake water mixing and greater catchment erosion, and low TIC, TOC, TOC/TN and HI suggest overall colder conditions and lower lake productivity and/or enhanced degradation of OM and dissolution of calcite. Lower calcite and OM contents are also observed in other cores from around the basin (Wagner et al., 2009a; Vogel et al., 2010a; Wagner et al., 2010), which most likely correlates to a cold phase associated with the Little Ice Age (LIA; Kaniewski et al., 2011; Goudeau et al., 2015). The LIA was potentially the result of changes in solar output and/or a regime shift in North Atlantic ocean circulation as a function of sea-ice/ocean feedbacks driven by volcanic eruptions (Rohling and Palike, 2005; Miller et al., 2012; Schleussner and Feulner, 2013).

In recent years (from ca. 1900 AD), OM concentrations have started to increase, which is most likely associated with enhanced nutrient input and anthropogenic-driven eutrophication processes (Matzinger et al., 2007).

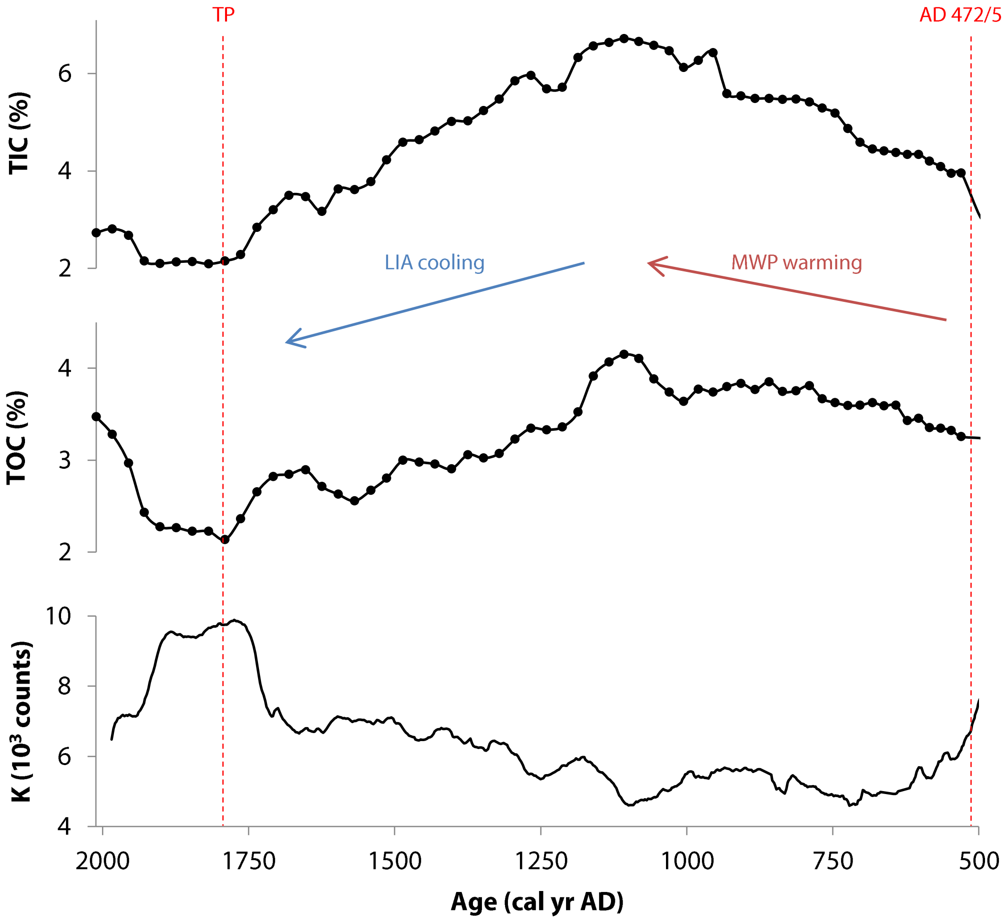

Figure 6.50 *Calcite (TIC), OM production (TOC) and erosion (K concentration; 11-point moving average) at Lake Ohrid over the last 1500 years (plotted against calendar age), showing the location of the AD 472/512 tephra, radiocarbon age from terrestrial plant matter (TP).*

6.6.5 A comparison of oxygen isotope data between Lake Ohrid and other Mediterranean records

The oxygen isotope record from Lake Ohrid ($\delta^{18}O_{calcite}$) shows higher values with a greater magnitude of variation before 9 ka, a transition to lower values centered on 8.9 ka, and a gradual progression to higher values between 8.9 ka and present (Figure 6.11). An overall low variance, especially when compared to the organic proxy data, is most likely due to the buffering effect of Lake Ohrid (large volume and long residence time) and the extended duration of the integrated signal. In addition, $\delta^{18}O_{calcite}$ can be considered a primary climate proxy in that changes can be explicitly attributed to climate forcing (Roberts et al., 2011a), rather than potentially being subject to anthropogenic influence (e.g. pollen, fire regimes).

Given that Lake Ohrid is sensitive to water balance, the lower $\delta^{18}O_{calcite}$ centred on ca. 9 ka suggests a progressive change to a more positive water balance (high P/E) and a climate characterised by humid conditions (Figure 6.51). The subsequent trend to higher values suggests a progressive transition to a drier climate. Although several short-term events are observed in the organic proxy record, only minor excursions are typically seen in $\delta^{18}O_{calcite}$. A mediated response to centennial-scale events implies that they either did not impact $\delta^{18}O_{lakewater}$ or temperature (controls on $\delta^{18}O_{calcite}$), or that any short-term events are effectively buffered by the lake itself (or by the sampling resolution). The general $\delta^{18}O_{calcite}$ trend is mirrored by previous, lower resolution records from Lake Ohrid (Co1202 and Lz1120; Figure 6.51), which suggests that lake water is well mixed and that higher resolution analyses do not show a greater amplitude of short-term variations in either $\delta^{18}O_{lakewater}$ or temperature (i.e. even when each 2 cm sample represents <10 years, decadal-scale variability is not recorded, implying a buffer functionality exists and confirms Lake Ohrid $\delta^{18}O_{calcite}$ is a function of longer-term climate change).

Comparison with Co1215 from Lake Prespa reveals a common interval of higher $\delta^{18}O_{calcite}$ between ca. 2-1 ka, which is interpreted as a period of drier conditions and lower lake levels. The excursion is more intense in Lake Prespa due to it having a smaller surface area to volume ratio and shorter lake water residence time, enhancing the response to periods of major lake level change (Leng et al., 2013).

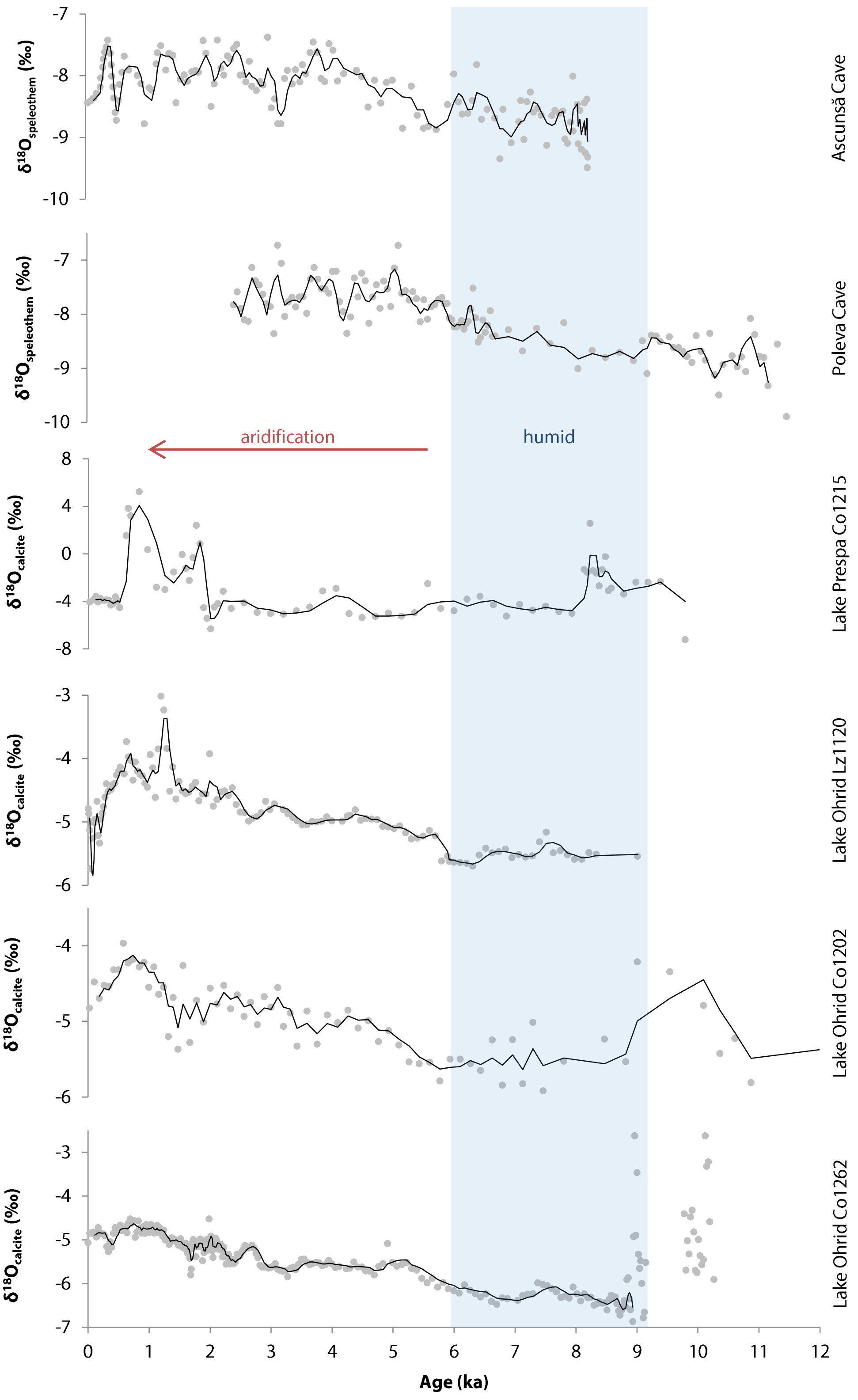

***Figure 6.51** Comparison of oxygen isotope records from the Balkan Peninsula, including Co1262, Lake Ohrid and Prespa cores Co1202, Lz1120, Co1215 (Leng et al., 2010a; Leng et al., 2013), and speleothem records from Poleva and Ascunsă caves in Romania (Constantin et al., 2007; Drăguşin et al., 2014), showing data points (grey dots) and 3-point running average (black lines).*

The millennial-scale trend to higher $\delta^{18}O_{calcite}$ after ca. 6 ka is not recorded in the Lake Prespa sequence, which could be a function of hydrology and lake size where winter recharge was sufficient to counteract summer evaporation in Prespa (Leng et al., 2013). In Lake Ohrid, the basin-wide trend to lower (early-mid Holocene) and subsequently higher (mid-late Holocene) $\delta^{18}O_{calcite}$ is consistent with speleothem records from south west Romania (ca. 450 km northeast of Ohrid), which are thought to respond to changes in regional hydrological balance and temperature over the Holocene (Figure 6.51; Poleva Cave; Constantin et al., 2007; Ascunsă Cave; Drăguşin et al., 2014). This trend is also observed in lake (Tigalmamine, Morocco; Lamb et al., 1989; Pamvotis, Greece; Frogley et al., 2001; Pergusa, Italy; Zanchetta et al., 2007a; Nar Gölü, Turkey; Dean et al., 2015) and speleothem (Soreq Cave, Israel; Bar-Matthews et al., 1997) isotope records from across the Mediterranean (5°W-35°E between 31-41°N), which show a consistent pattern of lower $\delta^{18}O$ in the early Holocene transitioning to higher values towards the late Holocene (Figure 6.52; Roberts et al., 2008). A stacked lake isotope record of inferred hydrological change for the eastern Mediterranean domain highlights a stable period of low $\delta^{18}O$ between 9-6 ka followed by a transition from wetter to drier conditions (higher $\delta^{18}O$) after 6 ka (Roberts et al., 2011a), which was most likely driven by a decline in the amount of water passing through the lake systems (Jones et al., 2007). Lower $\delta^{18}O$ and evidence for greater moisture availability is temporally and spatially consistent with the deposition of sapropel S1 in the Mediterranean Sea between ca. 9.5-6 ka (Ariztegui et al., 2000; Mercone et al., 2000; Roberts et al., 2008), during which surface salinities became almost homogenous across the whole basin (Kallel et al., 1997). Today a west-east salinity gradient exists due to differential evaporation across the basin, however the early Holocene pattern suggests enhanced freshwater input at the regional scale as the presence of organic-rich sapropel layers typically coincides with $\delta^{18}O$ minima (Rossignol-Strick, 1985; Tzedakis, 2007).

Figure 6.52 *Comparison of oxygen isotope records from the southern Mediterranean region (31-41°N), including Co1262, Lake Tigalmamine (Lamb et al., 1989), Lake Pergusa (Zanchetta et al., 2007a), Lake Pamvotis (Frogley et al., 2001), Nar Gölü (Dean et al., 2015), Soreq Cave (Bar-Matthews et al., 1999) and a stacked isotope record using lakes from the eastern Mediterranean (higher values = wetter, lower values = drier; Roberts et al., 2011a), showing data points (grey dots) and 3-point running average (black lines). Figure over page.*

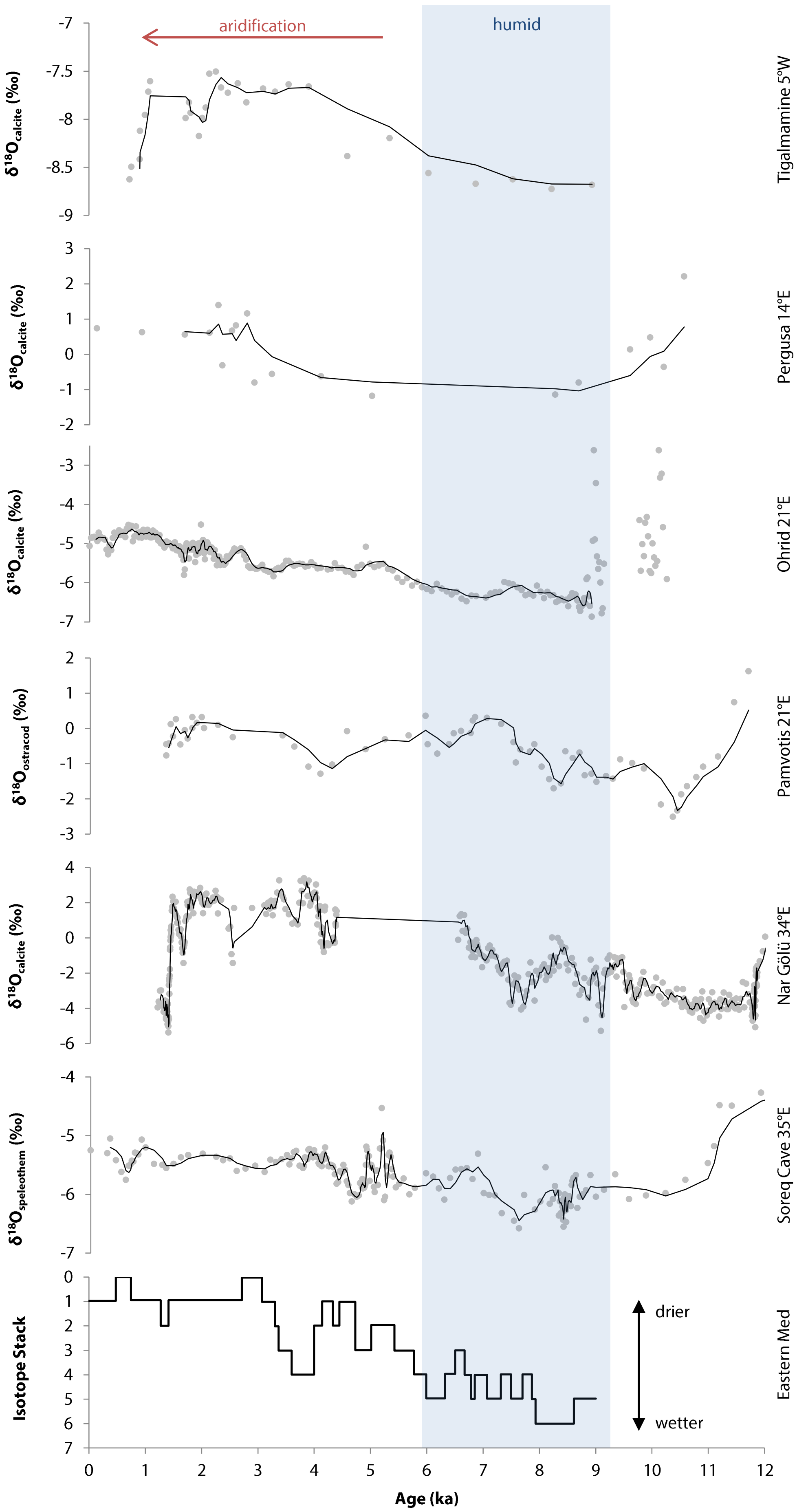
aridification
humid
$\delta^{18}O_{calcite}$ (‰)
-7
-7.5
-8
-8.5
-9
Tigalmamine 5°W
$\delta^{18}O_{calcite}$ (‰)
3
2
1
0
-1
-2
Pergusa 14°E
$\delta^{18}O_{calcite}$ (‰)
-3
-4
-5
-6
-7
Ohrid 21°E
$\delta^{18}O_{ostracod}$ (‰)
2
1
0
-1
-2
-3
Pamvotis 21°E
$\delta^{18}O_{calcite}$ (‰)
4
2
0
-2
-4
-6
Nar Gölü 34°E
$\delta^{18}O_{speleothem}$ (‰)
-4
-5
-6
-7
Soreq Cave 35°E
Isotope Stack
0
1
2
3
4
5
6
7
drier
wetter
Eastern Med
0
1
2
3
4
5
6
7
8
9
10
11
12
Age (ka)

An enhanced regime of regional precipitation is suggested by the almost synchronous excursion of lake isotope records to lower δ^{18}O (Figure 6.52), which is supported by lake level reconstructions inferring deeper water at lakes Xinias (Greece; Digerfeldt et al., 2000), Trifoglietti (southern Italy; Joannin et al., 2012) and Preola (Sicily; Magny et al., 2011b) (Figure 6.53), and is consistent with increased river discharge into the Gulf of Salerno (southern Italy; Naimo et al., 2005). A transition to lower sea surface δ^{18}O in the Adriatic (Siani et al., 2013), Aegean (Marino et al., 2009) and Ionian basins (Emeis et al., 2000) is also observed (−1.1‰; Paul et al., 2001), and pollen reconstructions from the Aegean Sea indicate precipitation during the time of sapropel formation was up to 50% higher in comparison to previous millennia (Kotthoff et al., 2008b). In addition, North African lakes (8-28°N) also typically show a highstand phase (maximum P/E balance) in the early Holocene with the largest positive precipitation anomaly between 15-21°N (Hoelzmann et al., 1998; Gasse and Roberts, 2004), which correlates with maximum sediment input (log Fe/Ca) and inferred higher discharge rates at the Nile delta (Figure 6.53; Revel et al., 2014). An intensification of the hydrological cycle across northern Africa during the early Holocene is thought to be related to a substantial migration of the intertropical convergence zone (ITCZ) in response to a precession minima and high summer insolation (Figure 6.53), resulting in an extension of African monsoonal precipitation over more northerly latitudes (Talbot et al., 2007; Tzedakis, 2007). The direct influence of the monsoon may have reached 24°N (Kuper and Kröpelin, 2006), and so would only have had an indirect influence on the Mediterranean through increased fresh water runoff into the Mediterranean Sea (Arz et al., 2003), thereby reducing deep-water ventilation and favouring sapropel deposition (Tzedakis, 2007). A north migration is supported by speleothem δ^{18}O records from Oman and Yemen, which suggest a rapid change to lower δ^{18}O similarly related to an intensification and shift of the Indian monsoon during the early Holocene (Fleitmann et al., 2007). The strength of the monsoon is controlled by the intensity of summer insolation, however its migration (along with the ITCZ) is driven by the latitudinal temperature gradient (LTG) (Davis and Brewer, 2009), shown today by a northward ITCZ migration during in boreal summer (weaker LTG) and a southward migration during in boreal winter (stronger LTG; Tzedakis et al., 2009).

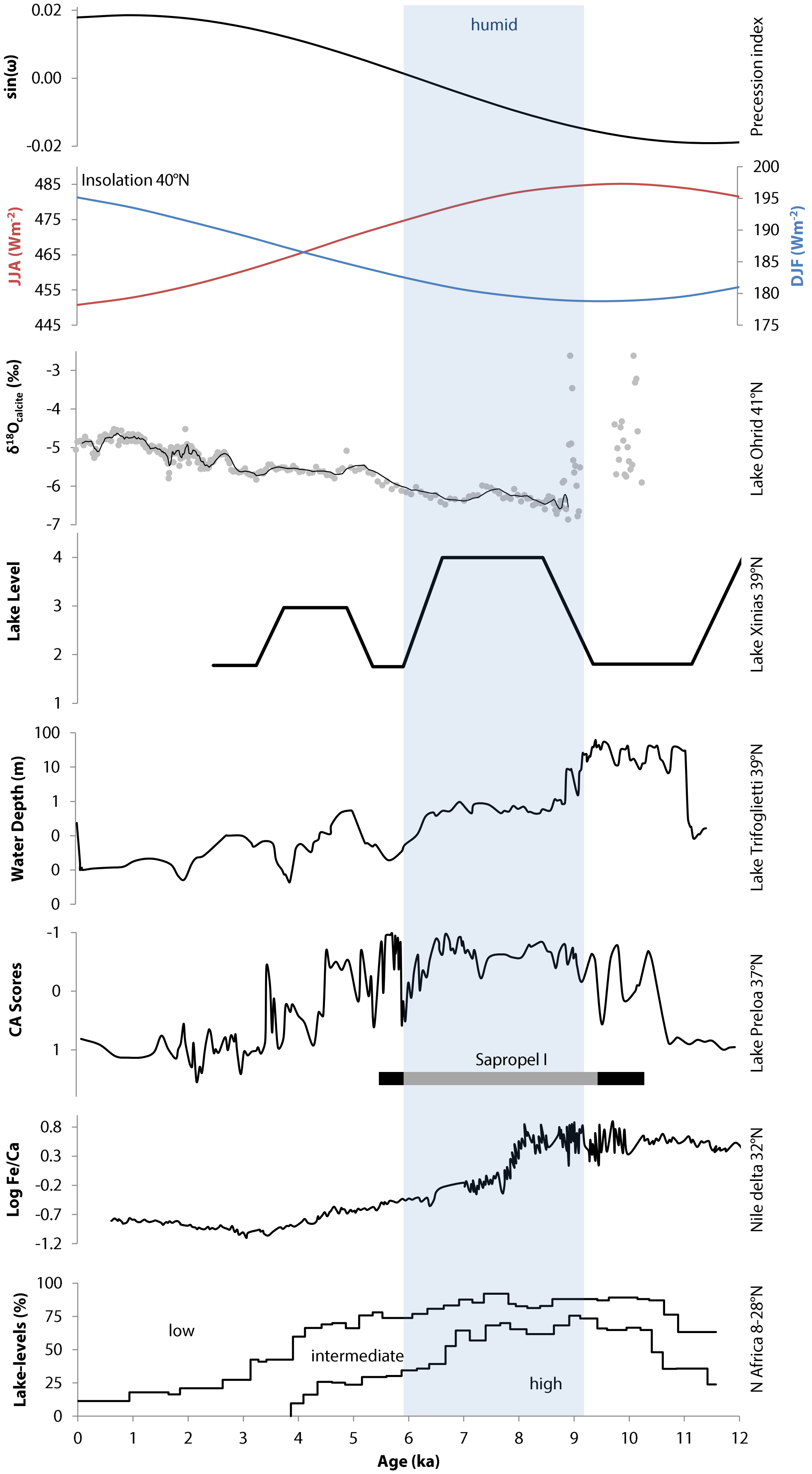
humid
sin(ω)
0.02
0.00
-0.02
Precession index
Insolation 40°N
JJA (Wm^{-2})
485
475
465
455
445
200
195
190
185
180
175
DJF (Wm^{-2})
δ^{18}O$_{calcite}$ (‰)
-3
-4
-5
-6
-7
Lake Ohrid 41°N
Lake Level
4
3
2
1
Lake Xinias 39°N
Water Depth (m)
100
10
1
0
0
0
Lake Trifoglietti 39°N
CA Scores
-1
0
1
Sapropel I
Lake Preloa 37°N
Log Fe/Ca
0.8
0.3
-0.2
-0.7
-1.2
Nile delta 32°N
Lake-levels (%)
100
75
50
25
0
low
intermediate
high
N Africa 8-28°N
0
1
2
3
4
5
6
7
8
9
10
11
12
Age (ka)

***Figure 6.53** Comparison of Co1262 $\delta^{18}O_{calcite}$ with lake level reconstructions from Lake Xinias (Digerfeldt et al., 2000), Lake Trifoglietti (Joannin et al., 2012), Lake Preola (Magny et al., 2011b), and North African lakes (Gasse and Roberts, 2004), discharge from the Nile delta (Revel et al., 2014), summer and winter insolation at 40°N and the precession index (Berger and Loutre, 1991). The duration of sapropel deposition (faster rate = grey bar, slower rate = black bar) in the Mediterranean Sea is also indicated (Mercone et al., 2000). Figure on previous page.*

6.6.6 Examining the drivers of regional climate change

The LTG is a function of the amount of insolation received at high and low latitudes (latitudinal insolation gradient; LIG), which can result in differential heating between the equator and poles. In the early-mid Holocene, an overall increase in summer insolation was proportionally greater at high latitudes in comparison to lower latitudes (weak LIG; Davis and Brewer, 2009). This would have resulted in relatively stable summer temperatures at the European scale but comprised relative warming at high latitudes and relative cooling at low latitudes (Figure 6.54), thereby forcing a weaker LTG (Figure 6.55). A weaker LTG enabled the northward expansion of the Hadley cell and strong summer insolation favoured the development of widespread intense monsoon conditions, which may further have contributed to low latitude surface cooling through increased cloud cover and evaporation associated with greater monsoonal precipitation (Braconnot et al., 2007).

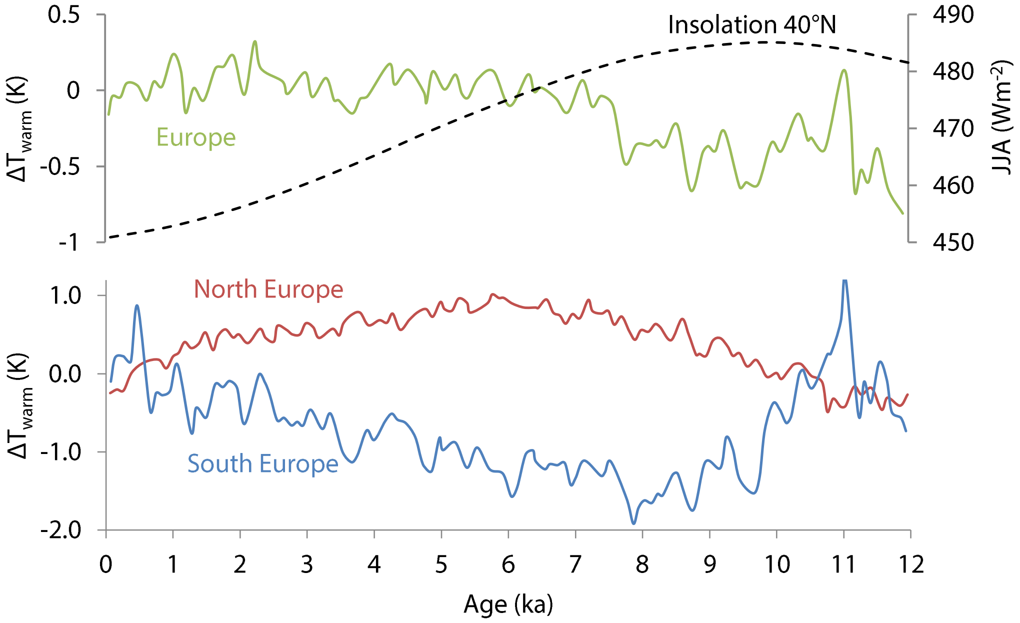

***Figure 6.54** Reconstructed summer temperatures (T_{warm}) for Europe (35-70°N), northern (55-70°N) and southern (35-45°N) Europe components (redrawn from Davis and Brewer, 2009), and summer (JJA) insolation at 40°N (Berger and Loutre, 1991).*

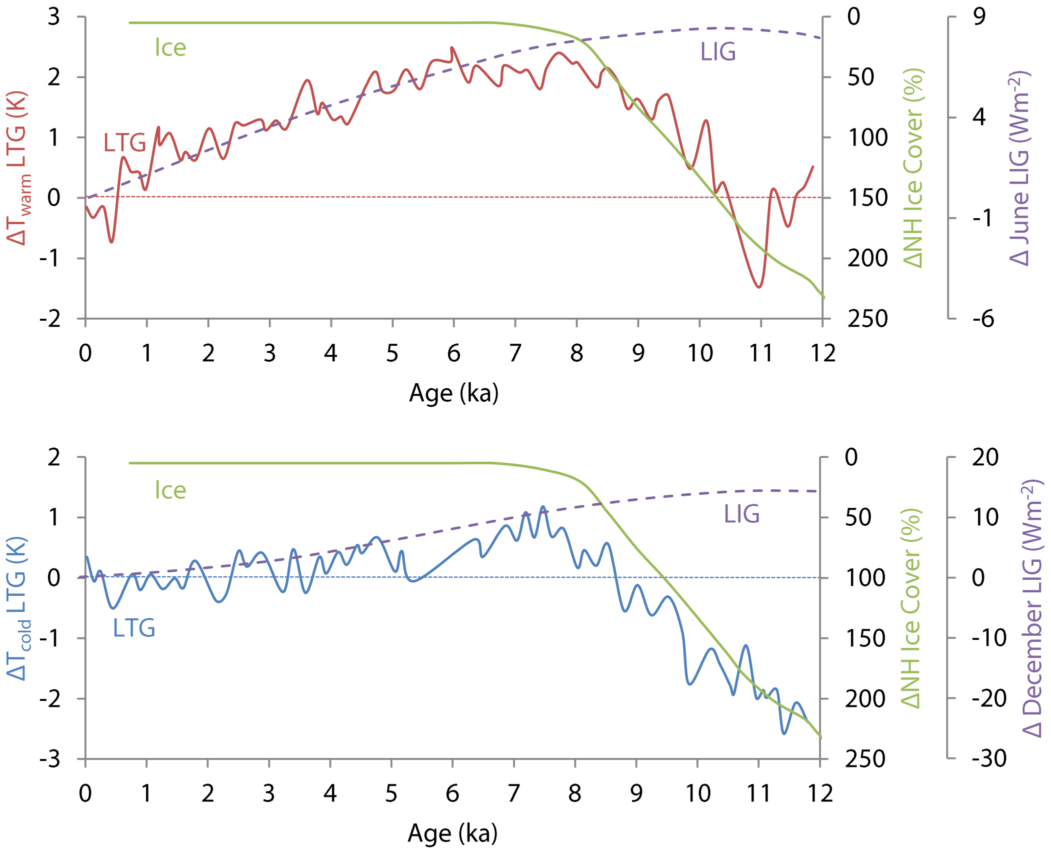

Figure 6.55 *Seasonal latitudinal temperature gradient (LTG; summer = red, winter = blue) over the Holocene calculated as the difference in temperature between North and South Europe (weak LTG = positive, strong LTG = negative), showing Northern Hemisphere ice cover (NH; green) and seasonal latitudinal insolation gradient (LIG; long dash purple) (redrawn from Davis and Brewer, 2009).*

Although a declining LIG is observed to force changes in the LTG in the mid-late Holocene, Northern Hemisphere (NH) ice cover strengthens the LTG in both summer and (more predominately) winter seasons in the earliest Holocene (Figure 6.55; Davis and Brewer, 2009). Peak insolation occurs at ca. 10 ka inferring that monsoon conditions should be most intense at this time (insolation maxima drives enhanced land-ocean pressure differences in summer months intensifying low level monsoonal flow; Rohling et al., 2009), which is confirmed by the prompt rise of North African lake levels and high Nile discharge in the earliest Holocene (Figure 6.53). However, a strong LTG due to NH ice cover restricts the northward migration of the ITCZ and southern Mediterranean conditions remain very dry, implied by higher δ^{18}O in lake and speleothem records (Figure 6.52), lower lake levels at Medina (Spain; Reed et al., 2001), Preola (Italy; Magny et al., 2011b), and Xinias (Greece; Digerfeldt et al., 2000), and restricted woodland development (Tzedakis, 2007). Enhanced dryness (and a stronger seasonality) may be in response to an insolation-forced intensification of the Indian monsoon system causing adiabatic descent over the eastern Mediterranean (Ziv et al., 2004; Jones et al., 2006), and a strengthened North Atlantic anticyclone blocking Atlantic depressions in the western Mediterranean (Tinner et al., 2009; Magny et al., 2013; Gaetani and Fontaine, 2014).

The progressive loss of NH ice cover through the early Holocene resulted in a weakening LTG and allowed a northward ITCZ shift, culminating in a very weak LTG at ca. 8 ka following the loss of the Fennoscandian ice sheet (Figure 6.55; Renssen et al., 2009; Magny et al., 2011a). A weak winter LTG is coincident with a change to mild and wet conditions in Northern Europe, where after 9 ka there is a distinct increase observed in annual precipitation at Lake Svanåvatnet (northern Norway; Bjune and Birks, 2008) and in temperature at Lake Toskaljavri (northwestern Finland; Seppä and Birks, 2002; Seppä et al., 2008). Wetter and milder conditions in northerly latitudes today are closely associated with the phase of the Arctic Oscillation (AO; and its regional expression, the North Atlantic Oscillation, NAO), which is the most prominent control on winter atmospheric circulation variability today (Hurrell et al., 2003) and shows a positive correlation to the winter LTG over the twentieth century (i.e. weak LTG coincides with +AO; Davis and Brewer, 2009).

A positive AO (NAO) index implies that a strong pressure contrast exists between the Azores High and the Icelandic low (Section 2.3), which results in the temperate westerlies being diverted northward bringing relatively warmer and wetter conditions to higher latitudes and drier conditions to mid-latitudes (i.e. driving a weaker LTG). The extent of northward penetration of warmer conditions is greatest when this pressure difference is enhanced (i.e. a higher AO index), causing westerlies to be strengthened that in turn drive warm Atlantic waters further north (Blindheim et al., 2000). An intrusion of warmer Atlantic waters is observed in sediment cores from the Norwegian Sea (Fronval and Jansen, 1996) and Barents Sea (Duplessy et al., 2001) during the early Holocene indicating a strong positive AO regime, which is supported by glacier variations in western Scandinavia (Nesje et al., 2000). The maximum extent of warming is observed to be congruous with the period of very weak winter LTG around 9-7 ka (Figure 6.56).

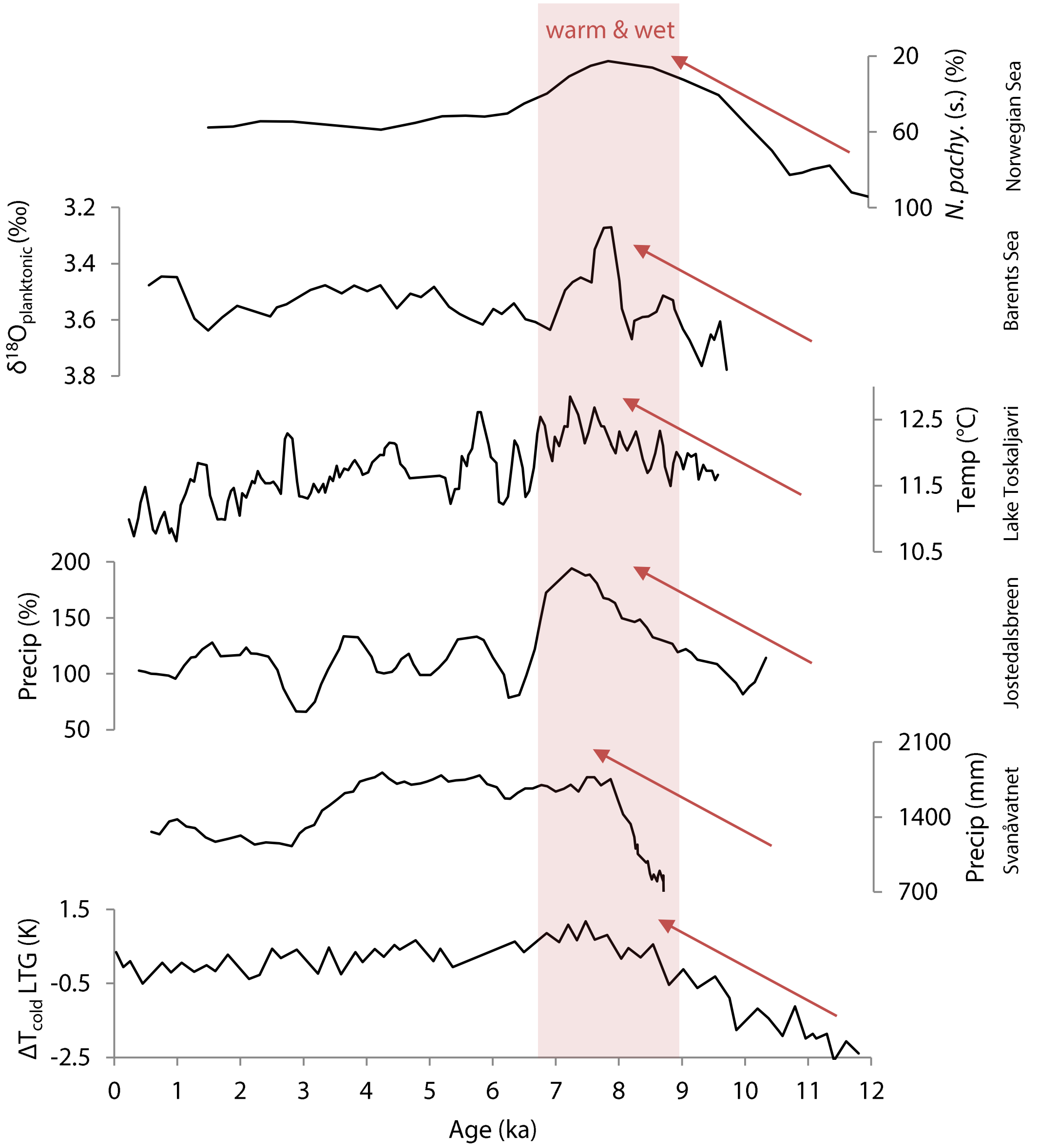

***Figure 6.56** High latitude (60-80°N) warming and +AO conditions inferred in records from the Norwegian Sea (*N. pachyderma (s.)*; Fronval and Jansen, 1996), Barents Sea (planktonic foraminifera; Duplessy et al., 2001), Lake Toskaljavri (temperature; Seppä and Birks, 2002), Jostedalsbreen (precipitation %; Nesje et al., 2000) and Lake Svanåvatnet (precipitation; Bjune and Birks, 2008), compared to winter (T_{cold}) LTG (Davis and Brewer, 2009).*

At the time when northerly latitudes received enhanced warmth and moisture from the diversion of the westerlies in the early-middle Holocene, mid-latitudes (including central Europe and the northern Mediterranean) became considerably drier (Figure 6.57). Positive oxygen isotope values indicate that a negative water balance existed at Lake Steisslingen in Germany (Mayer and Schwark, 1999) and at Lake Frassino in Italy (Baroni et al., 2006). Drier conditions are also suggested by a coincident decrease in detrital input at Lake Saint-Point (France; Magny et al., 2012b) and by lower lake levels at lakes Cerin (France; Magny et al., 2011a), Ledro (Italy; Magny et al., 2012a) and Accesa (Italy; Magny et al., 2007). The transition to a drier climate in mid-latitudes may correspond to a change in predominately summer environmental conditions, where the northern Mediterranean and central Europe underwent a reduction in summer precipitation alongside warmer summer temperatures (for example at lakes Ledro and Accesa; Peyron et al., 2013). This is supported by greater fire activity (measured as charcoal influx) in the north western Mediterranean (Vannière et al., 2011) and also in northern Romania (Lake Stiucii; Feurdean et al., 2013), which is dependent on decreasing summer rainfall and increasing summer temperature (Pausas, 2004; Vannière et al., 2011). This is exemplified by Lake Accesa, where there is a clear change to a more distinct seasonality in the early-mid-Holocene (mild winters and warm/dry summers) that can be characterised as a typical Mediterranean climate (Csa; Köppen, 1900; Peyron et al., 2011). However, the Accesa record also highlights the importance of seasonality in palaeoclimate reconstructions as although lake levels are low (Magny et al., 2007), the oxygen isotope records from nearby Corchia and Renella caves (ca. 130 km north of Lake Accesa) suggest a distinct increase in precipitation at this time (Zanchetta et al., 2007b; Zhornyak et al., 2011), which is most likely associated with greater autumn-winter precipitation (Tzedakis, 2007).

In contrast to more northern Mediterranean sites, an increase in winter (and summer) precipitation regimes is observed in records from more southerly locations (Magny et al., 2013), such as at Lake Pergusa where overall lower summer temperatures are reconstructed (Peyron et al., 2013). Higher lake levels at this time are also indicated at lakes Preola (Magny et al., 2011b), Trifoglietti (Joannin et al., 2012), Xinias (Digerfeldt et al., 2000), and Dojran (Francke et al., 2013), suggesting that summers were cooler (and perhaps wetter) such that water balance remained positive (unlike mid-latitude sites). Intense summer droughts are implied to be rare in the southern Mediterranean during the early Holocene as charcoal records suggest a reduction in fire activity in both western (Vannière et al., 2011) and eastern areas (Wick et al., 2003; Turner et al., 2008), however spatial variability in this signal could be due to human impact (Lawson et al., 2013).

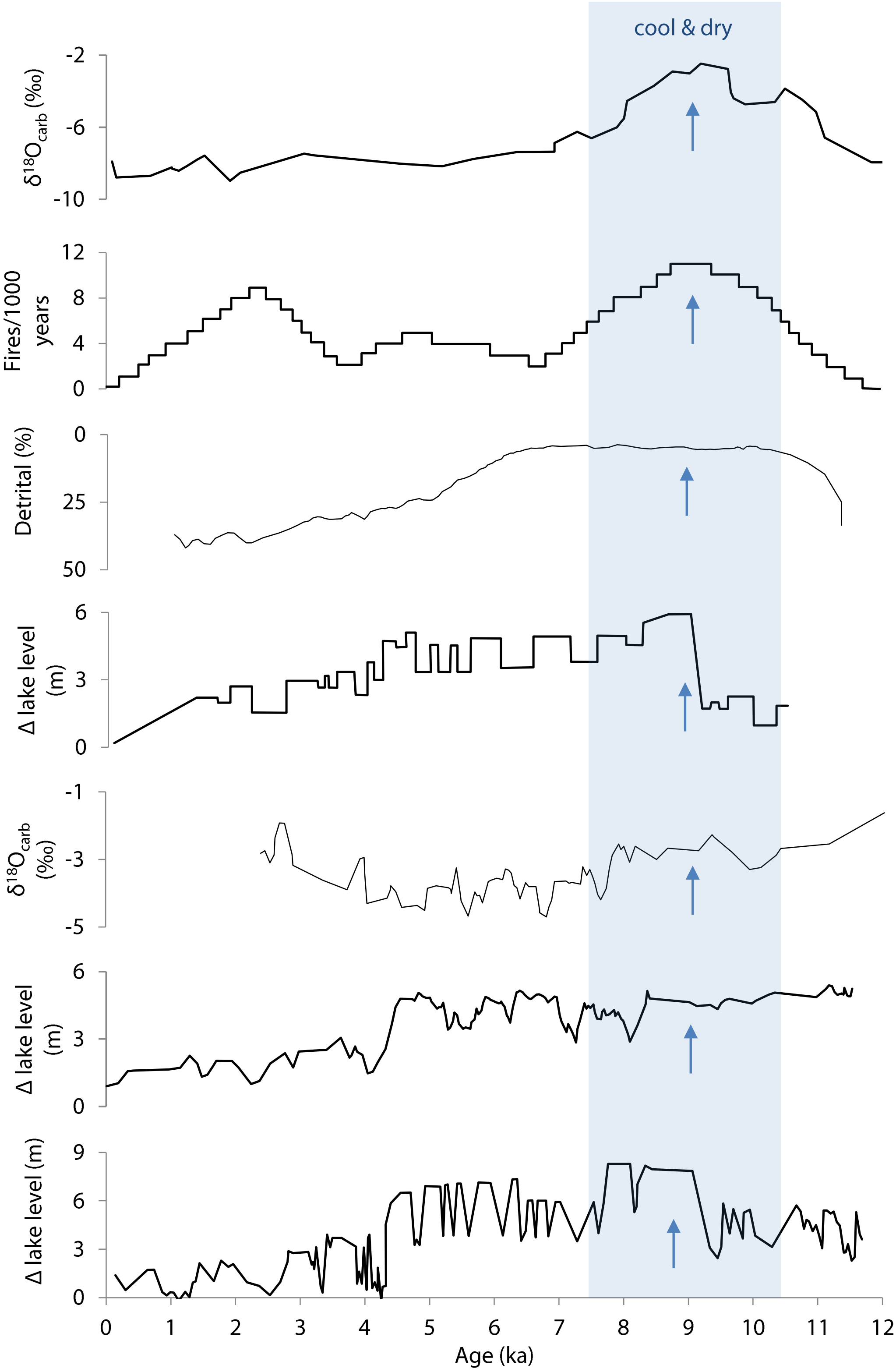

Figure 6.57 *Comparison of mid-European lake records (40-50°N), including Lake Steisslingen (Germany; Mayer and Schwark, 1999), Lake Stiucii (Romania; Feurdean et al., 2013), Lake Saint-Point (France; Magny et al., 2012b), Lake Cerin (France; Magny et al., 2011a), Lake Frassino (Italy; Baroni et al., 2006), Lake Ledro (Italy; Magny et al., 2012a), and Lake Accesa (Italy; Magny et al., 2007).*

A more humid southern Mediterranean is not necessarily compliant with a northward shift of the westerlies due to a positive AO in the early Holocene and the evidence for a wetter northern Europe (as shown in Figure 6.56). The additional moisture is not likely to have originated from direct precipitation delivered by the intensified African and Indian monsoon, as evidenced by records from the northern Red Sea (Arz et al., 2003) and Soreq Cave (Bar-Matthews et al., 2003), which instead suggest regional processes that operate in phase with (or as a result of) changes in the LTG and monsoon location/intensity (Rohling and Hilgen, 1991; Rohling et al., 2009). Increased precipitation during the early-mid Holocene in the Mediterranean could potentially be the result of several influences, including the formation of Mediterranean depressions due to a stronger temperature contrast between the sea and land in winter (Trigo et al., 2002; Magny et al., 2013) and/or generally enhanced SST and precipitation due to higher summer insolation (Tzedakis, 2007). In addition, given the northward position of the westerlies, a secondary Atlantic depression-track may have formed and extended over the entire Mediterranean during winter (Rohling and Hilgen, 1991, and references therein). Pollen-based reconstructions suggest that the majority of precipitation may have been in the form of intense events, and moreover imply that these were probably limited to autumn-winter months (Tzedakis, 2007; Sadori et al., 2011). Considering the overall regional trend to lower $\delta^{18}O$ in lakes and speleothems, including Lake Ohrid (Figure 6.52), this could therefore be explained by a larger proportion of Mediterranean-sourced water in precipitation (which was isotopically fresher during the sapropel event) and/or an overall increase in annual precipitation (driven by greater winter precipitation). Further, if precipitation was in the form of intense events, $\delta^{18}O_{precipitation}$ would be lower due to the amount effect (Leng and Marshall, 2004).

The early Holocene deposition of sapropel I in the Mediterranean Sea can be divided into two phases, separated by a ca. 0.5 ka episode of cooler and drier conditions characterised by a reduction in organic deposition (Ariztegui et al., 2000). This interval coincides with a climate deterioration associated with the 8.2 ka event, recognised in many NH records (Alley et al., 1997; Morrill, 2005) and correlates to a cooling trend across the southern Mediterranean (Section 6.6.4.3), including in the organic proxies from Lake Ohrid (Figure 6.41 and 6.42). If the abrupt event itself is considered, a freshwater pulse into the North Atlantic would weaken thermohaline circulation

(Renssen et al., 2002), thereby cooling northerly latitudes and strengthening the LTG (Davis and Brewer, 2009). A strong LTG would inhibit a northward ITCZ migration and weaken the North Atlantic anticyclone, resulting in the southward migration of westerlies and the advection of maritime air over European mid-latitudes establishing negative AO (NAO) conditions (Wanner et al., 2001; Trouet et al., 2009; Magny et al., 2013). This is observed in the Barents Sea planktonic foraminifera isotope record as a short-term reversal to colder conditions (i.e. less influence of warm Atlantic waters; Duplessy et al., 2001), whereas central European records indicate a wetter climate and higher lake levels (e.g. Magny et al., 2007; Magny et al., 2012a), and southern Mediterranean sequences suggest drier conditions (e.g. Pross et al., 2009; Desprat et al., 2013). This hydrological tripartition of Europe is recorded across the central and western Mediterranean (Magny et al., 2003), and suggests similar mechanisms (relating to changes in the LTG and AO index) control atmospheric circulation and climate at both the millennial-scale and for centennial events (Magny et al., 2013). Given the widespread extent of the 8.2 ka event, and considering the magnitude of change observed in the organic and pollen records from lakes Ohrid and Prespa (Figure 6.41; Wagner et al., 2009a; Aufgebauer et al., 2012; Leng et al., 2013; Panagiotopoulos et al., 2013), it is perhaps unexpected not to see a strong response in $\delta^{18}O_{calcite}$. However, a weak response to the 8.2 ka event is recorded in other western and central Mediterranean sites (Joannin et al., 2012; Peyron et al., 2013), and the isotope signal may have been buffered by due to relatively unchanged Mediterranean surface water $\delta^{18}O$ (Emeis et al., 2000; Zanchetta et al., 2007b). In addition, any increase in source $\delta^{18}O$ or lower water influx due to a drier climate (both driving increasing $\delta^{18}O_{lakewater}$) may have been counteracted by colder temperatures (as recorded at nearby Lake Maliq; Bordon et al., 2009). A colder temperature regime would have been facilitated by an expansion of sub-polar climate conditions and an intensified Siberian High leading to more frequent outbreaks of cold and dry northerly air flows over the central-eastern Mediterranean (Saaroni et al., 1996; Renssen et al., 2002; Rohling et al., 2002; Gogou et al., 2007; Rohling et al., 2009).

The end of sapropel deposition in the Mediterranean Sea at around 6 ka is coincident with the start of a progressive decline in summer insolation and a decrease (increase) in relative temperatures over northern (southern) Europe (Figure 6.54). This was most likely driven by a corresponding change in the differential amount of insolation received at low and high latitudes (stronger LIG) resulting in a strengthened LTG (Figure 6.55; Davis and Brewer, 2009). A decrease in summer insolation and an increasingly stronger LTG through the mid-late Holocene may have forced a weaker African/Indian monsoon system (reducing the land-sea pressure contrast during summer), also leading to a southerly migration of the ITCZ and an associated southward repositioning of the westerlies (i.e. similar to that described for the 8.2 ka event and opposite to the conditions of the early Holocene). A weaker monsoon and expansion of the North African desert belt at this time is implied by lower North African lake levels and a reduction in Nile discharge (Figure 6.53), thereby restricting the input of freshwater to the Mediterranean and instigating the cessation of sapropel deposition associated with a decline in stratification (Triantaphyllou et al., 2009). This is also synchronous with northern latitude cooling reconstructed at Lake Toskaljavri (Seppä and Birks, 2002), a decline in precipitation at Jostedalsbreen (Nesje et al., 2000), and a reduction in warm Atlantic waters entering the Norwegian and Barents Sea (Fronval and Jansen, 1996; Duplessy et al., 2001). Cooling in northern Europe suggests the southerly relocation of westerly winds, which is supported by increasing lake level (Magny et al., 2007; Magny et al., 2011a; Magny et al., 2012a), greater detrital input (Magny et al., 2012b) and lower δ^{18}O (Mayer and Schwark, 1999; Baroni et al., 2006) in central European lakes, and decreasing fire frequency in the northern Mediterranean area (above ca. 40°N; Vannière et al., 2011; Feurdean et al., 2013) due to an increase in summer precipitation (Peyron et al., 2013).

In opposition, southern Mediterranean sites (below ca. 40°N) show a transition to drier conditions (Magny et al., 2013), where lake levels are reconstructed to have been lower at Lake Xinias (Digerfeldt et al., 2000) and Lake Trifoglietti (Joannin et al., 2012), pollen concentrations decline (Sadori and Narcisi, 2001; Sadori et al., 2011) and a progressive increase is observed in δ^{18}O records across western (Lamb et al., 1989), central (Frogley et al., 2001; Zanchetta et al., 2007a), and eastern regions (Eastwood et al., 2007; Dean et al., 2015). The evolution to a drier climate is shown to have a transitionary phase towards drier conditions between the end of sapropel deposition and ca. 4.5-4 ka, and a period with dry conditions after 4 ka (e.g. Bar-Matthews et al., 1997; Magny et al., 2011b; Peyron et al., 2013). A distinct increase in charcoal influx (fire activity) through the mid-late Holocene in southern Mediterranean areas, especially after 4 ka (Wick et al., 2003; Vannière et al., 2011; Lawson et al., 2013; Panagiotopoulos et al., 2013), suggests that dry conditions are associated with a stronger precipitation seasonality and enhanced summer drought, which is confirmed by pollen-based reconstructions of summer precipitation (Figure 6.58; Sadori et al., 2008; Joannin et al., 2012).

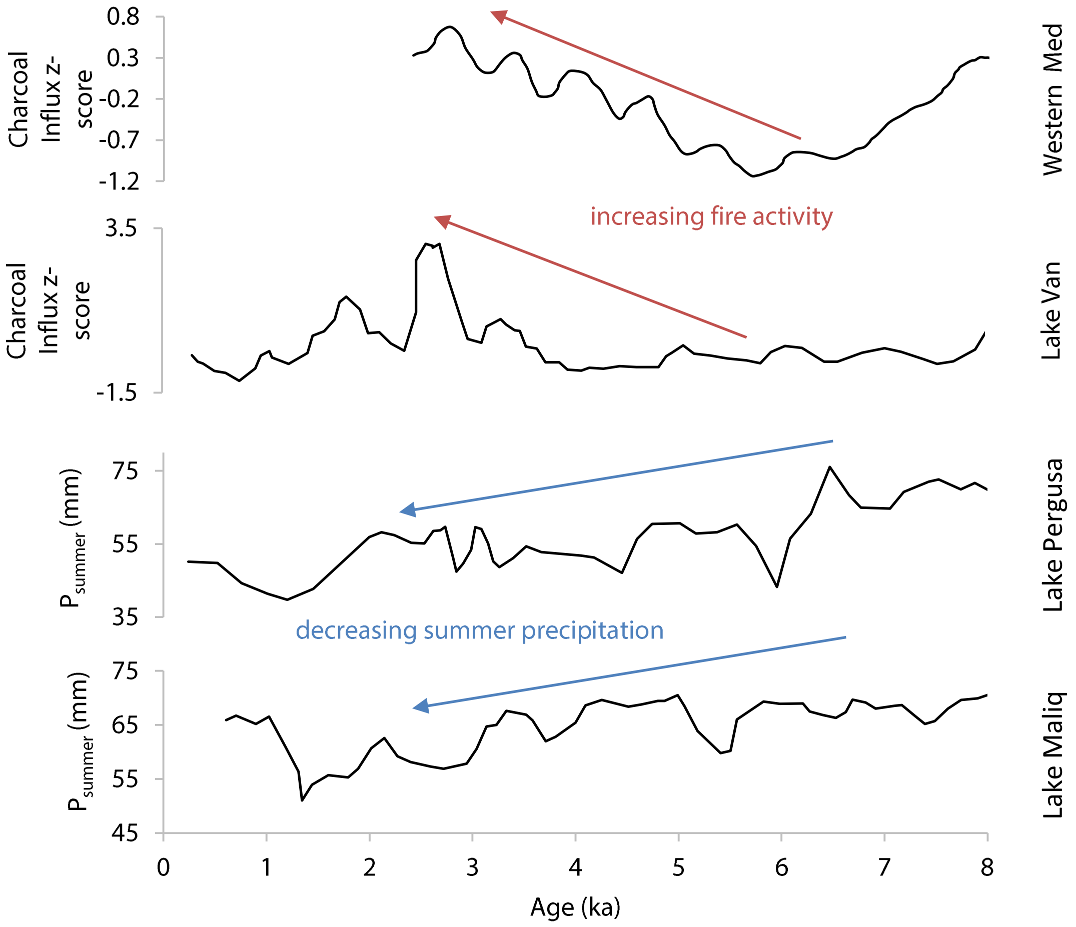

Figure 6.58 *Correlation between summer precipitation and fire activity in the southern Mediterranean (below ca. 40°N), showing a synthesis charcoal record for the western-central Mediterranean (Vannière et al., 2011), charcoal influx at Lake Van (Turkey; Wick et al., 2003), and pollen-based reconstructions of summer precipitation from Lake Pergusa (Sicily; Peyron et al., 2013) and Lake Maliq (Albania; Bordon et al., 2009).*

A pronounced environmental anomaly around 4 ka is observed across a broad spectrum of western-eastern Mediterranean (Carrion, 2002; Arz et al., 2006; Drysdale et al., 2006; Kotthoff et al., 2008a) and global sequences (Marchant and Hooghiemstra, 2004; Booth et al., 2005), which suggest an abrupt change in hydrological budget and widespread drought conditions in the Mediterranean that had a severe impact on human civilisation (Weiss et al., 1993; Roberts et al., 2011b). Superimposed on the general trend to drier conditions in the southern Mediterranean during the mid-late Holocene, a rapid stepped shift around ca. 4 ka to higher $\delta^{18}O_{speleothem}$ is recorded at Soreq Cave (Bar-Matthews et al., 1997) and also as a lake level lowering at Lake Preola (Magny et al., 2011b). This transition corresponds to lower lake levels in northern Africa and a weakened African monsoon (Gasse, 2000; Gasse and Roberts, 2004), potentially relating to the decline of positive AO (NAO) conditions and the crossing of an environmental threshold (Magny et al., 2013). A significant response around 4 ka is not seen in the Lake Ohrid isotope sequence, however a transition to higher $\delta^{18}O_{calcite}$ is recorded at Lake Prespa, which indicates this event may have either not been severe enough to limit winter recharge to Lake Ohrid, or the event was effectively buffered by the lake (although a decline in organic proxies is seen at Ohrid after 4 ka; Figure 6.45).

The continued decline of summer insolation through the late Holocene and a progressive increase in the precession index results in a maximum southward displacement of the ITCZ and a stronger LTG (Davis and Brewer, 2009). This results in the current general atmospheric circulation and seasonal Mediterranean climate pattern of today, promoting cooler SST and less evaporation (under lower summer insolation) leading to enhanced summer dryness over the southern Mediterranean (Peyron et al., 2013). A recent trend (ca. 0.7 ka) to lower $\delta^{18}O_{calcite}$ in Lake Ohrid, also observed in previous Ohrid records and in Lake Prespa (Figure 6.51; Leng et al., 2010a; Leng et al., 2013), is most likely in response to widespread forest clearance and decrease retention time in the catchment. Over the last several decades, enhanced freshening of lake water is expected as changes in water balance have been heavily influenced by anthropogenic activity, such as agricultural irrigation and the diversion of the River Sateska in 1962 (Matzinger et al., 2006b; Popovska and Bonacci, 2007).

6.7 Summary

This chapter contains new stable isotope ($\delta^{18}O_{calcite}$, $\delta^{13}C_{calcite}$, $\delta^{13}C_{organic}$) and geochemical data (TOC, TOC/TN, RE) from Lake Ohrid core Co1262. An age-model based on tephra, radiocarbon ages and cross-correlation was established that delivers robust chronological control of the entire sequence and suggests that the core covers the last ca. 12.3 ka (Wagner et al., 2012b). The multi-proxy investigation provides information on Late Glacial to Holocene climate and environmental changes in the lake and its catchment, and represents the highest resolution and best-dated record from Lake Ohrid to date.

At the millennial-scale, hydroclimate and environmental conditions at Lake Ohrid are found to be controlled by regional and hemispheric processes related to orbitally-driven changes in insolation and the associated differences in incident radiation received at higher and lower latitudes. In turn, orbital forcing determines the position of the ITCZ, strength of North Atlantic anticyclone and intensity and direction of Atlantic westerly winds. Variations in these parameters are intrinsically linked to the African-Indian monsoon system, modulation of atmospheric circulation (AO/NAO) and development of a hydrological tripartition separating mid-latitude European climate from that of northern Europe and the southern Mediterranean. The boundary between the lower two of these zones is around ca. 40°N (Magny et al., 2003; Magny et al., 2013; Peyron et al., 2013), which is also representative of a phase shift between high and low latitude temperature trends during the Holocene (Davis and Brewer, 2009). In addition, the local and regional environmental response to centennial-scale events suggests a similar control mechanism to those that govern millennial-scale trends (i.e. LTG variations).

The response in Co1262 to Late Glacial to Holocene climatic and environmental change is consistent with previous cores from Lake Ohrid and Lake Prespa, and from across the Balkan Peninsula. A comparison between Co1262 and records from the southern and eastern Mediterranean indicates a uniform response to orbital-driven variations in temperature and precipitation, which can be set against the context of European and Northern Hemisphere climate change over the present Interglacial period (summarised in Table 6.6).

Table 6.6 *Summary of drivers and responders for generalised synoptic climate trends in North Africa, the Mediterranean and Europe over the early-mid Holocene (ca. 11-6 ka) and the mid-late Holocene (ca. 6 ka − present).*

Driver/Responder	**Early-mid Holocene**	**Mid-late Holocene**
Lake Ohrid $\delta^{18}O_{calcite}$	Low	High
Precession	Minimum	Maximum
Obliquity	Maximum	Minimum
LIG/LTG	Weak	Strong
Summer insolation	Maxima	Minima
ITCZ shift	Northward	Southward
African-Indian Monsoon	Strong	Weak
North African lake level	High	Low
Nile discharge	High	Low
Mediterranean Sea	Sapropel	No Sapropel
North Atlantic anticyclone	Strong	Weak
Westerlies shift	Northward	Southward
NAO/AO index	Positive	Negative
Northern Europe climate	Wet	Dry
Mid-Europe and northern Mediterranean climate		
Climate	Dry	Wet
Lake level	Low	High
Summer precipitation	Low	High
Fire activity	High	Low
Southern Mediterranean and Near East climate		
Climate	Wet	Dry
Lake level	High	Low
Summer precipitation	High	Low
Fire activity	Low	High

Variations within the Co1262 correspond both spatially and temporally with the current understanding of Late Glacial to Holocene hydroclimate across the Mediterranean, Europe and North Africa, but both at a higher sampling resolution and with a better chronology than most available records. The data and interpretation of the Holocene core give context for longer-term reconstructions of climate and hydrology from the Scientific Collaboration on Past Speciation Conditions in Lake Ohrid (SCOPSCO) cores that likely date back to the Lower Pleistocene (Wagner et al., 2014).

CHAPTER 7 | SCOPSCO 5045

This chapter is based on the publication: Lacey J. H., Leng, M. J., Francke A., Sloane, H. J., Milodowski, A., Vogel, H., Baumgarten, H., & Wagner B. 2015. Mediterranean climate since the Middle Pleistocene: a 640 ka stable isotope record from Lake Ohrid (Albania/Macedonia). Biogeosciences Discussions, 12, 13427-13481.

7.1 **Introduction**

The Scientific Collaboration on Past Speciation Conditions in Lake Ohrid (SCOPSCO) project is a multi-disciplinary international research initiative to better understand the influence of climate change and major geological events on evolution and the generation of endemic populations (Wagner et al., 2014), by obtaining more precise information on:

i. The age and origin of the lake.
ii. Past seismotectonic activity in the region.
iii. Central Mediterranean climate and environmental change through the Quaternary.
iv. How evolution is influenced by major geological events and the triggers for speciation.

This chapter presents extensive isotope data from SCOPSCO cores and provides a hydroclimate reconstruction covering the last 640 ka, directly addressing SCOPSCO aim (iii). Ultimately, the isotope data will support other lines of multi-proxy evidence (generated by the wider research team) to address aim (iv). The chapter will provide information on the coring campaign, core processing and chronological control of the record, and utilise the new isotope data to discuss interglacial/interstadial (and glacial/stadial) variability. The new record is a regionally unique continental isotope stratigraphy that enables the evaluation of long-term hydroclimate change on the Balkan Peninsula, and facilitates comparison with other long and continuous records.

7.2 **Core recovery and processing**

7.2.1 Site selection

Sites were selected for the SCOPSCO drilling campaign based on a dense grid of hydro-acoustic and multichannel seismic surveys carried out over the period 2004 to 2009 (as for the Lini site, Section 6.1; Reicherter et al., 2011; Lindhorst et al., 2015). In addition to the Lini site, four more drill sites (DEEP, Cerava, Gradište, Struga) were initially proposed from several locations around the lake to answer specific research questions, one of which (Struga) was replaced with the Peštani site during the campaign for logistical reasons (Table 7.1, Figure 7.1).

Table 7.1 *SCOPSCO coring sites and research motivation (modified from Wagner et al., 2014).*

Site	Water depth (m)	# holes	Total drilled (m)	Total recovery (m)	Deepest drill depth (m.b.l.f.)	Composite profile length (m)	Research question
DEEP (5045-1)	243	6	2088.71	1526.06	568.92	544.88	Age/origin, tephrostratigraphy, evolution forcing, longest possible archive
Cerava (5045-2)	125	2	175.71	172.20	90.48	87.86	Lake level fluctuations, catchment dynamics, evolutionary processes
Gradište (5045-3)	131	3	327.35	224.46	123.41	114.07	Active tectonics, spring dynamics, evolutionary processes
Peštani (5045-4)	262	1	194.50	177.90	194.50	177.90	Recover bedrock-neighbouring sediments

The master site (DEEP 5045-1, 41°02’57”N, 20°42’54”E) is located in a central basin depression (243 m water depth, Figure 7.1) where seismic data indicated a thick sediment succession of ca. 800 m of sediment overlying the basement (Figure 7.2; Lindhorst et al., 2015). Importantly, seismic data showed that the sediment fill was free from unconformities and erosional features with no major hiatuses (unlike marginal cores, e.g. Lz1120; Wagner et al., 2009a), thereby providing the best potential for a long and continuous record of maximum age (Figure 7.3).

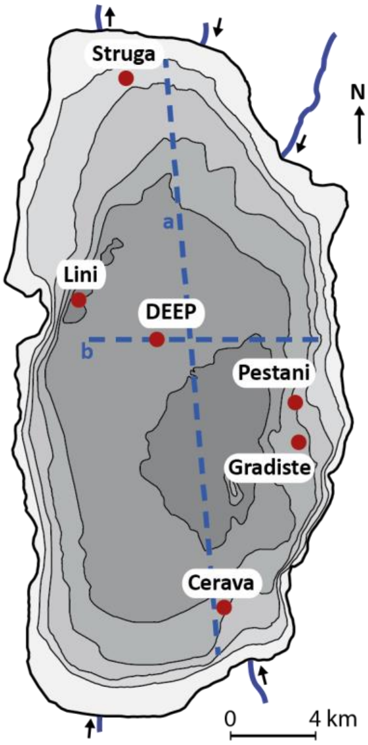

Figure 7.1 *Locations of the SCOPSCO drill sites (red dots) and line of seismic profiles shown in Figures 7.2 and 7.3.*

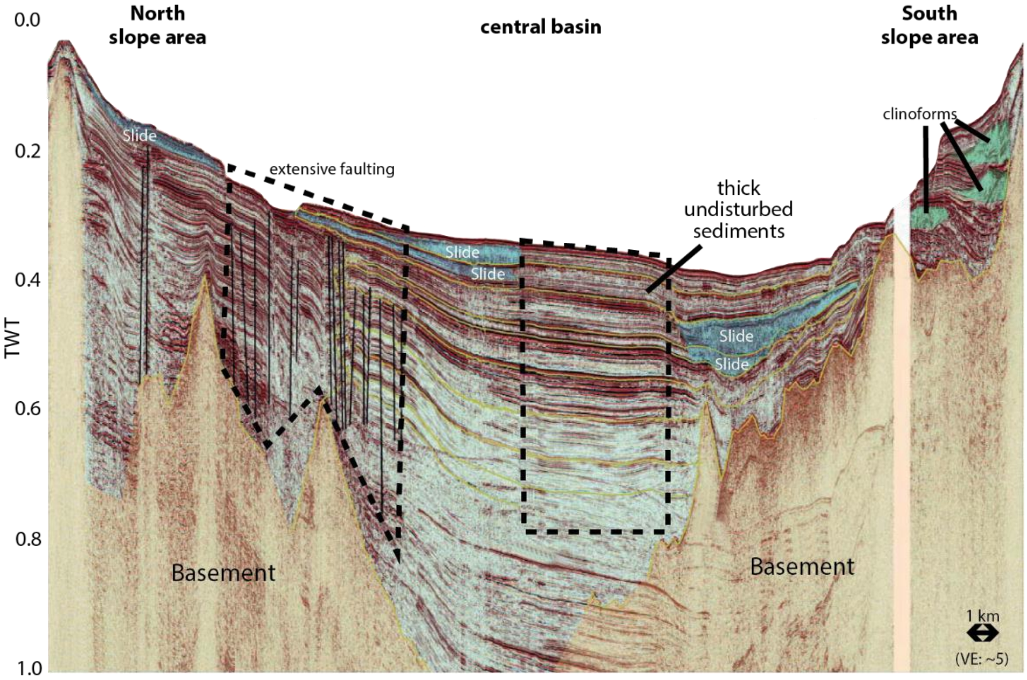

Figure 7.2 *Seismic cross section (line a, Figure 7.1) running north to south, showing the sedimentary and tectonic structure of Lake Ohrid (adapted from Wagner et al., 2014).*

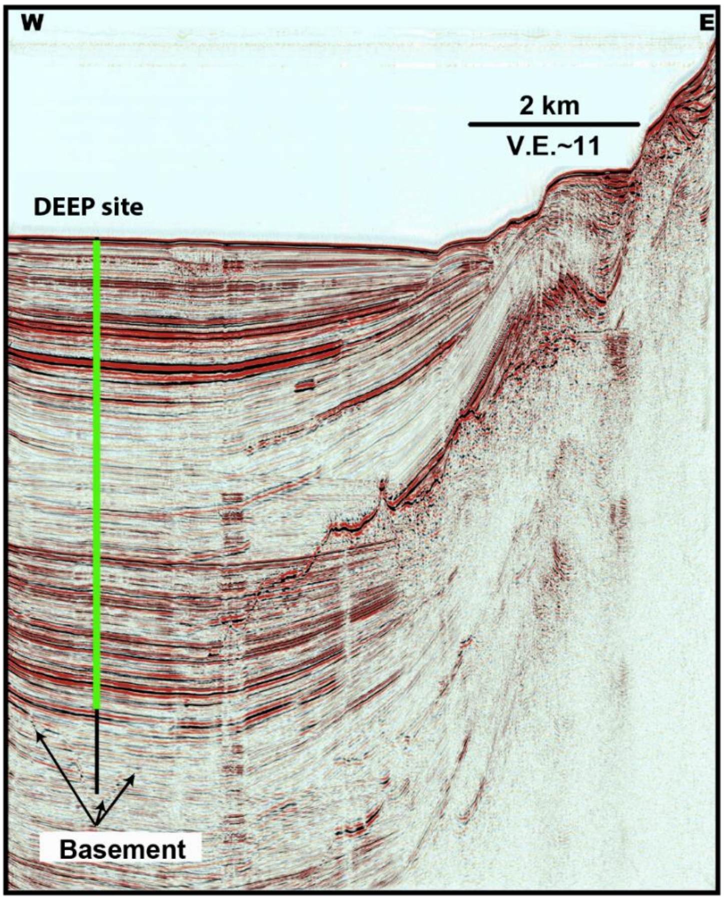

Figure 7.3 *Seismic cross section (line b, Figure 7.1) running west to east, showing the location of the DEEP site (green line = approximate depth of core recovery, black line = proposed target depth; adapted from Wagner et al., 2014; Lindhorst et al., 2015).*

7.2.2 Drill campaign and coring results

The SCOPSCO field campaign took place in March-June 2013, after being postponed from 2012 due to a fire on the container ship MSC Flaminia (equipment transport vessel from US to Europe). Coring was carried out using the Deep Lake Drilling System (DLDS; Figure 7.4a) operated by a team from the US-based corporation Drilling, Observation and Sampling of Earth’s Continental Crust (DOSECC). Different coring tools were used for drilling depending on the sediment depth and consistency, including a hydraulic piston corer (HPC, Figure 7.4b) for relatively soft uncompacted sediments, and rotary drill tools (extended nose, XTN and the Alien, ALN, Figure 7.4 b and c, respectively) for deeper, more consolidated sediments (Figure 7.5).

Figure 7.4 *a) DOSECC Deep Lake Drilling System ('the barge') used to core Lake Ohrid , b) hydraulic piston corer [i] and extended nose drill bit [ii], and c) the Alien drill bit. Core catcher can be seen in (b-ii) and (c).*

To maximise recovery six parallel holes were drilled at DEEP site (A-F), reaching a maximum depth of 569 m below the lake floor (b.l.f.) at which point gravel-pebble-sized grains restricted further penetration[11]. Holes 1A and 1E were restricted to surface sediments (<5 m b.l.f.), 1B and 1C reached down to 480 m b.l.f., 1D down to 569 m b.l.f., and spot coring was carried out in 1F (providing overlapping cores missing from the other holes; Francke et al., 2015). A total of 1526 m of sediment was recovered from the six parallel drill holes, which, taking into account overlap between the sediment cores, amounted to a total composite recovery of 545 m (95%) (increasing to 99% for the upper 430 m; Wagner et al., 2014). The base of the cores (>430 m) is dominated by shallow water facies characterised by fine-grained organic-rich material, coarser sediments containing shell fragments, distinct sand layers, and gravel-pebble

---

[11] The author assisted with SCOPSCO fieldwork for a three-week period in May 2013, helping to core part of the DEEP site, Cerava, Gradište and Peštani. As part of the science team, the author's main responsibility was to process the core once it had been retrieved.

grade material. In contrast, the upper core (<430 m) comprises mainly hemipelagic sediments (Figure 7.5). Following recovery, the cores were split into sections up to one-metre-long, stored in darkness at 4°C, and shipped to the University of Cologne (Germany) for storage.

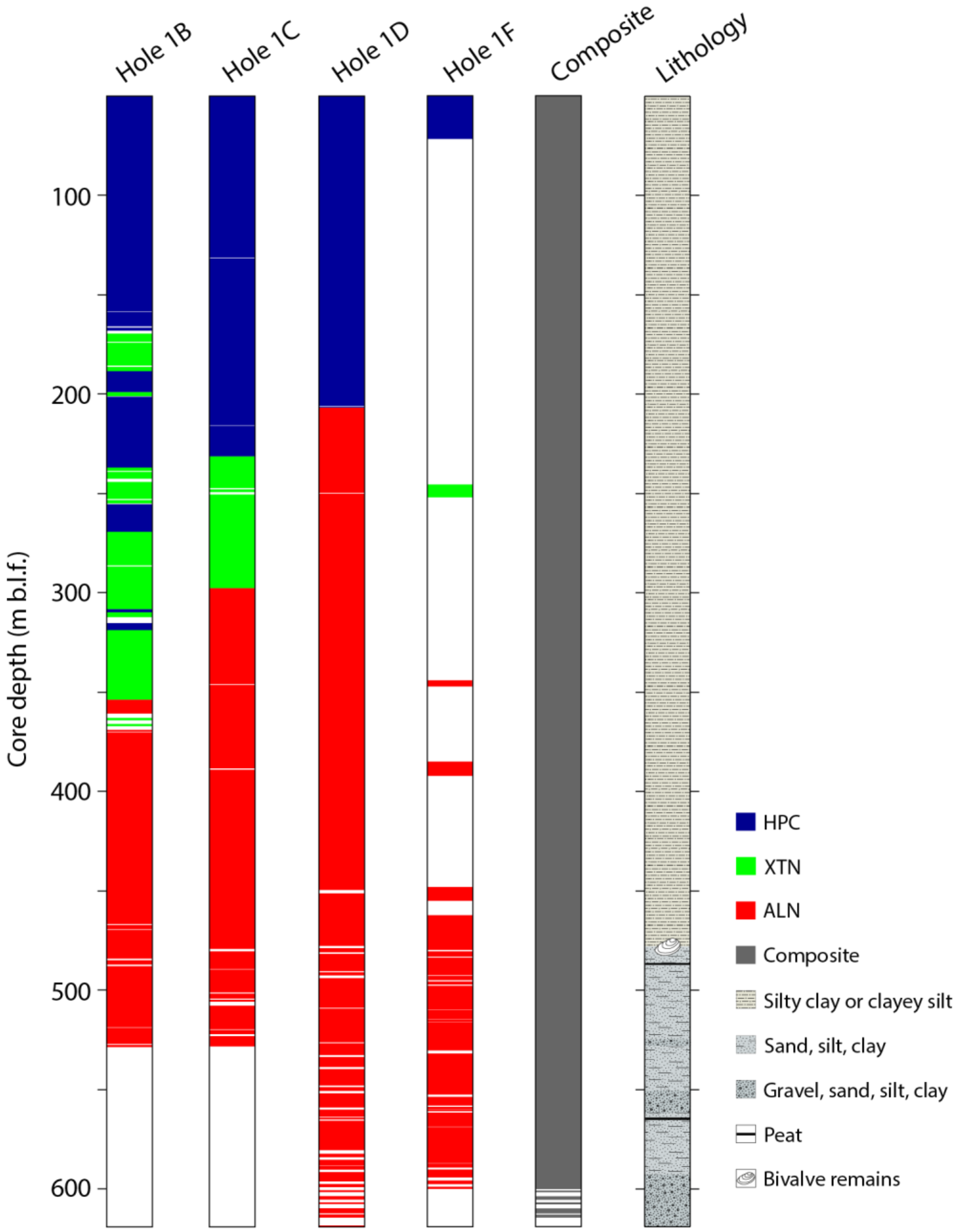

Figure 7.5 *Core recovery for holes 1B, 1C, 1D, and 1F, composite recovery profile (composite profile shown is based on field depth measurements) and lithology from DEEP site (redrawn from Wagner et al., 2014). Drill tools used in each hole are indicated, including the hydraulic piston corer (HPC, blue), extended nose drill bit (XTN, green), and the Alien (ALN, red). The composite recovery made up from overlapping parallel sections is in grey (core gaps are white). The lithology is also shown and based on core catcher samples.*

7.2.3 Core correlation

Core correlation was initially approximated in the field using individual holes and based on field depth measurements (as shown in Figure 7.5), and later a preliminary composite profile was produced (by Dr Alexander Francke, University of Cologne) from magnetic susceptibility (MS) data measured at 2 cm resolution on a Geotek multi-sensor core logger (MSCL) during fieldwork (using whole cores from holes 1B, 1C, 1D, and 1F). Cores selected for the profile were split (working and reference halves) and described, imaged at high-resolution, and scanned using X-ray fluorescence (XRF) at 2.5 mm resolution (by students at the University of Cologne, supervised by Dr A. Francke). The core correlation was then fine-tuned using the optical, lithological, and XRF data (where needed adjacent cores were opened and processed to provide additional precision to the correlation).

An initial composite profile was created for the DEEP site down to 247.79 m (metres composite depth, replacing field measurement ‘below lake floor’ depths), with 99.97% core recovery due to having no overlapping cores between two sections (Francke et al., 2015). The composite profile comprises two sections from core Co1261 (recovered in 2011 from DEEP site using a UWITEC gravity corer to give better core quality for surface sediments) and 386 sections from holes 1B, 1C, 1D, and 1F (Table 7.2). Given the scale of the SCOPSCO project and the time required for core handling, this thesis presents data from the initial composite profile (i.e. between the surface and 247.79 m correlated composite depth).

7.2.4 Core processing

All primary core processing was carried out at the University of Cologne and is detailed in full by Francke et al. (2015). In summary, split cores from the composite profile were sampled at 16 cm resolution, whereby a 2 cm slice (40.7 cm^3) of sediment was taken from each working core half and split into four sub-samples (for multi-proxy analyses). Smaller samples (5 cm^3) were removed midway between these (i.e. every other 8 cm) for higher resolution work. Samples for palaeomagnetic analyses were also taken every 50 cm. The sub-samples were freeze-dried and each aliquot was homogenised and ground to a fine powder (< 63 μm). Total carbon (TC) and total inorganic carbon (TIC) were measured using a DIMATOC 100 carbon analyser (as detailed in Section 4.1.1), and total organic carbon (TOC) was calculated as the difference between TC and TIC.

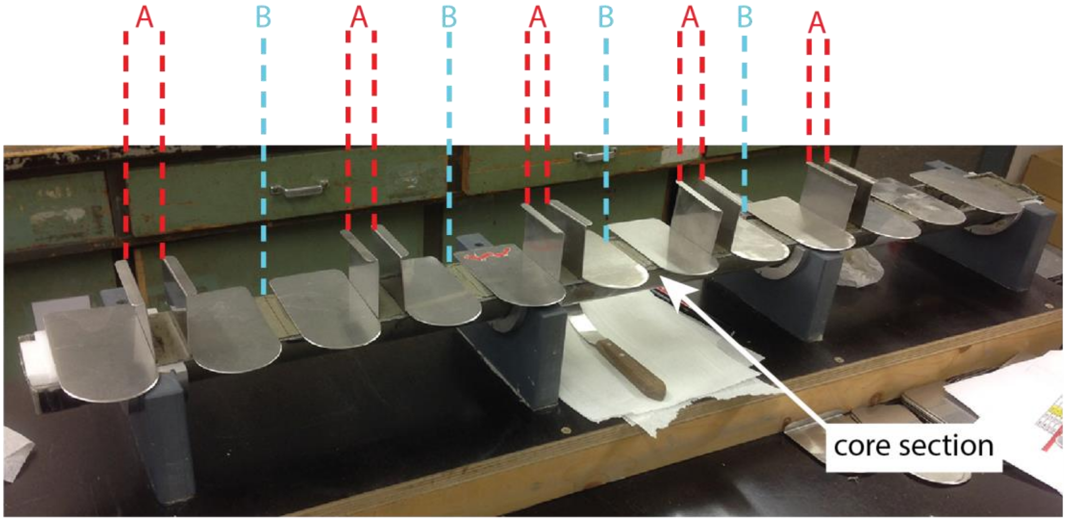

Figure 7.6 *Example of core processing technique used to extract samples at 16 cm ('a', red) and 8 cm ('b', blue) resolution. A set of metal plates were used to remove the 2 cm thick slices (another set was placed flat onto the core section to minimise disturbance) and cylindrical plastic vials were used for the 8 cm resolution samples.*

Relative concentration changes of carbonate phases in the sub-samples were determined at 32 cm resolution throughout the composite profile using Fourier transform infrared spectroscopy (FTIR) by Dr Hendrik Vogel, University of Bern, Switzerland (FTIR methodology is described in full by Lacey et al. (2015b) and Francke et al. (2015)).

7.2.5 Lithological overview

The DEEP site composite profile (surface to 247.79 m) predominantly comprises fine-grained hemipelagic sediments, with a decreasing water content top (ca. 70%) to bottom (ca. 32%) due to compaction over time (Francke et al., 2015). Decompaction of sediment layers is calculated to range between 10% and 30% downcore and the overall thickness is suggested to increase by 36 m after compaction is taken into account (Baumgarten et al., 2015). Francke et al. (2015) subdivide the hemipelagic sediments into three main lithotypes (defined by visual core description). Lithotype 1 sediments are characterised by high TIC, high TOC, high biogenic silica (bSi, diatom frustules), and low siliciclastic mineral abundance (low potassium, K, intensity and a reduction in fine <4 μm material). Lithotype 2 sediments have a lower concentration of TIC, variable TOC and bSi, and moderate clastic material (higher K intensity than lithotype 1). Lithotype 3 sediments are categorised as having very low TIC (apart from occasional TIC peaks to ca. 0.5%) and generally low TOC, low bSi and high clastic matter (increased fine fraction <4 μm content).

Anomalous event layers that do not correspond to the three main lithotypes can be attributed to tephra fallout deposits and Mass Wasting Deposits (MWD). Twelve tephra layers up to 15 cm thick have been identified by the presence of glass shards and geochemically correlated to known volcanic eruptions from the Italian Volcanic Provinces and wider Mediterranean area (Leicher et al., 2015). Conspicuous layers with a largely minerogenic composition were classified as MWD, and are predominantly between 0.1-3 cm thick comprising lenses or normal-graded layer (Francke et al., 2015).

7.3 Sampling

The DEEP site composite profile was sampled for oxygen and carbon isotope ratios on carbonate ($\delta^{18}O_{carbonate}$ and $\delta^{13}C_{carbonate}$) using 16 cm resolution sub-samples provided by the University of Cologne from the surface to a correlated depth of 247.79 m throughout zones with a high TIC content (up to 10% TIC, lithotype 1 and 2, Figure 7.7). Based on the Lini Co1262 record (Chapter 6) and other previous cores, high TIC content is thought to represent warmer interglacial/interstadial periods (Wagner et al., 2009a; Leng et al., 2010a; Vogel et al., 2010a; Wagner et al., 2010).

Within zones of overall low TIC (i.e. lithotype 2 and 3, assumed to correspond to glacial/stadial periods), intermittent spikes to higher TIC (mostly <0.5% but up to ca. 2%) were also sampled (Figure 7.7) and investigated using X-Ray Diffraction (XRD; see Section 4.4 for analytical method), as XRF showed that the recurrent spikes were high in Fe and Mn (Francke et al., 2015). Material was also taken across a number of these layers to provide polished epoxy resin-embedded thin sections for Scanning Electron Microscopy (SEM) and Energy-Dispersive X-Ray Spectroscopy (EDX) (see Sections 4.5 and 4.6 for analytical methods).

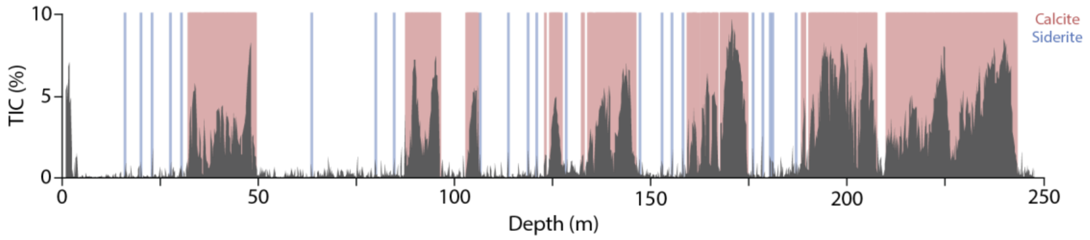

Figure 7.7 *Sampling horizons for calcite (red) and siderite (blue) from the SCOPSCO composite profile were based on TIC measurements (grey) provided by Dr Alexander Francke.*

7.4 Chronology

The age model for the SCOPSCO composite profile (upper 247.79 m of the DEEP site sequence) was established by Francke et al. (2015) using 1) tephrostratigraphical information, 2) tuning TOC (and TOC-related proxies) to trends in local daily insolation patterns (26 June at 41°N; Laskar et al., 2004) and to the winter season length, and 3) tuning high TIC content to minima of the Lisiecki and Raymo (2005) global benthic isotope stack (LR04).

Tephra layers correlated to well-known eruptions from Italian volcanoes by geochemical fingerprinting were used as first order tie points, providing a robust basis for the age model (Leicher et al., 2015). Correlated tephra layers include Mercato (8.5 ka*), Y-3 (29.1 ka*), Y-5 (39.6 ka), X-6 (109 ka), P11 (129 ka), Vico B (162 ka), Pozzolane Rosse (457 ka), Sabatini Fall A (496 ka), and A11/A12 (511 ka) (*calibrated 14C age, 40Ar/39Ar ages recalculated from the literature; Leicher et al. (2015)).

Second order tie points included the tuning of minima in TOC (and TOC-related proxies, e.g. TOC/TN) to increasing insolation and winter season length. Summer insolation is thought to drive aquatic productivity and lake water mixing is considered to be a function of winter season length. Minima and maxima in winter season length and insolation may have an opposing effect of the presence of TOC in sediments (low insolation = low TOC, however low winter season length reduces mixing, and vice versa). Therefore, TOC (and TOC-related proxies) is most likely low (poor preservation and production potential) during periods where summer insolation intensity and winter season length are balanced (i.e. at their inflection points). This was corroborated by tephra layers deposited during TOC minima that chronologically coincide with inflection points of summer insolation and winter season length.

Taking the first and second order tie points into consideration, the TIC record shows a good correspondence with peak interglacial conditions recorded by the LR04 global benthic isotope stack, where TIC maxima are temporally comparable to δ^{18}O minima. The stratigraphic position of the P11 tephra (129 ka) below a TIC maximum at 48 m infers that the TIC peak is most likely associated with interglacial conditions centred around 123 ka during the Eemian (MIS 5.5), which supports the association of TIC with the LR04 isotope stack. Third order tie points were therefore achieved by tuning LR04 δ^{18}O minima with TIC maxima.

Overall, nine tephra layers (1st order) and 45 correlation points (2nd and 3rd order) were incorporated into an age-depth model for the composite profile using the software package Bacon 2.2 (Blaauw and Christen, 2011), with 2σ uncertainty for ^{40}Ar/^{39}Ar tephra ages and ±1000 years applied to 2nd and 3rd order tie points to account for inaccuracies in the tuning process (Figure 7.8; Francke et al., 2015). The age model was compared and fine-tuned to the age model of borehole logging data, which was based on tuning potassium contents from downhole spectral gamma ray to LR04 and cyclostratigraphic analysis on gamma ray data from hole 1D (Baumgarten et al., 2015). Chronological information is discussed in detail in Francke et al. (2015), Leicher et al. (2015), and Baumgarten et al. (2015).

The age model implies that composite profile for the upper 247.79 m of sediments recovered from the DEEP site in Lake Ohrid represents the last ca. 640 ka and most likely covers Marine Isotope Stages (MIS) 16-1 (Lisiecki and Raymo, 2005). Hereafter results are presented and discussed within the MIS framework (lettered sub-stages are detailed by Railsback et al., 2015).

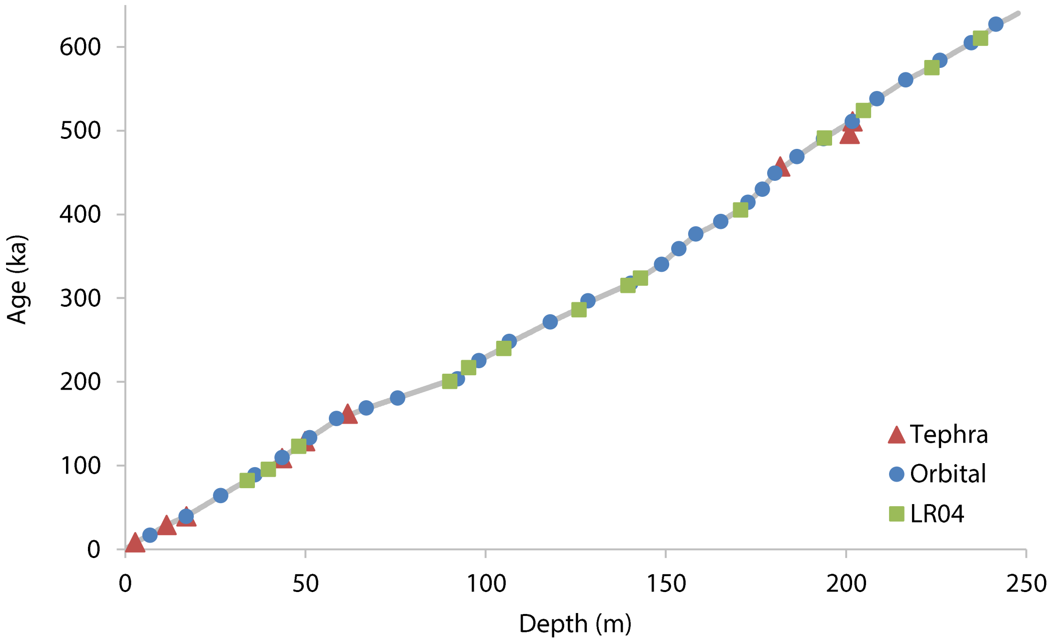

Figure 7.8 *Age model for the DEEP site composite sequence from the surface to 247.79 m, indicating a basal age of ca. 640 ka (redrawn from Francke et al., 2015).*

The age model was used to interpolate a date for each individual sample depth (every 16 cm), and therefore data can be shown as a time series plot. Given that tie points to the LR04 benthic $\delta^{18}O$ isotope stack and orbital parameters are used in the calculation of the age-depth model, care must be taken not to develop circular interpretation of the dataset through direct temporal comparison with these records. However, although this may preclude the direct comparison of leads/lags between terrestrial-marine realms and to some terrestrial records, assuming the overall error of the age model is within the region of a couple of thousand years, the relative magnitude of excursions can be compared (even if their exact timing cannot).

7.5 Results

A total of 651 samples were analysed from the composite profile for $\delta^{18}O_{calcite}$ and $\delta^{13}C_{calcite}$ (using the method described in Section 4.1), and the results are presented with TIC as a time series in Figure 7.9. As the Lini record provides the most extensive Holocene section recovered from Lake Ohrid to date (Co1262 = 7.84 m, compared to 4.63 m in the composite profile), the isotope stratigraphy from Co1262 is utilised to provide a higher resolution dataset for the composite profile (the Co1262 data is plotted using the age model calculated in Section 6.4).

Over the whole record, calcite occurs predominantly in interglacial/interstadial periods (i.e. odd-numbered MIS), and has mean $\delta^{18}O_{calcite} = -5.3 \pm 0.8‰$ (1σ, $n = 924$) and $\delta^{13}C_{calcite} = +0.4 \pm 0.6‰$ (1σ, $n = 924$), including Co1262 data. MIS 15 and 13 have similar $\delta^{18}O_{calcite}$, TIC remains relatively high through glacial MIS 14 and $\delta^{18}O_{calcite}$ is consistent with the bounding MIS values (MIS 15 to MIS 13 mean $\delta^{18}O_{calcite} = -5.5 \pm 0.7‰$ (1σ, $n = 294$). Minimum $\delta^{18}O_{calcite}$ for the whole record (−7.6‰) occurs at ca. 378 ka during MIS 11, which has mean $\delta^{18}O_{calcite} = -5.5 \pm 0.9‰$ (1σ, $n = 75$) and the largest overall variation. MIS 9 has the lowest mean $\delta^{18}O_{calcite}$ of the record (−5.8±0.9‰, 1σ, $n = 69$). A TIC spike centred around ca. 287 ka in MIS 8 (see later discussion on the attribution to MIS 9) has lower $\delta^{18}O_{calcite}$ than the values observed for MIS 9 (−6.5±0.5‰, 1σ, $n = 18$). MIS 7 shows similar values to the lower core and has mean $\delta^{18}O_{calcite} = -5.5 \pm 0.6‰$ (1σ, $n = 73$). MIS 5 contains the highest mean $\delta^{18}O_{calcite}$ (−4.6±0.8‰, 1σ, $n = 104$) and is observed to be similar to Holocene average $\delta^{18}O_{calcite}$ from Co1262 (−4.9±0.7‰, 1σ, $n = 280$). $\delta^{13}C_{calcite}$ is less variable than $\delta^{18}O_{calcite}$ when considering individual MIS, with mean values ranging between +0.0±0.7‰ for MIS 7 and +0.6±0.7‰ for MIS 5 (MIS 14 mean $\delta^{13}C_{calcite} = +0.8 \pm 0.5‰$, however this represents glacial stage).

Table 7.2 *Statistics for the Lake Ohrid 5045-1 composite profile split into MIS, showing total samples (n), mean ($\bar{x}$), standard deviation (1σ), correlation coefficient (r^2) and p-value for $\delta^{18}O_{calcite}$ and $\delta^{13}C_{calcite}$.*

MIS	n	$\delta^{18}O_{calcite}$		$\delta^{13}C_{calcite}$		r^2	*p*
		$\bar{x}$	1σ	$\bar{x}$	1σ		
All	924	−5.26	0.83	+0.43	0.57	0.09	<0.01
1	273	−4.90	0.65	+0.44	0.43	0.02	<0.01
5	104	−4.63	0.84	+0.65	0.73	0.28	<0.01
7	73	−5.47	0.64	+0.04	0.69	0.04	0.08
8	18	−6.49	0.53	+0.32	0.44	0.11	0.17
9	69	−5.82	0.85	+0.40	0.59	0.10	<0.01
11	75	−5.50	0.94	+0.22	0.40	0.10	<0.01
13	107	−5.47	0.70	+0.48	0.53	0.36	<0.01
14	51	−5.54	0.76	+0.79	0.46	0.38	<0.01
15	136	−5.44	0.65	+0.40	0.64	0.20	<0.01
16	18	−5.69	0.93	+0.46	0.36	0.00	0.85

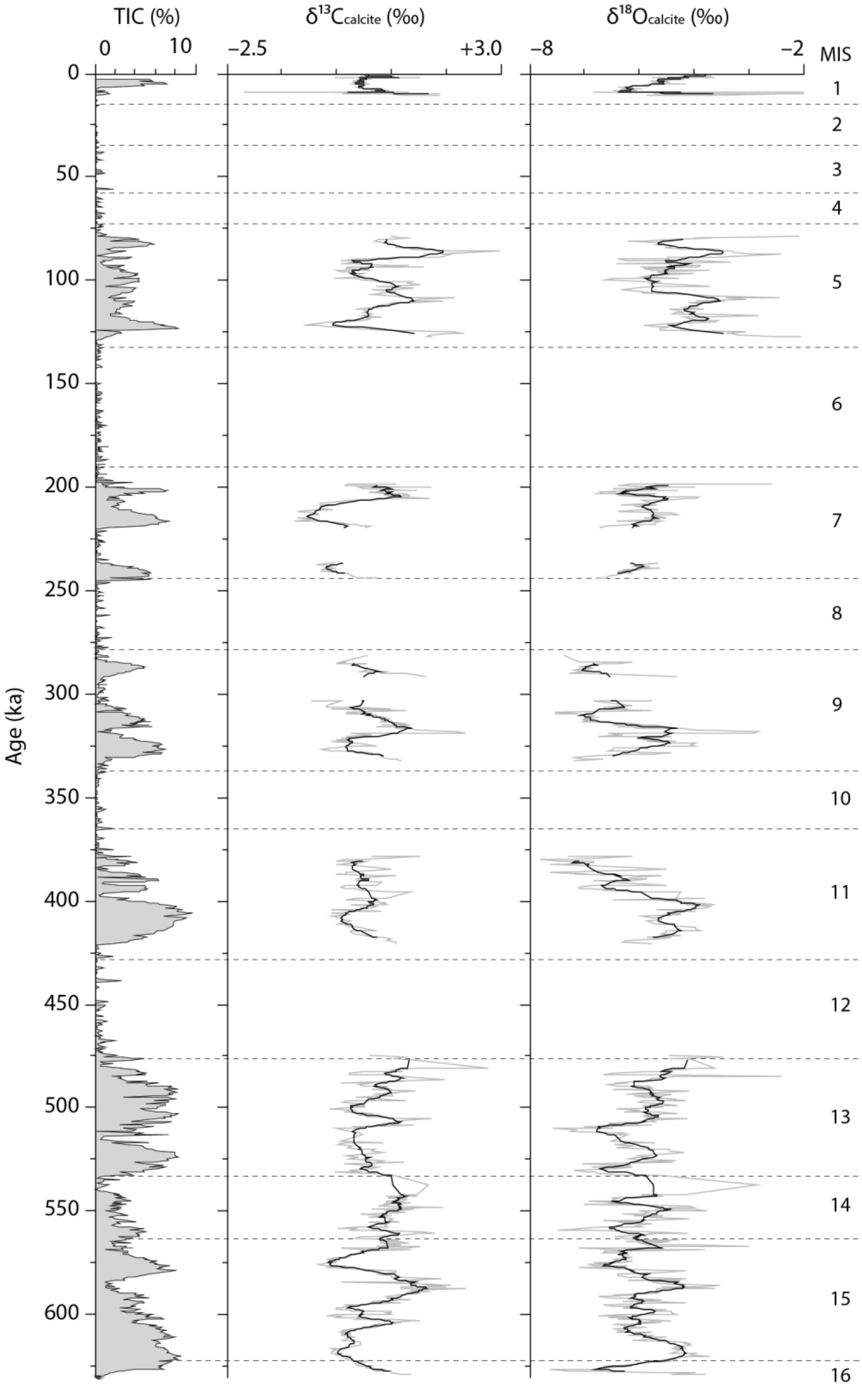

Figure 7.9 *Isotope results ($\delta^{18}O_{calcite}$ and $\delta^{13}C_{calcite}$) from the SCOPSCO DEEP site composite profile, showing TIC (Francke et al., 2015), the Holocene Co1262 dataset (Chapter 6), and MIS stratigraphy (Lisiecki and Raymo, 2005; Railsback et al., 2015). Calcite data is given as raw (grey line) and 9-point running average (black line).*

As TIC is negligible through glacial (even-numbered MIS) and stadial intervals, calcite isotope data is quasi-continuous through the SCOPSCO sequence. However, discrete horizons that have higher TIC are present in glacial periods, which are recognised as thin yellow-brown layers in visual core description and correlate to enhanced iron (Fe) and manganese (Mn) XRF intensities (Figure 7.10; Francke et al., 2015). Elevated TIC suggested that carbonate was present, and so several horizons identified from XRF data and visual descriptions were selected for XRD and thin section analysis.

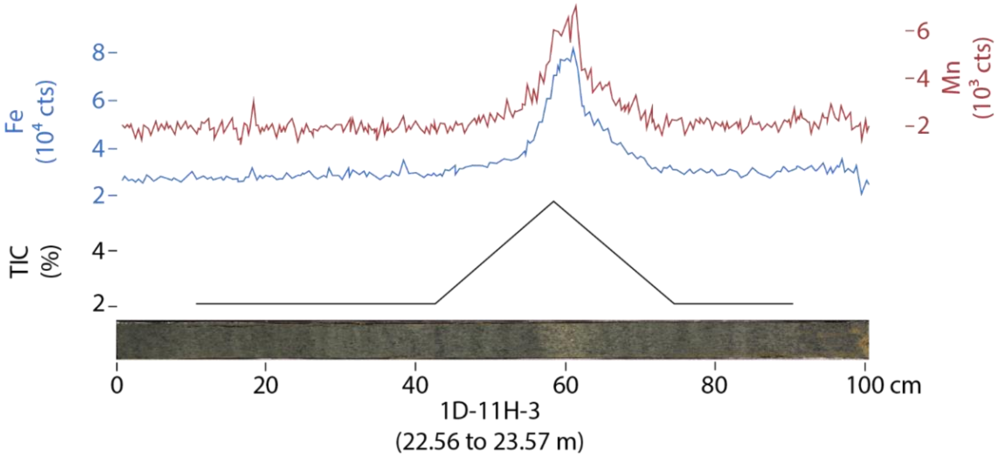

Figure 7.10 *A light yellow-brown layer in core 1D-11H-3 (at 60 cm section depth) between 22.56 and 23.57 m composite depth (ca. 56 ka) correlates to higher TIC, Fe and Mn (redrawn from Francke et al., 2015).*

XRD analysis was carried out on 30 samples taken from TIC peaks within areas of the composite profile with overall low-negligible inorganic carbonate. Samples were selected based on their overall TIC content, and analysis comprised 10 high (1-2%), 10 mid-range (0.75-1%) and 10 lower (0.65-0.75%) samples from glacial intervals. Analytical work and data processing was carried out using the methodology described in Section 4.4. Phase identification suggests that all of the samples contained siderite ($FeCO_3$), and that the best pattern fit was achieved using a pure siderite (main peak is around 2.80Å or 37.3°2θ; Doris Wagner, personal communication, March 2015; Figure 7.11). Although Fe-substitution is possible (for example, Mn or Ca), a shift in the peak position would be expected if the cation substitution was large, which was not observed in the analysis (inferring a relatively pure siderite).

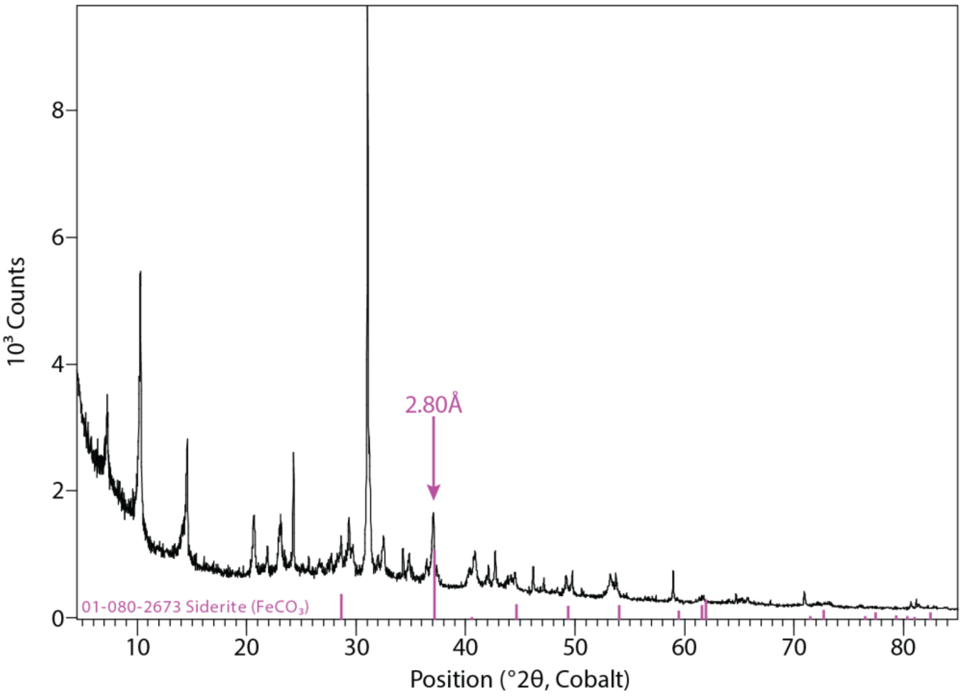

Figure 7.11 *X-ray diffraction plot of analysis results for vial 660 (106.5 m, ca. 246.4 ka), showing the reference pattern for siderite (*$FeCO_3$*) and the main siderite peak at 2.80Å (37.3°2θ).*

In addition to XRD analysis, material was taken from both calcite and siderite-bearing layers identified in the composite profile (from adjacent cores to preserve the integrity of the composite profile) and prepared using the methodology described in Section 4.5. A total of eight thin sections were made (by John Fletcher, BGS Thin Sectioning Department), six from glacial TIC spikes (TIC = ca. 1.5%) spanning a visually identifiable siderite layer and two from interglacial (high TIC = ca. 9%) locations. Scanned images of these thin sections highlight the sedimentological difference between lithotype 1 and lithotype 3 sediments (Figure 7.12).

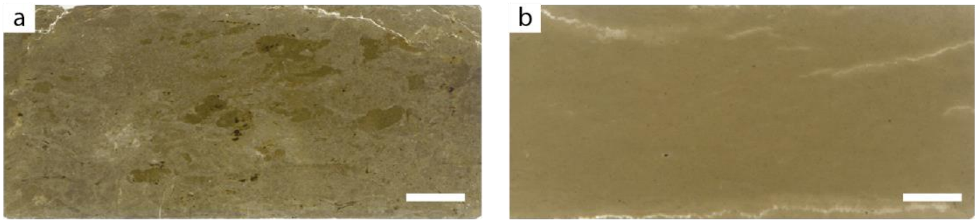

Figure 7.12 *Example of thin sections used to investigate diagenetic processes in core 5045-1, a) glacial section (siderite) from 147 m core depth, ca. 336 ka, and b) interglacial (calcite) section from 240 m core depth, ca. 620 ka, highlighting the sedimentological change between lithotype 1 and 3 (white scale bar = 5 mm).*

The thin sections were analysed using SEM and EDX to further qualify the carbonate minerals present in 5045-1 sediments, and to assess their mineralogical relationship with other phases in the core to elucidate their environment of deposition. SEM-EDX chemical characterisation of the thin section material confirms that the carbonate present in glacial TIC spikes is siderite. EDX spectra of individual mineral grains show elemental peaks for Fe, Mn, Ca, C, and O, suggesting that (contrary to XRD analysis) the siderite is not completely pure (i.e. $FeCO_3$), but may have a more complex, chemically distinct elemental nature (Figure 7.13). Individual SEM images will be discussed in further detail in Section 7.6.2.

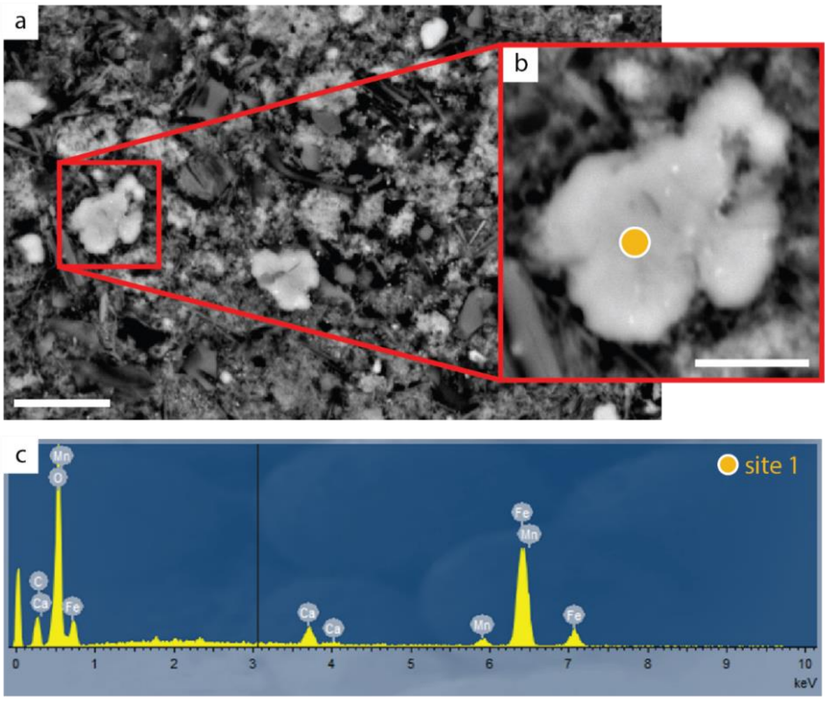

***Figure 7.13** a) back-scatter SEM image of glacial thin section (146 m, ca. 250 ka; scale bar = 10 μm), emphasising b) a carbonate grain (scale bar = 2 μm) showing the location of c) EDX spot analysis at 'site 1' indicating the chemical composition of the site of interest and confirming it to be siderite.*

FTIR data[12] have also been generated for the composite profile (by Dr Hendrik Vogel), which also confirm siderite to be present and give an indication of the relative abundance of siderite and calcite through the 5045-1 sequence (Figure 7.14). In general, siderite is abundant in zones with low calcite and is typically associated with

---

[12] FTIR spectroscopy passes infrared radiation through a sample and the spectrum acquired from the transmitted component represents the selectively adsorbed radiation providing a characteristic pattern specific to the particular molecular structure of a given mineral.

glacial periods (even-numbered MIS) as well as stadials. Siderite is absent toward the base of the core, only present in modest quantities within MIS 14, and increases upwards where the greatest number of siderite layers are observed in MIS 6 (although siderite is common throughout MIS 9-3).

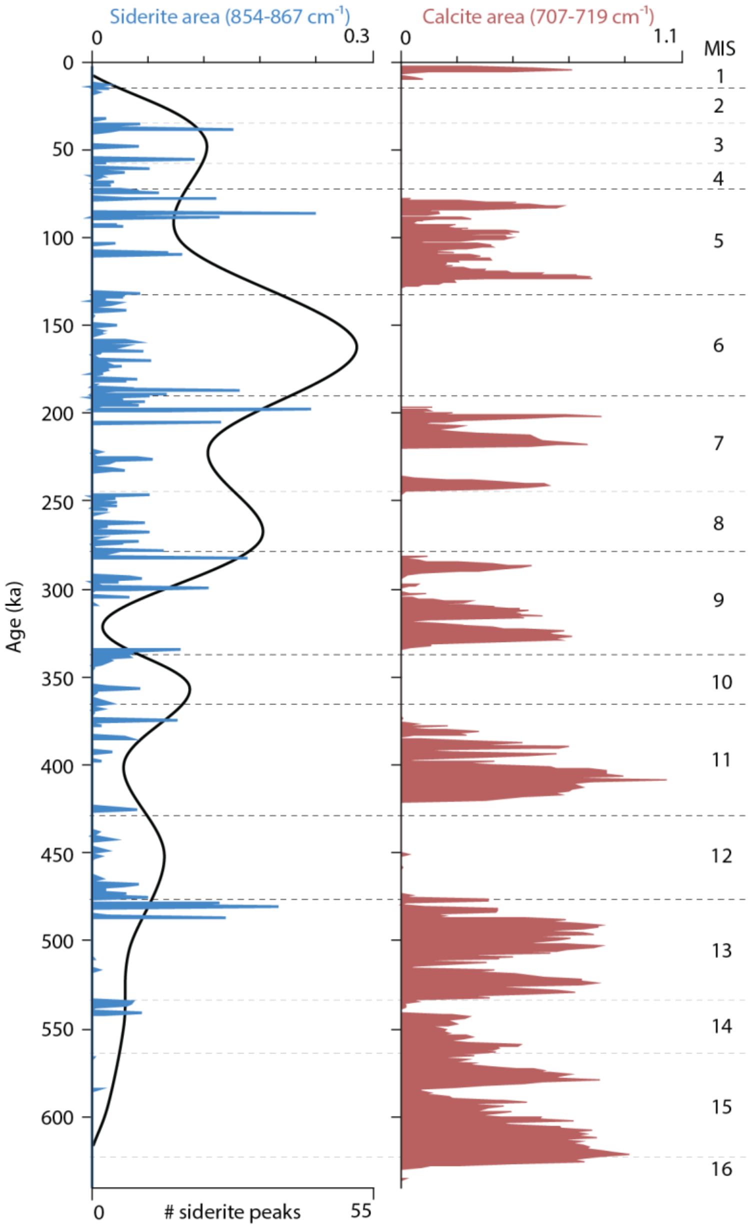

Figure 7.14 *FTIR spectroscopy data for siderite (blue) and calcite (red) from the composite profile (courtesy of Dr H. Vogel), showing the MIS stratigraphy (Lisiecki and Raymo, 2005; Railsback et al., 2015) and number of siderite peaks per MIS (black line, MIS 2-4 amalgamated).*

In total 22 samples were selected for oxygen and carbon isotope analysis on siderite ($\delta^{18}O_{siderite}$ and $\delta^{13}C_{siderite}$) based on the highest TIC peaks from glacial MIS (i.e. zones of overall low TIC; horizons are detailed in Figure 7.7), to provide an indication of glacial conditions and to support a more continuous record of hydroclimate variability over multiple glacial-interglacial cycles (Figure 7.15). Overall, mean $\delta^{18}O_{siderite}$ = −2.2±0.8‰ (1σ, *n* = 22) and $\delta^{13}C_{siderite}$ = +12.3±0.5‰ (1σ, *n* = 22). The lowest $\delta^{18}O_{siderite}$ are observed in MIS 3 (−3.1±0.7‰), and the highest in MIS 10 (−1.3±0.7‰), which also contains the lowest $\delta^{13}C_{siderite}$ (+11.9±0.4‰). The highest $\delta^{13}C_{siderite}$ are observed in MIS 12 (+12.6±0.2‰) and MIS 3 (+12.6±0.5‰).

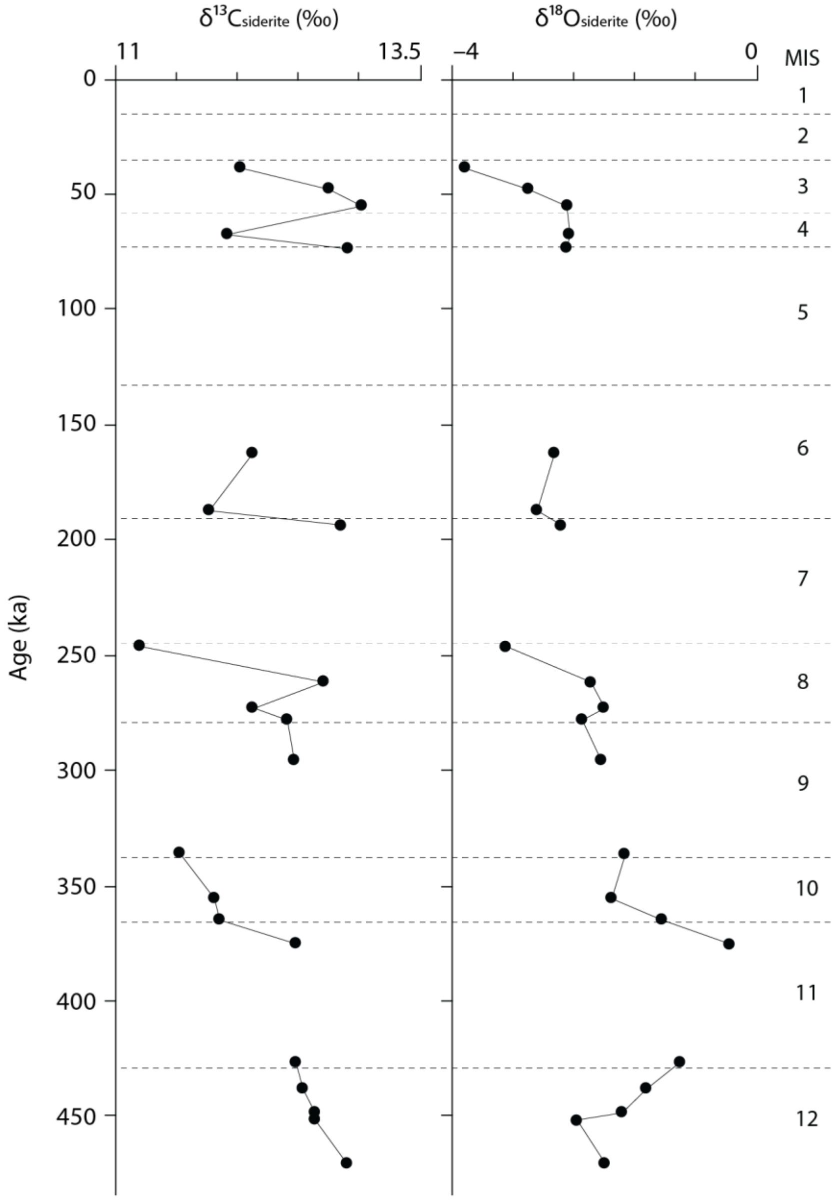

Figure 7.15 *Isotope results ($\delta^{18}O_{siderite}$ and $\delta^{13}C_{siderite}$) from the composite profile, showing siderite data (black dots) and MIS stratigraphy.*

7.6 Discussion

7.6.1 Oxygen isotope composition of calcite

The formation of calcite in surface waters is shown to be seasonally induced during summer months in response to elevated temperatures and the photosynthetic removal of CO_2 within the epilimnion (Matzinger et al., 2007). Assuming equilibrium conditions, $\delta^{18}O_{calcite}$ is a function of epilimnetic temperature and the oxygen isotope composition of lake water ($\delta^{18}O_{lakewater}$) at the time of calcite precipitation (Section 3.5; Leng and Marshall, 2004). Based on core top sediments and modern lake water isotope measurements, calcite is shown precipitate in equilibrium with lake water and is confirmed to be associated with summer conditions (see discussion in Section 6.6.3). These modern data suggest that the oxygen isotope record is primarily a function of water balance, where calcite is precipitated in warmer summer periods on an annual basis (also determined by the presence of Ca^{2+} and HCO_3^- ions), and $\delta^{18}O_{calcite}$ is likely driven by the proportion of winter recharge in relation to summer evaporation over extended timescales, given the lake water residence time. The isotope dataset from core Co1262 suggests a relatively stable isotope hydrology through the Holocene, where $\delta^{18}O_{calcite}$ responds to atmospheric circulation and climate change in association with variations in insolation and the latitudinal temperature gradient (LTG; Chapter 6). Although centennial-scale events may have had a marginal impact on the record, millennial-scale $\delta^{18}O_{calcite}$ trends in Co1262 are observed to reflect a coherent spatial pattern of regional climate variability during the Holocene, ultimately driven by orbital parameters. Therefore, isotope data from core Co1262, in addition to the modern isotope data available, are used as a ‘recent’ calibration for the 5045-1 record to provide an understanding of the processes driving isotope variations and to facilitate longer-term reconstructions. Moreover, this highlights an inherent assumption that the systematics of isotope variation have not varied significantly over the last 640 ka (this assumption is perhaps more tenable for the upper record, subsequent to the mid-Pleistocene transition where the dominant periodicity of climate-forcing changed from a 41 ka to 100 ka cyclicity).

Oxygen isotope data from the Holocene broadly fall between −6.5‰ and −2.0‰ (although values are typically no higher than −4.0‰), which is consistent with the 5045-1 record where values range between −7.6‰ and −2.3‰. Assuming that the main sources of moisture and $\delta^{18}O_{source}$ have remained relatively similar between interglacial/interstadial periods, this suggests that variations are a function of processes similar to Holocene conditions with no significant excursions beyond that predicted by the modern calibration. Considering that the glacial-interglacial variability in global $\delta^{18}O_{seawater}$ is approximately 1.0±0.1‰ (Schrag et al., 2002), or 1.2±0.1‰ in the Mediterranean (Paul et al., 2001), the difference in $\delta^{18}O_{source}$ between interglacials is likely to be minimal. In addition, the mean annual weighted isotope composition of modern water inflow to Lake Ohrid was calculated as $\delta^{18}O = -8.3‰$ (Chapter 5), from which at mean summer lake water temperatures (18°C) a hypothetical calcite precipitate would have $\delta^{18}O = -9.2‰$ (Chapter 6). As for the Holocene data, $\delta^{18}O_{calcite}$ is always higher than this (by +1.6‰ to +6.9‰) for the 5045-1 record, suggesting that lake water has been subject to a degree of evaporative fractionation throughout the last 640 ka (at least during interglacials/interstadials). Further, based on the interpretation of the calibration dataset, the lowest isotope values should occur when there is more water input (meaning lake water is more reflective of $\delta^{18}O_{precipitation}$) and highest when there is less water input and more evaporation (if only relative to a precipitation decrease, i.e. lower P/E).

A further differentiation should be considered between MIS and full interglacials. Comparing the average values and variability between MIS may misrepresent the magnitude of variation between interglacials (*sensu stricto*). Assuming that temperature variations positively correlate with calcite production, interglacial conditions should coincide with higher TIC. Figure 7.16 shows the difference between averages calculated for interglacials (taken as >6% TIC) and all $\delta^{18}O_{calcite}$ measurements from high TIC zones within a MIS. When discrete interglacials are taken into account, $\delta^{18}O_{calcite}$ is highest during MIS 11 coincident with the highest TIC. In contrast, when whole MIS are averaged, MIS 5 and the Holocene are observed to have particularly high $\delta^{18}O_{calcite}$. The magnitude of variation between interglacials may correspond to the relative strength of summer insolation, where generally higher summer insolation coincides with lower $\delta^{18}O_{calcite}$, as for the early Holocene in Co1262 (it is acknowledged the age model could create artificial synchroneity). Individual MIS and controls on isotope variation are discussed in further detail in Section 7.6.5.

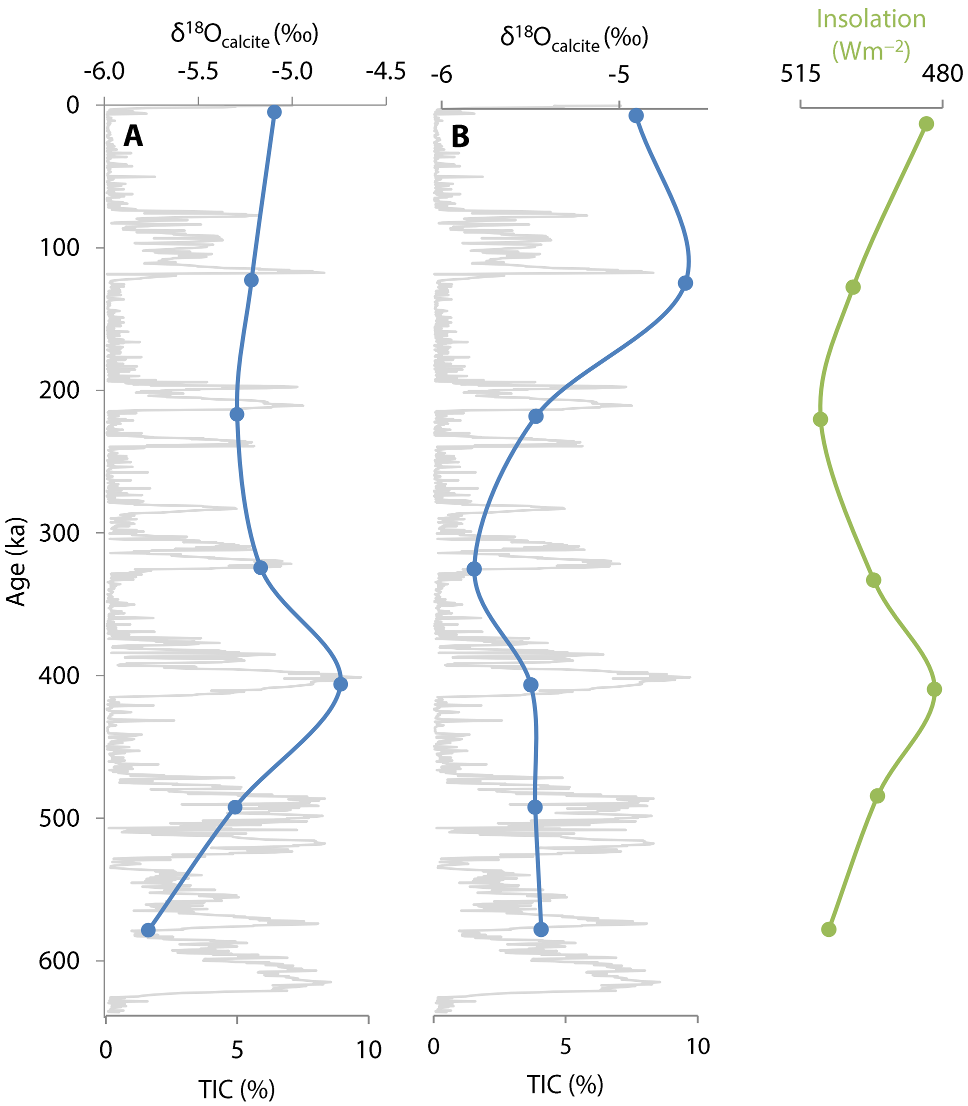

***Figure 7.16** Comparison between average $\delta^{18}O_{calcite}$ (blue dots) for MIS 1-15 defined by a) peak interglacial conditions (taken as >6% TIC), and b) all isotope data measured within a stage, showing TIC (grey line, 15-point running average) and summer (JJA) insolation maxima (40°N, Wm^{-2}) coinciding with each interglacial (Laskar et al., 2004).*

$\delta^{18}O_{calcite}$ data is limited to horizons with higher TIC, which typically correspond to interglacial and interstadial periods that are characterised by concomitant increases in both TIC and TOC (Francke et al., 2015). Calcite precipitation is observed to be related to phases of enhanced moisture availability in Co1262, where a greater quantity of Ca^{2+} and HCO_3^- ions are delivered through karst spring water. In addition, higher summer temperatures during interglacials will drive evaporation favouring the concentration of ions and enhancing calcite precipitation, which will be reinforced by warmer surface waters that lower the calcite saturation threshold (Lézine et al., 2010). Conversely, glacial sediments are typically characterised by low TIC and TOC that anti-correlate with K and titanium (Ti) profiles, indicating low productivity and increased clastic input (Vogel et al., 2010a; Baumgarten et al., 2015). Overall lower temperatures during glacial periods would lead to greater lake water mixing and more frequent deep convective overturn, which in turn would result in a more oxygenated water column. Enhanced mixing promotes the breakdown of water column stratification and the associated oxygenation of the water column increases the rate of aerobic decomposition of organic matter (OM), releasing CO_2 that reduces pH and increases calcite dissolution (Vogel et al., 2010a; Francke et al., 2015). Following extensive OM degradation, the TOC/TN ratio of sediments may be significantly reduced. This has been observed in previous cores from Lake Ohrid where during the Last Glacial TOC/TN were typically very low (4-5) compared to higher values in the Holocene and MIS 5 (Leng et al., 2010a). A decrease in TIC, TOC, and TOC/TN in core Co1262 during cool/dry phases correlated with an increase in Oxygen Index (Chapter 6), which also suggests OM was exposed to more intensive oxidative processes. Catchment permafrost may have also been prevalent in glacial periods, limiting the supply of Ca^{2+} and HCO_3^- ions by reducing the volume of karstic spring inflow (Belmecheri et al., 2009), which is supported by pollen-inferred mean annual temperatures for the Last Glacial down to −3°C (Bordon et al., 2009). Although there is no (or very limited) calcite in glacial periods, previous work has shown spikes in TIC during MIS 3-2 (Wagner et al., 2010), and similar increases in glacial TIC are observed throughout the 5045-1 composite profile (Figure 7.14; Francke et al., 2015). These TIC spikes are shown to comprise siderite, and are therefore analogous to those also found in Lake Prespa glacial sediments during MIS 4-2 (Leng et al., 2013).

7.6.2 Oxygen isotope composition of siderite

Within the 5045-1 record, multiple siderite-bearing horizons have been identified from visual core description, XRF results and FTIR spectroscopy (Francke et al., 2015). The presence of siderite was subsequently confirmed using XRD, and its morphology and geochemistry has been investigated using SEM-EDX (this thesis). SEM of thin sections from discrete higher TIC glacial intervals revealed a variable distribution of siderite, where a higher concentration of siderite crystals is contained within 'burrow-like' structures that impart a mottled texture to the sediment (Figure 7.17a-c). Individual siderite crystals were present as bright white grains of ca. 5 μm diametre

(Figure 7.17c) and siderite crystal clusters were around ca. 50-100 µm (Figure 7.17d), both of which appeared to be nucleating within an uncompacted clay matrix. Occasional (rare) dolomite grains were also observed that were large (>20 µm) and distinct from the fine clay matrix. The dolomite grains were typically found to be fringed by ca. 5 µm grains of siderite. Siderite comprised the principal carbonate component in these horizons, and apart from the infrequent dolomite crystals, no other form of carbonate was observed. The dolomite grains are assumed to be detrital as they are characteristically larger than most sedimentary components and have irregular margins. Given a higher accumulation of clastic-rich material in glacial periods (Baumgarten et al., 2015; Francke et al., 2015), a proportion of allochthonous dolomite derived from catchment rock is expected, however the overall small quantity is not thought to influence isotope measurements.

Individual siderite grains are observed to predominantly form within the open framework of the clay matrix, which suggests they precipitated in situ within the available pore space and are therefore most likely to be early diagenetic. A siderite grain shaped to the inner dimensions of a diatom frustule, fracturing it, provides further evidence for pre-compaction formation (Figure 7.17e). In addition, elongate siderite grains are seen to have grown within the confines of the matrix (Figure 7.17f). Authigenic siderite has been observed to precipitate in porewaters close to the sediment-water interface from dissolved ferrous iron (Fe^{2+}) and carbonate ions (Wersin et al., 1991; Lebeau et al., 2014). Siderite is generally formed under anoxic and reducing conditions, which typically have a high CO_2 partial pressure, elevated Fe and Ca, and a low sulphide concentration (Bahrig, 1988; Brauer and Negendank, 1993). The availability of dissolved Fe^{2+} for siderite formation is probably determined by the oxygen and sulphide content of porewater, as Fe^{2+} is readily oxidised to Fe^{3+} in the presence of molecular oxygen, and will preferentially react with H_2S to produce iron sulphide (Coleman, 1985; Lebeau et al., 2014). Therefore, siderite precipitation is most likely a function of the environmental setting and is dependent on the presence of redox-sensitive elements, which are influenced by changes in water column stratification that may vary seasonally (Balistrieri et al., 1992) as well as on a centennial to millennial scale (Katsuta et al., 2006).

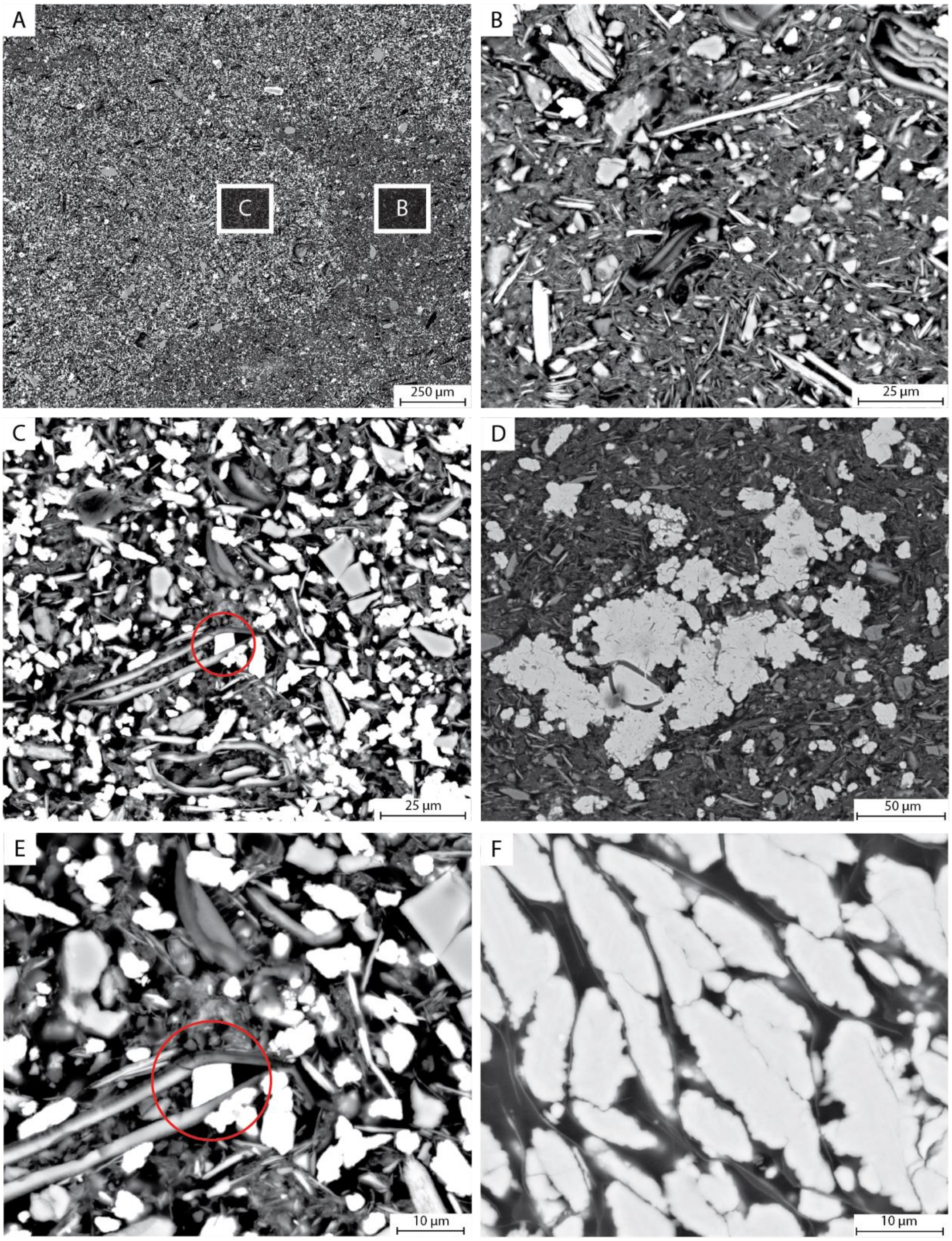

Figure 7.17 *Backscatter SEM images of glacial sediment thin sections, showing a) regions of high (brighter) and low (darker) siderite concentration, the locations of (b) and (c) are indicated, b) area of low siderite concentration, c) area of high siderite concentration (with focal point of (e) indicated), d) individual siderite grains amalgamating to form a larger crystal clyster, e) evidence for early diagenesis from siderite grain growing inside a diatom frustule (fracturing it), and f) siderite grains precipitating within the framework of the matrix. Individual scale bars are given for each SEM image.*

Discrete horizons enriched in Fe have previously been identified in Lake Ohrid (Vogel et al., 2010a), neighbouring Lake Prespa (Wagner et al., 2010; Leng et al., 2013), and in other ancient lakes, such as Lake Baikal (Granina et al., 2004). In Baikal, the formation of Fe-enriched layers up to approximately 25 cm below the sediment-water interface is thought to be related to bottom water redox conditions and significant changes in sedimentation regime. Assuming the siderite is formed in superficial sediments during the initial stages of diagenesis, like calcite, its isotope composition can be used as an indicator of depositional environment (Mozley and Wersin, 1992).

7.6.3 Comparison of $\delta^{18}O_{calcite}$ and $\delta^{18}O_{siderite}$

As with calcite, $\delta^{18}O_{siderite}$ is a function of both $\delta^{18}O_{lakewater}$ and the temperature of lake water at the time of precipitation. However, $\delta^{18}O_{calcite}$ and $\delta^{18}O_{siderite}$ cannot be directly compared as each have specific mineral-water fractionations and form under different temperature regimes (Leng et al., 2013). Although the temperature-dependent oxygen isotope fractionation between calcite and water has been extensively studied (Epstein et al., 1953; Craig, 1965; O'Neil et al., 1969), there are fewer studies into the siderite-water fractionation (Becker and Clayton, 1976; Carothers et al., 1988; Zhang et al., 2001) and published fractionation equations for siderite-water differ significantly at low temperatures (Krylov et al., 2008). In pedogenic siderites, the fractionation equations of Carothers et al. (1988) and Zhang et al. (2001) are observed to diverge below +30°C and it is suggested that the equation of Zhang et al. (2001) is more appropriate for defining equilibrium precipitation at lower temperatures (Ludvigson et al., 2013).

To enable comparison between calcite and siderite isotope measurements, $\delta^{18}O_{calcite}$ and $\delta^{18}O_{siderite}$ are converted to $\delta^{18}O_{lakewater}$ using specific mineral fractionation equations and different estimates for temperature at the time of precipitation (after Leng et al., 2013). For calcite data (interglacial/interstadial intervals), the equation of O'Neil et al. (1969) is used (Equation 7.1) and a precipitation temperature of +18°C is assumed to represent average summer conditions within the photic zone during the period of maximum phytoplankton activity (0-20 m water depth average temperature between June-August; Stankovic, 1960). For siderite data (glacial intervals), the equation of Zhang et al. (2001) is used (Equation 7.2) and a precipitation temperature of +5.8°C is assumed to represent average bottom water temperatures (average temperature measured during 1932-1951 at water depths between 250-285 m; Stankovic, 1960). The calculated $\delta^{18}O_{lakewater}$ for calcite and siderite using their respective fractionation equations and estimated formation temperatures are shown in Figure 7.18.

$$T = 16.9 - 4.38(\delta_c - \delta_w) + 0.1(\delta_c - \delta_w)^2 \qquad (7.1)$$

$$10^3 \ln \alpha_{sid-wt} = 2.56 \times 10^6 \times T^{-2}(K) + 1.69 \qquad (7.2)$$

Calculated $\delta^{18}O_{lakewater}$ from siderite are generally observed to be lower than those calculated for calcite, which suggests that the siderite-bearing horizons were deposited when Lake Ohrid was isotopically fresher in comparison to overall higher $\delta^{18}O_{lakewater}$ during interglacial/interstadial periods. The siderite horizons probably represent distinct abrupt and recurrent events in Lake Ohrid (Vogel et al., 2010a), however overall lower $\delta^{18}O_{lakewater}$ is nevertheless expected through glacial periods due to reduced lake water evaporation in response to decreased temperatures. Evaporation rates calculated for Eski Acıgöl in central Turkey infer glacial evaporation was around three times lower compared with that of the Late Holocene (0.4 m yr-1 vs. 1.1 m yr-1; Jones et al., 2007). A similar calculation performed for Lake Ohrid suggests that glacial evaporation may have been over four times lower than during the present interglacial (0.4 m yr^{-1} vs. 1.8 m yr^{-1}), after Jones et al. (2007) using the equation of Linacre (1992).

Higher evaporation rates are typically associated with closed lake basins and covariance between $\delta^{18}O$ and $\delta^{13}C$ (Talbot, 1990; Li and Ku, 1997), which is observed in the Lake Ohrid data as $\delta^{18}O_{calcite}$ and $\delta^{13}C_{calcite}$ have a moderate to strong covariance through MIS 16 to 5 (Figure 7.19), corroborating that evaporation rates were most likely higher during interglacial and interstadial periods. As rates of evaporation reduce, $\delta^{18}O_{lakewater}$ will be more susceptible to the influences of other controlling factors, such as variations in $\delta^{18}O_{precipitation}$, which may have had a greater importance in determining $\delta^{18}O_{lakewater}$ during glacial periods.

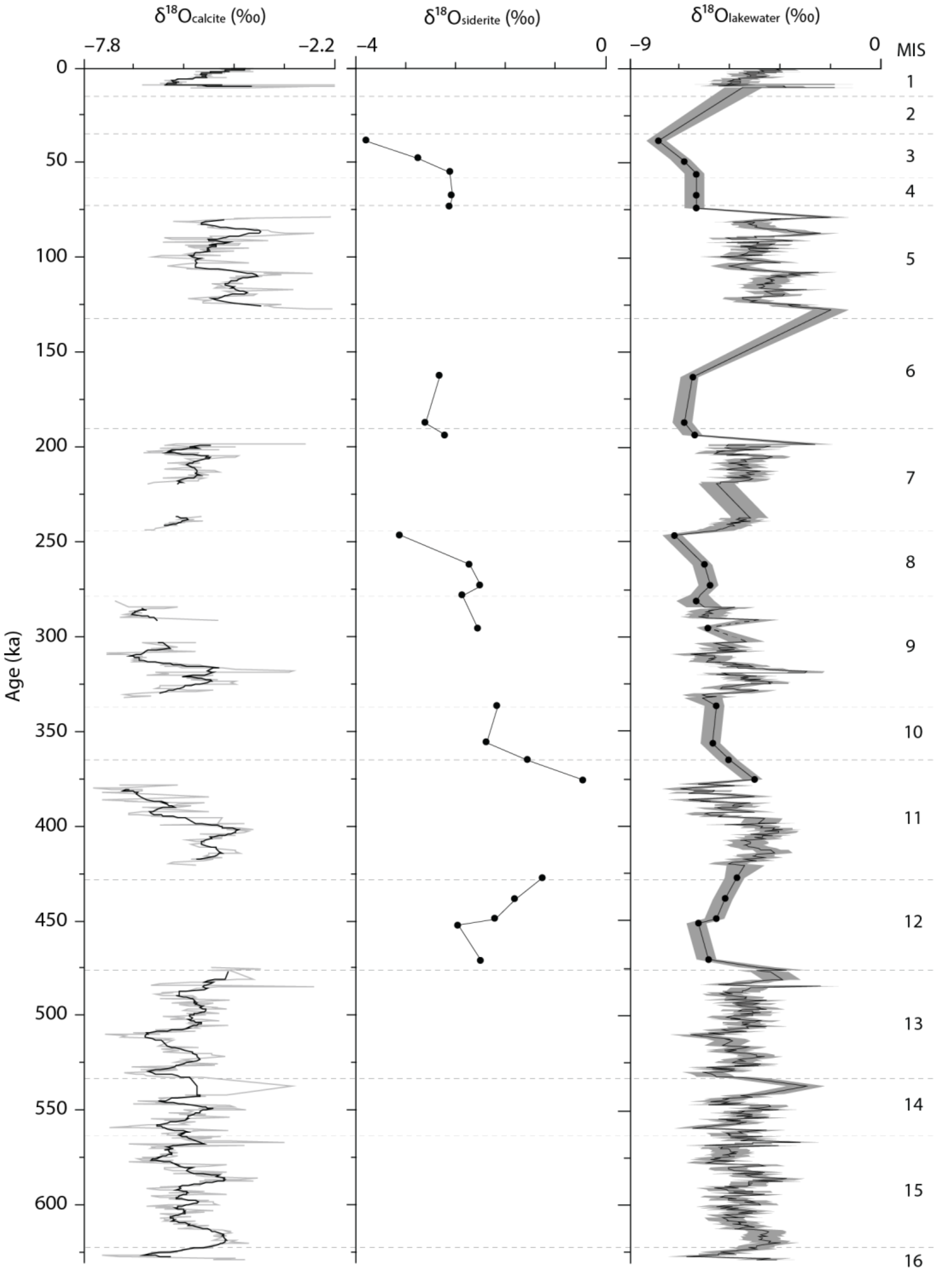

Figure 7.18 *$\delta^{18}O_{lakewater}$ reconstructed from $\delta^{18}O_{calcite}$ and $\delta^{18}O_{siderite}$ using palaeotemperature equations (O'Neil et al., 1969; Zhang et al., 2001) and estimates for temperature at the time of precipitation (calcite = 18°C, siderite = 5.8°C). $\delta^{18}O_{lakewater}$ range (grey) given between 15 to 21°C for calcite and 4 to 7°C for siderite.*

During colder intervals, $\delta^{18}O_{precipitation}$ would have been lower as a direct correlation exists between annual precipitation and temperature, where $\delta^{18}O_{precipitation}$ is reduced by roughly −0.6‰ for every 1°C drop in temperature at mid-high latitudes (Dansgaard, 1964; Leng & Marshall 2004). If a mean annual temperature difference of up to 9°C is assumed between interglacial and glacial periods, based on pollen-inferred temperature data from nearby Lake Maliq (Bordon et al., 2009) and reconstructed sea surface temperature (SST) from the Mediterranean Sea (Paul et al., 2001), $\delta^{18}O_{precipitation}$ would decrease by −5.4‰ in glacial periods. The generalised relationship between annual precipitation and temperature may not be accurate for Ohrid, however it is currently not possible to assess local variation as there is a lack of Global Network of Isotopes in Precipitation (GNIP) monitoring stations in the Balkan region (nearest >200 km from Lake Ohrid).

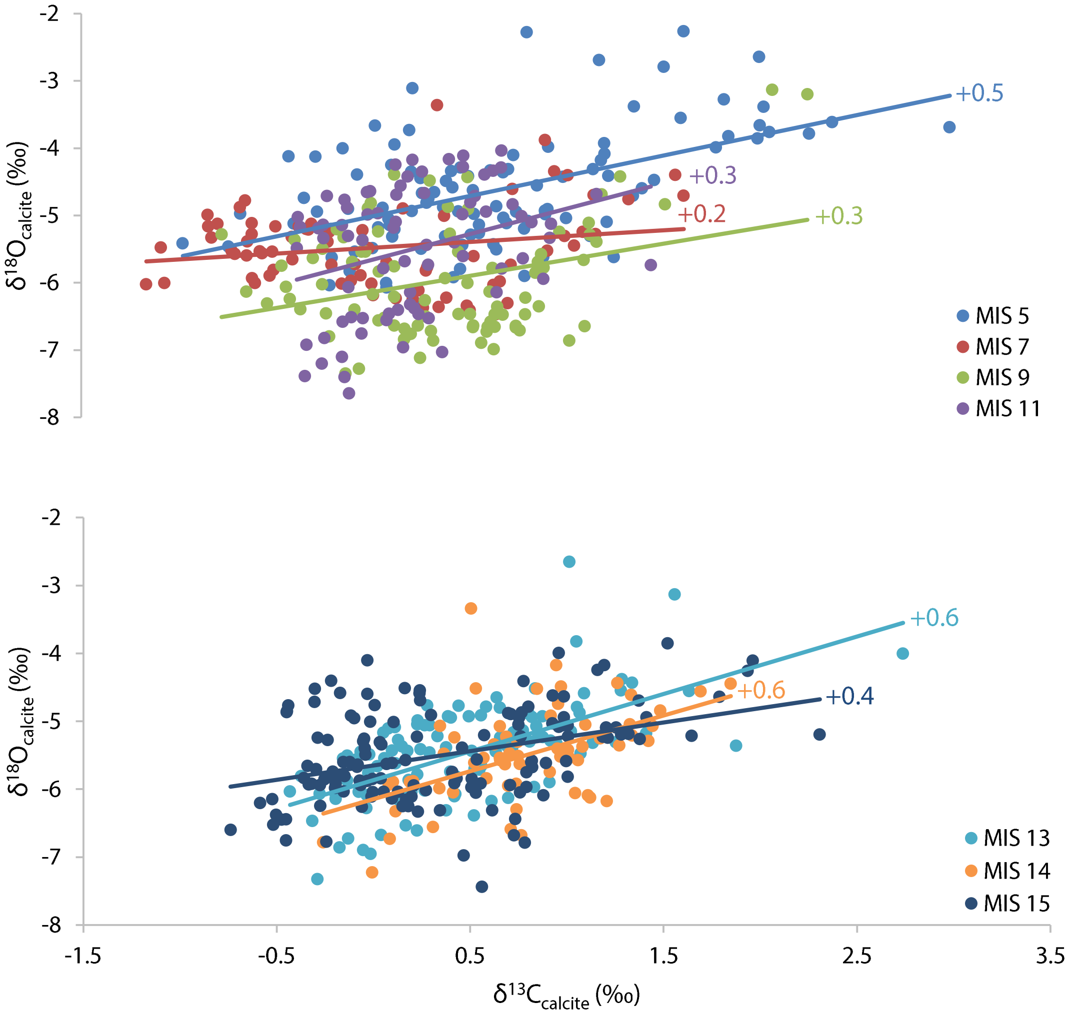

Figure 7.19 *Cross plot of $\delta^{18}O_{calcite}$ and $\delta^{13}C_{calcite}$ for MIS 16-5, showing linear regression and covariance (r) values (p = <0.001).*

When considering interglacial-glacial timescales, changes to $\delta^{18}O_{seawater}$ (the main source of atmospheric moisture) must also be considered, as ^{16}O is preferentially stored in polar ice causing glacial oceans to have higher $\delta^{18}O_{seawater}$. North Atlantic and Adriatic planktonic foraminifera indicate a $\delta^{18}O$ increase of around +3‰ during glacial periods (McManus, 1999; Siani et al., 2010), however the global ice volume component of this is nearer +1‰ (Schrag et al., 2002) and +1.2‰ for the Mediterranean Sea (Paul et al., 2001). The resultant net effect of temperature and source $\delta^{18}O_{sw}$ changes during glacial periods would therefore produce lower $\delta^{18}O_{precipitation}$.

In addition to more regional effects on $\delta^{18}O_{lakewater}$, local influences may also contribute to lower isotope values through glacial periods. Today, a significant proportion of winter precipitation occurs as snowfall at higher altitudes in the Ohrid-Prespa catchment, which is ultimately transferred to the lakes during spring when temperatures remain high enough for the snow to melt (Hollis and Stevenson, 1997; Popovska and Bonacci, 2007). Average winter temperatures at present are around 2°C, however winter temperature would have been considerably reduced during glacial periods and temperature during summer months may also have been lower (Bordon et al., 2009). If lower temperatures persisted throughout much of the year, a higher proportion of annual precipitation may have fallen in winter as snow. Snow is typically characterised as having much lower $\delta^{18}O$ than rainfall, which reflects in-cloud equilibrium conditions and cooler condensation temperatures (Darling et al., 2006), and so would provide a further potential source for low $\delta^{18}O$ during glacial periods. Changing proportions of snowfall (versus rainfall) are also suggested to similarly influence $\delta^{18}O_{lakewater}$ of Nar Gölü (central Turkey; Dean et al., 2013) and Lake Van (eastern Turkey; Kwiecien et al., 2014).

Temperatures may have been sufficiently reduced during glacials to also allow (at least discontinuous) permafrost to form in the Ohrid catchment, thereby decreasing input from karst waters and perhaps restricting the inflow of water from Lake Prespa (Belmecheri et al., 2009). Lake Prespa provides a large proportion of water input to Ohrid through the underground network of karst channels, which has higher $\delta^{18}O_{lakewater}$, when compared to measured precipitation (Chapter 5; Leng et al., 2010a, and references therein). This infers that during periods where glacial conditions were prevalent in the catchment, the inflow of water comprising high $\delta^{18}O$ from Lake Prespa may have reduced, and input would have instead been principally sourced from a combination of direct precipitation and surface run-off, both of which would result in lower $\delta^{18}O_{lakewater}$. A scenario of enhanced surface run-off is further supported by an increase in the amount of fine sand found in sediments during corresponding intervals in the Last Glacial and concomitant increases in Zr/Ti and Cr/Ti ratios, thought to be proxies for catchment erosion rates (Vogel et al., 2010a). Further, this would be facilitated by a decrease in catchment vegetation cover during glacial periods, as indicated by arboreal pollen abundance data (Sadori et al., 2015).

7.6.4 Carbon isotope composition of carbonate

When a carbonate mineral precipitates under equilibrium conditions, as with $\delta^{18}O$, it captures the $\delta^{13}C$ of the total dissolved inorganic carbon (TDIC) of lake water, which for most lakes (at a neutral pH) can be approximated to HCO_3^- (Chapter 3). In Lake Ohrid, $\delta^{13}C_{calcite}$ values average +0.42±0.48‰ through the Holocene, showing little variation between 7 ka and present (±0.27‰, 1σ). This is also observed for the 5045-1 record (Figure 7.9), where $\delta^{13}C_{calcite}$ values are overall high and generally consistent throughout the core (+0.4±0.6‰, 1σ, n=924), suggesting that $\delta^{13}C_{TDIC}$ has likewise remained relatively stable. $\delta^{13}C_{TDIC}$ is a function of carbon source and subsequent modification by in-lake processes (Section 3.6). Given reasonably high and stable $\delta^{13}C_{TDIC}$ values over the last 640 ka, the predominant driver of overall values is most likely to be either 1) the supply of geological carbon from dissolution in the catchment, or 2) equilibration with atmospheric CO_2. These processes are not mutually exclusive, however the resultant $\delta^{13}C_{TDIC}$ is similar between the two, where dissolution of carbonate rocks leads to hard waters entering the lake with $\delta^{13}C_{TDIC}$ values of approximately −1 to +1‰ (Leng et al., 2010a) and TDIC in equilibrium with atmospheric CO_2 has $\delta^{13}C_{TDIC}$ values of around +1‰ (varies with temperature up to +3‰ at 0°C; Mook et al., 1974).

Excursions away from the average value for $\delta^{13}C_{calcite}$ are most likely predominantly in response to variations in the input of isotopically light soil-derived CO_2 (see Sections 3.6 and 6.6). Although the systematics of $\delta^{13}C_{calcite}$ variation for individual stages are discussed in more detail in the following sections of this chapter, MIS 5 data are taken here as an example to highlight these relationships and validate the interpretation (Figure 7.20). There is a clear relationship between $\delta^{13}C_{calcite}$, $\delta^{18}O_{calcite}$ and arboreal pollen (AP) percentages, where lower $\delta^{13}C_{calcite}$ coincides with lower $\delta^{18}O_{calcite}$ and higher AP. Enhanced precipitation and water input is implied by lower $\delta^{18}O_{calcite}$, and facilitates the expansion of woodland in the catchment (higher AP) and promotes soil development. In combination with higher precipitation, a greater quantity of isotopically light soil-derived CO_2 may be available for transfer into the lake resulting in lower $\delta^{13}C_{calcite}$. The opposite is true for intervals of higher $\delta^{18}O_{calcite}$, higher $\delta^{13}C_{calcite}$, and lower AP. Therefore, variations in $\delta^{13}C_{calcite}$ are most likely driven by the relative proportion of isotopically light carbon from soils entering the lake offsetting the addition of lithospheric carbon and atmospheric exchange (also observed for Co1262, Section 6.6.2).

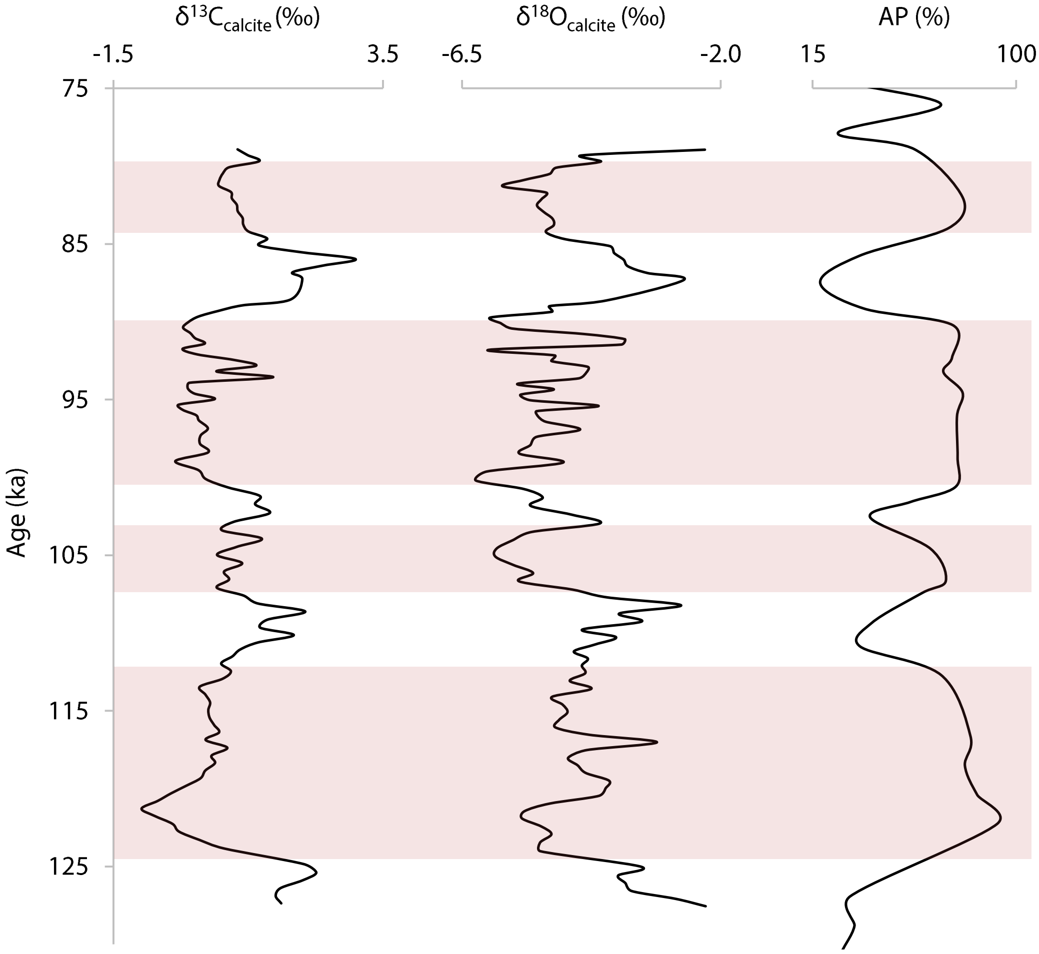

Figure 7.20 *$\delta^{18}O_{calcite}$ and $\delta^{13}C_{calcite}$ from MIS 5 plotted with arboreal pollen percentage (AP; Sadori et al., 2015), highlighting phases of low $\delta^{13}C_{calcite}$ (red bars).*

In contrast to $\delta^{13}C_{calcite}$, $\delta^{13}C_{siderite}$ is observed to be higher by at least +8‰, and has a mean value of +12.3±0.5‰ (1σ, n=22). Higher $\delta^{13}C$ is characteristic of siderite formed in non-marine sediments and is most probably associated to the incorporation of ^{13}C-enriched bicarbonate derived from methanogenesis. As lacustrine environments generally contain low sulphate concentrations, any sulphate that is present will rapidly become reduced at shallower levels in the sediment leaving a greater proportion of organic matter for methanogenic decomposition by bacteria (Mozley and Wersin, 1992). The metabolic pathway utilised by bacteria during the reduction of organic matter strongly fractionates in favour of light carbon (^{12}C), which, for isotopic mass balance, produces isotopically light methane and proportionally enriches the bicarbonate pool in ^{13}C. The methane is subsequently removed by ebullition or by emission through the stems of aquatic macrophytes, and the enriched bicarbonate is incorporated into TDIC (Curry et al., 1997). Methanogenic bicarbonate is therefore the probable cause for the isotopically heavy siderite, in the absence of evidence for other sources of high $\delta^{13}C$, for example intense aquatic productivity, dissolution of biogenic calcite, or volcanic CO_2 (Bahrig, 1988).

7.6.5 Climate and interglacial variability over the last 640 ka

The Late Quaternary is characterised by cyclic alternations between colder and warmer periods, the timing and magnitude of which are principally determined by orbital-induced climate oscillations and variations in atmospheric greenhouse gas content (Imbrie et al., 1984; Shackleton, 2000). This climate signal has been globally observed in deep marine sediments (Lisiecki and Raymo, 2005), ice cores (Jouzel et al., 2007), and continental sequences (Sun and An, 2005), which, when compared, indicate a broad correspondence over orbital timescales (Tzedakis et al., 1997; Lang and Wolff, 2011). However, extended high resolution continental sequences are still rare (Prokopenko et al., 2006; Tzedakis et al., 2006), especially when isotope stratigraphies are considered, and consequently the Lake Ohrid 5045-1 record can provide detailed information on how climate has changed over an extended timeframe. While glacial $\delta^{18}O$ is available from the analysis of authigenic siderite, the data are at low resolution and so comparison between glacial periods is not yet achievable. However, higher resolution $\delta^{18}O_{calcite}$ during warmer periods enables a more robust measure of variability and assessment of changing climate dynamics through the Late Quaternary.

7.6.5.1 MIS 16 to MIS 13

$\delta^{18}O_{calcite}$ and $\delta^{13}C_{calcite}$ are compared with other 5045-1 proxies and global records over MIS 16-13 in Figure 7.21. At the transition between MIS 16 and 15, an excursion to lower $\delta^{18}O_{calcite}$ occurs at ca. 627 ka, which is not observed in $\delta^{13}C_{calcite}$ suggesting that an initial phase of higher precipitation may have been associated with restricted catchment soil development and higher surface runoff. A period of colder conditions and sparse catchment vegetation at this time is inferred from low TOC, TOC/TN, and high K intensity (Francke et al., 2015). Decreasing $\delta^{13}C_{calcite}$ between 630-620 ka is most likely associated with the transition from glacial MIS 16 to interstadial MIS 15e, which is characterised by the low $\delta^{13}C_{calcite}$ until ca. 609 ka and a transition to higher $\delta^{18}O_{calcite}$. This suggests that precipitation had increased to allow for catchment forestation and soil development (i.e. lower $\delta^{13}C_{calcite}$), but perhaps either the increase was counteracted by summer evaporation driving higher $\delta^{18}O_{calcite}$ and/or source and temperature influences in $\delta^{18}O$ were more pervasive. Subsequent peaks to lower $\delta^{13}C_{calcite}$ at ca. 598 ka and 576 ka are probably associated with substages MIS 15c and MIS 15a, which are also associated with lower $\delta^{18}O_{calcite}$ and higher TOC (Francke et al., 2015), suggesting wetter and warmer conditions. A marked excursion to higher $\delta^{13}C_{calcite}$ and $\delta^{18}O_{calcite}$ at ca. 588 ka likely reflects stadial MIS 15b. Variability in $\delta^{13}C_{calcite}$, in conjunction with changes in TIC and K intensity, closely mirror the pattern of association derived from the Holocene calibration (Chapter 6), where warmer and wetter (interglacial/interstadial) periods are characterised by lower $\delta^{13}C_{calcite}$ as a result of catchment vegetation and soil development and the transfer of isotopically light soil-derived CO_2 to the lake. MIS 15e/c/a are defined by high arboreal pollen (AP) percentages at Tenaghi Philippon (Tzedakis et al., 2006; Pross et al., 2015) and at Lake Van (Litt et al., 2014), although Lake Van was probably still in its initial stages of formation during MIS 15 (Cukur et al., 2014). These substages are also associated with a shift to lower $\delta^{18}O$ in the global benthic oxygen isotope stack LR04 ($\delta^{18}O_{LR04}$; Lisiecki and Raymo, 2005) and Mediterranean isotope stack ($\delta^{18}O_{MEDSTACK}$; Wang et al., 2010).

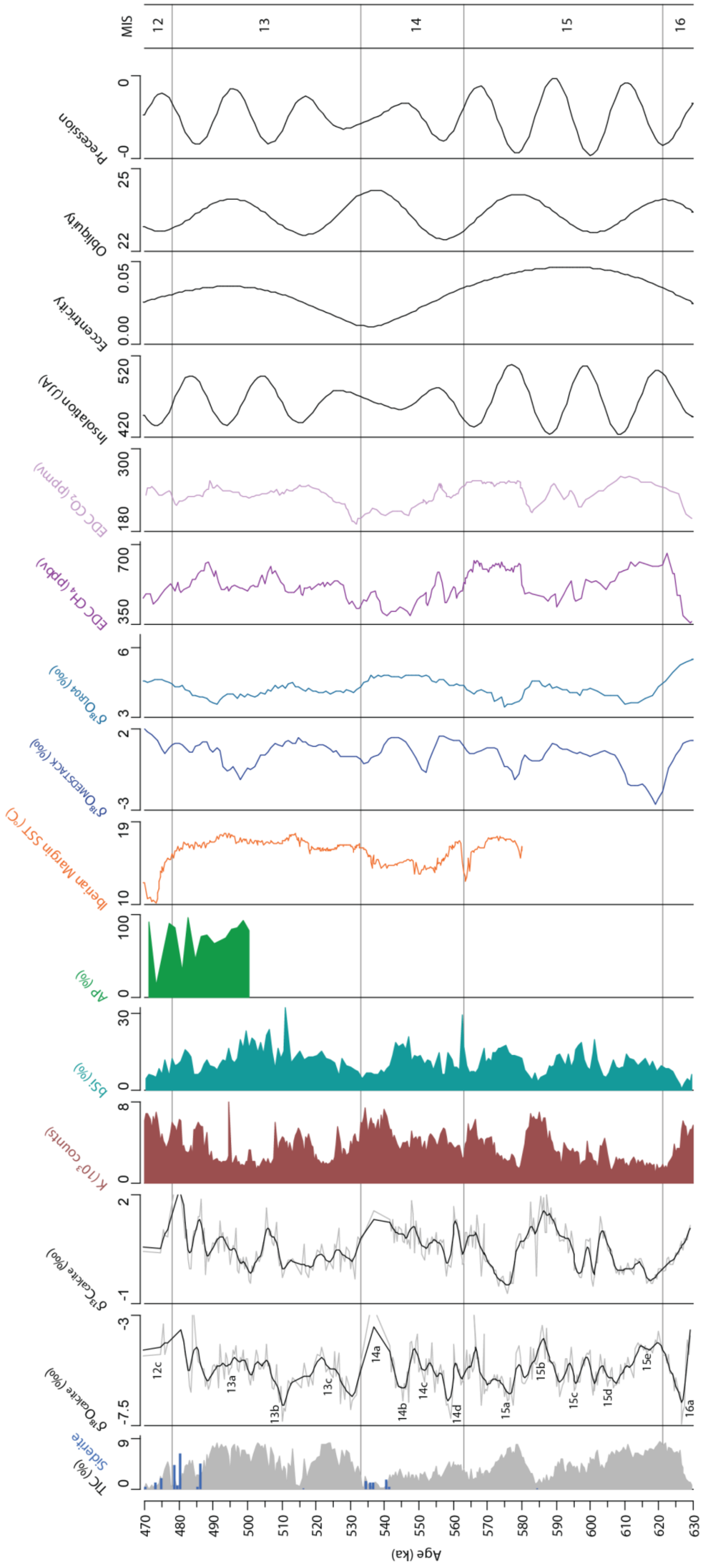

Figure 7.21 *Comparison of* $\delta^{18}O_{calcite}$ *and* $\delta^{13}C_{calcite}$ *data between MIS 16-13 (smooth span = 0.1), showing TIC, siderite occurrence, K intensity, bSi, and AP from core 5045-1 (Francke et al., 2015; Sadori et al., 2015), with regional and global records, including Iberian Margin SST (Rodrigues et al., 2011), planktonic* $\delta^{18}O_{MEDSTACK}$ *(Wang et al., 2010), benthic* $\delta^{18}O_{LR04}$ *stack (Lisiecki and Raymo, 2005), Epica Dome C (EDC)* CH_4 *and* CO_2 *(Loulergue et al., 2008; Lüthi et al., 2008), and summer (JJA) insolation at 41°N, eccentricity, obliquity and precession (Berger and Loutre, 1991; Laskar et al., 2004).*

Higher TIC thought to be related to MIS 15a, is concomitant with an excursion to the lowest $\delta^{18}O_{calcite}$ and $\delta^{13}C_{calcite}$ of the stage, which suggests that this was perhaps the warmest and wettest period of MIS 15. Extreme insolation-induced surface summer temperatures have been identified in climate simulations (Yin and Berger, 2011), and insolation maxima (precession minima) are in phase and reinforced by maximum orbital obliquity, which more commonly defines the early stages of strong interglacial climates and deglaciation (e.g. MIS 5, 9, 11; Jouzel et al., 2007; Hao et al., 2015). Insolation forcing may have therefore resulted in a severe loss of ice cover, above that experienced during other interglacials, preceding the inception of glacial MIS 14, which may have influenced the progression of glaciation as ice build-up is an important boundary condition for the onset of glaciation (Ruddiman, 2003; Hao et al., 2015).

MIS 14 at Lake Ohrid is the only glacial of the record to contain a higher proportion of TIC and TOC throughout most of the stage (Francke et al., 2015), indicating that temperatures did not decrease sufficiently enough to abate productivity and calcite production (isotope data are therefore available for the majority of MIS 14). $\delta^{18}O_{calcite}$ stays remarkably similar to that observed through MIS 15 (average MIS 14 = −5.5±0.8‰, MIS 15 = −5.4±0.6‰), and $\delta^{13}C_{calcite}$ shows a general trend of high and increasing values. Short-term excursions to lower $\delta^{18}O_{calcite}$ at ca. 559 and 546 ka suggest that although climate conditions during MIS 14 would have likely been wet ($\delta^{18}O_{calcite}$ consistent with interglacials), both wetter and drier periods occurred. Increasing $\delta^{13}C_{calcite}$ implies a progressive decline in the amount of soil-derived CO_2 being delivered to the lake and a reduction in catchment vegetation and soil development. A reduction in the amplitude of variations in $\delta^{13}C_{calcite}$ may be due to low orbital eccentricity, reducing the influence precessional variability.

Overall, MIS 14 was a particular weak glacial period (Lang and Wolff, 2011), and relatively low $\delta^{18}O_{LR04}$ suggests global ice volume was reduced in comparison to other glacial periods (Lisiecki and Raymo, 2005). Northern Hemisphere ice sheet growth is inferred to have been restricted during MIS 14 from Chinese loess successions (Hao et al., 2015), and a warm climate is suggested by relatively high (stadial-like) AP percentages at Tenaghi Philippon (Tzedakis et al., 2006), and high bSi and MS at Lake Baikal (Prokopenko et al., 2006). Comparatively high glacial summer and winter SST reconstructed from the Iberian margin (Rodrigues et al., 2011) and North Atlantic (Ruddiman et al., 1989) may have also contributed to a substantial increase in precipitation, promoting interglacial-like hydroclimate during MIS 14, driven by a different circulation pattern and greater influence of subtropical currents (Voelker et al., 2010).

The period between ca. 540-535 ka is characterised as having very low TIC, TOC and bSi in core 5045-1 (Francke et al., 2015), and is the only part of MIS 14 where $^{18}O/^{16}O$ and $^{13}C/^{12}C$ could not be measured (likely associated with MIS 14a). This suggests that full glacial conditions prevailed at Lake Ohrid, which is supported by the presence of siderite, and most likely corresponds to enhanced ice cover inferred from higher $\delta^{18}O_{MED}$ and $\delta^{18}O_{LR04}$ (Lisiecki and Raymo, 2005; Wang et al., 2010), and lower greenhouse gas (GHG) concentrations as measured in the EPICA Dome C ice core (EDC; Loulergue et al., 2008; Lüthi et al., 2008). As discussed for the Holocene calibration (Chapter 6), increasing Northern Hemisphere ice cover would strengthen the latitudinal temperature gradient (LTG), thereby weakening the North Atlantic anticyclone leading to progressively drier conditions over southern Europe and the Mediterranean.

Following MIS 14a, $\delta^{18}O_{calcite}$ and $\delta^{13}C_{calcite}$ are both relatively stable through MIS 13 (−5.5±0.7‰ and +0.5±0.5‰, respectively), and have a similar composition to MIS 15 and 14. Given that only minor oscillations are observed in the isotope data and that there is generally high TIC and low K intensity through the interval (ca. 535-480 ka), MIS 13 is therefore characterised by reasonably consistent climate conditions at Lake Ohrid. $\delta^{18}O_{calcite}$ is low at the inception of MIS 13c and becomes progressively higher between ca. 531-522 ka, with absolute values similar to the those observed from the early-late Holocene (ca. −6 to −4‰). The trend follows an increase in TIC, TOC and bSi, which suggests that temperature is increasing driving higher aquatic productivity (Francke et al., 2015). The subsequent decline in biogeochemical proxies centred around ca. 511 ka is concomitant with a transition to lower $\delta^{18}O_{calcite}$ ($\delta^{13}C_{calcite}$ is stable around +0.2‰ between 531-511 ka), and is most likely associated to the onset of stadial-like conditions during MIS 13b. Reconstructions of SST from marine cores suggest that temperature change was minimal during MIS13b and that only small variations are recorded over the duration of MIS 13 at the Iberian Margin (Rodrigues et al., 2011), which is supported by sustained high palaeoproductivity in the Ionian Sea (Maiorano et al., 2013) and a limited reduction in AP at Tenaghi Philippon (Tzedakis et al., 2006).

A shift to higher $\delta^{18}O_{calcite}$ and $\delta^{13}C_{calcite}$ is observed between 510-505 ka, which most likely represents the onset of MIS 13a, and is mirrored by increasing TIC, TOC and bSi (Francke et al., 2015). Increasing $\delta^{18}O_{calcite}$ and $\delta^{13}C_{calcite}$ suggest the start of MIS 13a was a particularly dry interval, and is perhaps related to a period of hydrological closure or greater evaporation (Talbot, 1990; Li and Ku, 1997). This interval is just beyond the current extent of pollen data from core 5045-1 (Sadori et al., 2015), and a better understanding of the $\delta^{13}C_{calcite}$ minimum may be gained when further information about catchment vegetation is available. Following this excursion, $\delta^{13}C_{calcite}$ decreases to a minimum at ca. 500 ka and $\delta^{18}O_{calcite}$ remains stable between ca. 505-487 ka, likely reflecting full interglacial conditions at Lake Ohrid.

The timing of interglacial conditions is unique within the 5045-1 record, and in a global context as maximum warmth (Jouzel et al., 2007) and minimum ice volume (Lisiecki and Raymo, 2005) occurred in the third substage, rather than in the first, after a glacial termination. This is probably in response to the weak preceding glacial stage (MIS 14) resulting in a low amplitude glacial termination (Voelker et al., 2010). In addition, the main phase of MIS 13a interglacial conditions is coincident with low summer insolation and a precessional maximum (Berger and Loutre, 1991; Laskar et al., 2004), alongside low $\delta^{18}O_{LR04}$ and $\delta^{18}O_{MEDSTACK}$, which suggests a high sea level and low global ice volume (ice volume expected to expand under precession maxima; Lisiecki and Raymo, 2005; Wang et al., 2010). As Rachmayani et al. (2015) show, although the precession index was high, summer temperatures remain high, which they attribute to the simultaneous high obliquity. High obliquity is associated with a greater amount of insolation and heat absorption at high latitudes, which would weaken the latitudinal insolation gradient (LIG) and LTG (Davis and Brewer, 2009), typically leading to a wetter climate in the southern Mediterranean (Chapter 6).

After ca. 490 ka $\delta^{18}O_{calcite}$ and $\delta^{13}C_{calcite}$ show a greater amplitude of variation, concomitant with overall lower TIC (Francke et al., 2015), which suggests a deterioration of climate conditions. Two spikes in TIC centred around ca. 483 and

477 ka show a short-lived transition to lower $\delta^{18}O_{calcite}$ and $\delta^{13}C_{calcite}$, associated with increased AP (Sadori et al., 2015) and K intensity (Francke et al., 2015) in core 5045-1, inferring an ephemeral reversal to warmer and wetter climates. Separating these high TIC, low isotope value intervals are excursions to lower AP and TIC (no calcite isotope data), characterised by the presence of siderite. This advocates that siderite is preferentially precipitated (and/or preserved) in colder/drier periods, where AP and TIC are lower and K intensity is higher.

7.6.5.2 MIS 11

$\delta^{18}O_{calcite}$ and $\delta^{13}C_{calcite}$ are compared with proxies from core 5045-1 and other global climate records through MIS 11 in Figure 7.22. Following a strong and relatively wet glacial MIS 12, AP percentages steadily increase after 424 ka (Sadori et al., 2015) and TIC production begins around ca. 421 ka (Francke et al., 2015). $\delta^{18}O_{calcite}$ is relatively low after the glacial termination (ca. −6‰), and an overall trend to higher $\delta^{18}O_{calcite}$ is observed over the next ca. 20 ka (maximum of −4‰ at ca. 401 ka). Within the first ca. 6 ka of MIS 11, there is a trend to higher $\delta^{18}O_{calcite}$ and lower $\delta^{13}C_{calcite}$, which is also been observed at the inception of other warm MIS (e.g. MIS 15). This trend could be a product of warming temperatures during the initial phases of the MIS, supporting soil development in the catchment but also increasing lake water evaporation, and/or related to a period of dry conditions.

A relatively rapid shift to higher $\delta^{18}O_{calcite}$ and $\delta^{13}C_{calcite}$ at ca. 413 ka may be related to an abrupt increase in evaporation corresponding to a positive covariation between $\delta^{18}O_{calcite}$ and $\delta^{13}C_{calcite}$ (Li and Ku, 1997). Similarly, a short-term reversal to colder SST is reconstructed around this time in core U1313 from the North Atlantic (Stein et al., 2009) and also lower GHG concentrations and temperature are observed in EDC ice cores (Jouzel et al., 2007; Lüthi et al., 2008). $\delta^{18}O_{calcite}$ and $\delta^{13}C_{calcite}$ transition to lower values through to ca. 407 ka after which an increase is observed to 398 ka (boundary with MIS 11b).

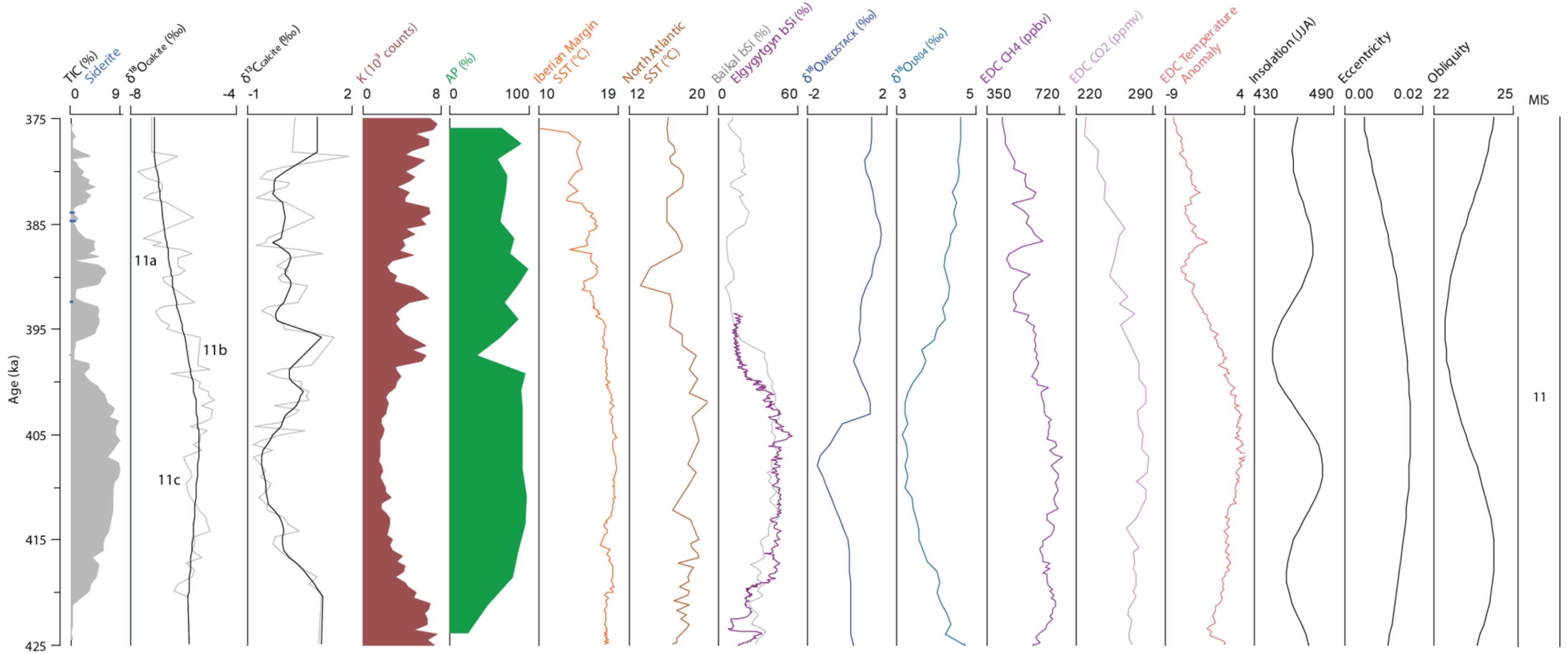

Figure 7.22 *Comparison of $\delta^{18}O_{calcite}$ and $\delta^{13}C_{calcite}$ data from MIS 11 (smooth span = 0.1), showing TIC, siderite occurrence, K intensity, and AP from core 5045-1 (Francke et al., 2015; Sadori et al., 2015), with regional and global records, including Iberian Margin SST (Rodrigues et al., 2011), North Atlantic SST (Stein et al., 2009), lakes Baikal and Elgygytgyn bSi (Prokopenko et al., 2006; Vogel et al., 2013), planktonic $\delta^{18}O_{MEDSTACK}$ (Wang et al., 2010), benthic $\delta^{18}O_{LR04}$ stack (Lisiecki and Raymo, 2005), EPICA Dome C (EDC) CH_4, CO_2 and air temperature anomaly (Jouzel et al., 2007; Loulergue et al., 2008; Lüthi et al., 2008), and summer (JJA) insolation at 41°N, eccentricity and obliquity (Berger and Loutre, 1991; Laskar et al., 2004).*

This period of time most likely corresponds to MIS 11c and generally warmer-wetter conditions at Lake Ohrid, supported by high TIC and pollen concentrations (Francke et al., 2015; Sadori et al., 2015). The transition to minimum $\delta^{18}O_{calcite}$ and $\delta^{13}C_{calcite}$ minima at ca. 407 ka is in phase with peak summer insolation, which also corresponds to high SST at the Iberian Margin (Rodrigues et al., 2011) high bSi at lakes Baikal and Elgygytgyn (Prokopenko et al., 2006; Vogel et al., 2013), and minima in $\delta^{18}O_{MEDSTACK}$ and $\delta^{18}O_{LR04}$ (Lisiecki and Raymo, 2005; Wang et al., 2010), suggesting a phase of peak interglacial conditions associated with a minimum in global ice volume. The overall progression of $\delta^{18}O_{calcite}$ at Lake Ohrid in MIS 11c also compares well with the development of CO_2, CH_4, and air temperature anomaly measured from the EDC Antarctic ice core record (Loulergue et al., 2008; Lüthi et al., 2008).

Overall, the first half of MIS 11 (equivalent to MIS 11c) shows relatively low variability in comparison to the second half of the stage and also to other warm MIS (e.g. MIS 15). A distinct maximum in $\delta^{13}C_{calcite}$ is observed at ca. 398-395 ka, which corresponds to higher $\delta^{18}O_{calcite}$, and is likely associated with colder and drier conditions during stadial MIS 11b. This is supported by higher K intensity, lower TIC and a substantial decrease in AP (Francke et al., 2015; Sadori et al., 2015). Generally higher $\delta^{13}C_{calcite}$ and AP between 395-378 ka suggest a return to wetter and warmer interstadial conditions during MIS 11a. However, the period after MIS 11c is characterised by higher variability and is punctuated by multiple stadial-interstadial events, which contrasts with the smooth climatic deterioration after MIS 11c observed in $\delta^{18}O_{LR04}$ (Lisiecki and Raymo, 2005). Minor variation in LR04 suggests individual records in the isotope stack differ during this interval as anomalous variations would have been smoothed implying an inconsistent pattern of climate change through this time (Candy et al., 2014). At Lake Ohrid, $\delta^{18}O_{calcite}$ and $\delta^{13}C_{calcite}$ imply that there were potentially four interstadial (ca. 394, 389, 386, 381 ka) and stadial (ca. 397, 392, 388, 384 ka) phases following MIS 11c and prior to the onset of glacial MIS 10, where the first stadial phase likely corresponds to MIS 11b (highest $\delta^{13}C_{calcite}$). Given that these events are short-lived, it is unlikely that they relate to orbital forcing and are most probably linked to abrupt climate events (Candy et al., 2014). These events may be linked with peaks in ice-rafted debris (IRD) and variations in SST reconstructed from North Atlantic and Iberian Margin marine cores (McManus, 1999; Desprat et al., 2005;

Stein et al., 2009; Rodrigues et al., 2011), also observed as variations in bSi from Lake Baikal (Prokopenko et al., 2006) and CH_4 measured in Antarctic ice cores (Loulergue et al., 2008).

In contrast to MIS 16-13 (Figure 7.21), during MIS 11 $\delta^{18}O_{calcite}$ shows a general pattern of increasing values between ca. 421-398 ka, and then decreasing values to the ca. 378 ka after which TIC is negligible (see lowess regression, Figure 7.22). This is largely different to the variation observed in $\delta^{13}C_{calcite}$, which shows two main phases of lower values separated by an excursion to higher values. For $\delta^{13}C_{calcite}$, this pattern of variability likely corresponds to the main substages of MIS 11 (11c, 11b, 11a) and is most probably related to peaks in summer insolation. The older peak is stronger than the younger, which is likely a function of higher obliquity modulating precessional summer insolation. However, although some of the variation in $\delta^{18}O_{calcite}$ may be due to changes in insolation, for example the transition to lower values around ca. 407 ka, overall the progression of $\delta^{18}O_{calcite}$ is similar to the general trend of $\delta^{18}O_{LR04}$ (Lisiecki and Raymo, 2005), and CH_4, CO_2 and the reconstructed temperature anomaly from Antarctic EDC ice cores (Jouzel et al., 2007; Loulergue et al., 2008). This suggests that as global temperatures increase and ice volume decreases, $\delta^{18}O_{calcite}$ at Lake Ohrid becomes higher, inferring that lake water became more evaporated (trend to a dry climate). Following the climatic optimum of MIS 11c, global ice volume increased and atmospheric GHG content decreased through MIS 11b and 11a, and $\delta^{18}O_{calcite}$ transitions to the lowest values of the entire 5045-1 core (−7.6‰ at 380 ka). Decreasing $\delta^{18}O_{calcite}$ also tracks progressively lower reconstructed SST in the North Atlantic and on the Iberian Margin (Stein et al., 2009; Rodrigues et al., 2011). However, a ca. −3.3‰ $\delta^{18}O_{calcite}$ change would require an average decrease of around 9°C (+0.36‰C^{-1}, Section 3.3.2), if the change was solely a function of temperature. Alternatives could be either a reduction in evaporation due to lower temperatures and/or a change in seasonality of precipitation. The progression to lower $\delta^{18}O_{calcite}$ within colder periods is expected given the reconstructed $\delta^{18}O_{lakewater}$ from glacial siderite is generally isotopically lower than interglacial $\delta^{18}O_{lakewater}$ calculated from calcite (Figure 7.18).

7.6.5.3 MIS 9

$\delta^{18}O_{calcite}$ and $\delta^{13}C_{calcite}$ are compared with proxies from core 5045-1 and other global climate records through MIS 9 in Figure 7.23. The initial ca. 4 ka of MIS 9 is marked by a transition to higher $\delta^{18}O_{calcite}$ and lower $\delta^{13}C_{calcite}$. After 329 ka $\delta^{18}O_{calcite}$ and $\delta^{13}C_{calcite}$ become coupled and minima are observed around 327 ka, which is assumed to correspond to peak interglacial conditions during MIS 9e. A distinction between the structure of interglacials is highlighted by MIS 11c and MIS 9e (e.g. Tzedakis et al., 2012). A maximum of ca. 6 ka elapses between the onset on calcite precipitation and peak interglacial conditions during MIS 9e, whereas MIS 11c is characterised by a prolonged interval of roughly 14 ka before the $\delta^{13}C_{calcite}$ minimum. This suggests that the onset of full interglacial conditions during MIS 9e was relatively rapid. The minimum in $\delta^{18}O_{calcite}$ and $\delta^{13}C_{calcite}$ at 327 ka is marginally offset (age model discrepancies) from the inferred minimum in global ice volume ($\delta^{18}O_{LR04}$), and peak sapropel deposition (Ziegler et al., 2010) and atmospheric GHG concentration in Antarctic ice cores around 333 ka (Jouzel et al., 2007; Loulergue et al., 2008; Lüthi et al., 2008). Peak warming indicated from Antarctic ice cores (Jouzel et al., 2007) is in phase with peak insolation and reinforced by high obliquity (Laskar et al., 2004). At Lake Ohrid $\delta^{18}O_{calcite}$ and $\delta^{13}C_{calcite}$ minimum are coincident with peaks in TIC, bSi and AP, and are offset from abrupt SST increases at the Iberian margin (Rodrigues et al., 2011) and $\delta^{18}O_{MEDSTACK}$ minimum (Wang et al., 2010). This suggests that the Ohrid age model could perhaps be refined for the initial stages of MIS 9e (inaccuracies may arise due to there being no absolute ages for MIS 9, i.e. no tephra occurrence; Francke et al., 2015). However, the overall pattern of variability is consistent between MIS 11c and MIS 9e, where directly after the period characterised by an opposing $\delta^{18}O_{calcite}$ and $\delta^{13}C_{calcite}$ trend, a minimum in isotope proxies occurs assumed to be related to full interglacial conditions. The transition to lower $\delta^{18}O_{calcite}$ and $\delta^{13}C_{calcite}$ is relatively short-lived (ca. 3.7 ka), after which there is rapid increase in both isotope proxies centred around ca. 325 ka as part of a longer trend to higher values culminating at ca. 319 ka. A transitory warm interval within the initial stages of MIS 9e is also suggested by pollen records from the Portuguese margin, which show a short forested interval of 3.6 ka (337-333 ka; Tzedakis et al., 2004; Roucoux et al., 2007).

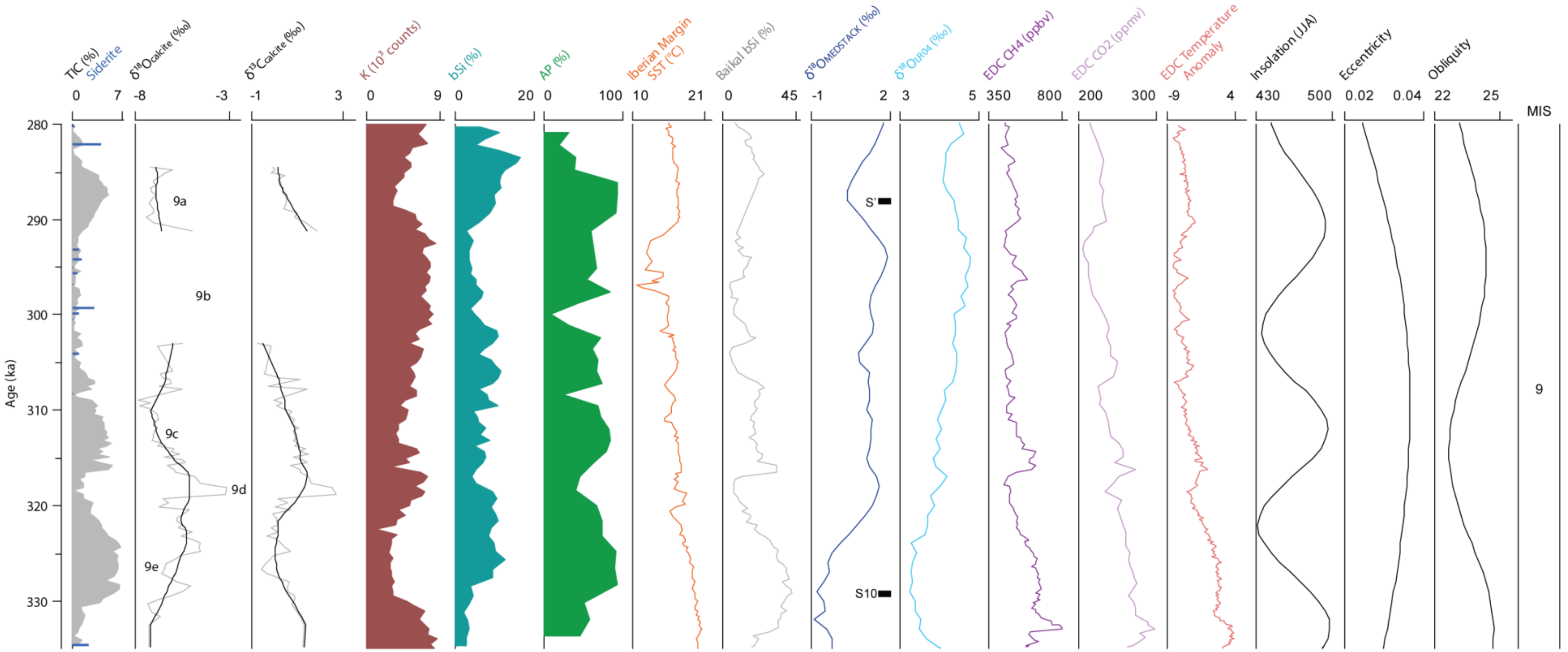

__Figure 7.23__ Comparison of $\delta^{18}O_{calcite}$ and $\delta^{13}C_{calcite}$ data from MIS 9 (smooth span = 0.1), showing TIC, siderite occurrence, K intensity, and AP from core 5045-1 (Francke et al., 2015; Sadori et al., 2015), with regional and global records, including Iberian Margin SST (Rodrigues et al., 2011), North Atlantic SST (Stein et al., 2009), Lake Baikal bSi (Prokopenko et al., 2006), planktonic $\delta^{18}O_{MEDSTACK}$ (Wang et al., 2010), intervals of Mediterranean sapropel deposition (Ziegler et al., 2010), benthic $\delta^{18}O_{LR04}$ stack (Lisiecki and Raymo, 2005), EPICA Dome C (EDC) CH_4, CO_2 and air temperature anomaly (Jouzel et al., 2007; Loulergue et al., 2008; Lüthi et al., 2008), and summer (JJA) insolation at 41°N, eccentricity and obliquity (Berger and Loutre, 1991; Laskar et al., 2004).

An abrupt excursion to the highest $\delta^{18}O_{calcite}$ and $\delta^{13}C_{calcite}$ of the stage observed between ca. 319-316 ka is coincident with lower TIC, bSi and AP, and an increase in K intensity (Francke et al., 2015; Sadori et al., 2015). A substantial reduction in *Pinus* populations at Lake Ohrid supports a severe deterioration to a dry climate (Sadori et al., 2015), which is also documented at Tenaghi Philippon (Tzedakis et al., 2004), and is most probably associated with stadial conditions during MIS 9d. In addition, lower SST at the Iberian margin (Rodrigues et al., 2011) and increasing global ice volume (Lisiecki and Raymo, 2005) at ca. 319 ka are coincident with lower CO_2, CH_4 and temperatures reconstructed from Antarctic ice cores (Jouzel et al., 2007; Loulergue et al., 2008; Lüthi et al., 2008). Peak stadial conditions during MIS 9d are thought to occur ca. 3 ka after a minimum in precessional summer insolation, which may be a function of an offset obliquity minimum centred around 314 ka (Laskar et al., 2004). Such an offset between precessional insolation and obliquity may have delayed the start of stadial conditions, unlike in MIS 11b where insolation and obliquity minimum coincide around 397 ka (Figure 7.22).

Following the stadial phase, MIS 9c is characterised by a general transition to lower $\delta^{18}O_{calcite}$ and $\delta^{13}C_{calcite}$. The initial phase of the transition is relatively rapid, where $\delta^{18}O_{calcite}$ decrease from peak stadial conditions of −3.1‰ at ca. 318 ka to −6.7‰ at ca. 313 ka, and also shows a higher amplitude of variation compared to the latter half of MIS 9c. Towards the final stages of MIS 9c large centennial-scale oscillations are present in both $\delta^{18}O_{calcite}$ and $\delta^{13}C_{calcite}$, which is coincident with a decrease in AP (Sadori et al., 2015) suggesting climate conditions became comparatively unstable prior to the inception of MIS 9b. After 309 ka $\delta^{18}O_{calcite}$ shows higher values suggesting a drier climate prevailed before TIC becomes negligible between ca. 303-291 ka. MIS 9b is suggested to be a prolonged period of very cold and dry conditions at Lake Ohrid, and the presence of siderite indicates that glacial-like climate persisted throughout much of the stadial phase. Low TIC and very low bSi imply that aquatic productivity was strongly reduced (Francke et al., 2015), and overall lower AP (in particular mesophilous trees) with higher non-arboreal pollen (NAP) supports a severe climate deterioration during MIS 9b (Sadori et al., 2015).

A progressive decrease in $\delta^{13}C_{calcite}$ after ca. 291 ka corresponds closely to increasing bSi and AP, and is associated with a rapid change to lower $\delta^{18}O_{calcite}$ during MIS 9a.

$\delta^{13}C_{calcite}$ shows a constant trend toward lower values between ca. 291-285 ka, suggesting that climate was relatively stable during MIS 9a and is not influenced by short-term abrupt events. Peak climate conditions around ca. 285 ka are also suggested by a concomitant maximum in bSi and AP (Francke et al., 2015; Sadori et al., 2015). $\delta^{18}O_{calcite}$ are consistently low between ca. 290-286 ka implying an isotopically fresh lake system. However, pollen data from Lake Ohrid shows that the interval between ca. 290-285 ka is characterised by a distinct rise of semi-deciduous *Quercus cerris* type forests, in opposition to deciduous *Quercus rober* type in MIS 9e and 9c, which suggests cooler and dryer conditions prevailed during MIS 9a (Sadori et al., 2015). Low $\delta^{18}O_{calcite}$ at this time might therefore be a function of a strong precipitation seasonality, where peak summer insolation drives extensive summer dryness and winter precipitation is enhanced, similar to suggested conditions during the early Holocene (Tzedakis, 2007).This is also supported by the deposition of sapropel S' around ca. 288 ka, which may be analogous with conditions surrounding the deposition of sapropel 1 between ca. 10-6.5 ka (Chapter 6; Ziegler et al., 2010). $\delta^{18}O_{calcite}$ shows an abrupt change to higher values at ca. 285 ka, after which a trend to lower values and higher $\delta^{13}C_{calcite}$ occurs. A sharp drop in AP and rise in NAP is also observed at this time (Sadori et al., 2015), coincident with a rapid decrease in bSi (Francke et al., 2015), suggesting the inception of glacial MIS 8. The trend to lower $\delta^{18}O_{calcite}$ is in agreement with lower $\delta^{18}O_{lakewater}$ reconstructed from siderite (Figure 7.18), suggesting the siderite-derived estimates of $\delta^{18}O_{lakewater}$ are reasonably robust.

7.6.5.4 MIS 7

$\delta^{18}O_{calcite}$ and $\delta^{13}C_{calcite}$ are compared with proxies from core 5045-1 and other global climate records through MIS 7 in Figure 7.24. MIS 7 is characterised by three separate phases of calcite preservation (Francke et al., 2015), which most likely correspond to MIS substages 7e, 7c, and 7a (Railsback et al., 2015), and therefore comprises a similar structure to other warm MIS (Tzedakis et al., 2003b). However, in contrast to other MIS, high amplitude changes in precessional summer insolation (Laskar et al., 2004), and subdued oscillations in atmospheric GHG concentrations (Petit et al., 1999; Loulergue et al., 2008) and global ice volume (Lisiecki and Raymo, 2005) are observed during MIS 7. The first peak in TIC between ca. 244 and 237 ka is associated with initially low but increasing $\delta^{18}O_{calcite}$ and high but decreasing $\delta^{13}C_{calcite}$ that both show a higher amplitude of variability after ca. 241 ka. Increasing $\delta^{18}O_{calcite}$ from ca. −6.5‰ to −5.0‰ suggests an initially wet climate with progressive trend to drier conditions through until ca. 237 ka (comparable to climatic development in the early-mid Holocene), however overall warm conditions and high moisture availability is likely given low $\delta^{13}C_{calcite}$ coincident with high TIC, bSi and AP (Francke et al., 2015; Sadori et al., 2015). This interval most probably corresponds to MIS 7e, and is coeval with warming indicated by arboreal expansion at Ioannina (Roucoux et al., 2008) and Tenaghi Philippon (Tzedakis et al., 2003b) in Greece, and Lake Van in Turkey (Litt et al., 2014), although the intensity of the climate optimum is comparably low (Desprat et al., 2006). Overall warming is supported by higher SST reconstructed for the Adriatic Sea (Piva et al., 2008), Alboran Sea (Martrat et al., 2004), and Iberian Margin (Martrat et al., 2007; Voelker and de Abreu, 2011). Temperature reconstructions from Antarctica suggest that MIS 7e was warmer than present and also the warmest phase of MIS 7 (Jouzel et al., 2007), which is in agreement with a global ice volume minimum associated with MIS 7e (Lisiecki and Raymo, 2005). This period of relative warmth is likely related to a peak in precessional summer insolation at ca. 241 ka (Laskar et al., 2004). However, in comparison to later substages, low eccentricity and obliquity result in a weakened insolation peak coincident with MIS 7e. In a global context, minimum ice volume and higher temperatures are therefore probably due to higher atmospheric CO_2 and CH_4 content in combination with an insolation peak during MIS 7e (Tzedakis et al., 2003b).

After the climate optimum during MIS 7e, an extended interval of colder climate (MIS 7d) is inferred to occur between ca. 237-220 ka by low TIC, bSi and AP, and high K intensity (Francke et al., 2015; Sadori et al., 2015). Due to low TIC isotope data is unavailable for this interval. Extreme cooling during MIS 7d is probably a function of very low insolation, obliquity and atmospheric GHG concentrations (Petit et al., 1999; Laskar et al., 2004; Jouzel et al., 2007), allowing the global ice volume to increase and reflect almost glacial levels (Lisiecki and Raymo, 2005).

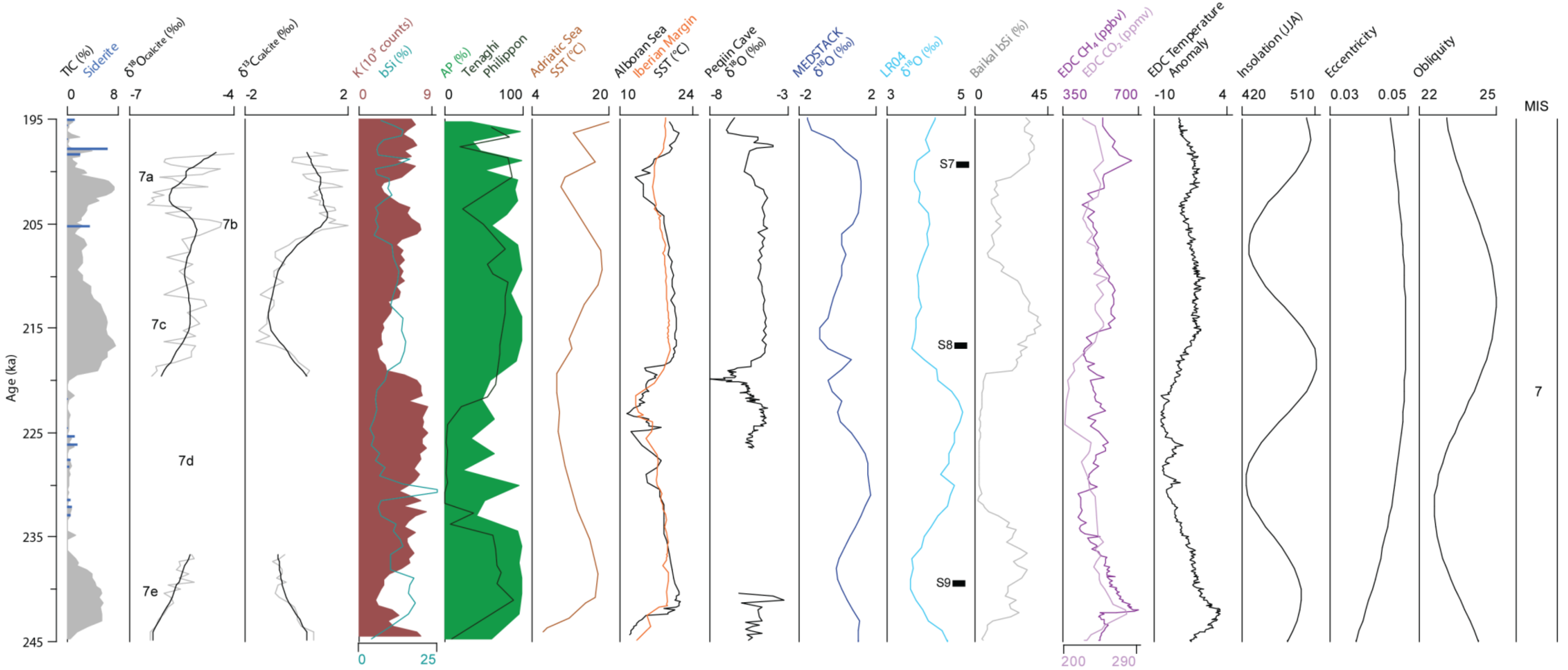

Figure 7.24 *Comparison of $\delta^{18}O_{calcite}$ and $\delta^{13}C_{calcite}$ data from MIS 7 (smooth span = 0.1), showing TIC, siderite occurrence, K intensity, bSi and AP from core 5045-1 (Francke et al., 2015; Sadori et al., 2015), with regional and global records, including Tenaghi Philippon AP (Tzedakis et al., 2003b), Adriatic Sea SST (Piva et al., 2008), Alboran Sea SST (Martrat et al., 2004), Iberian Margin SST (Martrat et al., 2007), Peqiin Cave $\delta^{18}O_{speleothem}$ (Bar-Matthews et al., 2003), planktonic $\delta^{18}O_{MEDSTACK}$ (Wang et al., 2010), intervals of Mediterranean sapropel deposition (Ziegler et al., 2010), benthic $\delta^{18}O_{LR04}$ stack (Lisiecki and Raymo, 2005), Lake Baikal bSi (Prokopenko et al., 2006), EPICA Dome C (EDC) CH_4, CO_2 and air temperature anomaly (Petit et al., 1999; Jouzel et al., 2007; Loulergue et al., 2008), and summer (JJA) insolation at 41°N, eccentricity and obliquity (Berger and Loutre, 1991; Laskar et al., 2004).*

Very cold conditions during this stadial phase are also inferred by the presence of siderite between ca. 233-225 ka, coinciding with AP minima. A relatively abrupt decrease in $\delta^{13}C_{calcite}$ after ca. 220 ka marks the onset of warmer conditions at Lake Ohrid, and the transition to interstadial MIS 7c. Similar to previous glacial terminations, $\delta^{18}O_{calcite}$ and $\delta^{13}C_{calcite}$ are inversely correlated between ca. 220-217 ka and increasing $\delta^{18}O_{calcite}$ suggests either glacial lake water was isotopically fresher (see Section 7.6.3), or the inception of MIS 7c was characterised by a particularly wet climate. Given that $\delta^{13}C_{calcite}$ decreases through this interval, it is perhaps more likely that lower $\delta^{18}O_{calcite}$ at the start of MIS 7c is related to a transition from glacial-like conditions. MIS 7c is a relatively long interstadial period (ca. 13 ka), comprising several oscillations from lower to higher $\delta^{18}O_{calcite}$, and although variations in $\delta^{13}C_{calcite}$ are coupled to changes in $\delta^{18}O_{calcite}$ after ca. 217 ka, the amplitude of fluctuations are more subdued. Excursions to higher $\delta^{18}O_{calcite}$ occur at ca. 216, 215, 213, 211, 209 and 208 ka, and are separated by phases of higher $\delta^{18}O_{calcite}$ suggesting rapid climate alternations with an average spacing $\approx$ 1.6 ka. The periodicity of these climate oscillations is similar to that observed for Holocene ice-rafting events in the North Atlantic region (Bond et al., 2001). Although less variable than $\delta^{18}O_{calcite}$, $\delta^{13}C_{calcite}$ reaches lower values in MIS 7c than during MIS 7e, which suggests climate was perhaps more favourable than during the full interglacial. This is supported by a higher TIC plateau and marginally higher AP during MIS 7c (Francke et al., 2015; Sadori et al., 2015).

Full interglacial conditions comparable to, or exceeding that experienced during MIS 7e are also indicated from other records, for example at Tenaghi Philippon a greater diversity of AP is observed along with a greater abundance of thermophilous taxa (Tzedakis et al., 2003b) and higher bSi in MIS 7c at Lake Baikal (Prokopenko et al., 2006). Particularly low $\delta^{13}C_{calcite}$ and high AP suggests that although atmospheric GHG concentrations were reduced compared to MIS 7e, higher summer insolation (maximum of last ca. 550 ka) during MIS 7c must be a crucial factor in determining environmental conditions both at Lake Ohrid, and across the Mediterranean region (Tzedakis et al., 2003b; Roucoux et al., 2008).

During MIS 7b, a change to stadial conditions is marked by an excursion to higher $\delta^{18}O_{calcite}$ and $\delta^{13}C_{calcite}$ between ca. 207-204 ka, where peak values coincide with the occurrence of siderite. Although siderite is present, TIC (calcite) is generally higher through this interval (> 2%) when compared to MIS 7d suggesting climate deterioration did not occur to the same extent. A short-term interval of cooling is advocated by an abrupt decrease in AP around ca. 205 ka (Sadori et al., 2015), which is likewise observed at Tenaghi Philippon (Tzedakis et al., 2003b) and Lake Van (Litt et al., 2014), and lower SST reconstructed for the Adriatic Sea (Piva et al., 2008), Alboran Sea (Martrat et al., 2004) and Iberian Margin (Martrat et al., 2007). In comparison to the previous stadial (MIS 7d), more temperate conditions are also implied by Antarctic ice core records (Jouzel et al., 2007) and a minimal change in global ice volume between MIS 7c and MIS 7b (Lisiecki and Raymo, 2005) suggests this was a relatively warm stadial phase, potentially due to a weak reduction in atmospheric CO_2 concentrations (Petit et al., 1999).

A distinct $\delta^{18}O_{calcite}$ decrease occurs at the end of MIS 7b, and defines the transition to the final interstadial phase of MIS 7. MIS 7a in Lake Ohrid is a relatively short interval (ca. 204-198 ka) that shows a decreasing $\delta^{13}C_{calcite}$ trend and increasing $\delta^{18}O_{calcite}$ similar to MIS 7e, however it is characterised by large amplitude coupled oscillations in both $\delta^{18}O_{calcite}$ and $\delta^{13}C_{calcite}$ to higher values at ca. 204, 201, 200 and 198 ka. Although at a lower sampling resolution, these fluctuations are also indicated by AP percentages (Sadori et al., 2015). A change in hydroclimate stability in late MIS 7 is also observed at Tenaghi Philippon (Tzedakis et al., 2003b) and in $\delta^{18}O_{speleothem}$ from Peqiin Cave (Israel; Bar-Matthews et al., 2003). Overall higher $\delta^{13}C_{calcite}$ in contrast to MIS 7e and 7c suggests a weaker climate amelioration than in the two previous interstadial periods. After ca. 198 ka siderite becomes abundant through MIS 6.

7.6.5.5 MIS 5

MIS 5 has been characterised as one of the strongest warm stages of the last 800 ka (Lang and Wolff, 2011), and is among the most studied intervals of the Quaternary from the European and Mediterranean regions (Frogley, 1999; Bar-Matthews et al., 2003; Tzedakis et al., 2003a; Drysdale et al., 2005; Brauer et al., 2007; Müller and Sánchez Goñi, 2007; Allen and Huntley, 2009; Pickarski et al., 2015; Wilson et al., 2015). At Lake Ohrid, the highest average $\delta^{18}O_{calcite}$ and $\delta^{13}C_{calcite}$ of the 5045-1 record are observed during MIS 5, suggesting that lake water was most evaporated during this stage, which could be related to severe lake level changes (up to 60 m below present) inferred during MIS 6 and MIS 5 (Lindhorst et al., 2010). The age model developed by Francke et al. (2015) is utilised in this section, however an alternative model incorporating tie points to independently-dated regional records has been proposed by Zanchetta et al. (2015), which is referred to where major discrepancies occur between the two chronological methods. $\delta^{18}O_{calcite}$ and $\delta^{13}C_{calcite}$ are compared with proxies from core 5045-1 and other global climate records through MIS 5 in Figure 7.25, and these relationships are highlighted during MIS 5e in Figure 7.26.

Initially high $\delta^{18}O_{calcite}$ and $\delta^{13}C_{calcite}$ around ca. 128 ka, coupled with low TIC and AP (Francke et al., 2015; Sadori et al., 2015), indicate cold-dry climate conditions and perhaps also reflect a lower lake level (Lindhorst et al., 2010), similar to reconstructed conditions at Lake Ioannina between ca. 140-131 ka (Wilson et al., 2015). A dry and cool climate may be associated with a North Atlantic cold episode, Heinrich Event 11, between ca. 135-130 ka initiated by a major meltwater pulse related to strong insolation and CO_2 forcing (Marino et al., 2015). Marino et al. (2015) suggest that this deglacial meltwater influx may account for ca. 70% of glacial-interglacial sea level change, and is coincident with low SST in the Alboran Sea (ca. 133 ka; Martrat et al., 2014). Based on correlation with marine cores (Marino et al., 2015) and speleothem (Drysdale et al., 2009; Regattieri et al., 2014) records, the chronology of the MIS 6-5 transition may be underestimated by ca. 4-5 ka (Zanchetta et al., 2015). Therefore, high $\delta^{18}O_{calcite}$ and $\delta^{13}C_{calcite}$ at ca. 128 ka may correspond to cool-dry conditions associated with North Atlantic HE 11 around ca. 133 ka.

A rapid transition to lower $\delta^{18}O_{calcite}$ and $\delta^{13}C_{calcite}$ at ca. 124 ka (ca. 130 ka; Zanchetta et al., 2015) is likely associated with the onset of full interglacial conditions during MIS 5e. An earlier onset of interglacial conditions is observed in other lacustrine (Frogley, 1999; Pickarski et al., 2015), speleothem (Bar-Matthews et al., 2003; Drysdale et al., 2005) and marine records (Grant et al., 2012; Martrat et al., 2014). This suggests that Ohrid isotope data (known to reflect regional hydroclimate; Chapter 6) can be correlated to other continental and marine proxy records to provide additional chronological control for the 5045-1 sequence (see Zanchetta et al., 2015).

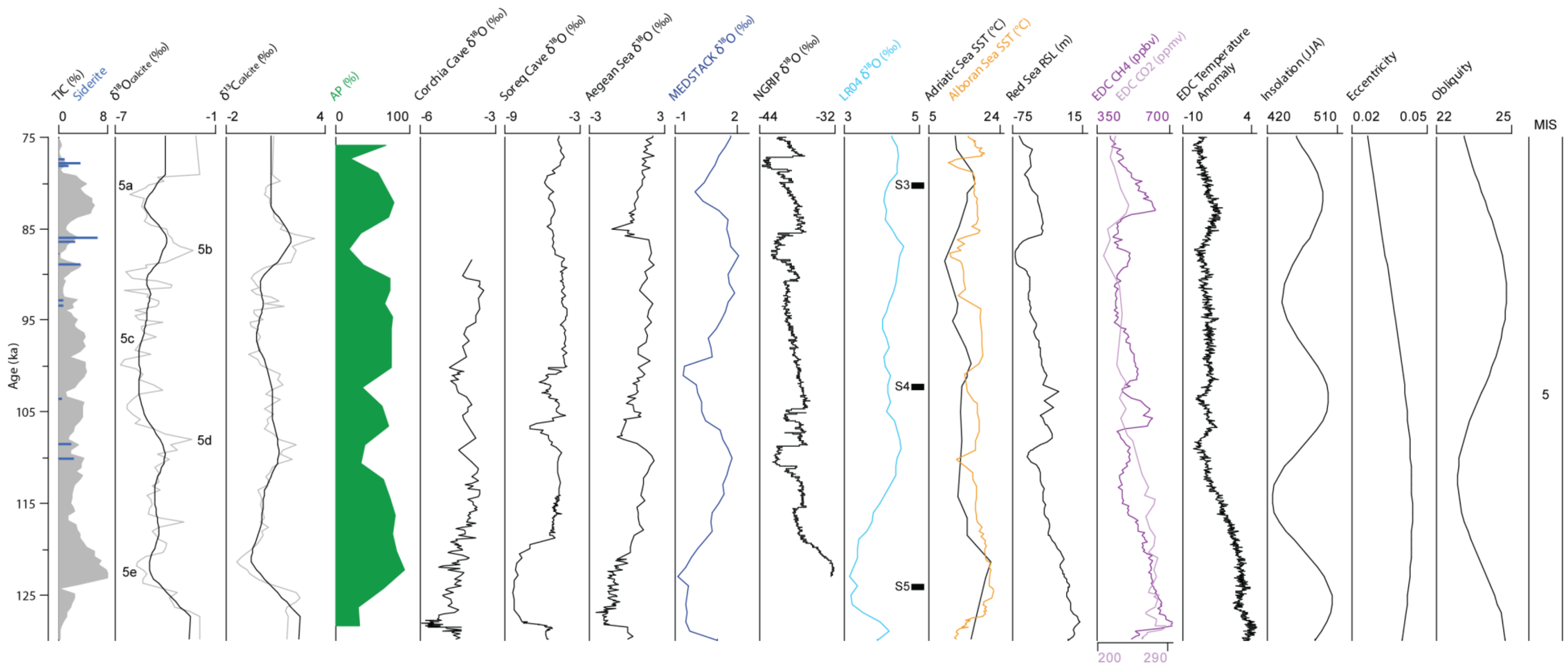

Figure 7.25 *Comparison of $\delta^{18}O_{calcite}$ and $\delta^{13}C_{calcite}$ data from MIS 5 (smooth span = 0.1), showing TIC, siderite occurrence, and AP from core 5045-1 (Francke et al., 2015; Sadori et al., 2015), with regional and global records, including Corchia Cave $\delta^{18}O_{speleothem}$ (Drysdale et al., 2005), Soreq Cave $\delta^{18}O_{speleothem}$ (Bar-Matthews et al., 2003), Aegean Sea $\delta^{18}O$ (Grant et al., 2012), planktonic $\delta^{18}O_{MEDSTACK}$ (Wang et al., 2010), NGRIP ice core $\delta^{18}O$ (NGRIP Members, 2004), intervals of Mediterranean sapropel deposition (Ziegler et al., 2010), benthic $\delta^{18}O_{LR04}$ stack (Lisiecki and Raymo, 2005), Adriatic Sea SST (Piva et al., 2008), Alboran Sea SST (Martrat et al., 2004), Red Sea (RSL) relative sea-level (Grant et al., 2012), EPICA Dome C (EDC) CH_4, CO_2 and air temperature anomaly (Petit et al., 1999; Jouzel et al., 2007; Loulergue et al., 2008), and summer (JJA) insolation at 41°N, eccentricity and obliquity (Berger and Loutre, 1991; Laskar et al., 2004).*

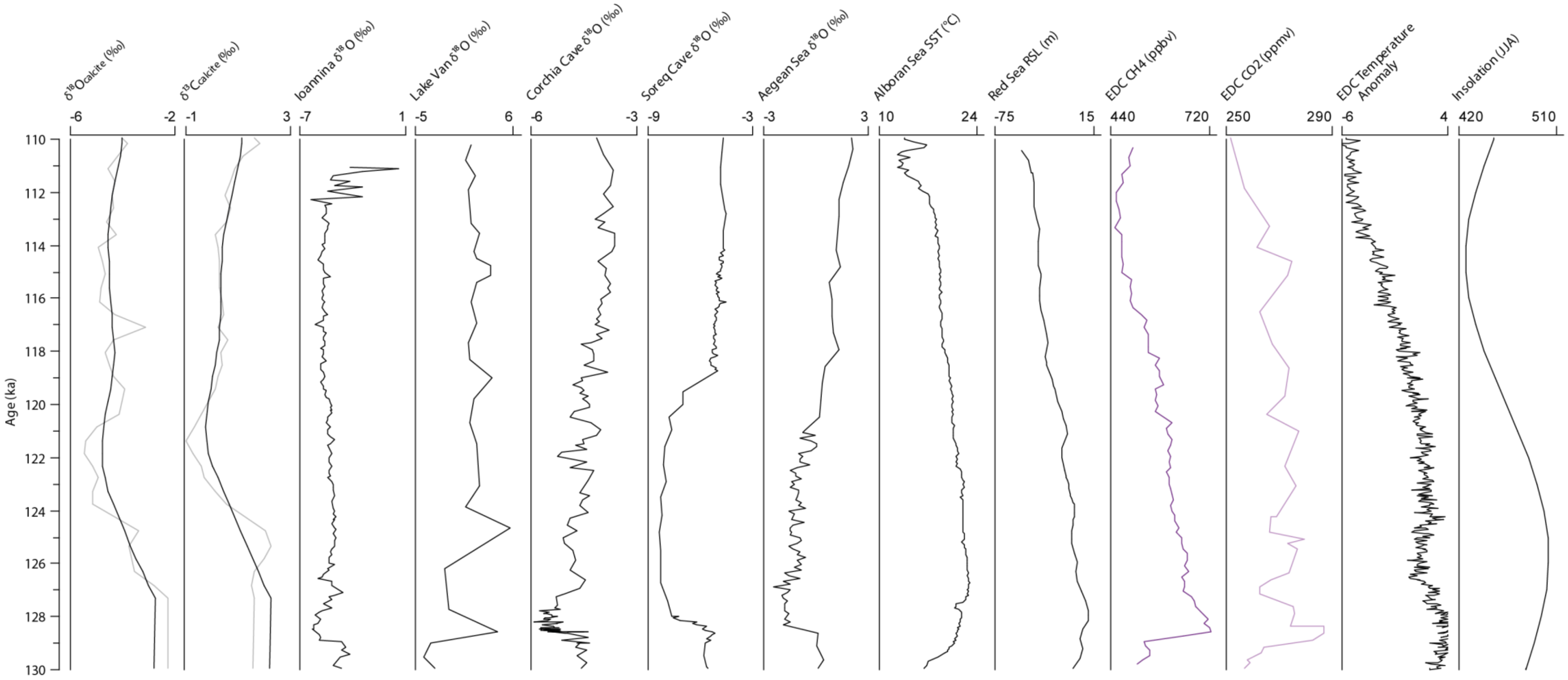

***Figure 7.26** Comparison of $\delta^{18}O_{calcite}$ and $\delta^{13}C_{calcite}$ data from MIS 5e (smooth span = 0.1), with regional and global records, including Lake Ioannina $\delta^{18}O$ (Frogley, 1999), Lake Van $\delta^{18}O$ (Pickarski et al., 2015), Corchia Cave $\delta^{18}O_{speleothem}$ (Drysdale et al., 2005), Soreq Cave $\delta^{18}O_{speleothem}$ (Bar-Matthews et al., 2003), Alboran Sea SST (Martrat et al., 2014), Red Sea (RSL) relative sea-level (Grant et al., 2012), EPICA Dome C (EDC) CH_4, CO_2 and air temperature anomaly (Petit et al., 1999; Jouzel et al., 2007; Loulergue et al., 2008), and summer (JJA) insolation at 41°N, (Laskar et al., 2004).*

Peak warming during MIS 5e is most probably coincident with the point of lowest $\delta^{18}O_{calcite}$ and $\delta^{13}C_{calcite}$ at around 3-4 ka following the sharp decline in isotope values (at ca. 122-121 ka using the age model of Francke et al. (2015)). However, although the overall trend of $\delta^{18}O_{calcite}$ and $\delta^{13}C_{calcite}$ is similar through MIS 5e (i.e. change from high to low values), lower $\delta^{18}O_{calcite}$ are observed at ca. 2 ka before $\delta^{13}C_{calcite}$. $\delta^{13}C_{calcite}$ closely follows the progression of vegetation development, showing the lowest values concomitant with peak AP at ca. 122 ka (Sadori et al., 2015), supporting the association of low $\delta^{13}C_{calcite}$ with catchment soil development. An initial interval of lower $\delta^{18}O_{calcite}$ centred on ca. 124 ka may instead be related to local effects of ice cap and snowfield meltwater entering the lake, decoupling terrestrial and lacustrine proxies (also obersved at Lake Ioannina; Wilson et al., 2015). Local ice caps on the mountains surrounding Lake Ohrid are indicated for the Last Glacial by catchment moraine deposits (Ribolini et al., 2011) and are likely to have been present during earlier glacial intervals, particularly in severe glacials such as MIS 6 (Francke et al., 2015). Overall, a change to lower $\delta^{18}O_{calcite}$ and $\delta^{13}C_{calcite}$ is most likely coincident with higher Mediterranean SST (Martrat et al., 2004; Piva et al., 2008; Martrat et al., 2014), greater regional precipitation (Frogley, 1999; Bar-Matthews et al., 2003; Drysdale et al., 2005), the deposition of sapropel S5 (Ziegler et al., 2010), and lower ice volume (Lisiecki and Raymo, 2005; Grant et al., 2012). An excursion to higher $\delta^{18}O_{calcite}$ and $\delta^{13}C_{calcite}$ around ca. 114 ka marks the end of the Last Interglacial, and infers interglacial conditions persisted for ca. 14-19 ka at Lake Ohrid (depending on age model), which is in broad agreement with reported durations from other regional sequences (Tzedakis, 2003; Brauer et al., 2007; Pickarski et al., 2015).

Higher $\delta^{18}O_{calcite}$ and $\delta^{13}C_{calcite}$ between ca. 114 and 107 ka suggest much drier climate conditions characterised MIS 5d, which is supported by the presence of siderite and a reduction in AP (Sadori et al., 2015). $\delta^{18}O_{calcite}$ shows a more gradual transition to higher values between ca. 114-110 ka, followed by an abrupt peak at ca. 108 ka. This trend is also observed at Lake Ioannina (Frogley, 1999), in SST reconstructions from the Alboran Sea (Martrat et al., 2004; Martrat et al., 2014), and also in the NGRIP ice core (NGRIP Members, 2004). The age model for 5045-1 is relatively well constrained during MIS 5d due to the presence of a tephra layer at ca. 109 and 110 ka (Francke et al., 2015; Leicher et al., 2015; Zanchetta et al., 2015), which infers that the coldest and driest period at Lake Ohrid (assumedly well-dated at ca. 108 ka), occurred around 2-3 ka after that observed in other records (Grant et al., 2012; Martrat et al., 2014). A minor offset (ca. 0.6 ka) is also present between $\delta^{18}O_{calcite}$ and $\delta^{13}C_{calcite}$ at Lake Ohrid, where $\delta^{13}C_{calcite}$ starts to decrease before $\delta^{18}O_{calcite}$ in phase with increasing AP (Sadori et al., 2015). Higher $\delta^{18}O_{calcite}$ could be due to the presence of siderite, however this is unlikely due to synchronous lowering $\delta^{13}C_{calcite}$ (siderite has much higher $\delta^{13}C$ due to methanogenesis; Section 7.6.4). The $\delta^{18}O_{calcite}$ peak at ca. 108 ka is therefore perhaps alternatively related to residence time effects and/or a differential response rate between $\delta^{18}O_{calcite}$ and $\delta^{13}C_{calcite}$ caused by winter precipitation being retained in the catchment (local snowfields/ice caps), whereas summer warming promoted vegetation growth and soil development at lower altitudes in the catchment. The minimum around ca. 108 ka is most likely associated with Greenland Stadial GS-25 (NGRIP Members, 2004).

Following stadial MIS 5d, $\delta^{18}O_{calcite}$ decreases by 2.8‰ between ca. 108-107 ka in MIS 5c suggesting that lake water became considerably fresher, where a minimum of −5.9‰ is observed between ca. 105-104 ka. After a short phase of higher values around ca. 102 ka, $\delta^{18}O_{calcite}$ further decreases to −6.3‰ at ca. 100 ka to the lowest values of MIS 5 and showing a 3.6‰ difference from peak stadial conditions during MIS 5d. Using the age model of Francke et al. (2015), the older $\delta^{18}O_{calcite}$ minimum corresponds to peak summer insolation, however using the model of Zanchetta et al. (2015) suggests that the younger $\delta^{18}O_{calcite}$ minimum is correspond to maximum insolation. The revised age model is further supported by $\delta^{13}C_{calcite}$, as there is a distinct stepped change at ca. 100 ka to lower values inferring peak interstadial conditions. In comparison to the large $\delta^{13}C_{calcite}$ excursion observed during MIS 5e, the initial phase of MIS 5c only shows a moderate change in $\delta^{13}C_{calcite}$ from stadial-like conditions during MIS 5d. The much larger change in $\delta^{18}O_{calcite}$ at the inception of MIS 5c infers either a large increase in precipitation (unlikely given relatively high $\delta^{13}C_{calcite}$ and restricted AP development at this time) or, as discussed previously, a decoupling between proxies due to meltwater influx. $\delta^{18}O_{calcite}$ and $\delta^{13}C_{calcite}$ must be somewhat decoupled in this interval as the amplitude of change observed in $\delta^{18}O_{calcite}$ is far greater than $\delta^{13}C_{calcite}$. This could therefore be due to a significant input of glacial meltwater, which would comprise very low $\delta^{18}O$ (Darling et al., 2006), compounding the effect of marginally elevated precipitation driving slightly lower $\delta^{13}C_{calcite}$ and higher AP (Sadori et al., 2015). A peak in $\delta^{18}O_{calcite}$ and $\delta^{13}C_{calcite}$ at ca. 102 ka is most probably associated with dry conditions during GS-24, also observed as a short-term shift to higher $\delta^{18}O$ at Soreq Cave (Bar-Matthews et al., 2003) and in the Aegean Sea (Grant et al., 2012). Subsequently, an extended period of low $\delta^{13}C_{calcite}$ between ca. 100-90 ka, concomitant with high AP (Sadori et al., 2015), suggests a largely more favourable climate. However, $\delta^{18}O_{calcite}$ shows high frequency and high amplitude oscillations throughout this interval. Apart from an excursion in both $\delta^{13}C_{calcite}$ and AP around ca. 93 ka (possibly related to GS-23), $\delta^{13}C_{calcite}$ does not reflect a similar variability. Considering $\delta^{18}O_{calcite}$ shows a similar amplitude excursion at ca. 93 ka to the other shifts that occur (approximately 1‰), these changes may perhaps be related to seasonality (i.e. a greater proportion of summer precipitation), temperature changes (i.e. warmer temperatures) or lake level changes (i.e. refilling the basin). Conversely $\delta^{18}O$ from Soreq Cave suggests a return to stadial-like conditions (higher $\delta^{18}O$) approximately 5 ka after GS-24, inferring this interval is characterised by lower regional precipitation and as such, the Ohrid isotope data is inconclusive. Although not available at present, diatom data and higher resolution pollen analyses may be able to further qualify the abrupt changes through this interval. Overall, $\delta^{18}O_{calcite}$ are observed to be lower in MIS 5c than during full interglacial conditions in MIS 5e, which could be due to the lake infilling after a lake water lowstand (Lindhorst et al., 2010). Alternatively, under higher insolation and atmospheric GHG concentrations during MIS 5e (Petit et al., 1999; Laskar et al., 2004; Loulergue et al., 2008), evaporation may have been stronger and forced higher $\delta^{18}O_{calcite}$, even under a regime of greater regional precipitation (Bar-Matthews et al., 2003; Drysdale et al., 2005).

After ca. 90 ka both $\delta^{18}O_{calcite}$ and $\delta^{13}C_{calcite}$ show a change to higher values, coincident with very low bSi, AP and high siderite abundance, which are assumed to be associated with stadial conditions during MIS 5b. The transition to higher values occurs over a shorter time interval compared to MIS 5d, inferring that MIS 5b probably experienced a more pronounced period of dry conditions and a larger climate deterioration. This is also suggested by higher $\delta^{18}O_{speleothem}$ at Soreq Cave (Bar-Matthews et al., 2003) and $\delta^{18}O_{MEDSTACK}$ (Wang et al., 2010), as well as by lower reconstructed SST from the Adriatic Sea (Piva et al., 2008) and Alboran Sea (Martrat et al., 2004). Moreover, this interval is characterised by very low atmospheric CO_2 (Petit et al., 1999) and increased global ice volume (Lisiecki and Raymo, 2005). A peak in $\delta^{13}C_{calcite}$ at ca. 86 ka is most likely related to an increase in the proportion of siderite, rather than being a direct measure of $\delta^{13}C_{TDIC}$ (although little change is observed in $\delta^{18}O_{calcite}$, probably due to the greater offset between $\delta^{13}C$ formed under methanogenic conditions). A rapid decrease in $\delta^{18}O_{calcite}$ after ca. 85 ka is thought to be related to the onset of interstadial conditions during MIS 5a, which is similar to previous cold-warm transitions in MIS 5 (i.e. more rapid in $\delta^{18}O_{calcite}$ than in $\delta^{13}C_{calcite}$). An overall decrease in $\delta^{13}C_{calcite}$ between ca. 85 and 81 ka infers that climate conditions may have been wetter towards the end of the stage, which is also advocated by low $\delta^{18}O_{calcite}$ at ca 81 ka. A transition to lower $\delta^{18}O_{speleothem}$ is also observed at Soreq Cave (Bar-Matthews et al., 2003) suggesting that regional rainfall may have increased toward the end of MIS 5a, which could be related to a coincident peak in precessional summer insolation (Laskar et al., 2004). A distinct rise in $\delta^{18}O_{calcite}$ around ca. 79 ka concomitant with a decrease in AP (Sadori et al., 2015) is most likely associated with lower reconstructed SST in the Alboran Sea (Martrat et al., 2004) and GS-21 (NGRIP Members, 2004). This suggests that glacial-like conditions were prevalent at Lake Ohrid prior to the boundary with glacial MIS 4 at 71 ka (Lisiecki and Raymo, 2005), and although isotope data are unavailable (due to low TIC), AP shows marked fluctuations and increasing NAP inferring an unstable climate characterised by an increasingly cool and dry environment (Sadori et al., 2015). After ca. 78 ka TIC becomes negligible and occasional minor peaks are related to the occurrence of siderite.

7.7 Summary

This chapter contains new stable isotope ($\delta^{18}O_{carbonate}$ and $\delta^{13}C_{carbonate}$) data from the SCOPSCO 5045-1 composite profile. Sediment cores recovered from Lake Ohrid represent one of the longest terrestrial palaeoclimate archives from the Mediterranean, and the isotope stratigraphy presented here is one of the most extensive and highly resolved available to date both regionally and worldwide. The upper 248 metres of the composite profile is discussed, which represents the last ca. 640 ka (Francke et al., 2015).

Francke et al. (2015) show the presence of TIC to be cyclical and observe phases of high TIC coincident with interglacials/interstadials and generally low TIC with glacials/stadials. Isotope data for calcite is continuous through intervals associated with high TIC. Discrete TIC peaks during glacials are confirmed to be siderite, which is the principle carbonate in these horizons. SEM-EDX shows that the siderite is early diagenetic and can be used, like calcite, as a proxy for lake water conditions at the time of precipitation.

To compare endogenic calcite and authigenic siderite, palaeotemperature equations and estimates for lake water temperature are used to reconstruct $\delta^{18}O_{lakewater}$. Glacial phases have lower $\delta^{18}O_{lakewater}$, and warmer stages have higher $\delta^{18}O_{lakewater}$. Overall, higher $\delta^{18}O_{lakewater}$ is most likely due to warmer temperatures and greater evaporation rates. Lower $\delta^{18}O_{lakewater}$ is probably due to reduced evaporation, lower air temperatures, a higher proportion of annual precipitation falling as isotopically light snow, and limited water input from Lake Prespa.

Given the quasi-continuous extent of isotope data for calcite, $\delta^{18}O_{calcite}$ and $\delta^{13}C_{calcite}$ are used to better understand interglacial and intra-interglacial variability through the Middle to Late Pleistocene (summarised in Figure 7.27). MIS 15-13 shows a period of stable $\delta^{18}O_{calcite}$, inferring that MIS 14 was a particularly weak glacial. A transition to lower $\delta^{18}O_{calcite}$ occurs in the later stages of MIS 11 and low $\delta^{18}O_{calcite}$ continues into MIS 9. A trend to higher values initiates with MIS 7 and evaporated conditions are observed in MIS 5. In all, this suggests a low-frequency progressive change between wetter and drier climate conditions. $\delta^{13}C_{calcite}$ shows sub-orbital oscillations with a varying amplitude about the long-term mean.

At glacial-interglacial transitions $\delta^{18}O_{calcite}$ typically shows low values (Figure 7.27), which is likely associated with lower glacial $\delta^{18}O_{lakewater}$ (siderite data) and/or an influx of low $\delta^{18}O$ meltwater from the catchment. Initially low values are probably the result of negligible TIC in the initial phases of deglaciation (i.e. calcite is only present after the peak influx of low $\delta^{18}O$). The majority of interglacial inceptions are directly followed by an increasing trend in $\delta^{18}O_{calcite}$, which suggests a short-term initial warming maxima, similar to that observed in atmospheric GHG concentrations (Figure 7.27).

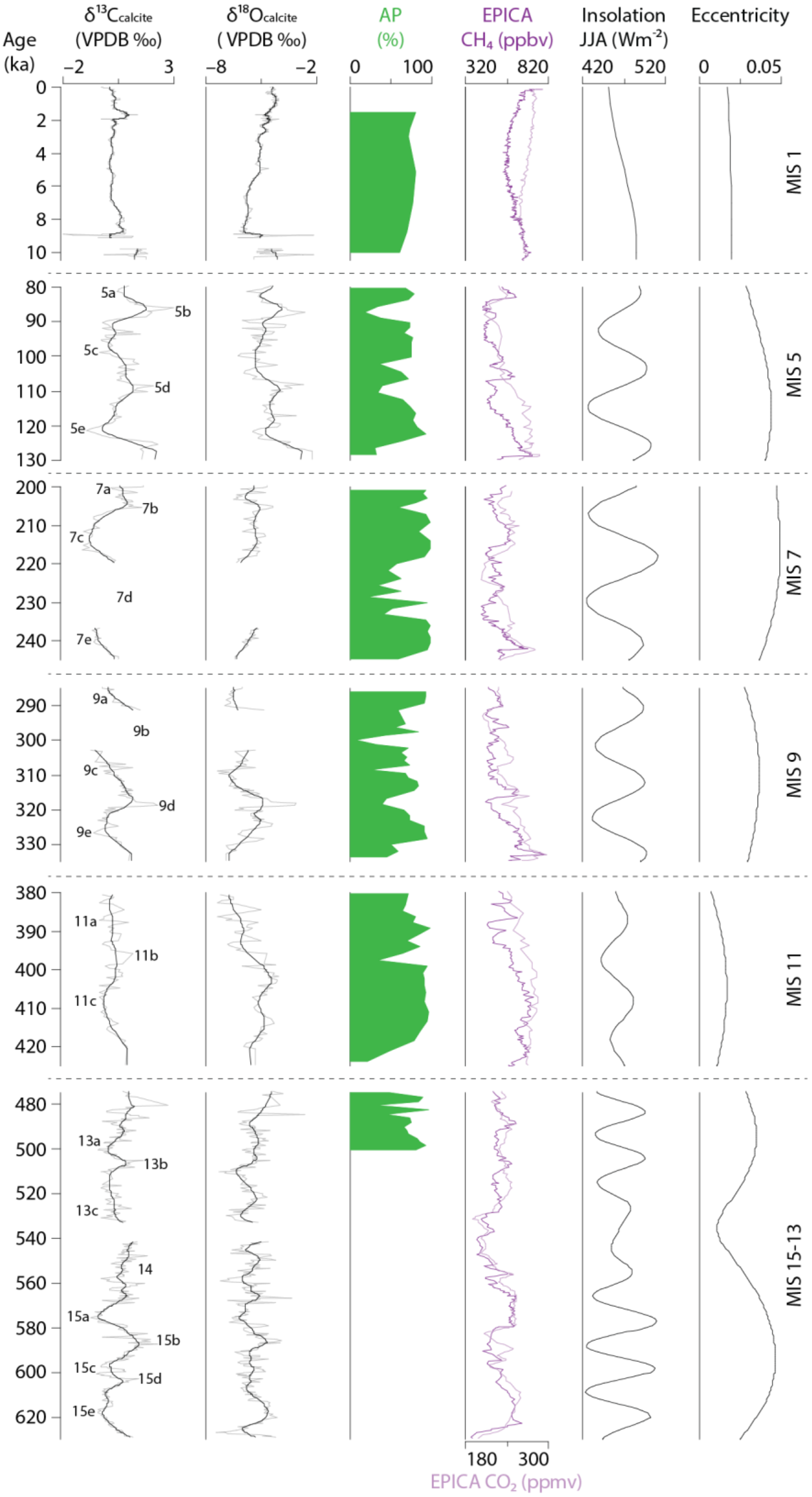

***Figure 7.27** Summary plot of $\delta^{13}C_{calcite}$, $\delta^{18}O_{calcite}$, and AP (Sadori et al., 2015) from Lake Ohrid through 'warm' MIS (stages and substages labelled), compared with Antarctic EPICA Dome C CO_2 (Lüthi et al., 2008) and CH_4 (Loulergue et al., 2008), summer (JJA) insolation at 40°N (Lasker et al. 2004), and orbital eccentricity (Berger and Loutre, 1991).*

A trend to lower values is observed in $\delta^{13}C_{calcite}$ at the start of interglacials, frequently inversely correlated to $\delta^{18}O_{calcite}$, which suggests an offset between $\delta^{18}O_{calcite}$ and $\delta^{13}C_{calcite}$ minima following glacial terminations. An offset between lower $\delta^{13}C_{calcite}$ and $\delta^{18}O_{calcite}$ may be linked to the development of catchment vegetation (AP %), and a lag in the production of catchment soils. The close association of $\delta^{13}C_{calcite}$ and AP is most likely driven by changes in summer insolation, which is in turn a function of orbital precession. Periods of high summer insolation are largely coincident with $\delta^{13}C_{calcite}$ minima (and AP maxima), where a greater amplitude of $\delta^{13}C_{calcite}$ variability is observed during high eccentricity and greater seasonality. This is highlighted when eccentricity maxima occur in parallel with insolation maxima (e.g. around 578 ka and 219 ka), which have the lowest $\delta^{13}C_{calcite}$ of the composite profile. Reduced variability in $\delta^{13}C_{calcite}$ mostly occurs during periods of low eccentricity, for example between MIS 14 to 13c, during MIS 11, and through the Holocene, emphasising the important influence of precessional insolation on the evolution of $\delta^{13}C_{calcite}$.

In contrast to lower $\delta^{18}O_{calcite}$ and $\delta^{13}C_{calcite}$ during interglacial and interstadial periods, stadial phases are typically associated with excursions to higher values (or an absence of data because of low calcite). This suggests that the drivers of isotope variation differ between full glacial periods and stadial phases, as calculated $\delta^{18}O_{lakewater}$ from siderite implies a change to lower values through glacials. A change to fresher lakewater conditions under deteriorating climate conditions is also implied through MIS 11. Decreasing $\delta^{18}O_{calcite}$ between ca. 400 and 380 ka is coincident with reducing AP and atmospheric GHG concentrations (Figure 7.27), inferring the onset of glacial conditions and supporting lower $\delta^{18}O$ during glacial phases. This opposes the transitions observed during warm stage stadial phases, for example MIS 9d and 5b, where higher $\delta^{18}O_{calcite}$ is accompanied by a change to higher $\delta^{13}C_{calcite}$ and lower AP. Given the overriding influence of orbital control on $\delta^{18}O_{calcite}$ and $\delta^{13}C_{calcite}$ during warmer stages, in particular eccentricity and precession, further comparisons should be made with other multi-proxy datasets (when available; e.g. diatoms, higher-resolution pollen) to elucidate the role of seasonality in determining the palaeoclimate and palaeoenvironmental evolution of Lake Ohrid.

CHAPTER 8 | SUMMARY OF RESEARCH

This study aimed to obtain detailed information on long-term climate and environmental change in the central Mediterranean region through the Late Quaternary using lacustrine isotope stratigraphy and geochemical data from ancient Lake Ohrid. To support a reliable interpretation of past climate variability the contemporary isotope system was modelled and hydrological balance reassessed. In addition, a Late Glacial to Holocene record was investigated using a high-resolution multi-proxy approach to provide a recent calibration and give context for the extended climate reconstruction.

8.1 Key conclusions

8.1.1 Modern isotope hydrology

- Lake Ohrid is an evaporative system with a complex hydrology.
- Evaporation from Lake Ohrid has an important influence on the overlying atmosphere, producing a moisture feedback effect (37% admixture of evaporate with atmosphere above the lake).
- Surface and sub-lacustrine springs form a larger proportion of water input (60%) than previously estimated, reducing the influence of direct precipitation (20%) and river inflow (20%).
- A component of groundwater outflow is inferred to comprise 13% of total water output.
- The calculated weighted average inflow $\delta^{18}O = -8.3‰$ and $\delta D = -56.3‰$.
- Variations in $\delta^{18}O_{lakewater}$ represent long-term fluctuations in water balance, and changes to the amount of precipitation input may have a greater direct influence on $\delta^{18}O_{lakewater}$ and P/E compared to evaporation.

8.1.2 Late Glacial to Holocene calibration

- Lini Co1262 is the longest Holocene sediment core recovered from Lake Ohrid (7.85 m) and provides one of the best-resolved lacustrine isotope and geochemical records available in the region. The age model suggests that the core covers the last ca. 12.3 ka.

- Organic proxies (TOC, TOC/TN, Rock-Eval, $\delta^{13}C_{organic}$) confirm a predominantly autochthonous source of organic matter and show a uniform response to both long-term trends and abrupt events.
- Aquatic productivity and carbonate production are low in the Late Glacial-Early Holocene, undergo an optimum during the Middle Holocene (maximum at ca. 5 ka), and reduce in the Late Holocene.
- Short-term excursions observed across organic proxies are coincident with major Holocene climate oscillations, one of the most prominent being associated cool and dry conditions during the 8.2 ka event, and confirm the overriding influence of the North Atlantic in the central Mediterranean.
- An environmental threshold must be surpassed before calcite is precipitated (and/or preserved), highlighted by the intervals following the Late Glacial-Holocene transition (ca. 11.1 ka) and the 8.2 ka event.
- A large water volume and long residence time effectively buffer $\delta^{18}O_{calcite}$ and $\delta^{13}C_{calcite}$ against short-term variations in $\delta^{18}O_{lakewater}$ and $\delta^{13}C_{TDIC}$, respectively.
- $\delta^{18}O_{calcite}$ is characterised by wetter conditions in the Early Holocene (centred on ca. 9 ka) and a progressive transition to drier conditions through the Middle-Late Holocene.
- Millennial-scale variability at Lake Ohrid is a function of regional water balance driven by insolation changes, which are primarily related to the precessional component of orbital cyclicity.

8.1.3 Late Quaternary palaeoenvironmental reconstruction

- SCOPSCO 5045-1 composite profile sediments spanning the last ca. 640 ka were analysed for $\delta^{18}O$ and $\delta^{13}C$ of carbonate, providing one of the most extensive continental isotope records available and facilitating a rare comparison of past interglacials from the same terrestrial sequence.
- Endogenic calcite is the primary carbonate mineral identified during interglacial and interstadial (high TIC) periods, however calcite is found to be negligible within glacial and stadial episodes.
- Intermittent TIC spikes (<2%) observed during glacial intervals were confirmed to comprise early diagenetic siderite.

- $\delta^{18}O_{calcite}$ and $\delta^{18}O_{siderite}$ were used to calculate $\delta^{18}O_{lakewater}$ to enable comparison between the two carbonate minerals.
- 'Warm' MIS are characterised by generally higher $\delta^{18}O_{lakewater}$ and 'cold' MIS by lower $\delta^{18}O_{lakewater}$, which is probably a composite function of changes in temperature, evaporation, seasonality, hydrology and type of precipitation (rain or snow).
- $\delta^{13}C_{siderite}$ is observed to be much higher than $\delta^{13}C_{calcite}$ most likely due to the effects of methanogenesis.
- $\delta^{18}O_{calcite}$ shows relatively stable conditions before ca. 450 ka, a wetter climate between ca. 400 and 250 ka, and a trend to drier climate conditions from ca. 250 ka to present. This may be linked to changes in orbital eccentricity controlling precessional insolation. $\delta^{13}C_{calcite}$ shows little low-frequency variability inferring a constant control on $\delta^{13}C_{TDIC}$ between MIS.
- At the millennial-scale, $\delta^{18}O_{calcite}$ and $\delta^{13}C_{calcite}$ are closely coupled, however $\delta^{13}C_{calcite}$ appears to better reflect regional-scale changes in climate and shows a strong similarity with palynological data from Lake Ohrid. In general, low $\delta^{18}O_{calcite}$ and $\delta^{13}C_{calcite}$ are associated with interglacial and interstadial periods and higher values occur during stadials, where oscillations are observed to be coincident with changes in precessional insolation, modulated by orbital obliquity.

8.2 Future work

The isotope and geochemical data from this thesis contribute toward the interdisciplinary SCOPSCO project and will be used, in conjunction with collaborators' datasets (e.g. pollen, diatoms), to better understand climate and environmental variability throughout the Pleistocene. This study has demonstrated the potential of isotope data for palaeoclimate reconstruction at Lake Ohrid and has provided one of the longest terrestrial isotope records worldwide (using only the upper half of the composite profile). As core-processing progresses, the key focus of future work will be to extend analyses over the remaining core material to deliver an isotope record covering the last 1.2 Ma. The current sampling resolution of 16 cm could be increased through interglacial intervals of particular interest, for example those with a similar orbital configuration to the Holocene (e.g. MIS 5, 11, 19).

To provide a continuous record of palaeoclimate change more glacial isotope data are required. There are numerous siderite-bearing horizons observed within each glacial interval, which means that intra-glacial variability could be quantified. It would also be important to assess the diagenetic properties of siderite throughout the composite profile. In certain intervals (yet to be analysed) calcite and siderite are contemporaneous, affording the opportunity to ascertain whether any offset occurs between the environments in which the minerals precipitate.

$\delta^{18}O_{calcite}$ and $\delta^{13}C_{calcite}$ are shown to be closely associated with changes in palynological data from Lake Ohrid. An interesting possibility is to utilise forthcoming pollen-based temperature reconstructions to better estimate past surface water conditions and more precisely reconstruct $\delta^{18}O_{lakewater}$. Further, $\delta^{18}O_{lakewater}$ calculated from carbonate could be combined with compound-specific hydrogen isotopic ratios (δD) of organic biomarkers to further elucidate palaeohydrological changes.

Although monitoring data are available for Lake Ohrid, there is ample potential for improvement. A comprehensive monitoring dataset would also allow for the development of a detailed isotope mass balance model (in particular for Lake Ohrid, but this could extend to the entire Ohrid-Prespa system). Ideally, limnological monitoring would be used to fully understand the response in $\delta^{18}O_{lakewater}$ to modern climate variations. This would greatly improve and support palaeoclimate reconstructions.

REFERENCES

Albrecht, C., and Wilke, T. (2008) Ancient Lake Ohrid: biodiversity and evolution. *Hydrobiologia* **615** (1), 103-140.

Albrecht, C., Trajanovski, S., Kuhn, K., Streit, B., and Wilke, T. (2006) Rapid evolution of an ancient lake species flock: Freshwater limpets (Gastropoda: Ancylidae) in the Balkan Lake Ohrid. *Organisms Diversity & Evolution* **6** (4), 294-307.

Albrecht, C., Vogel, H., Hauffe, T., and Wilke, T. (2010) Sediment core fossils in ancient Lake Ohrid: testing for faunal change in molluscs since the Last Interglacial period. *Biogeosciences Discussions* **7** (3), 3969-3999.

Allen, H. L., and Ocevski, B. T. (1977) Limnological studies in a large, deep, oligotrophic lake (Lake Ohrid, Yugoslavia). A summary of nutritional radiobioassay responses of the pelagial phytoplankton. *Hydrobiologia* **53** (1), 49-54.

Allen, J. R. M., and Huntley, B. (2009) Last Interglacial palaeovegetation, palaeoenvironments and chronology: a new record from Lago Grande di Monticchio, southern Italy. *Quaternary Science Reviews* **28** (15-16), 1521-1538.

Allen, J. R. M., Watts, W. A., McGee, E., and Huntley, B. (2002) Holocene environmental variability - the record from Lago Grande di Monticchio, Italy. *Quaternary International* **88**, 69-80.

Alley, R. B., Mayewski, P. A., Sowers, T., Stuiver, M., Taylor, K. C., and Clark, P. U. (1997) Holocene climatic instability: A prominent, widespread event 8200 yr ago. *Geology* **25** (6), 483-486.

Amataj, S., Anovski, T., Benischke, R., Eftimi, R., Gourcy, L. L., Kola, L., Leontiadis, I., Micevski, E., Stamos, A., and Zoto, J. (2007) Tracer methods used to verify the hypothesis of Cvijić about the underground connection between Prespa and Ohrid Lake. *Environmental Geology* **51** (5), 749-753.

Andrews, J. E., Riding, R., and Dennis, P. F. (1993) Stable isotopic compositions of Recent freshwater cyanobacterial carbonates from the British Isles: local and regional environmental controls. *Sedimentology* **40** (2), 303-314.

Anovski, T. (2001) *Progress in the Study of Prespa Lake Using Nuclear and Related Techniques, IAEA Regional Project RER/8/008*, Skopje, Macedonia.

Anovski, T., Andonovski, B., and Mineva, B. (1991) Study of the hydrological relationship between lakes Ohrid and Prespa. *In* Proceedings Proceedings of an IAEA international symposium, IAEA-SM-Vienna, 11-15 March 1991, Volume 319.

Anovski, T., Leontiadis, I., and Zoto, J. (2001) *Isotope Data*. *In* Anovski, T., (ed.), *Progress in the Study of Prespa Lake Using Nuclear and Related Techniques, IAEA Regional Project RER/8/008,* Skopje, Macedonia.

Anovski, T., Naumovski, J., Kacurkov, D., and Kirkov, P. (1980) A study of the origin of waters of St. Naum Springs, Lake Ohrid. *Fisika* **12** (76-86).

Ariztegui, D., Asioli, A., Lowe, J. J., Trincardi, F., Vigliotti, L., Tamburini, F., Chondrogianni, C., Accorsi, C. A., Bandini Mazzanti, M., Mercuri, A. M., Van Der Kaars, S., McKenzie, J. A., and Oldfield, F. (2000) Palaeoclimate and the formation of sapropel S1: Inferences from Late Quaternary lacustrine and marine sequences in the central Mediterranean region. *Palaeogeography, Palaeoclimatology, Palaeoecology* **158** (3-4), 215-240.

Ariztegui, D., Chondrogianni, C., Lami, A., Guilizzoni, P., and Lafargue, E. (2001) Lacustrine organic matter and the Holocene paleoenvironmental record of Lake Albano (central Italy). *Journal of Paleolimnology* **26** (283-292).

Arz, H. W., Lamy, F., Patzold, J., Muller, P. J., and Prins, M. A. (2003) Mediterranean Moisture Source for an Early-Holocene Humid Period in the Northern Red Sea. *Science* **300**, 118-121.

Arz, H. W., Lamy, F., and Pätzold, J. (2006) A pronounced dry event recorded around 4.2 ka in brine sediments from the northern Red Sea. *Quaternary Research* **66** (3), 432-441.

Aufgebauer, A., Panagiotopoulos, K., Wagner, B., Schaebitz, F., Viehberg, F. A., Vogel, H., Zanchetta, G., Sulpizio, R., Leng, M. J., and Damaschke, M. (2012) Climate and environmental change in the Balkans over the last 17 ka recorded in sediments from Lake Prespa (Albania/F.Y.R. of Macedonia/Greece). *Quaternary International* **274**, 122-135.

Ayusoa, R. A., De Vivo, B., Rolandi, G., Seal, R. R., and Paonea, A. (1998) Geochemical and isotopic (Nd−Pb−Sr−O) variations bearing on the genesis of volcanic rocks from Vesuvius, Italy. *Journal of Volcanology and Geothermal Research* **82** (1-4), 53-78.

Bahrig, B. (1988) Palaeo-environment information from deep water siderite (Lake of Laach, West Germany). *Geological Society, London, Special Publications* **40** (1), 153-158.

Balistrieri, L. S., Murray, J. W., and Paul, B. (1992) The cycling of iron and manganese in the water column of Lake Sammamish, Washington. *Limnology and Oceanography* **37** (3), 510-528.

Bar-Matthews, M., Ayalon, A., and Kaufman, A. (1997) Late Quaternary Paleoclimate in the Eastern Mediterranean Region from Stable Isotope Analysis of Speleothems at Soreq Cave, Israel. *Quaternary Research* **47** (2), 155-168.

Bar-Matthews, M., Ayalon, A., Kaufman, A., and Wasserburg, G. J. (1999) The Eastern Mediterranean paleoclimate as a reflection of regional events: Soreq cave, Israel. *Earth and Planetary Science Letters* **166** (1-2), 85-95.

Bar-Matthews, M., Ayalon, A., Gilmour, M., Matthews, A., and Hawkesworth, C. J. (2003) Sea−land oxygen isotopic relationships from planktonic foraminifera and speleothems in the Eastern Mediterranean region and their implication for paleorainfall during interglacial intervals. *Geochimica et Cosmochimica Acta* **67** (17), 3181-3199.

Barber, D. C., Dyke, A., Hillaire-Marcel, C., Jennings, A. E., Andrews, J. T., Kerwin, M. W., Bilodeau, G., McNeely, R., Southon, J., Morehead, M. D., and Gagnon, J. M. (1999) Forcing of the cold event of 8,200 years ago by catastrophic drainage of Laurentide lakes. *Nature* **400**, 344-348.

Baroni, C., Zanchetta, G., Fallick, A. E., and Longinelli, A. (2006) Mollusca stable isotope record of a core from Lake Frassino, northern Italy: hydrological and climatic changes during the last 14 ka. *The Holocene* **16** (6), 827-837.

Baumgarten, H., Wonik, T., Tanner, D. C., Francke, A., Wagner, B., Zanchetta, G., Sulpizio, R., Giaccio, B., and Nomade, S. (2015) Age depth-model for the past 630 ka in Lake Ohrid (Macedonia/Albania) based on cyclostratigraphic analysis of downhole gamma ray data. *Biogeosciences Discussions* **12**, 7671-7703.

Becker, R. H., and Clayton, R. N. (1976) Oxygen isotope study of a Precambrian banded iron-formation, Hamersley Range, Western Australia. *Geochimica et Cosmochimica Acta* **40**, 1153-1165.

Belmecheri, S., Namiotko, T., Robert, C., von Grafenstein, U., and Danielopol, D. L. (2009) Climate controlled ostracod preservation in Lake Ohrid (Albania, Macedonia). *Palaeogeography, Palaeoclimatology, Palaeoecology* **277** (3-4), 236-245.

Belmecheri, S., von Grafenstein, U., Andersen, N., Eymard-Bordon, A., Régnier, D., Grenier, C., and Lézine, A.-M. (2010) Ostracod-based isotope record from Lake Ohrid (Balkan Peninsula) over the last 140 ka. *Quaternary Science Reviews* **29** (27-28), 3894-3904.

Berger, A., and Loutre, M. F. (1991) Insolation values for the climate of the last 10 million years. *Quaternary Science Reviews* **10**, 297-317.

Berger, J.-F., and Guilaine, J. (2009) The 8200 cal BP abrupt environmental change and the Neolithic transition: A Mediterranean perspective. *Quaternary International* **200** (1−2), 31-49.

Bjune, A. E., and Birks, H. J. B. (2008) Holocene vegetation dynamics and inferred climate changes at Svanåvatnet, Mo i Rana, northern Norway. *Boreas* **37**, 146-156.

Blaauw, M. (2010) Methods and code for 'classical' age-modelling of radiocarbon sequences. *Quaternary Geochronology* **5**, 512-518.

Blaauw, M. and Christen, J. A. (2011) Flexible paleoclimate age-depth models using an autoregressive gamma process. *Bayesian Analysis* **6**, 457-474.

Blindheim, J., Borovkov, V., Hansen, B., Malmberg, S.-A., Turrell, W. R., and Osterhus, S. (2000) Upper layer cooling and freshening in the Nowegian Sea in relation to atmospheric forcing. *Deep-Sea Research I* **47**, 655-680.

Bond, G., Kromer, B., Beer, J., Muscheler, R., Evans, M. N., Showers, W., Hoffmann, S., Lotti-Bond, R., Hajdas, I., and Bonani, G. (2001) Persistent solar influence on north atlantic climate during the Holocene. *Science* **294**, 2130-2136.

Booth, R. K., Jackson, S. T., Forman, S. L., Kutzbach, J. E., Bettis, E. A., Kreigs, J., and Wright, D. K. (2005) A severe centennial-scale drought in midcontinental North America 4200 years ago and apparent global linkages. *The Holocene* **15** (3), 321-328.

Bordon, A., Peyron, O., Lézine, A.-M., Brewer, S., and Fouache, E. (2009) Pollen-inferred Late-Glacial and Holocene climate in southern Balkans (Lake Maliq). *Quaternary International* **200** (1-2), 19-30.

Bout-Roumazeilles, V., Combourieu Nebout, N., Peyron, O., Cortijo, E., Landais, A., and Masson-Delmotte, V. (2007) Connection between South Mediterranean climate and North African atmospheric circulation during the last 50,000yrBP North Atlantic cold events. *Quaternary Science Reviews* **26** (25-28), 3197-3215.

Bowen, G. J., and Wilkinson, B. (2002) Spatial distribution of $\delta^{18}O$ in meteoric precipitation. *Geology* **30** (4), 315-318.

Bowen, R. (1991) *Isotopes and climates*, London, Elsevier Science Publishers.

Braconnot, P., Otto-Bliesner, B., Harrison, S., Joussaume, S., Peterchmitt, J. Y., Abe-Ouchi, A., Crucifix, M., Driesschaert, E., Fichefet, T., Hewitt, C. D., Kageyama, M., Kitoh, A., Laîné, A., Loutre, M. F., Marti, O., Merkel, U., Ramstein, G., Valdes, P., Weber, S. L., Yu, Y., and Zhao, Y. (2007) Results of PMIP2 coupled simulations of the Mid-Holocene and Last Glacial Maximum - Part 1: experiments and large-scale features. *Climate of the Past* **3** (2), 261-277.

Brauer, A., Allen, J. R., Mingram, J., Dulski, P., Wulf, S., and Huntley, B. (2007) Evidence for last interglacial chronology and environmental change from Southern Europe. *Proceedings of the National Academy of Sciences USA* **104** (2), 450-455.

Brauer, A. and Negendank, J. F. W. 1993 *Paleoenvironmental reconstruction of the Late- and Postglacial sedimentary record of Lake Weinfelder Maar*. *In* Negendank, J. W. and Zolitschka, B. (eds.) *Paleolimnology of European Maar Lakes,* Volume 49, Springer Berlin Heidelberg, p. 223-235.

Brooks, J. L. (1950) Speciation in ancient lakes. *The Quarterly Review of Biology* **25** (1), 30-60.

Burchfiel, B. C., Nakov, R., Dumurdzanov, N., Papanikolaou, D., Tzankov, T., Serafimovski, T., King, R. W., Kotzev, V., Todosov, A., and Nurce, B. (2008) Evolution and dynamics of the Cenozoic tectonics of the South Balkan extensional system. *Geosphere* **4** (6), 919-938.

Candy, I., Schreve, D. C., Sherriff, J., and Tye, G. J. (2014) Marine Isotope Stage 11: Palaeoclimates, palaeoenvironments and its role as an analogue for the current interglacial. *Earth-Science Reviews* **128**, 18-51.

Caron, B., Sulpizio, R., Zanchetta, G., Siani, G., and Santacroce, R. (2010) The Late Holocene to Pleistocene tephrostratigraphic record of Lake Ohrid (Albania). *Comptes Rendus Geoscience* **342** (6), 453-466.

Carothers, W. W., Adami, L. H., and Rosenbauer, R. J. (1988) Experimental oxygen isotope fractionation between siderite-water and phosphoric acid liberated CO_2-siderite. *Geochimica et Cosmochimica Acta* **52**, 2445-2450.

Carrie, J., Sanei, H., and Stern, G. (2012) Standardisation of Rock−Eval pyrolysis for the analysis of recent sediments and soils. *Organic Geochemistry* **46**, 38-53.

Carrion, J. (2002) Patterns and processes of Late Quaternary environmentalchange in a montane region of southwestern Europe. *Quaternary Science Reviews* **21**, 2047-2066.

Celle-Jeanton, H., Gonfiantini, R., Travi, Y., and Sol, B. (2004) Oxygen-18 variations of rainwater during precipitation: application of the Rayleigh model to selected rainfalls in Southern France. *Journal of Hydrology* **289** (1−4), 165-177.

Channell, J. E. T., and Kozur, H. W. (1997) How many oceans? Meliata, Vardar, and Pindos oceans in Mesozoic Alpine paleogeography. *Geology* **25** (2), 183-186.

Cioni, R., Bertagnini, A., Santacroce, R., and Andronico, D. (2008) Explosive activity and eruption scenarios at Somma-Vesuvius (Italy): Towards a new classification scheme. *Journal of Volcanology and Geothermal Research* **178** (3), 331-346.

Clark, I. D. and Fritz, P. (1997) *Environmental Isotopes in Hydrogeology*, Boca Raton, Florida, CRC Press/Lewis Publishers.

Cohen, A. S. (2003) *Paleolimnology: The History and Evolution of Lake Systems*, Oxford, Oxford University Press.

Cohen, A. S. (2011) Scientific drilling and biological evolution in ancient lakes: lessons learned and recommendations for the future. *Hydrobiologia* **682** (1), 3-25.

Coleman, M. L. (1985) Geochemistry of diagenetic non-silicate minerals: kinetic considerations. *Philosophical Transactions of the Royal Society of London A* **315**, 39-56.

Collins-Pearson, J. (2013) Preparation of siderite ($FeCO_3$) for stable isotope analysis in palaeoenvironmental studies (MGeol thesis, University of Leicester, UK).

Coltelli, M., Del Carlo, P., and Vezzoli, L. (2000) Stratigraphic constraints for explosive activity in the past 100 ka at Etna Volcano, Italy. *International Journal of Earth Sciences* **89** (3), 665-677.

Combourieu-Nebout, N., Peyron, O., Bout-Roumazeilles, V., Goring, S., Dormoy, I., Joannin, S., Sadori, L., Siani, G., and Magny, M. (2013) Holocene vegetation and climate changes in the central Mediterranean inferred from a high-resolution marine pollen record (Adriatic Sea). *Climate of the Past* **9** (5), 2023-2042.

Constantin, S., Bojar, A.-V., Lauritzen, S.-E., and Lundberg, J. (2007) Holocene and Late Pleistocene climate in the sub-Mediterranean continental environment: A speleothem record from Poleva Cave (Southern Carpathians, Romania). *Palaeogeography, Palaeoclimatology, Palaeoecology* **243** (3-4), 322-338.

Craig, H. (1953) The geochemistry of the stable carbon isotopes. *Geochimica et Cosmochimica Acta* **3** (2-3), 53-92.

Craig, H. (1957) Isotopic standards for carbon and oxygen and correction factors for mass-spectrometric analysis of carbon dioxide. *Geochimica et Cosmochimica Acta* **12** (1−2), 133-149.

Craig, H. (1961) Isotopic Variations in Meteoric Waters. *Science* **133**, 1702-1703.

Craig, H. (1965) *The measurement of oxygen isotope palaeotemperatures*. *In* Tongiorgi, E. (ed.) *Stable Isotopes in Oceanographic Studies and Palaeotemperatures*, Pisa, Consiglio Nazionale delle Ricerche Laboratorio di Geologia Nucleare, p. 161-182.

Craig, H. and Gordon, L. I. (1965) *Deuterium and oxygen 18 variations in the ocean and marine atmosphere*. *In* Tongiogi, E. (ed.) *Stable Isotopes in Oceanographic Studies and Paleotemperatures*: Spoleto, Italy, p. 9-130.

Craig, H. and Keeling, C. D. (1963) The effects of atmospheric NO2 on the measured isotopic composition of atmospheric CO_2. *Geochimica et Cosmochimica Acta* **27** (5), 549-551.

Cristescu, M. E., Adamowicz, S. J., Vaillant, J. J., and Haffner, D. G. (2010) Ancient lakes revisited: from the ecology to the genetics of speciation. *Molecular Ecology* **19** (22), 4837-4851.

Crowley, T. J., and Lowery, T. S. (2000) How warm was the Medieval Warm Period? *Ambio* **29** (1), 51-54.

Cukur, D., Krastel, S., Schmincke, H. U., Sumita, M., Tomonaga, Y., and Namık Çağatay, M. (2014) Water level changes in Lake Van, Turkey, during the past ca. 600 ka: climatic, volcanic and tectonic controls. *Journal of Paleolimnology* **52** (3), 201-214.

Curry, B. B., Anderson, T. F., and Lohmann, K. C. (1997) Unusual carbon and oxygen isotopic ratios of ostracodal calcite from last interglacial (Sangamon episode) lacustrine sediment in Raymond Basin, Illinois, USA. *Journal of Paleolimnology* **17**, 421-435.

Cvetkoska, A., Levkov, Z., Reed, J. M., and Wagner, B. (2014) Late Glacial to Holocene climate change and human impact in the Mediterranean: The last ca. 17ka diatom record of Lake Prespa (Macedonia/Albania/Greece). *Palaeogeography, Palaeoclimatology, Palaeoecology* **406**, 22-32.

Cvijić, J. (1906) *Fundamentals of geography and geology of Macedonia and Old Serbia*, Belgrade (in Serbian), Serbian Academy of Sciences.

Cvijić, J. (1911) *Fundamentals of geography and geology of Macedonia and Old Serbia*, Beograd (in Serbian), Serbian Academy of Sciences.

Climate Wizard (CW) (2015) University of Washington and The Nature Conservancy, ClimateWizard.

Daley, T. J., Thomas, E. R., Holmes, J. A., Street-Perrott, F. A., Chapman, M. R., Tindall, J. C., Valdes, P. J., Loader, N. J., Marshall, J. D., Wolff, E. W., Hopley, P. J., Atkinson, T., Barber, K. E., Fisher, E. H., Robertson, I., Hughes, P. D. M., and Roberts, C. N. (2011) The 8200yr BP cold event in stable isotope records from the North Atlantic region. *Global and Planetary Change* **79** (3-4), 288-302.

Damaschke, M., Sulpizio, R., Zanchetta, G., Wagner, B., Böhm, A., Nowaczyk, N., Rethemeyer, J., and Hilgers, A. (2013) Tephrostratigraphic studies on a sediment core from Lake Prespa in the Balkans. *Climate of the Past* **9** (1), 267-287.

Dansgaard, W. (1964) Stable isotopes in precipitation. *Tellus* **16** (4), 436-468.

Darling, W. G., Bath, A. H., Gibson, J. J., and Rozanski, K. (2006) *Isotopes in Palaeoenvironmental Research: 1. Isotopes in Water*, Netherlands, Springer.

Davis, B. A. S. and Brewer, S. (2009) Orbital forcing and role of the latitudinal insolation/temperature gradient. *Climate Dynamics* **32** (2-3), 143-165.

Dean, J. R., Jones, M. D., Leng, M. J., Noble, S. R., Metcalfe, S. E., Sloane, H. J., Sahy, D., Eastwood, W. J., and Roberts, C. N. (2015) Eastern Mediterranean hydroclimate over the late glacial and Holocene, reconstructed from the sediments of Nar lake, central Turkey, using stable isotopes and carbonate mineralogy. *Quaternary Science Reviews* **124**, 162-174.

Dean, J. R., Jones, M. D., Leng, M. J., Sloane, H. J., Roberts, C. N., Woodbridge, J., Swann, G. E. A., Metcalfe, S. E., Eastwood, W. J., and Yiğitbaşıoğlu, H. (2013) Palaeo-seasonality of the last two millennia reconstructed from the oxygen isotope composition of carbonates and diatom silica from Nar Gölü, central Turkey. *Quaternary Science Reviews* **66**, 35-44.

Deines, P. (1980) *The isotopic composition of reduced organic carbon*. *In* Fritz, P. and Fontes, J. C. (eds.) *Handbook of Environmental Isotope Geochemistry*, Oxford, Elsevier.

Dejoux, C. (1994) *Lake Titicaca*. *In* Martens, K., Goddeeris, B., and Coulter, G. (eds.) *Speciation in Ancient Lakes,* Volume 44, Archiv für Hydrobiologie, p. 35-42.

Desprat, S., Combourieu-Nebout, N., Essallami, L., Sicre, M. A., Dormoy, I., Peyron, O., Siani, G., Bout Roumazeilles, V., and Turon, J. L. (2013) Deglacial and Holocene vegetation and climatic changes in the southern Central Mediterranean from a direct land−sea correlation. *Climate of the Past* **9** (2), 767-787.

Desprat, S., Sánchez Goñi, M. F., Turon, J.-L., Duprat, J., Malaizé, B., and Peypouquet, J.-P. (2006) Climatic variability of Marine Isotope Stage 7: direct land−sea−ice correlation from a multiproxy analysis of a north-western Iberian margin deep-sea core. *Quaternary Science Reviews* **25** (9-10), 1010-1026.

Desprat, S., Sánchez Goñi, M. F., Turon, J. L., McManus, J. F., Loutre, M. F., Duprat, J., Malaizé, B., Peyron, O., and Peypouquet, J. P. (2005) Is vegetation responsible for glacial inception during periods of muted insolation changes? *Quaternary Science Reviews* **24** (12-13), 1361-1374.

Digerfeldt, G., Olsson, S., and Sandgren, P. (2000) Reconstruction of lake-level changes in lake Xinias, central Greece, during the last 40,000 years. *Palaeogeography Palaeoclimatology Palaeoecology* **158**, 65-82.

Disnar, J. R., Guillet, B., Keravis, D., Di-Giovanni, C., and Sebag, D. (2003) Soil organic matter (SOM) characterization by Rock-Eval pyrolysis: scope and limitations. *Organic Geochemistry* **34**, 327-343.

Dotsika, E., Lykoudis, S., and Poutoukis, D. (2010) Spatial distribution of the isotopic composition of precipitation and spring water in Greece. *Global and Planetary Change* **71** (3-4), 141-149.

Downing, J. A., Prairie, Y. T., Cole, J. J., Duarte, C. M., Tranvik, L. J., Striegl, R. G., McDowell, W. H., Kortelainen, P., Caraco, N. F., Melack, J. M., and Middelburg, J. J. (2006) The global abundance and size distribution of lakes, ponds, and impoundments. *Limnology and Oceanography* **51** (5), 2388-2397.

Drăguşin, V., Staubwasser, M., Hoffmann, D. L., Ersek, V., Onac, B. P., and Veres, D. (2014) Constraining Holocene hydrological changes in the Carpathian−Balkan region using speleothem $\delta^{18}O$ and pollen-based temperature reconstructions. *Climate of the Past* **10** (4), 1363-1380.

Drummond, C. N., Patterson, W. P., and Walker, J. C. G. (1995) Climatic forcing of carbon-oxygen isotopic covariance in temperate-region marl lakes. *Geology* **23** (11), 1031-1034.

Drysdale, R., Zanchetta, G., Hellstrom, J., Maas, R., Fallick, A., Pickett, M., Cartwright, I., and Piccini, L. (2006) Late Holocene drought responsible for the collapse of Old World civilizations is recorded in an Italian cave flowstone. *Geology* **34** (2), 101.

Drysdale, R. N., Hellstrom, J. C., Zanchetta, G., Fallick, A. E., Sánchez Goñi, M. F., Couchoud, I., McDonald, J., Maas, R., Lohmann, G., and Isola, I. (2009) Evidence for Obliquity Forcing of Glacial Termination II. *Science* **325**, 1527-1531.

Drysdale, R. N., Zanchetta, G., Hellstrom, J. C., Fallick, A. E., and Zhao, J.-x. (2005) Stalagmite evidence for the onset of the Last Interglacial in southern Europe at 129 ± 1 ka. *Geophysical Research Letters* **32** (24).

Dumurdzanov, N., Serafimovski, T., and Burchfiel, B. C. (2005) Cenozoic tectonics of Macedonia and its relation to the South Balkan extensional regime. *Geosphere* **1** (1), 1.

Dumurdzanov, N., Todor Serafimovski, T., and Burchfield, B. C. (2004) *Evolution of the Neogene-Pleistocene Basins of Macedonia*, Boulder, Colorado, Geological Society of America, 1, p. 20.

Duplessy, J., Ivanova, E., Murdmaa, M. P., and Labeyrie, L. (2001) Holocene paleoceanography of the northern Barents Sea and variations of the northward heat transport by the Atlantic Ocean. *Boreas* **30**, 2-16.

Eastwood, W. J., Leng, M. J., Roberts, N., and Davis, B. (2007) Holocene climate change in the eastern Mediterranean region: a comparison of stable isotope and pollen data from Lake Gölhisar, southwest Turkey. *Journal of Quaternary Science* **22** (4), 327-341.

Eftimi, R., Amataj, S., and Zoto, J. (2007) *Groundwater circulation in two transboundary carbonate aquifers of Albania; their vulnerability and protection*. *In* Witkowski, A. J., Kowalczyk, A., and Vrba, J. (eds.) *Groundwater vulnerability assessment and maping,* Volume 11, The Netherlands, Taylor & Francis, p. 206-218.

Eftimi, R., Micevski, E., and Stamos, A. (2001) *Geological and hydrogeological conditions of the Prespa Region*. *In* Anovski, T. (ed.) *Progress in the Study of Prespa Lake Using Nuclear and Related Techniques, IAEA Regional Project RER/8/008*, Skopje, Macedonia, p. 11-22.

Eftimi, R., and Zoto, J. (1997) Isotope study of the connection of Ohrid and Prespa lakes, International Symposium "Towards Integrated Conservation and Sustainable Development of Transboundary Macro and Micro Prespa Lakes", Korcha, Albania.

Eicher, U. and Siegenthaler, U. (1976) Palynalogical andoxygen isotope investigations on late-Glacial sediment cores from Swiss lakes. *Boreas* **5**, 109-117.

Emeis, K. C., Struck, U., Schulz, H. M., Rosenberg, R., Bernasconi, S., Erlenkeuser, H., Sakamoto, T., and Martinez-Ruiz, F. (2000) Temperature and salinity variations of Mediterranean Sea surface waters over the last 16,000 years from records of planktonic stable oxygen isotopes and alkenone unsaturation ratios. *Palaeogeography Palaeoclimatology Palaeoecology* **158** (3-4), 259-280.

Epstein, S., Buchsbaum, R., Lowenstam, H. A., and Urey, H. C. (1953) Revised Carbonate-Water Isotopic Temperature Scale. *Geological Society of America Bulletin* **64** (11), 1315.

Espitalie, J., Deroo, G., and Marquis, F. (1985) La pyrolyse Rock-Eval et ses applications; deuxieme partie. *Revue de l'Institut Francais du Petrole* **40**, 755-784.

Espitalie, J., Laporte, J. L., Madec, M., Marquis, F., Leplat, P., Paulet, J., and Boutefeu, A. (1977) Rapid Method for Source Rock Characterization and for Determination of Their Petroleum Potential and Degree of Evolution. *Revue de l'Institut Francais du Petrole* **32** (1), 23-42.

Fernández-Chacón, F., Benavente, J., Rubio-Campos, J. C., Kohfahl, C., Jiménez, J., Meyer, H., Hubberten, H., and Pekdeger, A. (2010) Isotopic composition (δ^{18}O and δD) of precipitation and groundwater in a semi-arid, mountainous area (Guadiana Menor basin, Southeast Spain). *Hydrological Processes*, **24**, 1343-1356.

Feurdean, A., Liakka, J., Vannière, B., Marinova, E., Hutchinson, S. M., Mosburgger, V., and Hickler, T. (2013) 12,000-Years of fire regime drivers in the lowlands of Transylvania (Central-Eastern Europe): a data-model approach. *Quaternary Science Reviews* **81**, 48-61.

Fleitmann, D., Burns, S. J., Mangini, A., Mudelsee, M., Kramers, J., Villa, I., Neff, U., Al-Subbary, A. A., Buettner, A., Hippler, D., and Matter, A. (2007) Holocene ITCZ and Indian monsoon dynamics recorded in stalagmites from Oman and Yemen (Socotra). *Quaternary Science Reviews* **26** (1-2), 170-188.

Francke, A., Wagner, B., Just, J., Leicher, N., Gromig, R., Baumgarten, H., Vogel, H., Lacey, J. H., Sadori, L., Wonik, T., Leng, M. J., Zanchetta, G., Sulpizio, R., and Giaccio, B. (2015) Sedimentological processes and environmental variability at Lake Ohrid (Macedonia, Albania) between 640 ka and present day. *Biogeosciences Discussions* **12** (17), 15111-15156.

Francke, A., Wagner, B., Leng, M. J., and Rethemeyer, J. (2013) A Late Glacial to Holocene record of environmental change from Lake Dojran (Macedonia, Greece). *Climate of the Past* **9** (1), 481-498.

Francus, P. and Asikainen, C. A. (2001) Sub-sampling unconsolidated sediments: a solution for the preparation of undisturbed thin-sections from clay-rich sediments. *Journal of Paleolimnology* **26**, 323-326.

Friedman, I., and O'Neil, J. R. (1977) *Compilation of stable isotope fractionation factors of geochemical interest*. *In* Fleischer, M. (ed.) *Data of Geochemistry*, p. 440.

Fritz, P., Anderson, T. W., and Lewis, C. F. M. (1975) Late-Quaternary Climatic Trends and History of Lake Erie from Stable Isotope Studies. *Science* **190**, 267-269.

Frogley, M. R. (1999) Climate Variability in Northwest Greece During the Last Interglacial. *Science* **285**, 1886-1889.

Frogley, M. R., Griffiths, H. I., and Heaton, T. H. E. (2001) Historical biogeography and Late Quaternary environmental change of Lake Pamvotis, Ioannina (north-western Greece): evidence from ostracods. *Journal of Biogeography* **28** (6), 745-756.

Fronval, T., and Jansen, E. (1996) Rapid changes in ocean circulation and heat flux in the Nordic seas during the last interglacial period. *Nature* **383**, 806-810.

Gaetani, M. and Fontaine, B. (2014) Interacción entre el Monzón de África Occidental y el clima Mediterráneo en verano: Artículo de revisión. *Física de la Tierra* **25**, 41-55.

Gasse, F. (2000) Hydrological changes in the African tropics since the Last Glacial Maximum. *Quaternary Science Reviews* **19** (1-5), 189-211.

Gasse, F. and Roberts, C. N. (2004) *Late Quaternary hydrologic changes in the arid and semi-arid belt of Northern Africa*. *In* Diaz, H. F., and Bradley, R. S. (eds.) *The Hadley circulation: present, past and future*, London, Kluwer Academic Publishers, p. 313-345.

Gasse, F., Vidal, L., Van Campo, E., Demory, F., Develle, A.-L., Tachikawa, K., Elias, A., Bard, E., Garcia, M., Sonzogni, C., and Thouveny, N. (2015) Hydroclimatic changes in northern Levant over the past 400,000 years. *Quaternary Science Reviews* **111**, 1-8.

Gat, J. R., Klein, B., Kushnir, Y., Roether, W., Wernli, H., Yam, R., and Shemesh, A. (2003) Isotope composition of air moisture over the Mediterranean Sea: an index of the air–sea interaction. *Tellus* **55B**, 959-965.

Giaccio, B., Isaia, R., Sulpizio, R., and Zanchetta, G. (2008) Explosive volcanism in the central Mediterranean area during the late Quaternary-linking sources and distal archives. *Journal of Volcanology and Geothermal Research* **177** (1), v-vii.

Gibson, J. J., Birks, S. J., and Yi, Y. (2015) Stable isotope mass balance of lakes: a contemporary perspective. *Quaternary Science Reviews*.

Gibson, J. J., Prepas, E. E., and McEachern, P. (2002) Quantitative comparison of lake throughflow, residency, and catchment runoff using stable isotopes: modelling and results from a regional survey of Boreal lakes. *Journal of Hydrology* **262** (1-4), 128-144.

Gierlowski-Kordesch, E. H. and Park, L. E. (2004) Comparing species diversity in the modern and fossil record of lakes. *Journal of Geology* **112** (6), 703-717.

Giorgi, F. (2006) Climate change hot-spots. *Geophysical Research Letters* **33** (8).

Glavinov, A. (2012) Climate vulnerability assessment for Republic of Macedonia, SEEFCCA, Macedonia.

Gogou, A., Bouloubassi, I., Lykousis, V., Arnaboldi, M., Gaitani, P., and Meyers, P. A. (2007) Organic geochemical evidence of Late Glacial−Holocene climate instability in the North Aegean Sea. *Palaeogeography, Palaeoclimatology, Palaeoecology* **256** (1-2), 1-20.

Gorthner, A. (1994) What is an ancient lake? *Archiv Für Hydrobiologie* **44**, 97-100.

Goudeau, M. L. S., Reichart, G. J., Wit, J. C., de Nooijer, L. J., Grauel, A. L., Bernasconi, S. M., and de Lange, G. J. (2015) Seasonality variations in the Central Mediterranean during climate change events in the Late Holocene. *Palaeogeography, Palaeoclimatology, Palaeoecology* **418**, 304-318.

Granina, L., Müller, B., and Wehrli, B. (2004) Origin and dynamics of Fe and Mn sedimentary layers in Lake Baikal. *Chemical Geology* **205** (1-2), 55-72.

Grant, K. M., Rohling, E. J., Bar-Matthews, M., Ayalon, A., Medina-Elizalde, M., Ramsey, C. B., Satow, C., and Roberts, A. P. (2012) Rapid coupling between ice volume and polar temperature over the past 150,000 years. *Nature* **491**, 744-747.

Hadzisce, S. (1966) Das Mixophänomen im Ohridsee im Laufe der Jahre 1941/42−1964/65. *Verhandlungen des Internationalen Verein Limnologie* **16**, 134-138.

Hammarlund, D., Aravena, R., Barnekow, L., Buchardt, B., and Possnert, G. (1997) Multi-component carbon isotope evidence of early Holocene environmental change and carbon-flow pathways from a hard-water lake in northern Sweden. *Journal of Paleolimnology* **18** (3), 219-233.

Hammer, Ø., Harper, D. A. T., and Ryan, P. D. (2001) PAST: Paleontological statistics software package for education and data analysis. *Palaeontologia Electronica* **4** (1), 9.

Hao, Q., Wang, L., Oldfield, F., and Guo, Z. (2015) Extra-long interglacial in Northern Hemisphere during MISs 15-13 arising from limited extent of Arctic ice sheets in glacial MIS 14. *Science Reports* **5**, 12103.

Hare, A. A., Kuzyk, Z. Z. A., Macdonald, R. W., Sanei, H., Barber, D., Stern, G. A., and Wang, F. (2014) Characterization of sedimentary organic matter in recent marine sediments from Hudson Bay, Canada, by Rock-Eval pyrolysis. *Organic Geochemistry* **68**, 52-60.

Harms, U., Koeberl, C., and Zoback, M. D. (2007) *Continental Scientific Drilling: A Decade of Progress, and Challenges for the Future*, Springer-Verlag Berlin Heidelberg.

Heymann, C., Nelle, O., Dörfler, W., Zagana, H., Nowaczyk, N., Xue, J., and Unkel, I. (2013) Late Glacial to mid-Holocene palaeoclimate development of Southern Greece inferred from the sediment sequence of Lake Stymphalia (NE-Peloponnese). *Quaternary International* **302**, 42-60.

Hodell, D. A., and Schelske, C. L. (1998) Production, sedimentation, and isotopic composition of organic matter in Lake Ontario. *Limnology and Oceanography* **43** (2), 200-214.

Hoefs, J. (1980) *Stable Isotope Geochemistry*, Berlin, Springer-Verlag.

Hoefs, J. (2009) *Stable Isotope Geochemistry*, Berlin, Springer-Verlag.

Hoelzmann, P., Jolly, D., Harrison, S. P., Laarif, F., Bonnefille, R., and Pachur, H. J. (1998) Mid-Holocene land-surface conditions in northern Africa and the Arabian Peninsula: A data set for the analysis of biogeophysical feedbacks in the climate system. *Global Biogeochemical Cycles* **12** (1), 35-51.

Hoffman, J. S., Carlson, A. E., Winsor, K., Klinkhammer, G. P., LeGrande, A. N., Andrews, J. T., and Strasser, J. C. (2012) Linking the 8.2 ka event and its freshwater forcing in the Labrador Sea. *Geophysical Research Letters* **39,** L18703, 1-5.

Hoffmann, N., Reicherter, K., Fernández-Steeger, T., and Grützner, C. (2010) Evolution of ancient Lake Ohrid: a tectonic perspective. *Biogeosciences* **7** (10), 3377-3386.

Hollis, G. E., and Stevenson, A. C. (1997) The physical basis of the Lake Mikri Prespa systems: geology, climate, hydrology and water quality. *Hydrobiologia* **351**, 1-19.

Holtvoeth, J., Rushworth, D., Imeri, A., Cara, M., Vogel, H., Wagner, T., and Wolff, G. A. (2015) Improved end-member characterization of modern organic matter pools in the Ohrid Basin (Albania, Macedonia) and evaluation of new palaeoenvironmental proxies. *Biogeosciences Discussions* **12** (15), 12975-13039.

Holtvoeth, J., Vogel, H., Wagner, B., and Wolff, G. A. (2010) Lipid biomarkers in Holocene and glacial sediments from ancient Lake Ohrid (Macedonia, Albania). *Biogeosciences* **7** (11), 3473-3489.

Horita, J., and Wesolowski, D. J. (1994) Liquid-vapor fractionation of oxygen and hydrogen isotopes of water from the freezing to the critical temperature. *Geochimica et Cosmochimica Acta* **58** (16), 3425-3437.

Hudson, J. D. (1977) Stable isotopes and limestone lithification. *Journal of the Geological Society* **133** (6), 637-660.

Hurrell, J. W. (1995) Decadal Trends in the North Atlantic Oscillation: Regional Temperatures and Precipitation. *Science* **269**, 676-679.

Hurrell, J. W. (1996) Influence of variations in extratropical wintertime teleconnections on northern hemisphere temperature. *Geophysical Research Letters* **23** (6), 665-668.

Hurrell, J. W., and Deser, C. (2009) North Atlantic climate variability: The role of the North Atlantic Oscillation. *Journal of Marine Systems* **78** (1), 28-41.

Hurrell, J. W. and Dickson, R. R. (2005) *Climate variability over the North Atlantic*. *In* Stenseth, N. C., Ottersen, G., Hurrell, J. W., and Belgrano, A. (eds.) *Marine Ecosystems and Climate Variation*, Oxford University Press, p. 15-31.

Hurrell, J. W., Hoerling, M. P., and Folland, C. K. (2002) *Climatic variability over the North Atlantic*. *In* Pearce, R. P. (ed.) *International Geophysics*, Volume 83, Academic Press, p. 143-151.

Hurrell, J. W., Kushnir, Y., Ottersen, G., and Visbeck, M. (2003) *An overview of the North Atlantic Oscillation*), *The North Atlantic Oscillation: Climatic Significance and Environmental Impact*, Volume 134, Washington, DC, AGU, p. 1-35.

Imbrie, J., Hays, J. D., Martinson, D. G., McIntyre, A., Mix, A. C., Morley, J. J., Pisias, N. G., Prell, W. L., and Shackleton, N. (1984) *The orbital theory of Pleistocene climate : support from a revised chronology of the marine* δ^{18}*O record*. *In* Berger, A., Imbrie, J., Hays, H., Kukla, G., and Saltzman, B., (eds.) *Milankovitch and Climate (Part 1)*, Hingham, Mass., Reidel, p. 269–305.

Ito, E. (2001) *Application Of Stable Isotope Techniquesto Inorganic And Biogenic Carbonates*. *In* Last, W. and Smol, J. (eds.) *Tracking Environmental Change Using Lake Sediments*, Volume 2, Springer Netherlands, p. 351-371.

Jasechko, S., Gibson, J. J., and Edwards, T. W. D. (2014) Stable isotope mass balance of the Laurentian Great Lakes. *Journal of Great Lakes Research* **40** (2), 336-346.

Jin, L., Ogrinc, N., Hamilton, S. K., Szramek, K., Kanduc, T., and Walter, L. M. (2009) Inorganic carbon isotope systematics in soil profiles undergoing silicate and carbonate weathering (Southern Michigan, USA). *Chemical Geology* **264** (1-4), 139-153.

Joannin, S., Brugiapaglia, E., de Beaulieu, J. L., Bernardo, L., Magny, M., Peyron, O., Goring, S., and Vannière, B. (2012) Pollen-based reconstruction of Holocene vegetation and climate in southern Italy: the case of Lago Trifoglietti. *Climate of the Past* **8** (6), 1973-1996.

Johnsen, S. J., Clausen, H. B., Dansgaard, W., Fuhrer, K., Gundestrup, N., Hammer, C. U., Iversen, P., Jouzel, J., Stauffer, B., and steffensen, J. P. (1992) Irregular glacial interstadials recorded in a new Greenland ice core. *Nature* **359**, 311-313.

Johnson, T. C., Scholz, C. A., Talbot, M. R., Kelts, K., Ricketts, R. D., Ngobi, G., Beuning, K., Ssemmanda, I., and McGill, J. W. (1996) Late Pleistocene Desiccation of Lake Victoria and Rapid Evolution of Cichlid Fishes. *Science* **273**, 1091-1093.

Jones, M. D., Cuthbert, M. O., Leng, M. J., McGowan, S., Mariethoz, G., Arrowsmith, C., Sloane, H. J., Humphrey, K. K., and Cross, I. (2015) Comparisons of observed and modelled lake δ^{18}O variability. *Quaternary Science Reviews*, 1-12.

Jones, M. D., Roberts, C. N., and Leng, M. J. (2007) Quantifying climatic change through the last glacial–interglacial transition based on lake isotope palaeohydrology from central Turkey. *Quaternary Research* **67** (3), 463-473.

Jones, M. D., Roberts, C. N., Leng, M. J., and Türkeş, M. (2006) A high-resolution late Holocene lake isotope record from Turkey and links to North Atlantic and monsoon climate. *Geology* **34** (5), 361.

Jones, T. D., Lawson, I. T., Reed, J. M., Wilson, G. P., Leng, M. J., Gierga, M., Bernasconi, S. M., Smittenberg, R. H., Hajdas, I., Bryant, C. L., and Tzedakis, P. C. (2013) Diatom-inferred Late Pleistocene and Holocene palaeolimnological changes in the Ioannina basin, northwest Greece. *Journal of Paleolimnology* **49**, 185-204.

Jordanoska, B., Kunz, M. J., Stafilov, T., and Wuest, A. (2010) Temporal variability in physico-chemical properties of St. Naum karst springs feeding Lake Ohrid. *Ecology and Protection of the Environment* **13** (1-2), 3-11.

Jouzel, J., Masson-Delmotte, V., Cattani, O., Dreyfus, G., Falourd, S., Hoffmann, G., Minster, B., Nouet, J., Barnola, J. M., Chappellaz, J., Fischer, H., Gallet, J. C., Johnsen, S., Leuenberger, M., Loulergue, L., Luethi, D., Oerter, H., Parrenin, F., Raisbeck, G., Raynaud, D., Schilt, A., Schwander, J., Selmo, E., Souchez, R., Spahni, R., Stauffer, B., Steffensen, J. P., Stenni, B., Stocker, T. F., Tison, J. L., Werner, M., and Wolff, E. W. (2007) Orbital and Millennial Antarctic Climate Variability over the Past 800,000 Years. *Science* **317**, 793-796.

Juggins, S. (2015) Rioja: an R Package for the Analysis of Quaternary Science Data, Version 0.9-5 <https://cran.r-project.org/web/packages/rioja/citation.html>

Kallel, N., Paterne, M., Duplessy, J. C., Vergnaud-Grazzini, C., Pujol, C., Labeyrie, L., Arnold, M., Fontugne, M., and Pierre, C. (1997) Enhanced rainfall in the Mediterranean region during the last Sapropel Event. *Oceanologica Acta* **20** (5), 697-712.

Kaniewski, D., Van Campo, E., Paulissen, E., Weiss, H., Bakker, J., Rossignol, I., and Van Lerberghe, K. (2011) The medieval climate anomaly and the little Ice Age in coastal Syria inferred from pollen-derived palaeoclimatic patterns. *Global and Planetary Change* **78** (3-4), 178-187.

Katsuta, N., Takano, M., Kawakami, S.-i., Togami, S., Fukusawa, H., Kumazawa, M., and Yasuda, Y. (2006) Climate system transition from glacial to interglacial state around the beginning of the last termination: Evidence from a centennial- to millennial-scale climate rhythm. *Geochemistry, Geophysics, Geosystems* **7** (12), Q12006.

Kawanabe, H., Nishino, M., and Maehata, M. (2012) *Lake Biwa: Interactions between Nature and People*, Springer Netherlands.

Kim, S.-T., O’Neil, J. R., Hillaire-Marcel, C., and Mucci, A. (2007) Oxygen isotope fractionation between synthetic aragonite and water: Influence of temperature and Mg2+ concentration. *Geochimica et Cosmochimica Acta* **71** (19), 4704-4715.

Kim, S. T., and O'Neil, J. R. (1997) Equilibrium and nonequilibrium oxygen isotope effects in synthetic carbonates. *Geochimica et Cosmochimica Acta* **61** (16), 3461-3475.

Köppen, W. (1900) Versuch einer Klassifikation der Klimate, vorzugsweise nach ihren Beziehungen zur Pflanzenwelt. *Geographische Zeitschrift* **6**, 593-611.

Kostoski, G., Albrecht, C., Trajanovski, S., and Wilke, T. (2010) A freshwater biodiversity hotspot under pressure − assessing threats and identifying conservation needs for ancient Lake Ohrid. *Biogeosciences* **7** (12), 3999-4015.

Kotthoff, U., Koutsodendris, A., Pross, J., Schmiedl, G., Bornemann, A., Kaul, C., Marino, G., Peyron, O., and Schiebel, R. (2011) Impact of Lateglacial cold events on the northern Aegean region reconstructed from marine and terrestrial proxy data. *Journal of Quaternary Science* **26** (1), 86-96.

Kotthoff, U., Muller, U. C., Pross, J., Schmiedl, G., Lawson, I. T., van de Schootbrugge, B., and Schulz, H. (2008a) Lateglacial and Holocene vegetation dynamics in the Aegean region: an integrated view based on pollen data from marine and terrestrial archives. *The Holocene* **18** (7), 1019-1032.

Kotthoff, U., Pross, J., Müller, U. C., Peyron, O., Schmiedl, G., Schulz, H., and Bordon, A. (2008b) Climate dynamics in the borderlands of the Aegean Sea during formation of sapropel S1 deduced from a marine pollen record. *Quaternary Science Reviews* **27** (7-8), 832-845.

Krylov, A., Khlystov, O., Zemskaya, T., Minami, H., Hachikubo, A., Nunokawa, Y., Kida, M., Shoji, H., Naudts, L., Poort, J., and Pogodaeva, T. (2008) First discovery and formation process of authigenic siderite from gas hydrate‒bearing mud volcanoes in fresh water: Lake Baikal, eastern Siberia. *Geophysical Research Letters* **35** (5).

Kuglitsch, F. G., Toreti, A., Xoplaki, E., Della-Marta, P. M., Zerefos, C. S., Türkeş, M., and Luterbacher, J. (2010) Heat wave changes in the eastern Mediterranean since 1960. *Geophysical Research Letters* **37** (4), L04802.

Kuper, R., and Kröpelin, S. (2006) Climate-controlled Holocene occupation in the Sahara: Motor of Aftica's evolution. *Science* **313**, 803-807.

Kwiecien, O., Stockhecke, M., Pickarski, N., Heumann, G., Litt, T., Sturm, M., Anselmetti, F., Kipfer, R., and Haug, G.H. (2014) Dynamics of the last four glacial terminations recorded in Lake Van, Turkey. *Quaternary Science Reviews* **104**, 42-52.

Lacey, J. H., Francke, A., Leng, M. J., Vane, C. H., and Wagner, B. (2015a) A high-resolution Late Glacial to Holocene record of environmental change in the Mediterranean from Lake Ohrid (Macedonia/Albania). *International Journal of Earth Sciences* **104** (6), 1623-1638.

Lacey, J. H., Leng, M. J., Francke, A., Sloane, H. J., Milodowski, A., Vogel, H., Baumgarten, H., and Wagner, B. (2015b) Mediterranean climate since the Middle Pleistocene: a 640 ka stable isotope record from Lake Ohrid (Albania/Macedonia). *Biogeosciences Discussions* **12** (16), 13427-13481.

Lamb, H. F., Eicher, U., and Switsur, V. R. (1989) An 18 000-year record of vegetation, lake-level and climatic change from Tigalmamine, Middle Atlas, Morocco. *Journal of Biogeography* **16** (1), 65-74.

Lambevska, V. (2011) *The impact of climate change on food production in the former Yugoslav Republic of Macedonia*): *The impacts of climate change on food production in the Western Balkan RegionI,* Regional Environmental Center for Central and Eastern Europe, p. 62-80.

Lang, N. and Wolff, E. W. (2011) Interglacial and glacial variability from the last 800 ka in marine, ice and terrestrial archives. *Climate of the Past* **7**, 361-380.

Langford, F. F., and Blanc-Valleron, M. M. (1990) Interpreting Rock- Eval Pyrolisis data using graphs of pyrolizable hydrocarbons vs. total organic carbon. *AAPG Bulletin* **74** (6), 799-804.

Laskar, J., Robutel, P., Joutel, F., Gastineau, M., Correia, A. C. M., and Levrard, B. (2004) A long-term numerical solution for the insolation quantities of the Earth. *Astronomy & Astrophysics* **428**, 261-285.

Lawson, I., Frogley, M., Bryant, C., Preece, R., and Tzedakis, P. (2004) The Lateglacial and Holocene environmental history of the Ioannina basin, north-west Greece. *Quaternary Science Reviews* **23** (14-15), 1599-1625.

Lawson, I. T., Tzedakis, P. C., Roucoux, K. H., Galanidou, N., and Williams, J. (2013) The anthropogenic influence on wildfire regimes: charcoal records from the Holocene and Last Interglacial at Ioannina, Greece. *Journal of Biogeography* **40** (12), 2324-2334.

Le Bas, M. J., Le Maitre, R. W., Streckeisen, A., and Zanettin, B. (1986) A chemical classification of volcanic rocks based on the total alkali-silica diagram. *Journal of Petrology* **27**, 745-750.

Lebeau, O., Busigny, V., Chaduteau, C., and Ader, M. (2014) Organic matter removal for the analysis of carbon and oxygen isotope compositions of siderite. *Chemical Geology* **372**, 54-61.

LeGrande, A. N. and Schmidt, G. A. (2006) Global gridded data set of the oxygen isotopic composition in seawater. *Geophysical Research Letters* **33** (12).

Leicher, N., Zanchetta, G., Sulpizio, R., Giaccio, B., Francke, A., and Wagner, B. (2015) Mid-Pleistocene to Holocene sedimentation at Lake Ohrid (Macedonia, Albania) derived from lithologic and geochemical data. *Biogeosciences Discussions*, **12**, 15411-15460.

Lelieveld, J., Hadjinicolaou, P., Kostopoulou, E., Chenoweth, J., Maayar, M., Giannakopoulos, C., Hannides, C., Lange, M. A., Tanarhte, M., Tyrlis, E., and Xoplaki, E. (2012) Climate change and impacts in the Eastern Mediterranean and the Middle East. *Climatic Change* **114** (3-4), 667-687.

Leng, M. J., Baneschi, I., Zanchetta, G., Jex, C. N., Wagner, B., and Vogel, H. (2010a) Late Quaternary palaeoenvironmental reconstruction from Lakes Ohrid and Prespa (Macedonia/Albania border) using stable isotopes. *Biogeosciences* **7** (10), 3109-3122.

Leng, M. J., Jones, M. D., Frogley, M. R., Eastwood, W. J., Kendrick, C. P., and Roberts, C. N. (2010b) Detrital carbonate influences on bulk oxygen and carbon isotope composition of lacustrine sediments from the Mediterranean. *Global and Planetary Change* **71** (3-4), 175-182.

Leng, M. J., Lamb, A. L., Heaton, T. H. E., Marshall, J. D., Wolfe, B. B., Jones, M. D., Holmes, J. A., and Arrowsmith, C. (2006) *Isotopes in Palaeoenvironmental Research: 4. Isotopes in Lake Sediments*, Netherlands, Springer.

Leng, M. J., and Marshall, J. D. (2004) Palaeoclimate interpretation of stable isotope data from lake sediment archives. *Quaternary Science Reviews* **23** (7-8), 811-831.

Leng, M. J., Roberts, N., Reed, J. M., and Sloane, H. J. (1999) Late Quaternary palaeohydrology of the Konya Basin, Turkey, based on isotope studies of modern hydrology and lacustrine carbonates. *Journal of Paleolimnology* **22** (2), 187-204.

Leng, M. J., Wagner, B., Boehm, A., Panagiotopoulos, K., Vane, C. H., Snelling, A., Haidon, C., Woodley, E., Vogel, H., Zanchetta, G., and Baneschi, I. (2013) Understanding past climatic and hydrological variability in the Mediterranean from Lake Prespa sediment isotope and geochemical record over the Last Glacial cycle. *Quaternary Science Reviews* **66**, 123-136.

Leuenberger, M. C., Lang, C., and Schwander, J. (1999) Delta 15N measurements as a calibration tool for the paleothermometer and gas-ice age differences: A case study for the 8200 B.P. event on GRIP ice. *Journal of Geophysical Research: Atmospheres* **104** (18), 22163-22170.

Lewis, C. F. M., Miller, A. A. L., Levac, E., Piper, D. J. W., and Sonnichsen, G. V. (2012) Lake Agassiz outburst age and routing by Labrador Current and the 8.2 cal ka cold event. *Quaternary International* **260**, 83-97.

Lézine, A. M., von Grafenstein, U., Andersen, N., Belmecheri, S., Bordon, A., Caron, B., Cazet, J. P., Erlenkeuser, H., Fouache, E., Grenier, C., Huntsman-Mapila, P., Hureau-Mazaudier, D., Manelli, D., Mazaud, A., Robert, C., Sulpizio, R., Tiercelin, J. J., Zanchetta, G., and Zeqollari, Z. (2010) Lake Ohrid, Albania, provides an exceptional multi-proxy record of environmental changes during the last glacial−interglacial cycle. *Palaeogeography, Palaeoclimatology, Palaeoecology* **287** (1-4), 116-127.

Li, H. C. and Ku, T. L. (1997) δ^{13}C-δ^{18}O covariance as a paleohydrological indicator for closed-basin lakes. *Palaeogeography, Palaeoclimatology, Palaeoecology* **133** (1-2), 69-80.

Linacre, E. (1992), *Climate Data and Resources: A Reference and Guide*, London, Routledge.

Lindhorst, K., Vogel, H., Krastel, S., Wagner, B., Hilgers, A., Zander, A., Schwenk, T., Wessels, M., and Daut, G. (2010) Stratigraphic analysis of lake level fluctuations in Lake Ohrid: an integration of high resolution hydro-acoustic data and sediment cores. *Biogeosciences Discussions* **7** (3), 3651-3689.

Lindhorst, K., Krastel, S., Reicherter, K., Stipp, M., Wagner, B., and Schwenk, T. (2015) Sedimentary and tectonic evolution of Lake Ohrid (Macedonia/Albania). *Basin Research* **27**, 84-101.

Lionello, P., Abrantes, F., Voelker, A., Sierro, F. J., Naughton, F., Rodrigues, T., Cacho, I., Ariztegui, D., Brayshaw, D., Sicre, M.-A., and Batista, L. (2012) *1 - Paleoclimate Variability in the Mediterranean Region*. *In* Lionello, P. (ed.) *The Climate of the Mediterranean Region*, Oxford, Elsevier, p. 1-86.

Lisiecki, L. E., and Raymo, M. E. (2005) A Pliocene-Pleistocene stack of 57 globally distributed benthic δ^{18}O records. *Paleoceanography* **20** (1), PA1003.

Litt, T. and Anselmetti, F. S. (2014). Lake Van deep drilling project PALEOVAN. *Quaternary Science Reviews* **104**, 1-7.

Litt, T., Pickarski, N., Heumann, G., Stockhecke, M., and Tzedakis, P. C. (2014) A 600,000 year long continental pollen record from Lake Van, eastern Anatolia (Turkey). *Quaternary Science Reviews* **104**, 30-41.

Lojka, R., Drábková, J., Zajíc, J., Sýkorová, I., Franců, J., Bláhová, A., and Grygar, T. (2009) Climate variability in the Stephanian B based on environmental record of the Mšec Lake deposits (Kladno−Rakovník Basin, Czech Republic). *Palaeogeography, Palaeoclimatology, Palaeoecology* **280** (1-2), 78-93.

Lorenschat, J., Zhang, X., Anselmetti, F. S., Reed, J. M., Wessels, M., and Schwalb, A. (2014) Recent anthropogenic impact in ancient Lake Ohrid (Macedonia/Albania): a palaeolimnological approach. *Journal of Paleolimnology*, **6**, 524-550.

Loulergue, L., Schilt, A., Spahni, R., Masson-Delmotte, V., Blunier, T., Lemieux, B., Barnola, J. M., Raynaud, D., Stocker, T. F., and Chappellaz, J. (2008) Orbital and millennial-scale features of atmospheric CH4 over the past 800,000 years. *Nature* **453**, 383-386.

Ludvigson, G. A., González, L. A., Fowle, D. A., Roberts, J. A., Driese, S. G., Villarreal, M. A., Smith, J. J., and Suarez, M. B. (2013) *Paleoclimatic Applications and Modern Process Studies of Pedogenic Siderite*), *New Frontiers in Paleopedology and Terrestrial Paleoclimatology*, Volume 104, SEPM (Society for Sedimentary Geology), p. 79-87.

Lüthi, D., Le Floch, M., Bereiter, B., Blunier, T., Barnola, J. M., Siegenthaler, U., Raynaud, D., Jouzel, J., Fischer, H., Kawamura, K., and Stocker, T. F. (2008) High-resolution carbon dioxide concentration record 650,000-800,000 years before present. *Nature* **453**, 379-382.

Macedonio, G., Pareschi, M. T., and Santacroce, R. (1988) A numerical simulation of the Plinian Fall Phase of 79 A.D. eruption of Vesuvius. *Journal of Geophysical Research: Solid Earth* **93** (B12), 14817-14827.

Mackay, A. W., M.B., E., and Khursevich, G. (2010) *Diatoms in ancient lakes*. *In* Smol, J. P., and Stoermer, E. F. (eds.) *The Diatoms: Applications for the Environmental and Earth Sciences*, Cambridge University Press, p. 209-228.

Magny, M., Bégeot, C., Guiot, J., and Peyron, O. (2003) Contrasting patterns of hydrological changes in europe in response to holocene climate cooling phases. *Quaternary Science Reviews* **22** (15-17), 1589-1596.

Magny, M., de Beaulieu, J.-L., Drescher-Schneider, R., Vannière, B., Walter-Simonnet, A.-V., Miras, Y., Millet, L., Bossuet, G., Peyron, O., Brugiapaglia, E., and Leroux, A. (2007) Holocene climate changes in the central Mediterranean as recorded by lake-level fluctuations at Lake Accesa (Tuscany, Italy). *Quaternary Science Reviews* **26** (13−14), 1736-1758.

Magny, M., Vannière, B., Zanchetta, G., Fouache, E., Touchais, G., Petrika, L., Coussot, C., Walter-Simonnet, A. V., and Arnaud, F. (2009) Possible complexity of the climatic event around 4300-3800 cal. BP in the central and western Mediterranean. *Holocene* **19** (6), 823-833.

Magny, M., Bossuet, G., Ruffaldi, P., Leroux, A., and Mouthon, J. (2011a) Orbital imprint on Holocene palaeohydrological variations in west-central Europe as reflected by lake-level changes at Cerin (Jura Mountains, eastern France). *Journal of Quaternary Science* **26** (2), 171-177.

Magny, M., Vannière, B., Calo, C., Millet, L., Leroux, A., Peyron, O., Zanchetta, G., La Mantia, T., and Tinner, W. (2011b) Holocene hydrological changes in south-western Mediterranean as recorded by lake-level fluctuations at Lago Preola, a coastal lake in southern Sicily, Italy. *Quaternary Science Reviews* **30** (19-20), 2459-2475.

Magny, M., Joannin, S., Galop, D., Vannière, B., Haas, J. N., Bassetti, M., Bellintani, P., Scandolari, R., and Desmet, M. (2012a) Holocene palaeohydrological changes in the northern Mediterranean borderlands as reflected by the lake-level record of Lake Ledro, northeastern Italy. *Quaternary Research* **77** (3), 382-396.

Magny, M., Leroux, A., Bichet, V., Gauthier, E., Richard, H., and Walter-Simonnet, A. V. (2012b) Climate, vegetation and land use as drivers of Holocene sedimentation: A case study from Lake Saint-Point (Jura Mountains, eastern France). *The Holocene* **23** (1), 137-147.

Magny, M., Combourieu-Nebout, N., de Beaulieu, J. L., Bout-Roumazeilles, V., Colombaroli, D., Desprat, S., Francke, A., Joannin, S., Ortu, E., Peyron, O., Revel, M., Sadori, L., Siani, G., Sicre, M. A., Samartin, S., Simonneau, A., Tinner, W., Vannière, B., Wagner, B., Zanchetta, G., Anselmetti, F., Brugiapaglia, E., Chapron, E., Debret, M., Desmet, M., Didier, J., Essallami, L., Galop, D., Gilli, A., Haas, J. N., Kallel, N., Millet, L., Stock, A., Turon, J. L., and Wirth, S. (2013) North-south palaeohydrological contrasts in the central Mediterranean during the Holocene: tentative synthesis and working hypotheses. *Climate of the Past* **9** (5), 2043-2071.

Maiorano, P., Tarantino, F., Marino, M., and De Lange, G. J. (2013) Paleoenvironmental conditions at Core KC01B (Ionian Sea) through MIS 13−9: Evidence from calcareous nannofossil assemblages. *Quaternary International* **288**, 97-111.

Mann, M. E. (2002) Large-Scale Climate Variability and Connections with the Middle East in Past Centuries. *Climatic Change* **55** (3), 287-314.

Marchant, R., and Hooghiemstra, H. (2004) Rapid environmental change in African and South American tropics around 4000 years before present: a review. *Earth-Science Reviews* **66** (3-4), 217-260.

Marino, G., Rohling, E. J., Rodriguez-Sanz, L., Grant, K. M., Heslop, D., Roberts, A. P., Stanford, J. D., and Yu, J. (2015) Bipolar seesaw control on last interglacial sea level. *Nature* **522**, 197-201.

Marino, G., Rohling, E. J., Sangiorgi, F., Hayes, A., Casford, J. L., Lotter, A. F., Kucera, M., and Brinkhuis, H. (2009) Early and middle Holocene in the Aegean Sea: interplay between high and low latitude climate variability. *Quaternary Science Reviews* **28** (27-28), 3246-3262.

Martens, K. (1997) Speciation in ancient lakes. *Trends in Ecology & Evolution* **12** (5), 177-182.

Martrat, B., Grimalt, J. O., Lopez-Martinez, C., Cacho, I., Sierro, F. J., Flores, J. A., Zahn, R., Canals, M., Curtis, J. H., and Hodell, D. A. (2004) Abrupt temperature changes in the Western Mediterranean over the past 250,000 years. *Science* **306**, 1762-1765.

Martrat, B., Grimalt, J. O., Shackleton, N. J., De Abreu, L., Hutterli, M. A., and Stocker, T. F. (2007) Four Climate Cycles of Recurring Deep and Surface Water Destabilizations on the Iberian Margin. *Science* **27**, 502-507.

Martrat, B., Jimenez-Amat, P., Zahn, R., and Grimalt, J. O. (2014) Similarities and dissimilarities between the last two deglaciations and interglaciations in the North Atlantic region. *Quaternary Science Reviews* **99**, 122-134.

Matter, M., Anselmetti, F. S., Jordanoska, B., Wagner, B., Wessels, M., and Wüest, A. (2010) Carbonate sedimentation and effects of eutrophication observed at the Kališta subaquatic springs in Lake Ohrid (Macedonia). *Biogeosciences* **7** (11), 3755-3767.

Matzinger, A., Jordanoski, M., Veljanoska-Sarafiloska, E., Sturm, M., Müller, B., and Wüest, A. (2006a) Is Lake Prespa Jeopardizing the Ecosystem of Ancient Lake Ohrid? *Hydrobiologia* **553** (1), 89-109.

Matzinger, A., Schmid, M., Veljanoska-Sarafiloska, E., Patceva, S., Guseska, D., Wagner, B., Müller, B., Sturm, M., and Wüest, A. (2007) Eutrophication of ancient Lake Ohrid: Global warming amplifies detrimental effects of increased nutrient inputs. *Limnology and Oceanography* **52** (1), 338-353.

Matzinger, A., Spirkovski, Z., Patceva, S., and Wüest, A. (2006b) Sensitivity of Ancient Lake Ohrid to Local Anthropogenic Impacts and Global Warming. *Journal of Great Lakes Research* **32** (1), 158-179.

Mayer, B. and Schwark, L. (1999) A 15,000-year stable isotope record from sediments of Lake Steisslingen, Southwest Germany. *Chemical Geology* **161**, 315-337.

McCrea, J. M. (1950) On the Isotopic Chemistry of Carbonates and a Paleotemperature Scale. *The Journal of Chemical Physics* **18** (6), 849.

McKenzie, J. A. (1985) *Carbon isotopes and productivity in the lacustrine and marine environment*. *In* Stumm, W. (ed.) *Chemical Processes in Lakes*, New York, Wiley.

McManus, J. F. (1999) A 0.5-Million-Year Record of Millennial-Scale Climate Variability in the North Atlantic. *Science* **283**, 971-975.

NGRIP Members (2004) High-resolution record of Northern Hemisphere climate extending into the last interglacial period. *Nature* **431**, 147-151.

Mercone, D., Thomson, J., Croudace, I. W., Siani, G., Paterne, M., and Troelstra, S. R. (2000) Duration of S1, the most recent sapropel in the eastern Mediterranean Sea, as indicated by accelerator mass spectrometry radiocarbon and geochemical evidence *Paleoceanography* **15** (3), 336-347.

Meyers, P. A. (1994) Preservation of Elemental and Isotopic Source Identification of Sedimentary Organic-Matter. *Chemical Geology* **114** (3-4), 289-302.

Meyers, P. A. (1997) Organic geochemical proxies of paleoceanographic, paleolimnologic, and paleoclimatic processes. *Organic Geochemistry* **27** (5-6), 213-250.

Meyers, P. A. (2003) Applications of organic geochemistry to paleolimnological reconstructions: a summary of examples from the Laurentian Great Lakes. *Organic Geochemistry* **34** (2), 261-289.

Meyers, P. A. and Ishiwatari, R. (1993) Lacustrine organic geochemistryman overview of indicators of organic matter sources and diagenesis in lake sediments. *Organic Geochemistry* **20** (7), 867-900.

Meyers, P. A. and Lallier-Verges, E. (1999) Lacustrine sedimentary organic matter records of Late Quaternary paleoclimates. *Journal of Paleolimnology* **21** (3), 345-372.

Meyers, P. A. and Teranes, J. L. (2001) *Sediment Organic Matter*. *In* Last, W. M. and Smol, J. P. (eds.) *Tracking Environmental Change Using Lake Sediments*, Volume 2, Springer Netherlands, p. 239-269.

Meyers, P. A., Leenheer, M. J., and Bourbonniere, R. A. (1995) Diagenesis of Vascular Plant Organic Matter Components during Burial in Lake Sediments. *Aquatic Geochemistry* **1**, 35-52.

Miller, G. H., Geirsdóttir, Á., Zhong, Y., Larsen, D. J., Otto-Bliesner, B. L., Holland, M. M., Bailey, D. A., Refsnider, K. A., Lehman, S. J., Southon, J. R., Anderson, C., Björnsson, H., and Thordarson, T. (2012) Abrupt onset of the Little Ice Age triggered by volcanism and sustained by sea-ice/ocean feedbacks. *Geophysical Research Letters* **39** (2), L02708.

Mook, W. G., Bommerson, J. C., and Staverman, W. H. (1974) Carbon isotope fractionation between dissolved bicarbonate and gaseous carbon dioxide. *Earth and Planetary Science Letters* **22** (2), 169-176.

Morrill, C. (2005) How widespread were climate anomalies 8200 years ago? *Geophysical Research Letters* **32** (19).

Mozley, P. S. (1989) Relation between depositional environment and the elemental composition of early diagenetic siderite. *Geology* **17**, 704-706.

Mozley, P. S. and Wersin, P. (1992) Isotopic composition of siderite as an indicator of depositional environment. *Geology* **20**, 817-820.

Muço, B., Vaccari, F., Panza, G., and Kuka, N. (2002) Seismic zonation in Albania using a deterministic approach. *Tectonophysics* **344** (3-4), 277-288.

Müller, U. C., and Sánchez Goñi, M. F. (2007) *Vegetation dynamics in southern Germany during marine isotope stage 5 (~ 130 to 70 kyr ago). In* Frank Sirocko, M. C. M. F. S. G. and Thomas, L. (eds.) *Developments in Quaternary Sciences*, Volume 7, Elsevier, p. 277-287.

Muscheler, R., Beer, J., Kubik, P. W., and Synal, H. A. (2005) Geomagnetic field intensity during the last 60,000 years based on 10Be and 36Cl from the Summit ice cores and 14C. *Quaternary Science Reviews* **24** (16-17), 1849-1860.

Muscheler, R., Beer, J., and Vonmoos, M. (2004) Causes and timing of the 8200yr BP event inferred from the comparison of the GRIP 10Be and the tree ring Δ14C record. *Quaternary Science Reviews* **23** (20-22), 2101-2111.

Naimo, D., Adamo, P., Imperato, M., and Stanzione, D. (2005) Mineralogy and geochemistry of a marine sequence, Gulf of Salerno, Italy. *Quaternary International* **140-141**, 53-63.

Nesje, A., Lie, O., and Dahl, S. O. (2000) Is the North Atlantic Oscillation reflected in Scandinavian glacier mass balance records? *Journal of Quaternary Science* **15** (6), 587-601.

O'Neil, J. R., Clayton, R. N., and Mayeda, T. K. (1969) Oxygen Isotope Fractionation in Divalent Metal Carbonates. *The Journal of Chemical Physics* **51** (12), 5547-5558.

O’Neil, J. R., Clayton, R. N., and Mayeda, T. K. (1969) Oxygen isotope fractionation in divalent metal carbonates. *Journal of Chemical Physics* **51**, 5547-5558.

Panagiotopoulos, K., Aufgebauer, A., Schäbitz, F., and Wagner, B. (2013) Vegetation and climate history of the Lake Prespa region since the Lateglacial. *Quaternary International* **293**, 157-169.

Panagiotopoulos, K., Böhm, A., Leng, M. J., Wagner, B., and Schäbitz, F. (2014) Climate variability over the last 92 ka in SW Balkans from analysis of sediments from Lake Prespa. *Climate of the Past* **10** (2), 643-660.

Patience, A. J., Lallier-Verges, E., Alberic, P., Desprairies, A., and Tribovillard, N. (1996) Relationships between organo-mineral supply and early diagenesis in the lacustrine environment: a study of surficial sediments from the Lac du Bouchet (Haute Loire, France). *Quaternary Science Reviews* **15** (2), 213-221.

Paul, H. A., Bernasconi, S. M., Schmid, D. W., and McKenzie, J. A. (2001) Oxygen isotope composition of the Mediterranean Sea since the Last Glacial Maximum: Constraints from pore water analyses. *Earth and Planetary Science Letters* **192** (1), 1-14.

Pausas, J. G. (2004) Changes in Fire and Climate in the Eastern Iberian Peninsula (Mediterranean Basin). *Climatic Change* **63** (3), 337-350.

Penman, H. L. (1948) Natural Evaporation from Open Water, Bare Soil and Grass. *Proceedings of the Royal Society of London. Series A. Mathematical and Physical Sciences* **193**, 120-145.

Petit, J. R., Jouzel, J., Raynaud, D., Barkov, N. I., Barnola, J. M., Basile, I., Bender, M., Chappellaz, J., Davis, M., Delaygue, G., Delmotte, M., Kotlyakov, V. M., Legrand, M., Lipenkov, V. Y., Lorius, C., Pepin, L., Ritz, C., Saltzman, E., and Stievenard, M. (1999) Climate and atmospheric history of the past 420,000 years from the Vostok ice core, Antarctica. *Nature* **399**, 429-436.

Peyron, O., Goring, S., Dormoy, I., Kotthoff, U., Pross, J., de Beaulieu, J. L., Drescher-Schneider, R., Vanniere, B., and Magny, M. (2011) Holocene seasonality changes in the central Mediterranean region reconstructed from the pollen sequences of Lake Accesa (Italy) and Tenaghi Philippon (Greece). *The Holocene* **21** (1), 131-146.

Peyron, O., Magny, M., Goring, S., Joannin, S., de Beaulieu, J. L., Brugiapaglia, E., Sadori, L., Garfi, G., Kouli, K., Ioakim, C., and Combourieu-Nebout, N. (2013) Contrasting patterns of climatic changes during the Holocene across the Italian Peninsula reconstructed from pollen data. *Climate of the Past* **9** (3), 1233-1252.

Philandras, C. M., Nastos, P. T., Kapsomenakis, J., Douvis, K. C., Tselioudis, G., and Zerefos, C. S. (2011) Long term precipitation trends and variability within the Mediterranean region. *Natural Hazards and Earth System Science* **11** (12), 3235-3250.

Pickarski, N., Kwiecien, O., Djamali, M., and Litt, T. (2015) Vegetation and environmental changes during the last interglacial in eastern Anatolia (Turkey): a new high-resolution pollen record from Lake Van. *Palaeogeography, Palaeoclimatology, Palaeoecology* **435**, 145-158.

Piva, A., Asioli, A., Andersen, N., Grimalt, J. O., Schneider, R. R., and Trincardi, F. (2008) Climatic cycles as expressed in sediments of the PROMESS1 borehole PRAD1-2, central Adriatic, for the last 370 ka: 2. Paleoenvironmental evolution. *Geochemistry, Geophysics, Geosystems* **9** (3), n/a-n/a.

Popovska, C. and Bonacci, O. (2007) Basic data on the hydrology of Lakes Ohrid and Prespa. *Hydrological Processes* **21** (5), 658-664.

Prokopenko, A. A., Hinnov, L. A., Williams, D. F., and Kuzmin, M. I. (2006) Orbital forcing of continental climate during the Pleistocene: a complete astronomically tuned climatic record from Lake Baikal, SE Siberia. *Quaternary Science Reviews* **25** (23-24), 3431-3457.

Pross, J., Kotthoff, U., Muller, U. C., Peyron, O., Dormoy, I., Schmiedl, G., Kalaitzidis, S., and Smith, A. M. (2009) Massive perturbation in terrestrial ecosystems of the Eastern Mediterranean region associated with the 8.2 kyr B.P. climatic event. *Geology* **37** (10), 887-890.

Pross, J., Koutsodendris, A., Christanis, K., Fischer, T., Fletcher, W. J., Hardiman, M., Kalaitzidis, S., Knipping, M., Kotthoff, U., Milner, A. M., Müller, U. C., Schmiedl, G., Siavalas, G., Tzedakis, P. C., and Wulf, S. (2015) The 1.35-Ma-long terrestrial climate archive of Tenaghi Philippon, northeastern Greece: Evolution, exploration, and perspectives for future research. *Newsletters on Stratigraphy* **48** (3), 253-276.

Rachmayani, R., Prange, M., and Schulz, M. (2015) Intra-interglacial climate variability from Marine Isotope Stage 15 to the Holocene. *Climate of the Past Discussions* **11** (4), 3071-3107.

Raicich, F., Pinardi, N., and Navarra, A. (2003) Teleconnections between Indian monsoon and Sahel rainfall and the Mediterranean. *International Journal of Climatology* **23** (2), 173-186.

Railsback, L. B., Gibbard, P. L., Head, M. J., Voarintsoa, N. R. G., and Toucanne, S. (2015) An optimized scheme of lettered marine isotope substages for the last 1.0 million years, and the climatostratigraphic nature of isotope stages and substages. *Quaternary Science Reviews* **111**, 94-106.

Ramanampisoe, L. and Disnar, J. R. (1994) Primary control of paleoproduction on organic matter preservation and accumulation in the Kimmeridge rocks of Yorkshire (UK) *Organic Geochemistry* **21** (12), 1153-1167.

Reed, J. M., Cvetkoska, A., Levkov, Z., Vogel, H., and Wagner, B. (2010) The last glacial-interglacial cycle in Lake Ohrid (Macedonia/Albania): testing diatom response to climate. *Biogeosciences* **7** (10), 3083-3094.

Reed, J. M., Stevenson, A. C., and Juggins, S. (2001) A multi-proxy record of Holocene climatic change in southwestern spain: The Laguna de Medina, Cádiz. *Holocene* **11** (6), 707-719.

Regattieri, E., Giaccio, B., Zanchetta, G., Drysdale, R. N., Galli, P., Nomade, S., Peronace, E., and Wulf, S. (2015) Hydrological variability over the Apennines during the Early Last Glacial precession minimum, as revealed by a stable isotope record from Sulmona basin, Central Italy. *Journal of Quaternary Science* **30** (1), 19-31.

Regattieri, E., Zanchetta, G., Drysdale, R. N., Isola, I., Hellstrom, J. C., and Roncioni, A. (2014) A continuous stable isotope record from the penultimate glacial maximum to the Last Interglacial (159−121ka) from Tana Che Urla Cave (Apuan Alps, central Italy). *Quaternary Research* **82** (2), 450-461.

Reicherter, K., Hoffmann, N., Lindhorst, K., Krastel, S., Fernández-Steeger, T., Grützner, C., and Wiatr, T. (2011) Active basins and neotectonics: Morphotectonics of the Lake Ohrid Basin (FYROM and Albania). *Zeitschrift der Deutschen Gesellschaft fur Geowissenschaften* **162** (2), 217-234.

Reimer, P. J., Baillie, M. G. L., Bard, E., Bayliss, A., Beck, J. W., Blackwell, P. G., Ramsey, C. B., Buck, C. E., Burr, G. S., Edwards, R. L., Friedrich, M., Grootes, P. M., Guilderson, T. P., Hajdas, I., Heaton, T. J., Hogg, A. G., Hughen, K. A., Kaiser, K. F., Kromer, B., McCormac, F. G., Manning, S. W., Reimer, R. W., Richards, D. A., Southon, J. R., Talamo, S., Turney, C. S. M., van der Plicht, J., and Weyhenmeyer, C. E. (2009) IntCal09 and Marine09 radiocarbon age calibration curves, 0-50,000 years CAL BP. *Radiocarbon* **51** (4), 1111-1150.

Reimer, P. J., Bard, E., Bayliss, A., Beck, J. W., Blackwell, P. G., Bronk Ramsey, C., Buck, C. E., Cheng, H., Edwards, R. L., Friedrich, M., Grootes, P. M., Guilderson, T., Haflidason, H., Hajdas, I., Hatté, C., Heaton, T. J., Hoffmann, D. L., Hogg, A. G., Hughen, K. A., Kaiser, K. F., Kromer, B., Manning, S. W., Niu, M., Reimer, R. W., Richards, D. A., Scott, E. M., Southon, J. R., Staff, R. A., Turney, C. S. M., and van der Plicht, J. (2013) IntCal13 and Marine13 radiocarbon age calibration curves 0−50,000 years cal BP. *Radiocarbon* **55** (4), 1869-1887.

Renssen, H., Goosse, H., and Fichefet, T. (2002) Modeling the effect of freshwater pulses on the early Holocene climate: The influence of high-frequency climate variability. *Paleoceanography* **17** (2), 10-11-10-16.

Renssen, H., Seppä, H., Heiri, O., Roche, D. M., Goosse, H., and Fichefet, T. (2009) The spatial and temporal complexity of the Holocene thermal maximum. *Nature Geoscience* **2** (6), 411-414.

Revel, M., Colin, C., Bernasconi, S., Combourieu-Nebout, N., Ducassou, E., Grousset, F. E., Rolland, Y., Migeon, S., Bosch, D., Brunet, P., Zhao, Y., and Mascle, J. (2014) 21,000 Years of Ethiopian African monsoon variability recorded in sediments of the western Nile deep-sea fan. *Regional Environmental Change* **14** (5), 1685-1696.

Ribolini, A., Isola, I., Zanchetta, G., Bini, M., and Sulpizio, R. (2011) Glacial feature on the Galicica Mountains, Macedonia: preliminary report. *Geografia Fisica e Dinamica Quaternaria* **34**, 247-255.

Roberts, N., Brayshaw, D., Kuzucuoglu, C., Perez, R., and Sadori, L. (2011a) The mid-Holocene climatic transition in the Mediterranean: Causes and consequences. *The Holocene* **21** (1), 3-13.

Roberts, N., Eastwood, W. J., Kuzucuoglu, C., Fiorentino, G., and Caracuta, V. (2011b) Climatic, vegetation and cultural change in the eastern Mediterranean during the mid-Holocene environmental transition. *The Holocene* **21** (1), 147-162.

Roberts, N., Jones, M. D., Benkaddour, A., Eastwood, W. J., Filippi, M. L., Frogley, M. R., Lamb, H. F., Leng, M. J., Reed, J. M., Stein, M., Stevens, L., Valero-Garcés, B., and Zanchetta, G. (2008) Stable isotope records of Late Quaternary climate and hydrology from Mediterranean lakes: the ISOMED synthesis. *Quaternary Science Reviews* **27** (25-26), 2426-2441.

Robertson, A. (2004) Development of concepts concerning the genesis and emplacement of Tethyan ophiolites in the Eastern Mediterranean and Oman regions. *Earth-Science Reviews* **66** (3-4), 331-387.

Rodrigues, T., Voelker, A. H. L., Grimalt, J. O., Abrantes, F., and Naughton, F. (2011) Iberian Margin sea surface temperature during MIS 15 to 9 (580−300 ka): Glacial suborbital variability versus interglacial stability. *Paleoceanography* **26** (1).

Roelofs, A., and Kilham, P. (1983) The diatom stratigraphy and palaeoecology of lake Ohrid, Yugoslavia. *Palaeogeography, Palaeoclimatology, Palaeoecology* **42** (3−4), 225-245.

Rohling, E., Mayewski, P., Abu-Zied, R., Casford, J., and Hayes, A. (2002) Holocene atmosphere-ocean interactions: records from Greenland and the Aegean Sea. *Climate Dynamics* **18** (7), 587-593.

Rohling, E. J., Abu-Zied, R., Casford, C. S. L., Hayes, A., and Hoogakker, B. A. A. (2009) *The Marine Environment: Present and Past*. *In* Woodward, J. C. (ed.) *The Physical Geography of the Mediterranean*, Oxford, UK, Oxford University Press, p. 33-67.

Rohling, E. J., and Hilgen, F. J. (1991) The eastern Mediterranean climate at times of sapropel formation: a review. *Geologie en Mijnbouw* **70** (3), 253-264.

Rohling, E. J., and Palike, H. (2005) Centennial-scale climate cooling with a sudden cold event around 8,200 years ago. *Nature* **434**, 975-979.

Romanek, C. S., Grossman, E. L., and Morse, J. W. (1992) Carbon isotopic fractionation in synthetic aragonite and calcite: Effects of temperature and precipitation rate. *Geochimica et Cosmochimica Acta* **56** (1), 419-430.

Rosenbaum, J., and Sheppard, S. M. F. (1986) An isotopic study of siderites, dolomites and ankerites at high temperatures. *Geochimica et Cosmochimica Acta* **50** (6), 1147-1150.

Rosi, M., and Santacroce, R. (1983) The A.D. 472 “Pollena” eruption: volcanological and petrological data for this poorly-known, plinian-type event at vesuvius. *Journal of Volcanology and Geothermal Research* **17** (1-4), 249-271.

Rosqvist, G. C., Leng, M. J., and Jonsson, C. (2007) North Atlantic region atmospheric circulation dynamics inferred from a late-Holocene lacustrine carbonate isotope record, northern Swedish Lapland. *The Holocene* **17** (7), 867-873.

Rossignol-Strick, M. (1985) Mediterranean Quaternary sapropels, an immediate response of the African monsoon to variation of insolation. *Palaeogeography Palaeoclimatology Palaeoecology* **49**, 237-263.

Rossignol-Strick, M. (1995) Sea-land correlation of pollen records in the Eastern Mediterranean for the glacial-interglacial transition: Biostratigraphy versus radiometric time-scale. *Quaternary Science Reviews* **14** (9), 893-915.

Roucoux, K. H., Tzedakis, P. C., Abreu, L. d., and Shackleton, N. J. (2007) *Fine-tuning the land-ocean correlation for the late middle pleistocene of Southern Europe*. *In* Frank Sirocko, M. C. M. F. S. G., and Thomas, L. (eds.) *Developments in Quaternary Sciences*, Volume 7, Elsevier, p. 359-373.

Roucoux, K. H., Tzedakis, P. C., Frogley, M. R., Lawson, I. T., and Preece, R. C. (2008) Vegetation history of the marine isotope stage 7 interglacial complex at Ioannina, NW Greece. *Quaternary Science Reviews* **27** (13-14), 1378-1395.

Rozanski, K., Araguás-Araguás, L., and Gonfiantini, R. (1992) Relation Between Long-Term Trends of Oxygen-18 Isotope Composition of Precipitation and Climate. *Science* **258**, 981-985.

Rozanski, K., Araguás-Araguás, L., and Gonfiantini, R. (1993) *Isotopic Patterns in Modern Global Precipitation*. *In* Swart, P. K., Lohmann, K. C., Mckenzie, J., and Savin, S. (eds.) *Climate Change in Continental Isotopic Records*, Washington, D. C., American Geophysical Union.

Ruddiman, W. F. (2003) Orbital insolation, ice volume, and greenhouse gases. *Quaternary Science Reviews* **22** (15-17), 1597-1629.

Ruddiman, W. F., Raymo, M. E., Martinson, D. G., Clement, B. M., and Backman, J. (1989) Pleistocene evolution: Northern hemisphere ice sheets and North Atlantic Ocean. *Paleoceanography* **4** (4), 353-412.

Saaroni, H., Bitan, A., Alpert, P., and Ziv, B. (1996) Continental polar outbreaks into the Levant and Eastern Mediterranean. *International Journal of Climatology* **16** (10), 1175-1191.

Sadori, L., Jahns, S., and Peyron, O. (2011) Mid-Holocene vegetation history of the central Mediterranean. *The Holocene* **21** (1), 117-129.

Sadori, L., Koutsodendris, A., Masi, A., Bertini, A., Combourieu-Nebout, N., Francke, A., Kouli, K., Joannin, S., Mercuri, A. M., Panagiotopoulos, K., Peyron, O., Torri, P., Wagner, B., Zanchetta, G., and Donders, T. H. (2015) Pollen-based paleoenvironmental and paleoclimatic change at Lake Ohrid (SE Europe) during the past 500 ka. *Biogeosciences Discussions* **12** (18), 15461-15493.

Sadori, L. and Narcisi, B. (2001) The Postglacial record of environmental history from Lago di Pergusa, Sicily. *The Holocene* **11** (6), 655-671.

Sadori, L., Zanchetta, G., and Giardini, M. (2008) Last Glacial to Holocene palaeoenvironmental evolution at Lago di Pergusa (Sicily, Southern Italy) as inferred by pollen, microcharcoal, and stable isotopes. *Quaternary International* **181** (1), 4-14.

Sanei, H., Stasiuk, L. D., and Goodarzi, F. (2005) Petrological changes occurring in organic matter from Recent lacustrine sediments during thermal alteration by Rock-Eval pyrolysis. *Organic Geochemistry* **36** (8), 1190-1203.

Sangiorgi, F., Capotondi, L., Combourieu Nebout, N., Vigliotti, L., Brinkhuis, H., Giunta, S., Lotter, A. F., Morigi, C., Negri, A., and Reichart, G.-J. (2003) Holocene seasonal sea-surface temperature variations in the southern Adriatic Sea inferred from a multiproxy approach. *Journal of Quaternary Science* **18** (8), 723-732.

Santacroce, R., Cioni, R., Marianelli, P., Sbrana, A., Sulpizio, R., Zanchetta, G., Donahue, D. J., and Joron, J. L. (2008) Age and whole rock−glass compositions of proximal pyroclastics from the major explosive eruptions of

Somma-Vesuvius: A review as a tool for distal tephrostratigraphy. *Journal of Volcanology and Geothermal Research* **177** (1), 1-18.

Schleussner, C. F., and Feulner, G. (2013) A volcanically triggered regime shift in the subpolar North Atlantic Ocean as a possible origin of the Little Ice Age. *Climate of the Past* **9** (3), 1321-1330.

Schmidt, G. A., Bigg, G. R., and Rohling, E. J. (1999) Global Seawater Oxygen-18 Database 1.21 <http://data.giss.nasa.gov/o18data/>.

Schon, I. and Martens, K. (2004) Adaptive, pre-adaptive and non-adaptive components of radiations in ancient lakes: a review. *Organisms Diversity & Evolution* **4** (3), 137-156.

Schrag, D. P., Adkins, J. F., McIntyre, K., Alexander, J. L., Hodell, D. A., Charles, C. D., and McManus, J. F. (2002) The oxygen isotopic composition of seawater during the Last Glacial Maximum. *Quaternary Science Reviews* **21** (1−3), 331-342.

Schwalb, A. (2003) Lacustrine ostracodes as stable isotope recorders of late-glacial and Holocene environmental dynamics and climate. *Journal of Paleolimnology* **29** (3), 265-351.

Sebag, D., Debret, M., M'Voubou, M., Obame, R. M., Ngomanda, A., Oslisly, R., Bentaleb, I., Disnar, J. R., and Giresse, P. (2013) Coupled Rock-Eval pyrolysis and spectrophotometry for lacustrine sedimentary dynamics: Application for West Central African rainforests (Kamalete and Nguene lakes, Gabon). *The Holocene* **23** (8), 1173-1183.

Seppä, H. and Birks, H. J. B. (2002) Holocene Climate Reconstructions from the Fennoscandian Tree-Line Area Based on Pollen Data from Toskaljavri. *Quaternary Research* **57** (2), 191-199.

Seppä, H., MacDonald, G. M., Birks, H. J. B., Gervais, B. R., and Snyder, J. A. (2008) Late-Quaternary summer temperature changes in the northern-European tree-line region. *Quaternary Research* **69** (3), 404-412.

Shackleton, N. J. (2000) The 100,000-Year Ice-Age Cycle Identified and Found to Lag Temperature, Carbon Dioxide, and Orbital Eccentricity. *Science* **289**, 1897-1902.

Sharp, Z. (2007) *Principles of Stable Isotope Geochemistry*, New Jersey, Pearson Prentice Hall.

Siani, G., Magny, M., Paterne, M., Debret, M., and Fontugne, M. (2013) Paleohydrology reconstruction and Holocene climate variability in the South Adriatic Sea. *Climate of the Past* **9** (1), 499-515.

Siani, G., Paterne, M., and Colin, C. (2010) Late glacial to Holocene planktic foraminifera bioevents and climatic record in the South Adriatic Sea. *Journal of Quaternary Science* **25** (5), 808-821.

Spirkovski, Z., Avramovski, O., and Kodzoman, A. (2001) Watershed management in the Lake Ohrid region of Albania and Macedonia. *Lakes & Reservoirs: Research and Management* **6**, 237-242.

Stankovic, S. (1960) *The Balkan Lake Ohrid and Its Living World*, Den Haag, Uitgeverij Dr. W. Junk, Monographiae Biologicae.

Stein, M., Ben-Avraham, Z., Goldstein, S., Agnon, A., Ariztegui, D., Brauer, A., Haug, G., Ito, E., and Yasuda, Y. (2011) Deep Drilling at the Dead Sea. *Scientific Drilling* **11**, 46-47.

Stein, R., Hefter, J., Grützner, J., Voelker, A., and Naafs, B. D. A. (2009) Variability of surface water characteristics and Heinrich-like events in the Pleistocene midlatitude North Atlantic Ocean: Biomarker and XRD records from IODP Site U1313 (MIS 16-9). *Paleoceanography* **24** (2), PA2203.

Steindachner, F. (1892) Uber einige neue und seltene Fischarten usw. *Denkschriften der Akademie der Wissenschaften Wien, Mathematisch-naturwissenschaftliche* **59**, 357-384.

Steinman, B. A., Rosenmeier, M. F., Abbott, M. B., and Bain, D. J. (2010) The isotopic and hydrologic response of small, closed-basin lakes to climate forcing from predictive models: Application to paleoclimate studies in the upper Columbia River basin. *Limnology and Oceanography* **55** (6), 2231-2245.

Steinmann, P., Adatte, T., and Lambert, P. (2003) Recent changes in sedimentary organic matter from Lake Neuchâtel (Switzerland) as traced by Rock-Eval pyrolysis. *Eclogae Geologicae Helvetiae* **1**, 109-116.

Stuiver, M. (1970) Oxygen and carbon isotope ratios of fresh-water carbonates as climatic indicators. *Journal of Geophysical Research* **75** (27), 5247-5257.

Stuiver, M. and Reimer, P. J. (1993) Extended 14C data base and revised CALIB 3.0 14C age calibration program. *Radiocarbon* **35** (1), 215-230.

Sturany, R. (1894) Zur Molluskenfauna der europaischen Turke. *Annalen des kaiserlich koniglichen Naturhistorischen Hofmuseums* **9**, 369-394.

Sulpizio, R., Mele, D., Dellino, P., and Volpe, L. L. (2005) A complex, Subplinian-type eruption from low-viscosity, phonolitic to tephri-phonolitic magma: the AD 472 (Pollena) eruption of Somma-Vesuvius, Italy. *Bulletin of Volcanology* **67** (8), 743-767.

Sulpizio, R., Van Welden, A., Caron, B., and Zanchetta, G. (2010a) The Holocene tephrostratigraphic record of Lake Shkodra (Albania and Montenegro). *Journal of Quaternary Science* **25** (5), 633-650.

Sulpizio, R., Zanchetta, G., D'Orazio, M., Vogel, H., and Wagner, B. (2010b) Tephrostratigraphy and tephrochronology of lakes Ohrid and Prespa, Balkans. *Biogeosciences* **7**, 3273-3288.

Sun, Y. and An, Z. (2005) Late Pliocene-Pleistocene changes in mass accumulation rates of eolian deposits on the central Chinese Loess Plateau. *Journal of Geophysical Research* **110** (D23).

Swart, P. K., Burns, S. J., and Leder, J. J. (1991) Fractionation of the stable isotopes of oxygen and carbon in carbon dioxide during the reaction of calcite with phosphoric acid as a function of temperature and technique. *Chemical Geology* **86**, 89-96.

Talbot, M. R. (1990) A review of the palaeohydrological interpretation of carbon and oxygen isotopic ratios in primary lacustrine carbonates. *Chemical Geology: Isotope Geoscience section* **80** (4), 261-279.

Talbot, M. R., Filippi, M. L., Jensen, N. B., and Tiercelin, J.-J. (2007) An abrupt change in the African monsoon at the end of the Younger Dryas. *Geochemistry, Geophysics, Geosystems* **8** (3), Q03005.

Talbot, M. R. and Johannessen, T. (1992) A high resolution palaeoclimatic record for the last 27,500 years in tropical West Africa from the carbon and nitrogen isotopic composition of lacustrine organic matter. *Earth and Planetary Science Letters* **110** (1−4), 23-37.

Talbot, M. R. and Livingstone, D. A. (1989) Hydrogen Index and Carbon Isotopes of Lacustrine Organic-Matter as Lake Level Indicators. *Palaeogeography Palaeoclimatology Palaeoecology* **70** (1-3), 121-137.

Tančev, L. and Petkovski, L. (2006) *New large dams are necessary in FYR Macedonia*. *In* Berga, L., Buil, J. M., Bofill, E., De Cea, J. C., Garcia Perez, J. A., Mañueco, G., Polimon, J., Soriano, A., and Yagüe, J. (eds.) *Dams and Reservoirs, Societies and Environment in the 21st Century*, London, UK, Taylor & Francis, p. 365-372.

Tasevska, O., Jersabek, C., Kostoski, G., and Gušeska, D. (2012) Differences in rotifer communities in two freshwater bodies of different trophic degree (Lake Ohrid and Lake Dojran, Macedonia). *Biologia* **67** (3), 565-572.

R Core Team (2015) *R: A Language and Environment for Statistical Computing*. R Foundation for Statistical Computing, Vienna, Austria <http://www.r-project.org>

Thomas, E. R., Wolff, E. W., Mulvaney, R., Steffensen, J. P., Johnsen, S. J., Arrowsmith, C., White, J. W. C., Vaughn, B., and Popp, T. (2007) The 8.2ka event from Greenland ice cores. *Quaternary Science Reviews* **26** (1-2), 70-81.

Tinner, W., van Leeuwen, J. F. N., Colombaroli, D., Vescovi, E., van der Knaap, W. O., Henne, P. D., Pasta, S., D'Angelo, S., and La Mantia, T. (2009) Holocene environmental and climatic changes at Gorgo Basso, a coastal lake in southern Sicily, Italy. *Quaternary Science Reviews* **28** (15-16), 1498-1510.

Triantaphyllou, M. V., Ziveri, P., Gogou, A., Marino, G., Lykousis, V., Bouloubassi, I., Emeis, K. C., Kouli, K., Dimiza, M., Rosell-Melé, A., Papanikolaou, M., Katsouras, G., and Nunez, N. (2009) Late Glacial−Holocene climate variability at the south-eastern margin of the Aegean Sea. *Marine Geology* **266** (1-4), 182-197.

Trigo, R. M., Osborn, T. J., and Corte-Real, J. M. (2002) The North Atlantic Oscillation influence on Europe: climate impacts and associated physical mechanisms. *Climate Research* **20**, 9-17.

Trouet, V., Esper, J., Graham, N. E., Baker, A., Scourse, J. D., and Frank, D. C. (2009) Persistent Positive North Atlantic Oscillation Mode Dominated the Medieval Climate Anomaly. *Science* **324**, 78-80.

Turner, R., Roberts, N., and Jones, M. D. (2008) Climatic pacing of Mediterranean fire histories from lake sedimentary microcharcoal. *Global and Planetary Change* **63** (4), 317-324.

Tzedakis, C. (2003) Timing and duration of Last Interglacial conditions in Europe: a chronicle of a changing chronology. *Quaternary Science Reviews* **22** (8-9), 763-768.

Tzedakis, P. C. (2007) Seven ambiguities in the Mediterranean palaeoenvironmental narrative. *Quaternary Science Reviews* **26** (17-18), 2042-2066.

Tzedakis, P. C., Andrieu, V., deBeaulieu, J. L., Crowhurst, S., Follieri, M., Hooghiemstra, H., Magri, D., Reille, M., Sadori, L., Shackleton, N. J., and Wijmstra, T. A. (1997) Comparison of terrestrial and marine records of changing climate of the last 500,000 years. *Earth and Planetary Science Letters* **150** (1-2), 171-176.

Tzedakis, P. C., Frogley, M. R., and Heaton, T. H. E. (2003a) Last Interglacial conditions in southern Europe: evidence from Ioannina, northwest Greece. *Global and Planetary Change* **36** (3), 157-170.

Tzedakis, P. C., McManus, J. F., Hooghiemstra, H., Oppo, D. W., and Wijmstra, T. A. (2003b) Comparison of changes in vegetation in northeast Greece with records of climate variability on orbital and suborbital frequencies over the last 450 000 years. *Earth and Planetary Science Letters* **212** (1-2), 197-212.

Tzedakis, C., Roucoux, K. H., De Abreu, L., and Shackleton, N. (2004) The Duration of Forest Stages in Southern Europe and Interglacial Climate Variability. *Science* **306**, 2231-2235.

Tzedakis, P. C., Hooghiemstra, H., and Pälike, H. (2006) The last 1.35 million years at Tenaghi Philippon: revised chronostratigraphy and long-term vegetation trends. *Quaternary Science Reviews* **25** (23-24), 3416-3430.

Tzedakis, P. C., Pälike, H., Roucoux, K. H., and de Abreu, L. (2009) Atmospheric methane, southern European vegetation and low-mid latitude links on orbital and millennial timescales. *Earth and Planetary Science Letters* **277** (3-4), 307-317.

Tzedakis, P. C., Channell, J. E. T., Hodell, D. A., Kleiven, H. F., and Skinner, L. C. (2012) Determining the natural length of the current interglacial. *Nature Geoscience* **5** (2), 138-141.

Usdowski, E., and Hoefs, J. (1990) Kinetic $^{13}C^{12}C$ and $^{18}O^{16}O$ effects upon dissolution and outgassing of CO_2 in the system CO_2H_2O. *Chemical Geology: Isotope Geoscience Section* **80** (2), 109-118.

USGS (2015) USGS Earthquake Hazards Program.

Valiantzas, J. D. (2006) Simplified versions for the Penman evaporation equation using routine weather data. *Journal of Hydrology* **331** (3-4), 690-702.

van der Schriek, T. and Giannakopoulos, C. (2015) Reconstruction of hydro-climatic changes in the S Balkans from the Medieval Warm Period to the present based on a high-resolution lake level stage record derived from beach ridge sediments of Lake Prespa (Greece, Albania, FYROM). *In* Proceedings 15th EMS / 12th ECAM2015, Volume 12, EMS2015-169.

Vannière, B., Power, M. J., Roberts, N., Tinner, W., Carrion, J., Magny, M., Bartlein, P., Colombaroli, D., Daniau, A. L., Finsinger, W., Gil-Romera, G., Kaltenrieder, P., Pini, R., Sadori, L., Turner, R., Valsecchi, V., and Vescovi, E. (2011) Circum-Mediterranean fire activity and climate changes during the mid-Holocene environmental transition (8500-2500 cal. BP). *The Holocene* **21** (1), 53-73.

Vasconcelos, C., McKenzie, J. A., Warthmann, R., and Bernasconi, S. M. (2005) Calibration of the $\delta^{18}O$ paleothermometer for dolomite precipitated in microbial cultures and natural environments. *Geology* **33** (4), 317.

Verpoorter, C., Kutser, T., Seekell, D. A., and Tranvik, L. J. (2014) A global inventory of lakes based on high-resolution satellite imagery. *Geophysical Research Letters* **41** (18), 6396-6402.

Voelker, A., and de Abreu, L. (2011) A Review of Abrupt Climate Change Events in the Northeastern Atlantic Ocean (Iberian Margin): Latitudinal, Longitudinal, and Vertical Gradients), *Abrupt Climate Change: Mechanisms, Patterns, and Impacts,* AGU, p. 15-37.

Voelker, A. H. L., Rodrigues, T., Billups, K., Oppo, D., McManus, J., Stein, R., Hefter, J., and Grimalt, J. O. (2010) Variations in mid-latitude North Atlantic surface water properties during the mid-Brunhes (MIS 9−14) and their implications for the thermohaline circulation. *Climate of the Past* **6** (4), 531-552.

Vogel, H., Meyer-Jacob, C., Melles, M., Brigham-Grette, J., Andreev, A. A., Wennrich, V., Tarasov, P. E., and Rosén, P. (2013) Detailed insight into Arctic climatic variability during MIS 11c at Lake El'gygytgyn, NE Russia. *Climate of the Past* **9** (4), 1467-1479.

Vogel, H., Rosén, P., Wagner, B., Melles, M., and Persson, P. (2008) Fourier transform infrared spectroscopy, a new cost-effective tool for quantitative analysis of biogeochemical properties in long sediment records. *Journal of Paleolimnology* **40** (2), 689-702.

Vogel, H., Wagner, B., Zanchetta, G., Sulpizio, R., and Rosén, P. (2010a) A paleoclimate record with tephrochronological age control for the last glacial-interglacial cycle from Lake Ohrid, Albania and Macedonia. *Journal of Paleolimnology* **44** (1), 295-310.

Vogel, H., Wessels, M., Albrecht, C., Stich, H. B., and Wagner, B. (2010b) Spatial variability of recent sedimentation in Lake Ohrid (Albania/Macedonia). *Biogeosciences* **7**, 3333-3342.

Vogel, H., Zanchetta, G., Sulpizio, R., Wagner, B., and Nowaczyk, N. (2010c) A tephrostratigraphic record for the last glacial-interglacial cycle from Lake Ohrid, Albania and Macedonia. *Journal of Quaternary Science* **25** (3), 320-338.

Wagner, B., and Wilke, T. (2011) Preface "Evolutionary and geological history of the Balkan lakes Ohrid and Prespa". *Biogeosciences* **8** (4), 995-998.

Wagner, B., Reicherter, K., Daut, G., Wessels, M., Matzinger, A., Schwalb, A., Spirkovski, Z., and Sanxhaku, M. (2008a) The potential of Lake Ohrid for long-term palaeoenvironmental reconstructions. *Palaeogeography, Palaeoclimatology, Palaeoecology* **259** (2-3), 341-356.

Wagner, B., Sulpizio, R., Zanchetta, G., Wulf, S., Wessels, M., Daut, G., and Nowaczyk, N. (2008b) The last 40 ka tephrostratigraphic record of Lake Ohrid, Albania and Macedonia: a very distal archive for ash dispersal from Italian volcanoes. *Journal of Volcanology and Geothermal Research* **177** (1), 71-80.

Wagner, B., Lotter, A. F., Nowaczyk, N., Reed, J. M., Schwalb, A., Sulpizio, R., Valsecchi, V., Wessels, M., and Zanchetta, G. (2009a) A 40,000-year record of environmental change from ancient Lake Ohrid (Albania and Macedonia). *Journal of Paleolimnology* **41** (3), 407-430.

Wagner, B., Wilke, T., Krastel, S., Grazhdani, S., Reicherter, K., Trajanovski, S., and Zanchetta, G. (2009b) Scientific collaboration on past speciation conditions in Lake Ohrid : SCOPSCO Workshop report. *Scientific Drilling* **7**, 51-53.

Wagner, B., Vogel, H., Zanchetta, G., and Sulpizio, R. (2010). Environmental change within the Balkan region during the past ca. 50 ka recorded in the sediments from lakes Prespa and Ohrid. *Biogeosciences* **7** (10), 3187-3198.

Wagner, B., Aufgebauer, A., Vogel, H., Zanchetta, G., Sulpizio, R., and Damaschke, M. (2012a) Late Pleistocene and Holocene contourite drift in Lake Prespa (Albania/F.Y.R. of Macedonia/Greece). *Quaternary International* **274**, 112-121.

Wagner, B., Francke, A., Sulpizio, R., Zanchetta, G., Lindhorst, K., Krastel, S., Vogel, H., Rethemeyer, J., Daut, G., Grazhdani, A., Lushaj, B., and Trajanovski, S. (2012b) Possible earthquake trigger for 6th century mass wasting deposit at Lake Ohrid (Macedonia/Albania). *Climate of the Past* **8** (6), 2069-2078.

Wagner, B., Wilke, T., Krastel, S., Zanchetta, G., Sulpizio, R., Reicherter, K., Leng, M. J., Grazhdani, A., Trajanovski, S., Francke, A., Lindhorst, K., Levkov, Z., Cvetkoska, A., Reed, J. M., Zhang, X., Lacey, J. H., Wonik, T., Baumgarten, H., and Vogel, H. (2014) The SCOPSCO drilling project recovers more than 1.2 million years of history from Lake Ohrid. *Scientific Drilling* **17**, 19-29.

Wang, P., Tian, J., and Lourens, L. J. (2010) Obscuring of long eccentricity cyclicity in Pleistocene oceanic carbon isotope records. *Earth and Planetary Science Letters* **290** (3-4), 319-330.

Wanner, H., Brönnimann, S., Casty, C., Gyalistras, D., Luterbacher, J., Schmutz, C., Stephenson, D. B., and Xoplaki, E. (2001) North Atlantic Oscillation − Concepts And Studies. *Surveys in Geophysics* **22** (4), 321-381.

Watzin, M. C., Puka, V., and Naumoski, T. B. (2002) *Lake Ohrid and its watershed, state of the environment report*, Macedonia, Tirana, Lake Ohrid Conservation Project.

Weiss, H., Courty, M. A., Wetterstrom, W., Guichard, F., Senior, L., Meadow, R., and Curnow, A. (1993) The Genesis and Collapse of Third Millennium North Mesopotamian Civilization. *Science* **261**, 995-1004.

Wersin, P., Hohener, P., Giovanoli, R., and Stumm, W. (1991) Early diagenetic influences on iron transformations in a fresh-water lake sediment. *Chemical Geology* **90**, 233-252.

Wetzel, R. G. (1983) *Limnology*, USA, Saunders College Publishing.

Wick, L., Lemcke, G., and Sturm, M. (2003) Evidence of Lateglacial and Holocene climatic change and human impact in eastern Anatolia: High-resolution pollen, charcoal, isotopic and geochemical records from the laminated sediments of Lake Van, Turkey. *Holocene* **13** (5), 665-675.

Williams, D. F., Kuzmin, M. I., Prokopenko, A. A., Karabanov, E. B., Khursevich, G. K., and Bezrukova, E. V. (2001) The Lake Baikal drilling project in the context of a global lake drilling initiative. *Quaternary International* **80−81**, 3-18.

Wilson, G. P., Reed, J. M., Frogley, M. R., Hughes, P. D., and Tzedakis, P. C. (2015) Reconciling diverse lacustrine and terrestrial system response to penultimate deglacial warming in southern Europe. *Geology* **43** (9), 819-822.

Wilson, G. P., Reed, J. M., Lawson, I. T., Frogley, M. R., Preece, R. C., and Tzedakis, P. C. (2008) Diatom response to the Last Glacial−Interglacial Transition in the Ioannina basin, northwest Greece: implications for Mediterranean palaeoclimate reconstruction. *Quaternary Science Reviews* **27** (3-4), 428-440.

WMO (2015) World Weather Information Service, Hong Kong, Hong Kong Observatory <http://worldweather.wmo.int>

Xoplaki, E. (2002) Climate variability over the Mediterranean (Doctoral thesis, University of Bern).

Yin, Q. Z. and Berger, A. (2011) Individual contribution of insolation and CO2 to the interglacial climates of the past 800,000 years. *Climate Dynamics* **38** (3-4), 709-724.

Zanchetta, G., Borghini, A., Fallick, A. E., Bonadonna, F. P., and Leone, G. (2007a) Late Quaternary palaeohydrology of Lake Pergusa (Sicily, southern Italy) as inferred by stable isotopes of lacustrine carbonates. *Journal of Paleolimnology* **38** (2), 227-239.

Zanchetta, G., Drysdale, R. N., Hellstrom, J. C., Fallick, A. E., Isola, I., Gagan, M. K., and Pareschi, M. T. (2007b) Enhanced rainfall in the Western Mediterranean during deposition of sapropel S1: stalagmite evidence from Corchia cave (Central Italy). *Quaternary Science Reviews* **26** (3-4), 279-286.

Zanchetta, G., Sulpizio, R., Roberts, N., Cioni, R., Eastwood, W. J., Siani, G., Caron, B., Paterne, M., and Santacroce, R. (2011) Tephrostratigraphy, chronology and climatic events of the Mediterranean basin during the Holocene: An overview. *The Holocene* **21** (1), 33-52.

Zanchetta, G., Regattieri, E., Giaccio, B., Wagner, B., Sulpizio, R., Francke, A., Vogel, L. H., Sadori, L., Masi, A., Sinopoli, G., Lacey, J. H., Leng, M. L., and Leicher, N. (2015) Aligning MIS5 proxy records from Lake Ohrid (FYROM) with independently dated Mediterranean archives: implications for core chronology. *Biogeosciences Discussions* **12** (20), 16979-17007.

Zhang, C. L., Horita, J., Cole, D. R., Zhou, J. Z., Lovley, D. R., and Phelps, T. J. (2001) Temperature-dependent oxygen and carbon isotope fractionations of biogenic siderite. *Geochimica et Cosmochimica Acta* **65** (14), 2257-2271.

Zhang, X., Reed, J., Wagner, B., Francke, A., and Levkov, Z. (2014) Lateglacial and Holocene climate and environmental change in the northeastern Mediterranean region: diatom evidence from Lake Dojran (Republic of Macedonia/Greece). *Quaternary Science Reviews* **103**, 51-66.

Zhang, X., Reed, J. M., Lacey, J. H., Francke, A., Leng, M. J., Levkov, Z., and Wagner, B. (2015) Complexity of diatom response to Lateglacial and Holocene climate and environmental change in ancient, deep, and oligotrophic Lake Ohrid (Macedonia/Albania). *Biogeosciences Discussions*, **12**, 14343-14375.

Zhornyak, L. V., Zanchetta, G., Drysdale, R. N., Hellstrom, J. C., Isola, I., Regattieri, E., Piccini, L., Baneschi, I., and Couchoud, I. (2011) Stratigraphic evidence for a “pluvial phase” between ca 8200−7100 ka from Renella cave (Central Italy). *Quaternary Science Reviews* **30** (3-4), 409-417.

Ziegler, M., Tuenter, E., and Lourens, L. J. (2010) The precession phase of the boreal summer monsoon as viewed from the eastern Mediterranean (ODP Site 968). *Quaternary Science Reviews* **29** (11-12), 1481-1490.

Ziv, B., Saaroni, H., and Alpert, P. (2004) The factors governing the summer regime of the eastern Mediterranean. *International Journal of Climatology* **24** (14), 1859-1871.

Zocatelli, R., Turcq, B., Boussafir, M., Cordeiro, R. C., Disnar, J. R., Costa, R. L., Sifeddine, A., Albuquerque, A. L. S., Bernardes, M. C., and Jacob, J. (2012) Late Holocene paleoenvironmental changes in Northeast Brazil recorded by organic matter in lacustrine sediments of Lake Boqueirão. *Palaeogeography, Palaeoclimatology, Palaeoecology* **363-364**, 127-134.